Characterization and expression of protein(s) involved in gold nanoparticle formations by *Thermus scotoductus* SA-01

Mariana Erasmus

Characterization and expression of protein(s) involved in gold nanoparticle formations by *Thermus scotoductus* SA-01

By

Mariana Erasmus

Submitted in fulfillment of the requirements for the degree

MAGISTER SCIENTIAE

In the

Department of Microbial, Biochemical and Food Biotechnology

Faculty of Natural and Agricultural Sciences

University of the Free State

Bloemfontein

Republic of South Africa

May 2010

Supervisor: Prof. E. van Heerden

Co-supervisor: Prof. J. Albertyn

I dedicate this dissertation to my family, for giving me the opportunity to study as well as for their constant love and support throughout this research.

“All human discoveries seem to be made only for the purpose of confirming more and more strongly the truth contained in the Sacred Scriptures.”

~ John Herschel (1792 – 1871), British Astronomer

“The most exciting phrase to hear in science, the one that heralds the most discoveries, is not ‘Eureka’ (I found it!), but ‘That’s funny…’”

~ Isaac Asimov (1920 – 1992), American Author & Biochemistry Professor

CONTENTS

ACKNOWLEDGEMENTS……..**ix**

LIST OF SYMBOLS AND ABBREVIATIONS……**xi**

LIST OF FIGURES……**xvi**

LIST OF TABLES……..**xxxii**

CHAPTER 1: LITERATURE REVIEW

1.1 NANOTECHNOLOGY AND NANOMATERIALS……...**1**

1.2 METAL NANOPARTICLES……**4**

1.2.1 Iron, Cobalt, Copper & Nickel…….....**5**

1.2.2 Cadmium, Palladium & Vanadium.....**6**

1.2.3 Platinum……**7**

1.2.4 Silver……..**8**

1.2.5 Gold……..**10**

1.3 OXIDE NANOPARTICLES……...**13**

1.3.1 Magnetite.....**13**

1.3.2 Zinc Oxide…….....**14**

1.4 METALLOID AND SEMICONDUCTOR NANOPARTICLES……**15**

1.4.1 Silicon & Germanium……..**15**

1.5 DIFFERENT TYPES OF NANOSCALE STRUCTURES.....15

1.5.1 Nanoparticles.....16

1.5.2 Nanotubes.....16

1.5.3 Nanowires.....17

1.5.4 Nanoshells.....18

1.5.5 Other Nanoscale Structures.....18

1.6 PHYSICO-CHEMICAL PROPERTIES OF NANOMATERIALS.....19

1.7 METHODS USED IN THE PRODUCTION OF NANOMATERIALS.....22

1.7.1 Physical & Chemical Methods.....23

1.7.2 Biological Methods.....25

1.8 APPLICATIONS IN NANOTECHNOLOGY.....28

1.9 CONCLUSIONS.....30

REFERENCES.....32

— · · — · · — · · — · · — · · — · · — · · —

CHAPTER 2: INTRODUCTION TO PRESENT STUDY

2.1 INTRODUCTION.....44

2.2 AIMS OF THIS STUDY.....45

REFERENCES.....47

— · · — · · — · · — · · — · · — · · — · · —

CHAPTER 3: EXPRESSION AND CHARACTERIZATION OF AN ABC TRANSPORTER, PEPTIDE-BINDING PROTEIN FROM *THERMUS SCOTODUCTUS* SA-01 IN A MESOPHILIC HOST

3.1 INTRODUCTION……**49**

3.2 MATERIALS AND METHODS……**52**

3.2.1 Bacterial Strains and Culture Conditions……..**52**

3.2.2 Plasmids……**52**

3.2.3 Genomic DNA Isolation……..**56**

3.2.4 Polymerase Chain Reaction……..**57**

3.2.5 Ligation into pGEM®-T Easy……..**58**

3.2.6 Preparation of *Escherichia coli* TOP10 and BL21(DE3) Competent Cells……...**58**

3.2.7 Transformation into *Escherichia coli* TOP10……**59**

3.2.8 Evaluation of the Insert Size……**59**

3.2.9 Preparation of the pET-22b(+) and pET-28b(+) Expression Plasmids……**60**

3.2.10 Evaluation of the Insert Size……**61**

3.2.11 Sequencing……**61**

3.2.12 Transformation into *Escherichia coli* BL21 (DE3)……...**62**

3.2.13 Expression and Fractionation of the ABC Transporter, Peptide-Binding Protein……**62**

3.2.14 Purification of the ABC Transporter, Peptide-Binding Protein……**63**

3.2.14.1 Expression in pET-22b(+)……..**63**

3.2.14.2 Expression in pET-28b(+)……..**63**

3.2.15 Characterization of the ABC Transporter, Peptide-Binding Protein in *Escherichia coli*……**64**

3.2.15.1 SDS-PAGE Analysis……..**64**

3.2.15.2 Protein Concentrations……..**64**

3.2.15.3 Gold Reduction Assay……...**65**

3.2.15.4 Surface Plasmon Resonance……..**66**
3.2.15.5 Transmission Electron Microscopy……..**68**
3.2.15.6 Energy Dispersive X-ray Spectrometry and Selected-Area Electron Diffraction……**68**
3.2.15.7 Nanotrac Particle Size Analyzer……..**68**
3.2.15.8 Scanning Auger Nanoprobe……**69**
3.2.15.9 The Effect of Methyl Viologen Concentrations on Gold Reduction and Nanoparticle Formation……..**69**
3.2.15.10 The Effect of Sodium Dithionite Concentrations on Gold Reduction and Nanoparticle Formation…….**69**
3.2.15.11 The Effect of Protein Concentrations on Gold Reduction and Nanoparticle Formation……..**70**
3.2.15.12 The Effect of Denatured Protein on Gold Reduction and Nanoparticle Formation……**70**
3.2.15.13 The Effect of Exposure Time on Gold Reduction and Nanoparticle Formation……**70**
3.2.15.14 The Effect of $HAuCl_4$ Concentrations on Gold Reduction and Nanoparticle Formation……..**71**
3.2.15.15 The Effect of Temperature on Gold Reduction and Nanoparticle Formation……**71**
3.2.15.16 The Effect of pH on Gold Reduction and Nanoparticle Formation……**71**
3.2.15.17 The Effect of Different Disulphide Bond Reducing Agents on Gold Reduction and Nanoparticle Formation……**72**
3.2.16 Mechanism Hypothesis……..**72**

3.3 RESULTS AND DISCUSSIONS……..**74**
3.3.1 Selection of the ABC Transporter, Peptide-Binding Protein…**74**
3.3.2 Genomic DNA Isolation and Polymerase Chain Reaction……**75**
3.3.3 Cloning into pGEM®-T Easy……..**75**

3.3.4 Cloning into pET-22b(+) and pET-28b(+)……**76**
3.3.5 Expression of the ABC Transporter, Peptide-Binding Protein……**79**
3.3.6 Purification of the ABC Transporter, Peptide-Binding Protein……**80**
3.3.6.1 Expression in pET-22b(+)……**80**
3.3.6.2 Expression in pET-28b(+)……**82**
3.3.7 Characterization of the ABC Transporter, Peptide-Binding Protein in *Escherichia coli*……**85**
3.3.7.1 The Effect of Methyl Viologen Concentrations on Gold Reduction and Nanoparticle Formation……..**86**
3.3.7.2 The Effect of Sodium Dithionite Concentrations on Gold Reduction and Nanoparticle Formation…….**90**
3.3.7.3 The Effect of Protein Concentrations on Gold Reduction and Nanoparticle Formation……..**93**
3.3.7.4 The Effect of Denatured Protein on Gold Reduction and Nanoparticle Formation……**97**
3.3.7.5 The Effect of Exposure Time on Gold Reduction and Nanoparticle Formation……**99**
3.3.7.6 The Effect of $HAuCl_4$ Concentrations on Gold Reduction and Nanoparticle Formation……**103**
3.3.7.7 The Effect of Temperature on Gold Reduction and Nanoparticle Formation……...**107**
3.3.7.8 The Effect of pH on Gold Reduction and Nanoparticle Formation……..**112**
3.3.7.9 The Effect of Different Disulphide Bond Reducing Agents on Gold Reduction and Nanoparticle Formation……..**122**
3.3.8 Mechanism Hypothesis……**127**

3.4 CONCLUSIONS……...**130**

REFERENCES.....**131**

CHAPTER 4: EXPRESSION AND CHARACTERIZATION OF AN ABC TRANSPORTER, PEPTIDE-BINDING PROTEIN FROM *THERMUS SCOTODUCTUS* SA-01 IN A THERMOPHILIC HOST

4.1 INTRODUCTION.....**136**

4.2 MATERIALS AND METHODS.....**138**

4.2.1 Bacterial Strains and Culture Conditions.....**138**

4.2.2 Plasmids.....**138**

4.2.3 Genomic DNA Isolation.....**142**

4.2.4 Polymerase Chain Reaction.....**142**

4.2.5 Ligation into pGEM®-T Easy.....**144**

4.2.6 Preparation of *Escherichia coli* TOP10 Competent Cells.....**144**

4.2.7 Transformation into *Escherichia coli* TOP10.....**144**

4.2.8 Ligation into pET-22b(+) and pET-28b(+).....**144**

4.2.9 Evaluation of the Insert Size and Sequencing.....**145**

4.2.10 Preparation of the pWUR and pMK184 Expression Plasmids.....**146**

4.2.11 Evaluation of the Insert Size and Sequencing.....**147**

4.2.12 Transformation into *Thermus thermophilus* HB27.....**147**

4.2.13 Expression and Fractionation of the ABC Transporter, Peptide-Binding Protein.....**148**

4.2.14 Purification of the ABC Transporter, Peptide-Binding Protein.....**148**

4.2.14.1 Expression in pWUR and pMK184.....**148**

4.2.15 Characterization of the ABC Transporter, Peptide-Binding Protein in *Thermus thermophilus* HB27.....**148**

4.2.15.1 SDS-PAGE and Western Blot Analysis.....**149**

4.2.15.2 Protein Concentrations……**149**
4.2.15.3 Gold Reduction Assay……**149**
4.2.15.4 Surface Plasmon Resonance……**149**
4.2.15.5 Transmission Electron Microscopy……**150**
4.2.15.6 Energy Dispersive X-ray Spectrometry and Selected-Area Electron Diffraction……**150**
4.2.15.7 The Effect of the Assay Components (Sodium Dithionite and Methyl Viologen) on Gold Reduction and Nanoparticle Formation……...**150**
4.2.15.8 The Effect of Denatured Protein on Gold Reduction and Nanoparticle Formation……...**151**
4.2.15.9 The Effect of $HAuCl_4$ Concentrations on Gold Reduction and Nanoparticle Formation……**151**
4.2.15.10 The Effect of Temperature on Gold Reduction and Nanoparticle Formation……...**151**
4.2.15.11 The Effect of pH on Gold Reduction and Nanoparticle Formation……..**152**
4.2.15.12 The Effect of Different Disulphide Bond Reducing Agents on Gold Reduction and Nanoparticle Formation……..**152**
4.2.16 Mechanism Hypothesis……**152**

4.3 RESULTS AND DISCUSSIONS……**153**
4.3.1 Genomic DNA Isolation and Polymerase Chain Reaction…..**153**
4.3.2 Cloning into pGEM®-T Easy……**154**
4.3.3 Cloning into pET-22b(+) and pET-28b(+).....**155**
4.3.4 Cloning into pWUR and pMK184……**158**
4.3.5 Expression of the ABC Transporter, Peptide-Binding Protein……...**162**
4.3.6 Purification of the ABC Transporter, Peptide-Binding Protein……...**163**

4.3.6.1 Expression in pWUR and pMK184……**163**

4.3.7 Characterization of the ABC Transporter, Peptide-Binding Protein in *Thermus thermophilus* HB27……..**168**

4.3.7.1 The Effect of the Assay Components (Sodium Dithionite and Methyl Viologen) on Gold Reduction and Nanoparticle Formation……...**169**

4.3.7.2 The Effect of Denatured Protein on Gold Reduction and Nanoparticle Formation……...**173**

4.3.7.3 The Effect of $HAuCl_4$ Concentrations on Gold Reduction and Nanoparticle Formation……**175**

4.3.7.4 The Effect of Temperature on Gold Reduction and Nanoparticle Formation……...**179**

4.3.7.5 The Effect of pH on Gold Reduction and Nanoparticle Formation……..**183**

4.3.7.6 The Effect of Different Disulphide Bond Reducing Agents on Gold Reduction and Nanoparticle Formation……..**187**

4.3.8 Mechanism Hypothesis……**191**

4.4 CONCLUSIONS……...**193**

REFERENCES……**194**

— · · — · · — · · — · · — · · — · · — · · —

CHAPTER 5: CONCLUSIONS……..**197**

— · · — · · — · · — · · — · · — · · — · · —

SUMMARY……**200**

OPSOMMING……...**202**

— · · — · · — · · — · · — · · — · · — · · —

ACKNOWLEDGEMENTS

I wish to express my gratitude and appreciation to all of the following without whom none of this would have been possible:

- My supervisors, **Prof. Esta van Heerden** and **Prof. Koos Albertyn**, for their invaluable assistance in finalizing this script, as well as for all their supervision and trust throughout this study, but also for all the years so far that I had the opportunity to gain knowledge under their guidance, because they helped me to grow and to become a better scientist.

- **Prof. José Berenguer** and **Eloy Ferreras** (CBMSO, Universidad Autónoma de Madrid, Spain) for all their supportive advice and for sharing their knowledge with me, as well as for all their help and everything I have learned during the time I have spend in Prof. Berenguer's lab.

- **Prof. Gaëtan Borgonie** and **Myriam Clayes** (Ghent University, Belgium) for their help with the TEM work, but also for the invaluable friendship of Prof. Borgonie and for always being such a big encouragement to me.

- **Prof. Jan Neethling** (NMMU, Port Elizabeth, South Africa) for his help with the TEM, EDX and SAED work.

- **Prof. Hendrik Swart** and **Dr. Liza Coetsee** (Department of Physics, UFS, Bloemfontein, South Africa) for their help with the Nanoprobe work.

- **Isabel Coetzee** and **Swiss Lab** (Pty) Ltd (Midrand, Johannesburg, South Africa) for their help with the Nanotrac work.

- **Everyone in the Department of Microbiology, Biochemistry and Food Biotechnology** from the UFS, who shared ideas, made suggestions, helped where they could and for their guidance and interest shown, especially **Dr. Jacqui van Marwijk** for all her help.

- **All my friends and the members of the Extreme Biochemistry group** for their friendship, for supporting me through good and bad times, for sharing in my success and failures and for their care and understanding, inside and outside of this department.

- The **National Research Foundation** (NRF), the **Oppenheimer Memorial Trust**, the **Ernst and Ethel Eriksen Trust**, **Whitehead Scientific** and **BioPAD (TIA)** for financial support during this study.

- My family - my parents **Rassie and Ria Erasmus** and my sister and brother-in-law **Elilyia and Morné Shardelow**, for all the sacrifices they made, their unfailing love, their endless understanding and support and for financial assistance, not only for the time of this study, but throughout my life.

- Above all to **God**, my Creator, my Friend, and my Saviour for giving me the ability to do all of this and for all His love and guidance during these years and throughout my life.

LIST OF SYMBOLS AND ABBREVIATIONS

ºC	Degrees Celsius
%	Percentage
&	And
<	Less than
>	Greater than
±	Approximately
®	Registered Trademark
A	Absorbance
ABC	ATP-Binding Cassette
a-*lac*Z	Coding Site
Amp^r	Ampicillin Resistance Gene
ATCC	American Type Culture Collection
atm	atmosphere
ATP	Adenosine Triphosphate
BBInternational	British Biocell International
BCA	Bicinchoninic Acid
BLAST	Basic Local Alignment Search Tool
$Bleo^r$	Bleomycin Resistance Gene
bp	base pair
BSA	Bovine Serum Albumin
CBMSO	Centro de Biología Molecular “Severo Ochoa”
CDs	Compact Discs
CdS	Cadmium-Sulphide
ClustalW	Multiple Sequence Alignment Tool
cm	centimetre
CNT	Carbon Nanotubes
CT	Carbon Tetrachloride
CTAB	Cetyltrimethyl Ammonium Bromide
CVD	Chemical Vapour Deposition

ddH_2O	Double Distilled Water
DMF	Dimethyl Formamide
DNA	Deoxyribonucleic Acid
dNTPs	Deoxyribonucleotide Triphosphates
DTT	Dithiothreitol
e^-	Electron
e.g.	exempli gratia/for example
EBI	European Bioinformatics Institute
EDTA	Ethylene Diaminetetraacetic Acid
EDX	Energy Dispersive X-ray Spectrometry
et al.	et alii/ and others
EtBr	Ethidium Bromide
etc.	et cetera/and so on
EtOH	Ethanol
eV	electron Volt
FED	Field Emission Display
g	gram
$g.L^{-1}$	gram per Litre
gDNA	Genomic DNA
GMR-HD	Giant Magnetoresistive Hard Disk
H^+	Hydrogen Ion
His-Tag	Histidine-Tag
Inc.	Incorporation
IPTG	Isopropyl β-D-1-Thiogalactopyranoside
IR-blocking	Infrared Blocking
IT	Information technology
Kan^r	Kanamycin Resistance Gene
kb	kilobase pair
kDa	kilo Dalton
keV	kiloelectron Volt
km	kilometre
kV	kilo Volt
*Lac*I	Coding Site
*Lac*Z	Coding Site

LB	Luria-Bertani
L-DOPA	L-3,4-Dihydroxyphenylalanine
LEDs	Light-Emitting Diodes
M	Molar
mAu	milli Absorbance units
$\mu g.ml^{-1}$	microgram per millilitre
µl	microlitre
µm	micrometre
µM	micromolar
$mg.ml^{-1}$	milligram per millilitre
ml	millilitre
$ml.min^{-1}$	millilitre per minute
mM	millimolar
MOPS	3-(N-Morpholino)Propanesulfonic Acid Hemisodium Salt
Mr	Relative Molecular Mass
MRAM	Magnetoresistive Random Access Memory
$mS.cm^{-1}$	millisiemens per centimetre
$MV^{\bullet+}$	Methyl Viologen, Free Radical Ion
MV^{0}	Elemental Methyl Viologen
MV^{2+}	Methyl Viologen
MWCO	Molecular Weight Cut-Off
nA	nano Ampere
NAD(P)H	Reduced Nicotinamide Adenine Dinucleotide Phosphate
NCBI	National Center for Biotechnology Information
ng	nanogram
$ng.\mu l^{-1}$	nanogram per Microlitre
nm	nanometre
NMMU	Nelson Mandela Metropolitan University
NTA	Nitrilotriacetic Acid
OD	Optical Density
OLED	Organic Light Emitting Diode
Ori	Origin of Plasmid Replication
ORI ColE1	Origin of Plasmid Replication
Ori*Eco*	Origin for Replication in *E. coli*

PCBs	Printed Circuit Boards
PCR	Polymerase Chain Reaction
PECVD	Plasma-Enhanced Chemical Vapour Deposition
PGM	Platinum Group Metals
pH	Measure of the Acidity or Basicity of a Solution
PhD	Philosophiae Doctor
pI	Isoelectric Point
$pmol.\mu l^{-1}$	picomoles per microlitre
(Pty) Ltd	Proprietary Limited
RepA	Minimal Replicon for Replication in *Thermus* sp.
RFLP	Restriction Fragment Length Polymorphisms
RNase	Ribonuclease
rpm	revolutions per minute
SAED	Selected-Area Electron Diffraction
SDS	Sodium Dodecyl Sulphate
SDS-PAGE	Sodium Dodecyl Sulphate-Polyacrylamide Gel Electrophoresis
SEM	Scanning Electron Microscopy
SERS	Surface Enhanced Raman Scattering
SH-SH	Reduced Disulphide Bond
SOC	Super Optimal, Catabolite Repression
sp(s).	species
sp.	species
SPR	Surface Plasmon Resonance
S-S	Disulphide Bond
TA	3-Thiopheneacetic Acid
TAE	Tris-Acetic Acid-EDTA
TCE	Trichloroethylene
TE	Tris-EDTA
TEM	Transmission Electron Microscopy
TfbI	Transformation buffer I
TfbII	Transformation buffer II
TM	Trademark
Tm	Melting Temperature
TOP	Tri-*n*-Octylphosphine

TOPO	Tri-*n*-Octylphosphine Oxide
Tris-HCl	2-Amino-2-(Hydroxymethyl)-1,3-Propandiol, Hydrochloric Acid
TX-100	Triton X-100
TYG	Tryptone, Yeast Extract, Glucose
U	Units
UV	Ultraviolet
UV-Vis	Ultraviolet-Visible
$V.cm^{-1}$	Volts per centimetre
v/v	volume per volume
v/v/v	volume per volume per volume
WR	Working Reagent
x	Times
x g	Acceleration due to Gravity
X-Gal	5-Bromo-4-Chloro-3-Indolyl-beta-D-Galactopyranosidehosphate

LIST OF FIGURES

Figure 1.1: Nanoscale objects have at least one measurement (height, length, depth) between 1 and 100 nanometre (Taken from http://www.discovernano.northwestern.edu)……**2**

Figure 1.2: Dark-field (A) and bright-field (B) TEM micrographs of platinum nanoparticles produced by cells of *Shewanella algae*. Scale bars in A and B are equal to 700 nm and 100 nm respectively (Taken from Konishi *et al*., 2007a)……**8**

Figure 1.3: TEM micrographs of silver nanoparticles produced by cells of *Plectonema boryanum* UTEX 485. Scale bars in A and B are equal to 500 nm and 50 nm respectively (Taken from Lengke *et al*., 2007a)……**10**

Figure 1.4: An increase in the size of nanoparticles results in a change of colour, from yellow/orange to red/pink, to purple, to blue, due to the surface plasmon vibrations of the gold nanoparticles (Taken from http://www.news.wustl.edu).....**11**

Figure 1.5: TEM micrographs of gold nanoparticles produced by cells of *Shewanella algae*. Scale bars in A and B are equal to 500 nm and 200 nm respectively (Taken from Konishi *et al*., 2007b)……...**12**

Figure 1.6: TEM micrographs of magnetite nanoparticles produced by iron-reducing bacteria. Scale bars in A and B are both equal to 200 nm (Taken from Moon *et al*., 2007)……**14**

Figure 1.7: TEM micrographs showing different shapes of nanoparticles with (A) mainly tetrahedral, (B) mainly cubical and (C) mainly spherical nanoparticles. Scale bars in A and B are equal to 10 nm and in C, 15 nm (Taken from Narayanan & El-Sayed, 2004)……..**16**

Figure 1.8: TEM micrographs of (A) nanowires and (B) the tip of a single nanowire, indicated in (A). Scale bars in A and B are equal to 20 nm and 2 nm respectively (Taken from Lee *et al*., 2006)……**18**

Figure 3.1: Vector map of pET-22b(+), indicating the ampicillin resistance gene, the ColE1 origin of plasmid replication, the *Lac*I coding site and the multiple cloning site under the T7 promoter. Sequence of the pET-22b(+) cloning region, showing the *Eco*RI and *Nde*I sites where the gene was inserted to yield a construct with no His-Tag……**54**

Figure 3.2: Vector map of pET-28b(+), indicating the kanamycin resistance gene, the ColE1 origin of plasmid replication, the *Lac*I coding site and the multiple cloning site under the T7 promoter. Sequence of the pET-28b(+) cloning region, showing the ribosome binding site, the thrombin cleavage site fusion and the *Eco*RI and *Nde*I sites where the gene was inserted to yield a construct with a N-terminal His-Tag……**55**

Figure 3.3: Standard curve for the Micro BCA™ protein assay kit (PIERCE) at 60ºC, using BSA as protein standard. Error bars indicate standard deviations and are smaller than the symbols used……**65**

Figure 3.4: An increase in the size of nanoparticles results in a change of colour, from pink, to purple, to blue, due to the surface plasmon vibrations of the gold nanoparticles (Taken from http://www.webexhibits.org).....**67**

Figure 3.5: UV-Vis spectra of colloidal gold. An increase in the size of nanoparticles results in a shift to bigger wavelengths and forming bigger peaks. Au1 will represent the pink colour in Figure 3.4 and Au4 to the blue colour (Taken from Šlouf *et al.*, 2006)……**67**

Figure 3.6: Homology model of the *T. scotoductus* ABC transporter, peptide-binding protein. The surface exposed disulphide bond, hypothesized to be involved in the gold reduction and nanoparticle formation process, can be seen in yellow (Taken from van Marwijk, (2009)……..**73**

Figure 3.7: (A) Genomic DNA isolated from *T. scotoductus* SA-01 (Lane 2) with the GeneRuler™ DNA ladder (Lane 1). (B) The amplified ABC transporter, peptide-binding gene of ± 1.9 kb, using primers 1 and 2 (Lane 3), negative control (Lane 2) and the MassRuler™ DNA ladder (Lane 1)….**75**

Figure 3.8: The amplified ABC transporter, peptide-binding gene of ± 1.9 kb, using primers 1 and 2, inserted into the pGEM®-T Easy Vector system of ± 3 kb (Lanes 2 - 11) and the MassRuler™ DNA ladder (Lane 1)……..**76**

Figure 3.9: (A) The empty, digested pET-22b(+) and pET-28b(+) vectors (Lanes 2 and 3 respectively), and the MassRuler™ DNA ladder (Lane 1). (B) The ABC transporter, peptide-binding gene of ± 1.9 kb, inserted into pET-22b(+) of ± 5.5 kb (Lanes 2 - 11) and inserted into pET-28b(+) of ± 5.5 kb (Lanes 13 - 22) and the MassRuler™ DNA ladder (Lanes 1 and 12)…...**77**

Figure 3.10: Sequence alignments of the ABC transporter, peptide-binding gene from *T. scotoductus* SA-01 and clone 9 in pET-28b(+), showing 100% identity……**79**

Figure 3.11: Overexpression of the ABC transporter, peptide-binding protein of ± 70 kDa. Lane 1 represents the Precision Plus Protein™ Standard. Lanes 2 and 6 are the negative control's 4 hours of pET-22b(+) and pET-28b(+) respectively. Lanes 3 – 5 are the overexpressed clone 7 in pET-22b(+) 0 hours; 2 hours and 4 hours respectively. Lanes 7 – 9 are the overexpressed clone 9 in pET-28b(+) 0 hours; 2 hours and 4 hours respectively……**80**

Figure 3.12: Purification of clone 7 in pET-22b(+), with the Sephacryl S200HR (Gel-filtration) column. (A) Elution profile obtained, showing the protein eluted between ± 150 and 200 ml [A_{280} (▬); Conductivity (▬)]. (B) SDS-PAGE with lane 1 representing the Precision Plus Protein™ Standard and lanes 2 – 10 the fractions selected from the elution profile to determine which fractions contained the ± 70 kDa protein. (C) Activity determinations with tube 1 representing the blank, containing no protein and showing a black colour and tubes 2 – 7 are the fractions in B (lanes 2 – 7), showing a pink/purple colour, which proved that the protein has gold reduction activity……**81**

Figure 3.13: Purification of clone 9 in pET-28b(+), with the Nickel NTA (HisTrapFF) column. (A) Elution profile obtained, showing the protein eluted between ± 200 and 220 ml [A_{280} (▬); Conductivity (▬)]. (B) SDS-PAGE with lane 1 representing the Precision Plus Protein™ Standard and lanes 2 – 5 the fractions selected from the elution profile to determine which fractions contained the ± 70 kDa protein. (C) Activity determinations with tube 1 representing the blank, containing no protein and showing a black colour and tubes 2 – 5 are the fractions in B (lanes 2 – 5), showing a pink/purple

colour, which proved that the protein has gold reduction activity……..**83**

Figure 3.14: Purification of clone 9 in pET-28b(+), with the Sephacryl S200HR (Gel-filtration) column. (A) Elution profile obtained, showing the protein eluted between ± 150 and 200 ml [A_{280} (▬); Conductivity (▬)]. (B) SDS-PAGE with lane 1 representing the Precision Plus Protein™ Standard and lanes 2 – 10 the fractions selected from the elution profile to determine which fractions contained the ± 70 kDa protein. (C) Activity determinations with tube 1 representing the blank, containing no protein and showing a blackish colour and tubes 2 – 6 are the fractions in B (lanes 6 – 10), showing a pink/purple colour, which proved that the protein has gold reduction activity……..**84**

Figure 3.15: The different colours obtained through the gold reduction assay at varying methyl viologen concentrations, indicating gold nanoparticle formation. The odd numbers (1 – 9) indicate protein reactions for 0 µM; 1.5 µM; 2.5 µM; 3.5 µM and 4.5 µM respectively and the even numbers (2 – 10) the corresponding blank reactions……**86**

Figure 3.16: UV-Vis absorption spectra of the surface plasmon resonance recorded for the different methyl viologen concentrations, indicating gold nanoparticle production through a change in the absorbance around 540 - 560 nm. (A) The protein reactions and (B) the corresponding blank reactions. [0 µM (▬); 1.5 µM (▬); 2.5 µM (▬); 3.5 µM (▬); 4.5 µM (▬)]……...**87**

Figure 3.17: TEM micrographs for the different methyl viologen concentrations, indicating the shapes, sizes and amounts of gold nanoparticles obtained. All scale bars are equal to 1000 nm……...**88**

Figure 3.18: EDX spectrum recorded for the nanoparticles produced at different methyl viologen concentrations, showing a typical pattern for all the samples and indicates that the nanoparticles are gold……...**88**

Figure 3.19: Methyl viologen (MV^{2+}) either reacts with sodium dithionite *via* an ion exchange reaction, to form MV^0, in reaction 1 or it can accept electrons from sodium dithionite to form the free radical ion ($MV^{\bullet+}$), in reaction 2..**89**

Figure 3.20: The different colours obtained through the gold reduction assay at varying sodium dithionite concentrations, indicating gold nanoparticle formation. The odd numbers (1 – 13) indicate protein reactions for 0 µM; 1 µM; 2 µM; 3 µM; 4 µM; 5 µM and 6 µM respectively and the even numbers (2 – 14) the corresponding blank reactions……...**91**

Figure 3.21: UV-Vis absorption spectra of the surface plasmon resonance recorded for the different sodium dithionite concentrations, indicating gold nanoparticle production through a change in the absorbance around 540 - 560 nm. (A) The protein reactions and (B) the corresponding blank reactions. [0 µM ( ); 1 µM ( ); 2 µM ( ); 3 µM ( ); 4 µM ( ); 5 µM ( ); 6 µM ( )]……**91**

Figure 3.22: TEM micrographs for the different sodium dithionite concentrations, indicating the shapes, sizes and amounts of gold nanoparticles obtained. All scale bars are equal to 1000 nm……...**92**

Figure 3.23: EDX spectrum recorded for the nanoparticles produced at different sodium dithionite concentrations, showing a typical pattern for all the samples and indicates that the nanoparticles are gold……...**93**

Figure 3.24: The different colours obtained through the gold reduction assay at varying protein concentrations, indicating gold nanoparticle formation. The odd numbers (1 – 11) indicate protein reactions for 0 µg.ml^{-1}; 10 µg.ml^{-1}; 20 µg.ml^{-1}; 30 µg.ml^{-1}; 40 µg.ml^{-1} and 50 µg.ml^{-1} respectively and the even numbers (2 – 12) the corresponding blank reactions……...**94**

Figure 3.25: UV-Vis absorption spectra of the surface plasmon resonance recorded for the different protein concentrations, indicating gold nanoparticle production through a change in the absorbance around 540 - 560 nm. (A) The protein reactions and (B) the corresponding blank reactions. [0 µg.ml^{-1} ( ); 10 µg.ml^{-1} ( ); 20 µg.ml^{-1} ( ); 30 µg.ml^{-1} ( ); 40 µg.ml^{-1} ( ); 50 µg.ml^{-1} ( )]……**95**

Figure 3.26: TEM micrographs for the different protein concentrations, indicating the shapes, sizes and amounts of gold nanoparticles obtained. All scale bars are equal to 1000 nm……**96**

Figure 3.27: EDX spectrum recorded for the nanoparticles produced at different protein concentrations, showing a typical pattern for all the samples and indicates that the nanoparticles are gold……...**96**

Figure 3.28: The different colours obtained through the gold reduction assay with denatured protein and various electron donors, indicating gold nanoparticle formation. The odd numbers (1 – 5) indicate protein reactions for sodium dithionite; dithiothreitol and β-mercaptoethanol respectively and the even numbers (2 – 6) the corresponding blank reactions……..**97**

Figure 3.29: UV-Vis absorption spectra of the surface plasmon resonance recorded for the denatured protein and various electron donors, indicating insignificant nanoparticle production through no change in the absorbance around 540 - 560 nm. (A) Protein reactions with the different electron donors and (B) the corresponding blank reactions. [Sodium dithionite (▬); Dithiothreitol (▬); β-mercaptoethanol (▬)]……...**98**

Figure 3.30: TEM micrographs of gold nanoparticles for the denatured protein with different electron donors, indicating the shapes, sizes and amounts of gold nanoparticles obtained. All scale bars are equal to 1000 nm……...**99**

Figure 3.31: The different colours obtained through the gold reduction assay at various exposure times, indicating gold nanoparticle formation. The odd numbers (1 – 19) indicate protein reactions for 30 minutes; 1 hour; 2 hours; 4 hours; 6 hours; 8 hours; 10 hours; 12 hours; 24 hours and 48 hours respectively and the even numbers (2 – 20) the corresponding blank reactions……**100**

Figure 3.32: UV-Vis absorption spectra of the surface plasmon resonance recorded for the different exposure times, indicating gold nanoparticle production through a change in the absorbance around 540 - 560 nm. (A) The protein reactions and (B) the corresponding blank reactions. [30 minutes (▬); 1 hour (▬); 2 hours (▬); 4 hours (▬); 6 hours (▬); 8 hours (▬); 10 hours (▬); 12 hours (▪▪▪); 24 hours (▪▪▪); 48 hours (▪▪▪)]……**101**

Figure 3.33: TEM micrographs for the different exposure times, indicating the shapes, sizes and amounts of gold nanoparticles obtained. All scale bars are equal to 1000 nm……**102**

Figure 3.34: EDX spectrum recorded for the nanoparticles produced at different exposure times, showing a typical pattern for all the samples and indicates that the nanoparticles are gold……**103**

Figure 3.35: The different colours obtained through the gold reduction assay at varying $HAuCl_4$ concentrations, indicating gold nanoparticle formation. The odd numbers (1 – 13) indicate protein reactions for 0 mM; 0.5 mM; 1.0 mM; 2.0 mM; 5.0 mM; 7.5 mM and 10 mM respectively and the even numbers (2 – 14) the corresponding blank reactions……**104**

Figure 3.36: UV-Vis absorption spectra of the surface plasmon resonance recorded for the different $HAuCl_4$ concentrations, indicating gold nanoparticle production through a change in the absorbance around 540 - 560 nm. (A) The protein reactions and (B) the corresponding blank reactions. [0 mM ( ); 0.5 mM ( ); 1.0 mM ( ); 2.0 mM ( ); 5.0 mM ( ); 7.5 mM ( ); 10 mM ( )]……..**104**

Figure 3.37: TEM micrographs for the different $HAuCl_4$ concentrations, indicating the shapes, sizes and amounts of gold nanoparticles obtained. Scale bars in 0 mM – 5.0 mM are equal to 1000 nm and in 10.0 mM the scale bar is equal to 20 mm……**106**

Figure 3.38: EDX spectrum recorded for the nanoparticles produced at different $HAuCl_4$ concentrations, showing a typical pattern for all the samples and indicates that the nanoparticles are gold……**106**

Figure 3.39: The different colours obtained through the gold reduction assay at varying temperatures, indicating gold nanoparticle formation. The odd numbers (1 – 11) indicate protein reactions for 30ºC; 37ºC; 42ºC; 55ºC; 65ºC and 85ºC respectively and the even numbers (2 – 12) the corresponding blank reactions……**108**

Figure 3.40: UV-Vis absorption spectra of the surface plasmon resonance recorded for the different temperatures, indicating gold nanoparticle production through a change in the absorbance around 540 - 550 nm. (A) The protein reactions and (B) the corresponding blank reactions. [30ºC ( ); 37ºC ( ); 42ºC ( ); 55ºC ( ); 65ºC ( ); 85ºC ( )]……**109**

Figure 3.41: TEM micrographs for the different temperatures, indicating the shapes, sizes and amounts of gold nanoparticles obtained. All scale bars are equal to 1000 nm……**111**

Figure 3.42: EDX spectrum recorded for the nanoparticles produced at different temperatures, showing a typical pattern for all the samples and indicates that the nanoparticles are gold……..**111**

Figure 3.43: The different colours obtained through the gold reduction assay at varying pH values, indicating gold nanoparticle formation. The odd numbers (1 – 7) indicate protein reactions for pH 3.6; 5.5; 7.5 and 9.0 respectively and the even numbers (2 – 8) the corresponding blank reactions……..**113**

Figure 3.44: UV-Vis absorption spectra of the surface plasmon resonance recorded for the different pH values, indicating gold nanoparticle production through a change in the absorbance around 540 - 550 nm. (A) The protein reactions and (B) the corresponding blank reactions. [pH 3.6 ( ); pH 5.5 ( ); pH 7.5 ( ); pH 9.0 ( )]……...**113**

Figure 3.45: TEM micrographs for the different pH values, indicating the shapes, sizes and amounts of gold nanoparticles obtained. All scale bars are equal to 1000 nm……**115**

Figure 3.46: (A) TEM micrograph of a gold nanoparticle with (B) corresponding selected-area electron micro-diffraction pattern for pH 9.0. The scale bar in A is equal to 230 nm……...**115**

Figure 3.47: EDX spectrum recorded for the nanoparticles produced at different pH values, showing a typical pattern for all the samples and indicates that the nanoparticles are gold……**116**

Figure 3.48: Size distribution for the gold nanoparticles obtained at (A) pH 7.5 and (B) pH 9.0……**119**

Figure 3.49: SEM micrographs for pH 7.5, indicating different shapes and sizes of gold nanoparticles obtained. Scale bars in A and B are equal to 500 nm and 200 nm, respectively……...**119**

Figure 3.50: (A and C) SEM micrographs of gold nanoparticles with (B and D) corresponding selected-area Auger spectra, indicating the gold from the nanoparticles. [Area 1 ( ); Area 2 ( ); Area 3 ( )]. Scale bars in A and C are equal to 500 nm and 200 nm, respectively……..**120**

Figure 3.51: Elemental map tests done with ten frames, indicating the presence and distribution of the gold from the nanoparticles……**121**

Figure 3.52: The different colours obtained through the gold reduction assay with various electron donors, indicating gold nanoparticle formation. The odd numbers (1 – 5) indicate protein reactions for sodium dithionite; dithiothreitol and β-mercaptoethanol respectively and the even numbers (2 – 6) the corresponding blank reactions……...**122**

Figure 3.53: UV-Vis absorption spectra of the surface plasmon resonance recorded for the different electron donors, indicating gold nanoparticle production through a change in the absorbance around 540 - 580 nm. (A) The protein reactions and (B) the corresponding blank reactions. [Sodium dithionite ( ); Dithiothreitol ( ); β-mercaptoethanol ( )]……**123**

Figure 3.54: (A) TEM micrograph of a gold nanoparticle with (B) corresponding selected-area electron micro-diffraction pattern for sodium dithionite as electron donor. (C and D) TEM micrographs for dithiothreitol and (E and F) TEM micrographs for β-mercaptoethanol, indicating the shapes, sizes and amounts of gold nanoparticles obtained. The scale bars in A, C, D, E and F are equal to 430 nm; 580 nm; 580 nm; 910 nm and 300 nm respectively……..**124**

Figure 3.55: EDX spectrum recorded for the nanoparticles produced with different electron donors, showing a typical pattern for all the samples and indicates that the nanoparticles are gold……**125**

Figure 3.56: Size distribution for the gold nanoparticles obtained with sodium dithionite as the electron donor……..**127**

Figure 3.57: No significant change in colour obtained through the gold reduction assay with iodoacetic acid and the various electron donors, indicating negative nanoparticle formation. The odd numbers (1 – 5) indicate protein reactions for sodium dithionite; dithiothreitol and β-mercaptoethanol respectively and the even numbers (2 – 6) the corresponding blank reactions……**128**

Figure 3.58: UV-Vis absorption spectra of the surface plasmon resonance recorded for the iodoacetic acid with the various electron donors, indicating no nanoparticle production through no change in the absorbance around 540 - 560 nm. (A) Protein reactions with the different electron donors and (B) the corresponding blank reactions. [Sodium dithionite (▬); Dithiothreitol (▬); β-mercaptoethanol (▬)]……**128**

Figure 3.59: TEM micrographs of gold nanoparticles for iodoacetic acid with the different electron donors, no formation of gold nanoparticles. All scale bars are equal to 1000 nm……**129**

▬ · · ▬ · · ▬ · · ▬ · · ▬ · · ▬ · · ▬ · · ▬

Figure 4.1: Vector map of pWUR, indicating the bleomycin resistance gene, the ori*Eco* origin for replication in *E. coli*, minimal replicon (RepA) for replication in *Thermus* sp. and the multiple cloning site under the PslpA and Plac promoters, showing the *Eco*RI and *Xba*I sites where the gene was inserted……**140**

Figure 4.2: Vector map of pMK184, indicating the kanamycin resistance gene, the ori*Eco* origin for replication in *E. coli*, the a-*lac*Z coding site, minimal replicon (RepA) for replication in *Thermus* sp. and the multiple cloning site under the PslpA and Plac promoters, showing the *Eco*RI and *Xba*I sites where the gene was inserted……...**141**

Figure 4.3: (A) Genomic DNA isolated from *T. scotoductus* SA-01 (Lane 2) with the GeneRuler™ DNA ladder (Lane 1). (B) The amplified ABC transporter, peptide-binding gene of ± 1.9 kb for construct 1 (Lane 3); construct 2 (Lane 4) and construct 3 (Lane 5); negative control (Lane 2) and the MassRuler™ DNA ladder (Lane 1)……...**153**

Figure 4.4: The amplified ABC transporter, peptide-binding gene of ± 1.9 kb, inserted into the pGEM®-T Easy Vector system of ± 3 kb, for (A) Construct 1 (Lanes 2 - 11) and the GeneRuler™ DNA ladder (Lane 1). (B) Construct 2 (Lanes 2 - 11) and the GeneRuler™ DNA ladder (Lane 1). (C) Construct 3 (Lanes 2 - 11) and the GeneRuler™ DNA ladder (Lane 1).**155**

Figure 4.5: (A) The empty, digested pET-22b(+) and pET-28b(+) vectors (Lanes 2 and 3 respectively), and the MassRuler™ DNA ladder (Lane 1). (B) The ABC transporter, peptide-binding gene of ± 1.9 kb, inserted into the pET vectors of ± 5.5 kb. Clone 1, inserted into pET-22b(+) (Lanes 2 - 11); clone 5, inserted into pET-28b(+) (Lanes 12 – 19, 21 and 22); clone 3, inserted into pET-22b(+) (Lanes 23 – 32) and the GeneRuler™ DNA ladder (Lanes 1 and 20)……**156**

Figure 4.6: Sequence alignments of the ABC transporter, peptide-binding gene from *T. scotoductus* SA-01 and clone 6 in pET-22b(+) (Construct 1), showing 100% identity……**158**

Figure 4.7: (A) The empty, digested pWUR and pMK184 vectors (Lanes 2 and 3 respectively), and the GeneRuler™ DNA ladder (Lane 1). (B) The ABC transporter, peptide-binding gene of ± 1.9 kb, inserted into pWUR of ± 4.5 kb. Construct 1 (Lanes 2 - 11); construct 2 (Lanes 12 - 21); construct 3 (Lanes 22 - 31) and the GeneRuler™ DNA ladder (Lane 1). (C) The ABC transporter, peptide-binding gene of ± 1.9 kb, inserted into pMK184 of ± 5 kb. Construct 1 (Lanes 2 - 11); construct 2 (Lanes 12 - 21); construct 3 (Lanes 22 - 31) and the GeneRuler™ DNA ladder (Lane 1)……**160**

Figure 4.8: Sequence alignments of the ABC transporter, peptide-binding gene from *T. scotoductus* SA-01 and clone 2 in pWUR (Construct 2), showing 100% identity……...**162**

Figure 4.9: Expression of the ABC transporter, peptide-binding protein of ± 70 kDa. Lane 1 represents the Precision Plus Protein™ Standard. Lanes 2 and 6 are the negative controls of pWUR and pMK184 respectively. Lanes 3 – 5 are the expressed clone 10 (Construct 1); clone 2 (Construct 2) and clone 7 (Construct 3) in pWUR respectively. Lanes 7 and 8 are the expressed clone 4 (Construct 2) and clone 4 (Construct 3) in pMK184 respectively……..**163**

Figure 4.10: Elution profiles obtained after purification with the Nickel NTA (HisTrapFF) column, showing the protein eluted between ± 170 and 200 ml [A_{280} (—); Conductivity (—)]. (A) Clone 10 (Construct 1) in pWUR. (B) Clone 2 (Construct 2) in pWUR. (C) Clone 7 (Construct 3) in pWUR. (D) Clone 4 (Construct 2) in pMK184. (E) Clone 4 (Construct 3) in pMK184……**164**

Figure 4.11: SDS-PAGE with Coomassie blue staining, for the fractions selected from the elution profile to determine which fractions contained the ± 70 kDa protein. (A) The Precision Plus Protein™ Standard (Lane 1); pWUR negative control (Lanes 2 – 5) and Clone 10 (Construct 1) in pWUR (Lanes 6 – 9). (B) The Precision Plus Protein™ Standard (Lane 1); Clone 2 (Construct 2) in pWUR (Lanes 2 – 5) and Clone 7 (Construct 3) in pWUR (Lanes 6 – 9). (C) The Precision Plus Protein™ Standard (Lane 1); Clone 4 (Construct 2) in pMK184 (Lanes 2 – 5) and Clone 4 (Construct 3) in pMK184 (Lanes 6 – 9)……**165**

Figure 4.12: SDS-PAGE with Silver staining, for the fractions selected from the elution profile to determine which fractions contained the ± 70 kDa protein. (A) The Precision Plus Protein™ Standard (Lane 1); pWUR negative control (Lanes 2 – 5) and Clone 10 (Construct 1) in pWUR (Lanes 6 – 9). (B) The Precision Plus Protein™ Standard (Lane 1); Clone 2 (Construct 2) in pWUR (Lanes 2 – 5) and Clone 7 (Construct 3) in pWUR (Lanes 6 – 9). (C) The Precision Plus Protein™ Standard (Lane 1); Clone 4 (Construct 2) in pMK184 (Lanes 2 – 5) and Clone 4 (Construct 3) in pMK184 (Lanes 6 – 9)……**166**

Figure 4.13: Western blot with His-Tag detection, confirming the presence of the protein of ± 70 kDa, for Clone 2 (Construct 2) in pWUR and Clone 4 (Construct 2) in pMK184 (Lanes 3 and 5 respectively). The PageRuler™ Prestained Protein Ladder can be seen in lane 1, the pWUR negative control in lane 4 and a positive control of ± 40 kDa in lane 2……..**167**

Figure 4.14: Activity determinations done at (A) 65ºC and (B) 85ºC, with tube 6 representing the blank, containing no protein and showing no activity and tubes 1 – 5 are the pooled fractions for Clone 10 (Construct 1) in pWUR; Clone 2 (Construct 2) in pWUR; Clone 7 (Construct 3) in pWUR; Clone 4 (Construct 2) in pMK184 and Clone 4 (Construct 3) in pMK184, respectively, showing a pink/purple colour, which proved that the protein has gold reduction activity……**168**

Figure 4.15: The different colours obtained through the gold reduction assay with or without sodium dithionite and methyl viologen, indicating gold nanoparticle formation at 65ºC and 85ºC. The odd numbers (1 and 3; 5 and 6; 9 and 10) indicate protein reactions for both components, only dithionite and only methyl viologen respectively and the even numbers (2 and 4; 6 and 8; 10 and 12) the corresponding blank reactions……**170**

Figure 4.16: UV-Vis absorption spectra of the surface plasmon resonance recorded for with or without sodium dithionite and methyl viologen at 85ºC, indicating gold nanoparticle production through a change in the absorbance around 540 - 570 nm. (A) The protein reactions and (B) the corresponding blank reactions. [Sodium dithionite and methyl viologen (▬); Sodium dithionite (▬); Methyl viologen (▬)]……**171**

Figure 4.17: (A, C and D) TEM micrographs for the different assay components at 85ºC, indicating the shapes, sizes and amounts of gold nanoparticles obtained with (B) corresponding selected-area electron micro-diffraction pattern for sodium dithionite and methyl viologen. Scale bars in A, C and D are equal to 910 nm; 910 nm and 580 nm respectively……**172**

Figure 4.18: EDX spectrum recorded for the nanoparticles produced with the different assay components at 85ºC, showing a typical pattern for all the samples and indicates that the nanoparticles are gold……**173**

Figure 4.19: The different colours obtained through the gold reduction assay with denatured protein and various electron donors, indicating gold nanoparticle formation for 65ºC (1 – 6) and 85ºC (7 – 12). The odd numbers (1 – 5 and 7 - 11) indicate protein reactions for sodium dithionite; dithiothreitol and β-mercaptoethanol respectively and the even numbers (2 – 6 and 8 - 12) the corresponding blank reactions……...**174**

Figure 4.20: UV-Vis absorption spectra of the surface plasmon resonance recorded for the denatured protein and various electron donors at 85ºC, indicating insignificant nanoparticle production through no change in the absorbance around 540 - 560 nm. (A) The protein reactions and (B) the corresponding blank reactions. [Sodium dithionite (▬); Dithiothreitol (▬); β-mercaptoethanol (▬)]……..**175**

Figure 4.21: The different colours obtained through the gold reduction assay at varying $HAuCl_4$ concentrations, indicating gold nanoparticle formation for 65ºC (1 – 14) and 85ºC (15 – 28) respectively. The odd numbers (1 – 13 and 15 - 27) indicate protein reactions for 0 mM; 0.5 mM; 1.0 mM; 2.0 mM; 5.0 mM; 7.5 mM and 10 mM respectively and the even numbers (2 – 14 and 16 - 28) the corresponding blank reactions……**176**

Figure 4.22: UV-Vis absorption spectra of the surface plasmon resonance recorded for the different $HAuCl_4$ concentrations at 85ºC, indicating gold nanoparticle production through a change in the absorbance around 540 - 550 nm. (A) The protein reactions and (B) the corresponding blank reactions. [0 mM (▬); 0.5 mM (▬); 1.0 mM (▬); 2.0 mM (▬); 5.0 mM (▬); 7.5 mM (▬); 10 mM (▬)]……..**177**

Figure 4.23: (A, B and C) TEM micrographs for the different $HAuCl_4$ concentrations at 85ºC, indicating the shapes, sizes and amounts of gold nanoparticles obtained with (D) corresponding selected-area electron ring pattern for 2.0 mM. Scale bars in A, B and C are equal to 300 nm; 580 nm and 730 nm respectively……**178**

Figure 4.24: EDX spectrum recorded for the nanoparticles produced at different $HAuCl_4$ concentrations at 85ºC, showing a typical pattern for all the samples and indicates that the nanoparticles are gold……**179**

Figure 4.25: The different colours obtained through the gold reduction assay at varying temperatures, indicating gold nanoparticle formation. The odd numbers (1 – 11) indicate protein reactions for 30ºC; 37ºC; 42ºC; 55ºC; 65ºC and 85ºC respectively and the even numbers (2 – 12) the corresponding blank reactions……**180**

Figure 4.26: UV-Vis absorption spectra of the surface plasmon resonance recorded for the different temperatures, indicating gold nanoparticle production through a change in the absorbance around 540 - 560 nm. (A) The protein reactions and (B) the corresponding blank reactions. [30ºC (▬); 37ºC (▬); 42ºC (▬); 55ºC (▬); 65ºC (▬); 85ºC (▬)]……**180**

Figure 4.27: (A and C) TEM micrographs for gold nanoparticles with (B and D) corresponding selected-area electron micro-diffraction and ring pattern for 65ºC and 85ºC respectively, indicating the shapes, sizes and amounts of gold nanoparticles obtained. Scale bars in A and C are equal to 800 nm and 1000 nm respectively……..**182**

Figure 4.28: EDX spectrum recorded for the nanoparticles produced at 65ºC and 85ºC, showing a typical pattern for all the samples and indicates that the nanoparticles are gold……**182**

Figure 4.29: The different colours obtained through the gold reduction assay at varying protein concentrations, indicating gold nanoparticle formation for 65ºC (1 – 8) and 85ºC (9 – 16) respectively. The odd numbers (1 – 7 and 9 - 15) indicate protein reactions for pH 3.6; 5.5; 7.5 and 9.0 respectively and the even numbers (2 – 8 and 10 - 16) the corresponding blank reactions...**184**

Figure 4.30: UV-Vis absorption spectra of the surface plasmon resonance recorded for the different pH values at 85ºC, indicating gold nanoparticle production through a change in the absorbance around 550 - 650 nm. (A) The protein reactions and (B) the corresponding blank reactions. [pH 3.6 (▬); pH 5.5 (▬); pH 7.5 (▬); pH 9.0 (▬)]……..**185**

Figure 4.31: TEM micrographs for the different pH values at 85ºC, indicating the shapes, sizes and amounts of gold nanoparticles obtained. Scale bars are equal to 1000 nm; 910 nm; 430 nm and 900 nm respectively……..**186**

Figure 4.32: (A) TEM micrograph of gold nanoparticles with (B) corresponding selected-area electron micro-diffraction pattern for pH 9.0 at 85ºC. The scale bar in A is equal to 900 nm……**186**

Figure 4.33: EDX spectrum recorded for the nanoparticles produced at different pH values at 85ºC, showing a typical pattern for all the samples and indicates that the nanoparticles are gold……..**187**

Figure 4.34: The different colours obtained through the gold reduction assay with various electron donors, indicating gold nanoparticle formation for 65ºC (1 – 6) and 85ºC (7 – 12) respectively. The odd numbers (1 – 5 and 7 - 11) indicate protein reactions for sodium dithionite; dithiothreitol and β-mercaptoethanol respectively and the even numbers (2 – 6 and 8 - 12) the corresponding blank reactions……**188**

Figure 4.35: UV-Vis absorption spectra of the surface plasmon resonance recorded for the different electron donors at 85ºC, indicating gold nanoparticle production through a change in the absorbance around 550 - 600 nm. (A) The protein reactions and (B) the corresponding blank reactions. [Sodium dithionite (▬); Dithiothreitol (▬); β-mercaptoethanol (▬)]……**188**

Figure 4.36: (A) TEM micrograph of gold nanoparticles with (B) corresponding selected-area electron micro-diffraction pattern for sodium dithionite as electron donor at 85ºC. (C and D) TEM micrographs for dithiothreitol and β-mercaptoethanol at 85ºC respectively, indicating the shapes, sizes and amounts of gold nanoparticles obtained. The scale bars in A, C and D are equal to 910 nm; 910 nm and 580 nm respectively……**190**

Figure 4.37: EDX spectrum recorded for the nanoparticles produced with the different electron donors at 85ºC, showing a typical pattern for all the samples and indicates that the nanoparticles are gold……**190**

Figure 4.38: A slight change in colour obtained through the gold reduction assay with iodoacetic acid and the various electron donors, indicating ineffective nanoparticle formation for 65ºC (1 – 6) and 85ºC (7 – 12). The odd numbers (1 – 5 and 7 - 11) indicate protein reactions for sodium dithionite; dithiothreitol and β-mercaptoethanol respectively and the even numbers (2 – 6 and 8 - 12) the corresponding blank reactions……...**191**

Figure 4.39: UV-Vis absorption spectra of the surface plasmon resonance recorded for the iodoacetic acid with the various electron donors at 85ºC, indicating ineffective nanoparticle production through small changes in the absorbance around 540 - 560 nm. (A) The protein reactions and (B) the corresponding blank reactions. [Sodium dithionite (▬); Dithiothreitol (▬); β-mercaptoethanol (▬)]……..**192**

LIST OF TABLES

Table 1.1: Physical properties for materials at the nanoscale, that differs from the macroscale (Taken from Bhat, 2003)……...**4**

Table 1.2: Different parameters used for classification of nanoparticles (Taken from Luther, 2004)….....**19**

Table 1.3: Several of the microorganisms used in the synthesis of nanoparticles and the different types of metal nanoparticles which they can produce (Adapted from Mandal *et al.*, 2006)……**27**

Table 1.4: Several applications in which nanomaterials are being used (Adapted from Bhat, 2003; Luther, 2004)……...**29**

Table 3.1: Bacterial strains and plasmids used for cloning and expression in a mesophilic host……..**53**

Table 3.2: Oligonucleotide primers used for PCR amplification and sequencing. Underlined sequences indicate the introduced restriction sites for *Nde*I and *Eco*RI in primers 1 and 2 respectively……**57**

Table 3.3: Constructs obtained when using a combination of primers 1 and 2 with the pET-22b(+) and pET-28b(+) vectors respectively…….**58**

Table 3.4: The average size percentage of the nanoparticles present at (A) pH 7.5 and (B) pH 9.0…….**117**

Table 3.5: Size distribution of the nanoparticles present at (A) pH 7.5 and (B) pH 9.0……..**118**

Table 3.6: The average size percentage of the nanoparticles present with sodium dithionite as the electron donor…….**126**

Table 3.7: Size distribution of the nanoparticles present with sodium dithionite as the electron donor……..**126**

Table 4.1: Bacterial strains and plasmids used for cloning and expression in a thermophilic host…….**139**

Table 4.2: Oligonucleotide primers used for PCR amplification and sequencing. Underlined sequences indicate the introduced restriction sites for *Nde*I in primers 1 and 5 and *Eco*RI in primers 2 and 6 respectively…….**143**

Table 4.3: Constructs obtained when using a combination of primers 1, 2, 5 and 6 with the pET-22b(+) and pET-28b(+) vectors respectively.....**143**

Table 4.4: Constructs used for downstream experiments, after ligation in the pET-22b(+) and pET-28b(+) vectors respectively……..**145**

CHAPTER 1

LITERATURE REVIEW

1.1 NANOTECHNOLOGY AND NANOMATERIALS

Nanotechnology has become a field of increasing importance and a highly promising discipline in science, engineering and technology (Bhat, 2003; Sargent, 2010). There are several definitions describing nanotechnology, but ultimately it can be defined as the study, synthesis, design, manipulation, properties and applications of functional materials, devices and systems through the control of matter at the nanometre scale (Bhat, 2003; Scott *et al.,* 2008). To put this into perspective; the size of one hydrogen atom is roughly 0.1 nanometre, a virus approximately 100 nanometres and a red blood cell about 10 000 nanometres (Figure 1.1) (Bhat, 2003). For materials to be considered as "nano", is has to be between 1 and 1000 nanometres, or at least have one distinctive measurement (height, length or depth) in the nanometre range (Bhat, 2003; Karn & Bergeson, 2009). These materials can consist of groups of single elements, e.g. metals; groups of compounds, e.g. metal oxides, tubes wires and branching structures, or an endless amount of combinations. They can be regular and geometric such as crystals or irregular such as foam (Bhat, 2003; Karn & Bergeson, 2009).

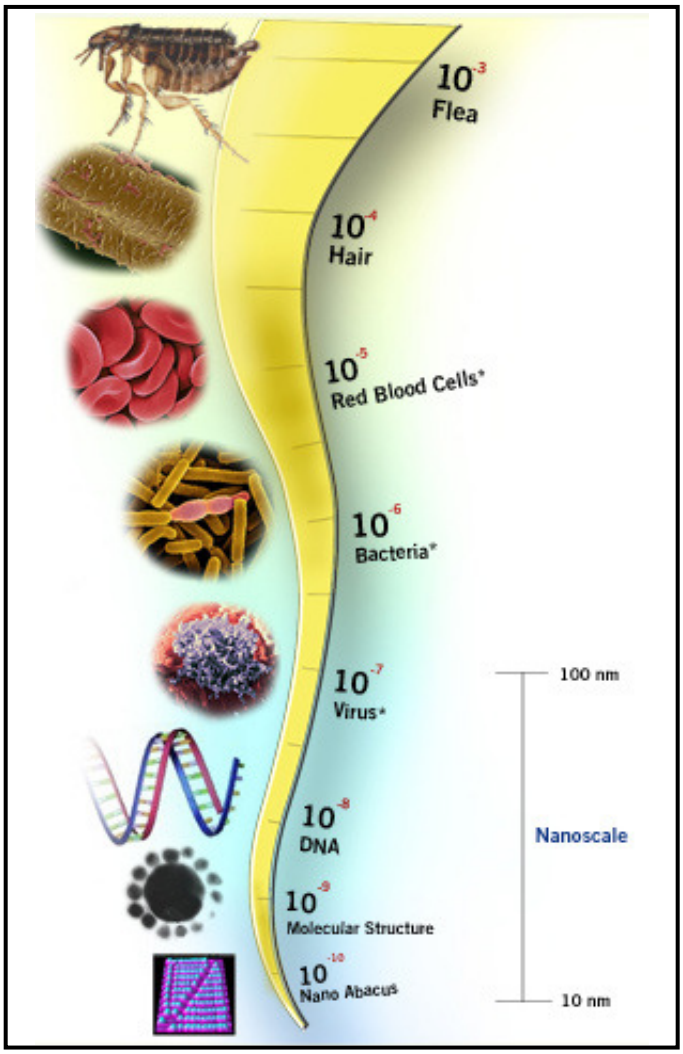

Figure 1.1: Nanoscale objects have at least one measurement (height, length, depth) between 1 and 100 nanometre (Taken from http://www.discovernano.northwestern.edu).

The field of nanotechnology is relatively extensive and is not only about nano-sizing the identified and existing materials or devices, but to study and develop new and unknown matter and systems with novel and significantly enhanced physical, chemical and biological properties that can be seen within the nanometre range, but not be observed in bulk materials (Bhat, 2003; Gardea-Torresdey *et al.*, 2003). Research in nanotechnology has been made possible due to the development and improvement of instruments for work at these levels, such as the development of the electron microscope in 1931, the use of individual atoms in 1989 and the single molecule organic switch in 1999. To ensure fast growing research in nanotechnology, even better and

newer instruments and techniques are being developed for the function of working with nanomaterials (Bhat, 2003).

Nanotechnology are generally seen as having enormous potential with guaranteed impacts in various disciplines, such as healthcare, IT and energy storage and has generated great interest due to its expected impact on the energy, chemical, electronics and space industries and drug and gene delivery (Gardea-Torresdey *et al.*, 2003; Mandal *et al.*, 2006). Nanomaterials are usually designed to be unique, but all these different nanotechnologies have one thing in common - the small dimensions that they function with, making use of the fact that, at this scale, materials can behave much differently from when they are in larger form. For example, nanomaterials can be stronger or lighter, or conduct heat or electricity in a different way. They can even change colour; particles of gold can appear red, blue, green or gold, depending on their size (Karn & Bergeson, 2009).

Nanomaterials show different physical and chemical properties (Table 1.1) which are very sensitive towards size and shape, but as materials become smaller, it is more difficult to control these parameters; however these properties become much more dependant on size and shape. In addition to the physical and chemical methods, biological procedures, using for instance various types of microorganisms, have the ability to produce nanoparticles that are of exceptional importance due to their effectiveness and flexibility. (Kasuya *et al.*, 2002; Krumov *et al.*, 2009).

Table 1.1: Physical properties for materials at the nanoscale, that differs from the macroscale (Taken from Bhat, 2003).

• Not only miniaturization but changes in physical properties
• Laws of quantum physics
• Surface behaviour dominates bulk material behaviour
• Metals become harder
• Ceramics become softer
• Composites and alloys of a whole variety possible
• Thin polymers less permeable
• Stronger, more heat resistant, transparent
• Increased chemical resistance, reduced weight
• Different interactions with light/other radiation
• New electrical properties
• Novel biological properties

These special properties are already used in making computer chips, CDs, mobile phones, etc. However, researchers are progressively finding out more about the nanoscale world and aim to use nanotechnologies to create new devices that are faster, lighter, stronger or more efficient and that operate at the scale of atoms and molecules, but have applications in the existent world. This then may effectively become the way of living and producing products through the advantage of science and technology (Kasuya *et al.*, 2002; Krumov *et al.*, 2009).

1.2 METAL NANOPARTICLES

The synthesis of metal nanoparticles is of interest due to their unique, size-dependant, physical, chemical, optical, electronic and magnetic properties. They have been found to be significant in many different applications such as catalysis, biosensing, biolabelling, nonlinear optical devices, optical recording media, electronics, photography, photonics, information storage, surface enhanced Raman scattering (SERS) and controlled drug delivery (Sun & Xia, 2002; Inasawa *et al.*, 2003; Miyazaki *et al.*, 2003; Swami *et al.*, 2003; Lengke *et al.*, 2006a; Lengke *et al.*, 2006b; Lengke *et al.*, 2007b). Several of the transition metals have been used to produce nanoparticles and in particular, precious

metals like gold, silver and platinum nanoparticles have been studied extensively due to their strong optical absorption in the visible region and their promising behaviour in especially catalysis (Mandal *et al*., 2002; Šlouf *et al*., 2006).

Well-controlled shapes, sizes, composition, crystallinity and solid or hollow structures primarily determine the basic properties of metal nanoparticles that make them so exceptional in these applications. These properties differ significantly from when the metals are used in bulk form. (Sun & Xia, 2002; Inasawa *et al*., 2003; Miyazaki *et al.*, 2003).

1.2.1 Iron, Cobalt, Copper & Nickel

The chemical synthesis of monodisperse noble metal nanoparticles has been achieved with great success, but as far as the synthesis of iron, cobalt, copper and nickel are concerned, much improvement is still needed in the way nanoparticles are being produced with these metals (Masala & Seshadri, 2004; Korbekandi *et al*., 2009).

Cobalt nanoparticles are being synthesized, using the thermal decomposition (200ºC) of dicobaltoctacarbonyl [$Co_2(CO)_8$] with tri-*n*-octylphosphine oxide (TOPO) as a surfactant. However, by using this process, polydisperse nanocrystals will be obtained. The same method can be used for homogeneous synthesis of iron nanoparticles, using iron pentacarbonyl [$Fe(CO)_5$] instead of the $Co_2(CO)_8$ and at higher temperatures (Masala & Seshadri, 2004). There are a few other processes that can be used for the production of monodisperse cobalt nanoparticles, such as the reduction of cobalt chloride or acetates in solution using a superhydride solution, polyalcohols or sodium borohydride ($NaBH_4$), with a stabilizer. The stabilizer is generally a mixture between oleic acid and an alkylphosphine, but can also be tri-*n*-octylphosphine (TOP), tributylamine or hexadecylamine (Masala & Seshadri, 2004).

Compared to silver, platinum and gold, not much work has been done on copper nanoparticles since it is easily oxidized, but methods used for nanoparticle production, may include chemical reduction of copper in solution or the reduction in reverse micelles (Masala & Seshadri, 2004; Kim *et al*., 2006; Pedersen & Wang, 2007). The problem of

using these methods is that the particles produced are irregularly shaped and the size distributions are very broad (Masala & Seshadri, 2004). Monodispersed copper nanoparticles have been produced through thermal decomposition of a copper-oleate complex, having the advantage of dispersibility in organic solvent and reduction stability (Kim *et al*., 2006). Another method for synthesizing copper nanoparticles includes the use of the iron storage protein, apoferritin, sequestering inorganic material and hydroxylate it to produce nanoparticles which are size-controlled. This same protein can also be used for making nickel nanoparticles (Okuda *et al*., 2003). No further reports could be obtained for other biological methods used for the synthesis of these nanoparticles.

As in the case of cobalt, nickel nanoparticles can also be produced by the reduction of metal acetates in solution using polyalcohols or sodium borohydride ($NaBH_4$), with a stabilizer, such as oleic acid, TOP, tributylamine or hexadecylamine (Masala & Seshadri, 2004; Hou *et al*., 2005). Nickel nanoparticles have also been produced successfully, using nickel chloride as the precursor, hydrazine as the reducing agent and palladium as the nucleation agent. When using this method at temperatures higher than 80ºC, high purity nickel will be obtained. At lower temperatures, nickel hydroxide in a precipitate form will also be obtained (Chou & Huang, 2001). Another method for synthesizing nickel nanoparticles includes the use of femtosecond laser ablation in vacuum. This method produces films of nickel nanoparticles with unusual properties in the field of magnetic materials, conducting materials and catalysis (Amoruso *et al*., 2005; Chen *et al*., 2007).

1.2.2 Cadmium, Palladium & Vanadium

Semiconductor cadmium-sulphide (CdS) nanoparticles have been successfully produced, using the fungus *Fusarium oxysporum* by exposure to aqueous cadmium ions (Cd^{2+}) and sulphate (SO_4^{2-}). This method yield technologically significant, exceptionally stable, extracellular CdS nanoparticles in solution (Ahmad *et al*., 2002).

Palladium nanoparticles are generally synthesized by the chemical reduction of metal salt such as a chloride or a halide in solution, with a stabilizer. Other successfully used

reducing agents include citrate, hydrogen, $NaBH_4$, potassium bitartarate, superhydrides, amines and alcohols (Masala & Seshadri, 2004; Lengke *et al.*, 2007b). Nanoparticle production from palladium has also been found to be effective, by the interaction of cyanobacterial biomass from *Plectonema boryanum* UTEX 485 with aqueous palladium(II)chloride [($PdCl_2^0$)]. Pd(0) are being precipitated as crystalline and elongate nanoparticles in solution and as encrusted nanoparticles on the cyanobacterial cells. Palladium nanoparticles can be successfully used as catalyst for *in situ* remediation of trichloroethylene (TCE) and carbon tetrachloride (CT) from contaminated groundwater (Lengke *et al.*, 2007b).

Vanadium is a profuse element and an important resource for several industrial applications, such as vanadium alloys, oxidation catalysis in sulphuric acid manufacturing, automobile catalytic converters, photographic development, textile dyeing, and ceramic colouring. Bacteria, such as *Shewanella oneidensis* have been found to be able to reduce vanadate ion V(V) to vanadyl ion V(IV), by coupling anaerobic oxidation of lactate, formate, and pyruvate to the reduction of vanadium pentoxide V(V). The vanadyl ion V(IV) will then precipitate as a solid (Carpentier *et al.*, 2003).

1.2.3 Platinum

The technique most often used for platinum nanoparticle production, like in the case of palladium, involves the reduction of metal salt such as a chloride, with a stabilizer. Other reducing agents used include $NaBH_4$, potassium bitartarate, superhydrides, amines and alcohols (Masala & Seshadri, 2004). Nanoparticles from the platinum group metals (PGM) are generally used in industrial and automotive catalysts, due to their high corrosion resistance and oxidation stability at high temperatures (Lengke *et al.*, 2006b; Lengke *et al.*, 2007b). Chemical reduction of the platinum has been widely developed for the depositing of PGM from related metal salt solutions with different reducing agents, but these methods involves heating at very high temperatures to conclude the reduction of soluble PGM ions (Konishi *et al.*, 2007a).

Several microorganisms have been found to produce platinum nanoparticles. Amongst these is the metal ion-reducing bacterium, *Shewanella algae* (Figure 1.2) (Konishi *et al.*,

2007a). Resting cells of this bacterium were able to reduce aqueous $PtCl_6^{2-}$ ions into elemental platinum at room temperature and neutral pH within 60 minutes. Lactate was used as the electron donor and the particles were located in the periplasm (Konishi *et al*., 2007a). The fungus, *Fusarium oxysporum*, was successfully used for inter- and extracellular production of platinum nanoparticles (Riddin *et al*., 2006). The cyanobacteria, *Plectonema boryanum* UTEX 485 were able to reduce $PtCl_4^0$ to yield precipitation of Pt(II)-organic material as amorphous spherical nanoparticles in solutions and dispersed nanoparticles within bacterial cells (Lengke *et al*., 2006b).

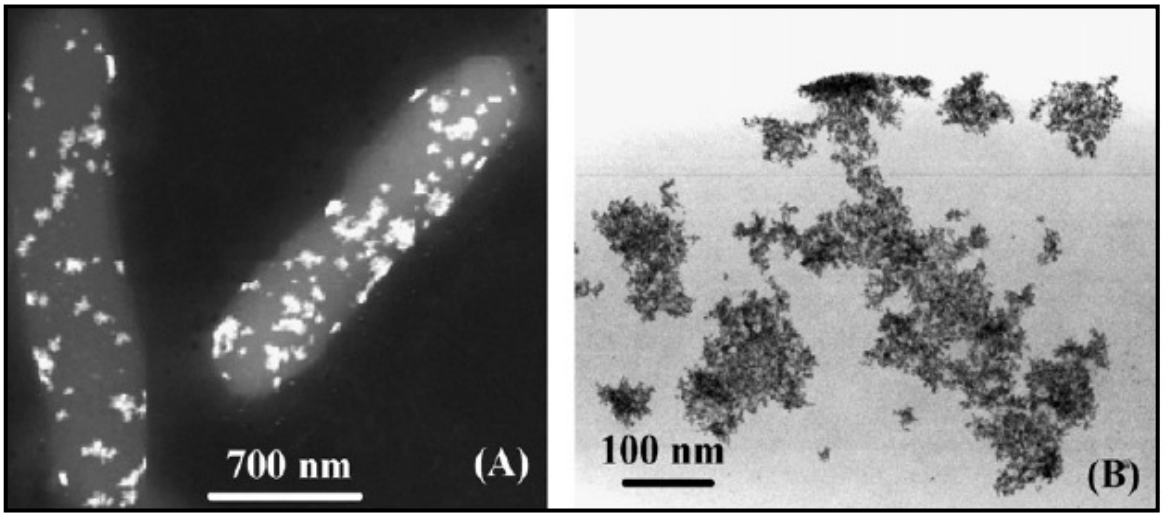

Figure 1.2: Dark-field (A) and bright-field (B) TEM micrographs of platinum nanoparticles produced by cells of *Shewanella algae*. Scale bars in A and B are equal to 700 nm and 100 nm respectively (Taken from Konishi *et al*., 2007a).

Other successful methods for the production of aqueous colloidal platinum nanoparticles, to be used as a reduction catalyst, include photochemical, pulse-radiolytical, and thermal methods (Furlong *et al*., 1984; Lengke *et al*., 2006b).

1.2.4 Silver

Silver nanoparticles are widely used due to their unique shape-dependent optical, electrical, and chemical properties that have possible applications in nanotechnology such as photographic reactions, catalysis, chemical analysis, biolabelling, sensors antimicrobial agents and filters (Bhainsa & D'Souza, 2006; Lengke *et al*., 2007a).

Nearly monodisperse silver nanoparticles can be synthesized by the reduction of a salt, usually silver nitrate ($AgNO_3$) or silver acetate ($AgC_2H_3O_2$) in solution, with a stabilizer. As in the case of the other metals, many variations of this process have been successfully used with different reducing agents, such as $NaBH_4$, sodium citrate, potassium bitartarate, dimethyl formamide (DMF), ascorbic acid, and alcohols (Masala & Seshadri, 2004).

Microorganisms used for the production of silver nanoparticles include *Pseudomonas stutzeri* AG259, *Escherichia coli*, *Vibrio cholerae*, *Pseudomonas aeruginosa*, *Salmonella typhi*, *Phoma* sp. 3.2883, and *Staphylococcus aureus*. The organisms produced both intra- and extracellular silver nanoparticles from $AgNO_3$ (Klaus *et al.*, 1999; Lengke *et al.*, 2007a). *Aspergillus fumigatus* and *Fusarium oxysporum* produced extracellular and intracellular silver nanoparticles respectively (Ahmad *et al.*, 2003a; Bhainsa & D'Souza, 2006). The cyanobacteria, *Plectonema boryanum* UTEX 485 were also able to reduce $AgNO_3$ to yield precipitation of spherical and octahedral nanoparticles and silver platelets in solutions (Figure 1.3) (Lengke *et al.*, 2007a). Other organisms that have been successful in producing silver nanoparticles include the fungi *Verticillium* sp. (AAT-TS-4) and *Hormoconis resina, Lactobacillus* strains, commonly found in buttermilk, and *Penicillium* sp(s). (Mukherjee *et al.*, 2001a; Nair & Pradeep, 2002; Sadowski *et al.*, 2008; Maliszewska *et al.*, 2009; Varshney *et al.*, 2009).

Other methods include Neem (*Azadirachta indica*) leaf broth in the extracellular synthesis of pure metallic and bimetallic silver nanoparticles and plant leaf extracts, including Pine, Persimmon, Ginkgo, Magnolia and Platanus (Shankar *et al.*, 2004; Song & Kim, 2009).

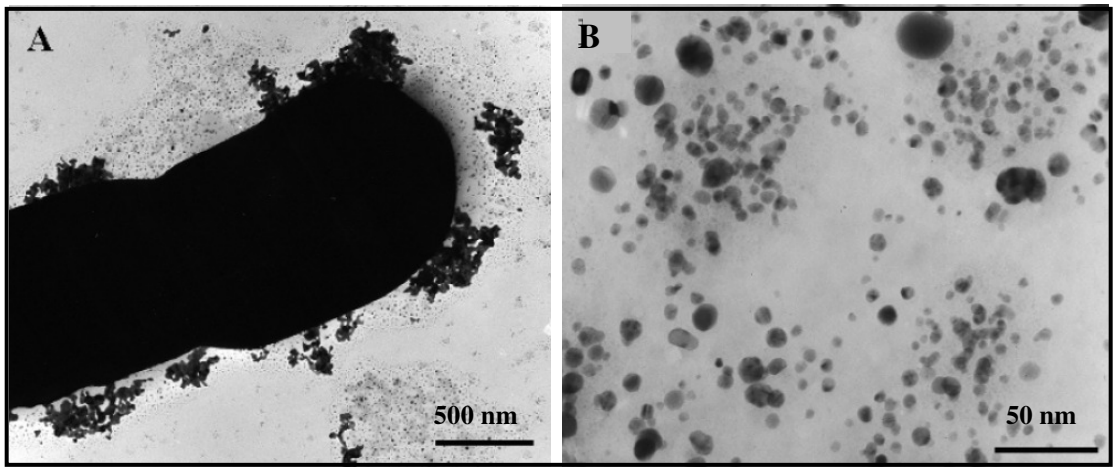

Figure 1.3: TEM micrographs of silver nanoparticles produced by cells of *Plectonema boryanum* UTEX 485. Scale bars in A and B are equal to 500 nm and 50 nm respectively (Taken from Lengke *et al*., 2007a).

1.2.5 Gold

As with the other metals discussed above, gold are also generally prepared by the reduction of a metal salt, such as a chloride or a halide in solution with a stabilizer. The first efficient studies of this process were done by Michael Faraday in 1857, who obtained colloidal gold by reducing an aqueous solution of $AuCl_4^-$ with phosphorus. Since then, different reducing agents and stabilizers have been used for the development of moderate conditions that can be used for the production of large amounts of nanoparticles of reproducible quality (Faraday, 1857; Masala & Seshadri, 2004).

Gold nanoparticles have been widely studied due to its optical and thermodynamic properties and because it is the most stable of all the metal nanoparticles (Inasawa *et al*., 2003; Huang & Yang, 2005). Important material features of gold include its nobility and its resistance to surface oxidation, which would obstruct the process of nanoscale technologies and devices based on other metals. The optical properties of gold at the nanoscale are of great importance due to gold nanoparticles varying in colour, from yellow/orange to red/pink to purple to blue (Figure 1.4), depending on particle size. This important property can be effectively used in a number of applications such as colours and coatings, in non-linear optical devices and optical recording media. Furthermore,

gold nanoparticles are catalytically active towards a variety of commercially essential reactions and due to these unique properties, gold are now being used in exciting new nanotechnology applications. This includes innovative electronic materials and devices, cancer treatments, biomedical techniques for monitoring body fluids, catalysts for pollution control, chemical processing, colours and coatings as well as fuel cells (Corti *et al*., 2003). When used in bulk form, gold is an inert, soft, yellow metal, with a face centred cubic structure and a melting point of 1064ºC, but these appearances differ significantly for gold nanoparticles (Corti *et al*., 2003; Bönnemann & Nagabhushana, 2004).



Figure 1.4: An increase in the size of nanoparticles results in a change of colour, from yellow/orange to red/pink, to purple, to blue, due to the surface plasmon vibrations of the gold nanoparticles (Taken from http://www.news.wustl.edu).

Microorganisms, used for the production of gold nanoparticles include pro- and eukaryotic algal genera such as *Lyngbya majuscula*, *Spirulina subsalsa* (Cyanophyceae) and *Rhizoclonium hieroglyphicum* (Chlorophyceae) (Chakraborty *et al*., 2009). These organisms were used for the bio-recovery of gold out of aqueous solutions. The media used turned purple in colour indicating reduction of Au(III) to Au(0) and formation of nanoparticles at intra- and extracellular level (Chakraborty *et al*., 2009). The fungus, *Rhizopus oryzae* have showed *in situ* reduction of chloroauric acid ($HAuCl_4$) (Das *et al*., 2009). The filamentous cyanobacterium, *Plectonema boryanum* UTEX 485, has been reacted with aqueous $Au(S_2O_3)_2^{3-}$ and $AuCl_4^-$ to yield precipitation of cubic gold nanoparticles at membrane vesicles and admixed with gold sulphide within cells and encrusted on the cyanobacteria. Reaction with $AuCl_4^-$ resulted in the precipitation of octahedral gold platelets in solutions and nanoparticles of gold within bacterial cells

(Lengke *et al*., 2006a). Other microorganisms include *Lactobacillus* strains, hyperthermophilic and mesophilic dissimilatory Fe(III)-reducing *bacteria* and *archaea*. *Shewanella algae* is capable of reducing Au(III) to Au(0) with hydrogen (H_2) as the electron donor (Figure 1.5) (Konishi *et al*., 2007b). *Candida utilis* formed finely dispersed intracellular particles and *Fusarium oxysporum* and *Pseudomonas aeruginosa* formed extracellular nanoparticles (Karamushka & Gadd, 1999; Kashefi *et al*., 2001; Mukherjee *et al*., 2002; Nair & Pradeep, 2002; Konishi *et al*., 2007b). *Rhodopseudomonas capsulate*, the alkalothermophilic (extremophilic) actinomycete, *Thermomonospora* sp., the alkalotolerant actinomycete, *Rhodococcus* sp. and the fungus, *Verticillium* sp. (AAT-TS-4) have all be shown to reduce gold and produce nanoparticles (Mukherjee *et al*., 2001b; Ahmad *et al*., 2003c; He *et al*., 2007; Husseiny *et al*., 2007). In theory, these methods, when used with controlled parameters, should be able to give monodisperse nanoparticles with ideal properties, but in practice, there has been limited success in controlling the shape of the particles.

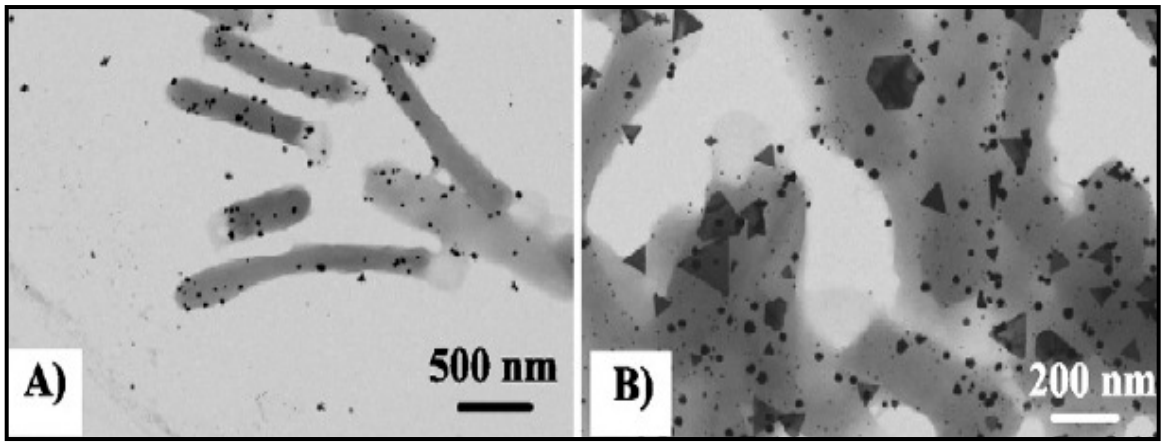

Figure 1.5: TEM micrographs of gold nanoparticles produced by cells of *Shewanella algae*. Scale bars in A and B are equal to 500 nm and 200 nm respectively (Taken from Konishi *et al*., 2007b).

Other effectively used methods include the possibility of using live Alfalfa plants, sugar beet pulp, wheat biomass, oat (*Avena sativa*) biomass or by reducing chloroauric acid ($HAuCl_4$) with 3-thiopheneacetic acid (TA). TA is a heterocyclic compound which can be polymerized by specific chemical methods or *via* electrochemical synthesis to form poly(3-thiopheneacetic acid) (Gardea-Torresdey *et al*., 1999; Armendariz *et al*., 2002; Gardea-Torresdey *et al*., 2002a; Armendariz *et al*., 2004; Huang & Yang, 2005; Castro *et*

al., 2009). Gold nanoparticles have also been formed by 308 nm laser irradiation without the use of any stabilizers, *via* UV photoactivation of $HAuCl_4$ in variable concentrations of TX-100, using citrate and ascorbic acid as the reducing agents and through the use of Neem (*Azadirachta indica*) leaf broth in the extracellular synthesis of pure metallic and bimetallic gold nanoparticles (Sau *et al*., 2001; Mandal *et al*., 2002; Inasawa *et al*., 2003; Pei *et al*., 2004; Shankar *et al*., 2004).

Several other metals that have also been found to be successful in the formation of nanoparticles include mercury, chromium, manganese and zinc and have been used in various applications, such as catalysis, energy storage, magnetic data storage, sensors and in the making of steel (Pang *et al.*, 2007; Bondi *et al*., 2009). Nanoparticles have also been produced, using oxides and metalloids or semiconductors (Masala & Seshadri, 2004).

1.3 OXIDE NANOPARTICLES

Oxides, especially those of the transition metals, compose a very significant material class. These present nearly every known property and they participate in a variety of functions. Oxides are also amongst the most stable materials formed, due to the high oxygen content in the Earth's atmosphere. Transition metal oxides, such as titanium dioxide (TiO_2), Zirconium Oxide (Zirconia, ZrO_2) and the oxides of iron (Fe_3O_4 and Fe_2O_3), those of the early transition metals, are fairly biocompatible or not very toxic, being the major advantage of oxide materials. Much work has been done on oxide nanoparticles, but research on metal nanoparticles outweighs the research done on oxide nanoparticles. This may be due to the synthesis not being developed very well and because capping of particles at the required size, to avoid more growth and giving stability through the coordinative saturation of dangling bonds on the particle surface, is not so deeply understood (Luther, 2004; Masala & Seshadri, 2004).

1.3.1 Magnetite

Magnetite (Fe_3O_4) was initially used in biology due to its strong magnetic properties. Afterwards, it has also been used in medicine for the magnetic separation of biochemical

products and cells and also the magnetic guidance of particle systems for site-specific drug delivery (Dresco *et al.*, 1999).

The most widely used method for the production of magnetite particles is by co-precipitation from a solution of ferrous iron [Fe(II)] and ferric iron [Fe(III)] salts using alkali metal hydroxide (Dresco *et al.*, 1999). Magnetite nanoparticles are also being synthesized by co-precipitation of acidic solutions of Fe(II) and Fe(III). Lauric acid and decanoic acid are added as the surfactants (Fu *et al.*, 2001) or by using magnetotactic and iron-reducing bacteria (Figure 1.6) (Sastry *et al.*, 2003; Masala & Seshadri, 2004; Moon *et al.*, 2007).

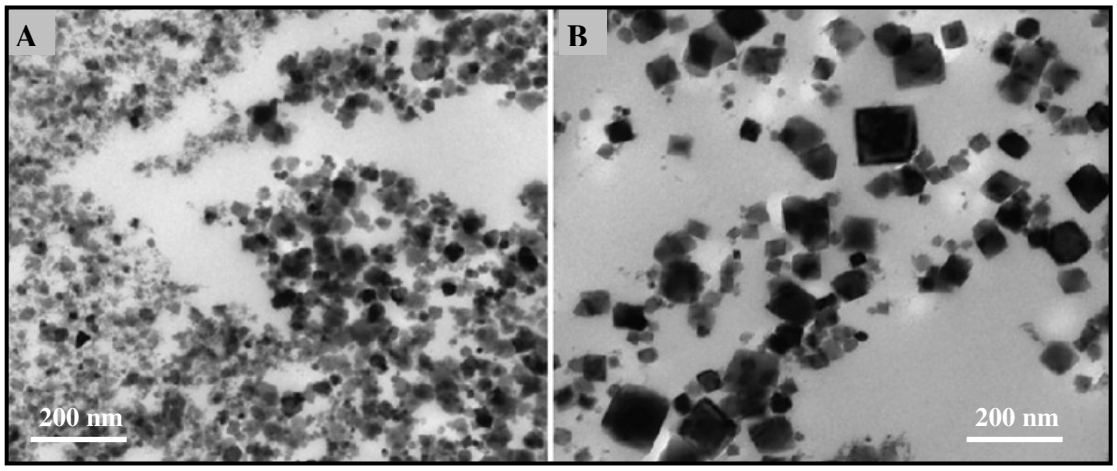

Figure 1.6: TEM micrographs of magnetite nanoparticles produced by iron-reducing bacteria. Scale bars in A and B are both equal to 200 nm (Taken from Moon *et al.*, 2007).

1.3.2 Zinc Oxide

Zinc Oxide (ZnO) nanoparticles is an n-type semiconductor that has been receiving much interest due to several applications such as optoelectronic devices, solar cells, gas sensors, optical waveguides, light emitting diodes and laser diodes (Sridevi & Rajendran, 2009).

ZnO crystallites have been synthesized by several methods, including solgel method, wet chemical synthesis, microwave synthesis, chemical vapour deposition and hydrothermal synthesis. ZnO nanoparticles and nanorods have been successfully

produced using the hydrothermal method with cetyltrimethyl ammonium bromide (CTAB) as surfactant. Several types of ZnO nanomaterials formed include prismatic forms, ellipsoidal, flowers, spheres, nanorods, nanowires and whiskers (Sridevi & Rajendran, 2009).

1.4 METALLOID AND SEMICONDUCTOR NANOPARTICLES

The production of group IV semiconductors, silicon and germanium, has not been widely studied. But more attention has been given to these metals due to several studies done; proposing that luminescence in porous silicon and silicon nanoparticles may be caused by quantum confinement (Masala & Seshadri, 2004).

1.4.1 Silicon & Germanium

Initial work done on the preparation of silicon nanoparticles from the gas phase, was the first step towards the study of the photophysics of these materials. The first work done on a solution route to produce silicon nanocrystals, involved the reduction of tetrachlorosilane ($SiCl_4$) and organotrichlorosilane ($RSiCl_3$) by sodium metal in a non-polar organic solvent at high temperatures (385ºC) and high pressure (> 100 atm). This method gave R-capped, hexagonal-shaped silicon nanoparticles. The same principle can also be applied to germanium. Silicon and germanium nanoparticles can also be synthesized on a small scale by laser ablation and ultrasonic methods and by using diatoms (Sastry *et al*., 2003; Masala & Seshadri, 2004).

1.5 DIFFERENT TYPES OF NANOSCALE STRUCTURES

One of the major advantages of nanotechnology is that by integrating nanoscale structures into materials, their functions can be improved and their applications being increased. Several different types of nanoscale structures have been produced up to date and include the following: nanoparticles, nanowires, nanotubes, nanolayers, nanopores, nanoshells, nanocrystals, nanocubes, nanorods, nanoplates, nanobelts,

nanotadpoles and quantum dots (Rao & Cheetham, 2001; Aitken *et al*., 2004; Luther 2004; Perez-Luna *et al*., 2004; Silberglitt, 2004; He *et al*., 2008).

1.5.1 Nanoparticles

Nanoparticles are composed out of a number of atoms or molecules and can have several sizes and shapes (Figure 1.7), such as amorphous, crystalline, spherical, needles, etc. Nanoparticles can be in the form of dry powders or liquid dispersions and can be used for coatings, components and devices that may or may not maintain the nanostructure of the specific raw materials. Nanoparticles are extensively used for industrial scale fabrication such as carbon black, polymer dispersions, micronized drugs, magnetic device, optoelectronics and electronic applications (Luther, 2004; Narayanan & El-Sayed, 2004; Silberglitt, 2004), and are already being sold by several companies, such as British Biocell International (BBInternational) and PlasmaChem (http://www.britishbiocell.co.uk; http://www.plasmachem.com).

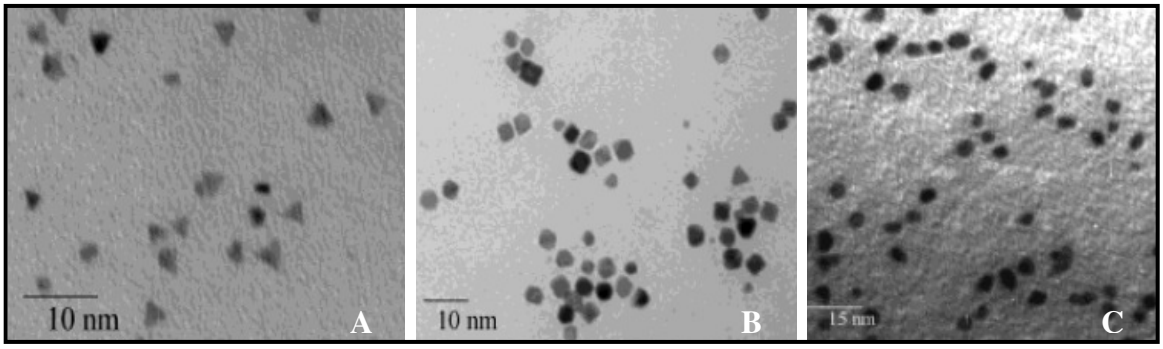

Figure 1.7: TEM micrographs showing different shapes of nanoparticles with (A) mainly tetrahedral, (B) mainly cubical and (C) mainly spherical nanoparticles. Scale bars in A and B are equal to 10 nm and in C, 15 nm (Taken from Narayanan & El-Sayed, 2004).

1.5.2 Nanotubes

Much interest has been created about nanotubes, due to their unique arrangement of properties such as high conductivity, high tensile strength, high temperature capability, plus nanoscale dimensionality, logics, data storage or wiring and microwave amplifiers

(Luther, 2004; Silberglitt, 2004). Nanotubes are a novel form of nanoscale structures and it has been shown that ultra traces of ions and molecules that are far too sensitive for conventional electrodes can be detected by nanotube ensemble electrodes (Aitken *et al.*, 2004; Shao *et al.*, 2005). Nanotubes are widely used in commercial applications, such as an additive to graphite in most of the lithium ion batteries used in cell phones and laptop computers, field emitters, conductive plastics and gas detection (Silberglitt, 2004). One of the most promising and simplest versions of linear nanoscale structures, are the carbon nanotubes (CNT). These structures have great tensile strength and are said to be 100 times stronger than steel, but only being one sixth of its weight. This unique property makes them the strongest, smallest fibre known. Nanotubes are generally being synthesized using laser ablation, arc discharge, chemical vapour deposition (CVD) or plasma-enhanced CVD (PECVD) (Aitken *et al.*, 2004; Luther, 2004; Silberglitt, 2004).

1.5.3 Nanowires

Nanowires are small, conducting or semi-conducting nanostructures with a single crystal arrangement, a diameter of a few tenths of a nanometre and a large aspect ratio (Figure 1.8). They are being used as an alternative to nanotubes as interconnectors for the transport of electrons in nanoelectronic devices. Nanowires are also being used in nanobarcodes, LEDs and thermoelectric devices (Aitken *et al.*, 2004; Silberglitt, 2004). Nanowires are usually made by filling a template with a vapour and let the nanowire grow. The deposition process can be electrochemical or chemical vapour deposition and the template can be made through etching or the use of other nanoscale structures, such as nanotubes (Aitken *et al.*, 2004).

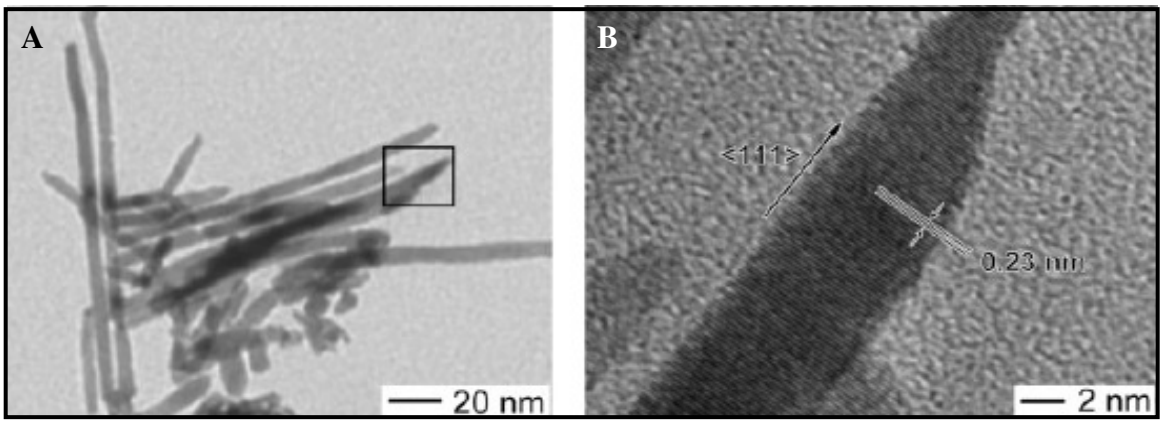

Figure 1.8: TEM micrographs of (A) nanowires and (B) the tip of a single nanowire, indicated in (A). Scale bars in A and B are equal to 20 nm and 2 nm respectively (Taken from Lee *et al.*, 2006).

1.5.4 Nanoshells

Nanoshells are usually made out of a dielectric core, such as silica, coated by a thin metallic film. The structures are generally produced through formation of dielectric cores, followed by the attachment of very small colloidal gold particles on their surface. These gold particles can then react as nucleation sites for additional reduction of gold chloride. In this way, the dielectric core will become covered by a continuous metallic film. Nanoshells are used in SERS, decreasing the rate of photo oxidation of semiconducting polymers and in controlled drug delivery. It has also been found that nanoshells can have a metallic core instead of the dielectric core (Perez-Luna *et al.*, 2004).

1.5.5 Other Nanoscale Structures

Several other structures with nano size ranges can be found. Amongst there are the nanolayers and the nanopores. Nanolayers have a wide range of functionalities and physical effects, such as mechanical, wetting, thermal, chemical, biological, electronical, magnetic and optical properties (Luther, 2004). Nanopores have several industrial applications, due to their applications in thermal insulation, controllable material

separation and release and their use as templates or filters in chemistry and catalysis (Luther, 2004).

1.6 PHYSICO-CHEMICAL PROPERTIES OF NANOMATERIALS

Nanomaterials connect the gap between the molecular level and the bulk form by displaying different physico-chemical properties that can be used in several new products, devices and technological applications. The most important physical and chemical properties of nanoparticles depends on their shape, size and size distribution, chemical composition of the element phases, the presence of interfaces, the interactions between the element atoms and morphological sub-structure of the material. Nanoparticles can be classified with reference to different parameters (some of which can be seen in table 1.2), such as organic or inorganic compounds, crystalline or amorphous states and can be found in the form of a powder, an aerosol (mainly solid or liquid phase in air), a suspension (mainly solid in liquids), an emulsion (two liquid phases), colloids, aggregates or single particles (Rao & Cheetham, 2001; Bönnemann & Nagabhushana, 2004; Luther, 2004; Riddin *et al.*, 2006).

Table 1.2: Different parameters used for classification of nanoparticles (Taken from Luther, 2004).

Classification	**Examples**
Dimension	
• 3 dimensions < 100 nm	Particles, quantum dots, hollow spheres, etc.
• 2 dimensions < 100 nm	Tubes, fibres, wires, platelets, etc.
• 1 dimension < 100 nm	Films, coatings, multilayer, etc.
Phase composition	
• Single-phase solids	Crystalline, amorphous particles and layers, etc.
• Multi-phase solids	Matrix composites, coated particles, etc.
• Multi-phase systems	Colloids, aerogels, ferrofluids, etc.
Manufacturing process	
• Gas phase reaction	Flame synthesis, condensation, CVD, etc.
• Liquid phase reaction	Sol-gel, precipitation, hydrothermal processing
• Mechanical phase reaction	Ball milling, plastic deformation, etc.

The surface and interfacial properties of the nanoparticles may be adapted with the presence of chemical agents or surfactants. These agents can prevent aggregation by protecting the particle charge and by modifying the outmost layer of the particles. The stability of the particles can also be influenced by surface energy, tension and stress (Bönnemann & Nagabhushana, 2004). Nanomaterials also have several other important properties such as improved hardness and ductility and special thermodynamic, optical, magnetic, mechanical, catalytic, sterical, biological and electronic properties that can increase the surface area of the particles as catalysts and their significance in surface coatings. These properties depend strongly on the shape and size of the particles (Mulholland & Bauer, 2000; Bönnemann & Nagabhushana, 2004; He *et al.*, 2008).

The size of the particles is one of the most important properties that influence the behaviour of the particle. The properties of many general materials increase considerably when reduced to a nano-scale size and the overall increase in the particle surface area results in increased reactivity with their environment and furthermore an increase in particle surface energy results in a decrease in melting point. A decrease in size will result in an increase in the diffusion coefficient the vapour pressure required for condensation, the surface area per mass and the force field between particles or between a particle and a surface. As the particle size keep on decreasing, there will be more atoms at the surface that are coordinatively vastly unsaturated and the particle may become a macro molecule or a molecular cluster. A decrease in size will also make it very difficult to measure the diameter of the particle (Tojo, 1997; Mulholland & Bauer, 2000; Bönnemann & Nagabhushana, 2004; Luther, 2004; Riddin *et al.*, 2006). An increase in the size of the cluster will also have a big influence on some of the properties of the material, such as the melting temperature. For instance, gold particles in the nanometre range melt between 500 – 600ºC, but gold in bulk form melts at 1064ºC, leading to the verification that the surface of the particles is a very important factor to consider, however there are some irregularities where metal nanoparticles such as a tin nanocluster, melt at higher temperatures than the bulk form. This may be due to different structural arrangements in the nano form than that of the bulk form (Bönnemann & Nagabhushana, 2004).

Particle size can be adjusted by changing the preparation conditions, for example, nanoparticles need sufficient reaction time to form particles that are homogeneous in

size, however too long reaction time may lead to the deterioration of size distribution (Zweers *et al.*, 2003; Pei *et al.*, 2007). Temperature, the time exposed to heat and the nature of the chemical reductant used, may also influence the size and distribution of the particles (Panigrahi *et al.*, 2006; Pei *et al.*, 2007). The rate of particle formation can be correlated with the incubation temperature where an increase in temperature will allow faster particle formation and the rate of reduction can influence the type of particle formed. For example, spherical particles are more likely to be formed at low reduction rates, while formation of nanorod and platelet-like particles are more likely to be formed at high reduction rates (Gericke & Pinches, 2006a). Even though there has been limited success in controlling the size and shape of the particles, it can be achieved in some occasions by working with reduced metal concentrations and low temperatures, but longer incubation times, to allow the particles to be formed at a slower rate (Mulholland & Bauer, 2000; Gericke & Pinches, 2006a).

The shape and size of nanoparticles can also be controlled by changing the pH of the reaction. For example, when fulvic acid is used in the synthesis of gold nanoparticles, the reaction kinetics strongly depend on the pH of the solution. At a decrease in pH, the reaction rate increase, therefore the rate of ionization of carboxylic and phenolic acidic groups increases at higher pH. This will yield more negatively charged molecules. Alternatively, when Au(III) is in the presence of chloride, the main gold species in the pH range of 11 – 8 is $Au(OH)_4^-$. This result in an increase in the solution pH and an increase in the electrostatic repulsion between the Au(III) complex ions and the fulvic acid macromolecules, therefore the reaction kinetics will slow down. An increase in size with a decrease in pH may also be due to a decrease in the molecular charge of the fulvic macromolecules that are protecting the metal colloids, due to a lower ionization of the acidic groups. The lower ionic strength of the solution of the complex may assist the interaction among nanoparticles and thus aggregation will take place (Dos Santos *et al.*, 2005). In the case of using *Avena sativa* for producing nanoparticles, it was proved that the percentage of Au(III) bound to the biomass decreased when the reaction pH increased, showing that the binding of Au(III) is higher at low pH values. This proposes that the gold-biomass interaction takes place through ionic binding, because Au(III) acts as an anion in aqueous solutions, therefore the biomass may have more positive functional groups at low pH values, allowing the Au(III) ions to get closer to the binding sites (Armendariz *et al.*, 2004). It was also proposed that Au(III) binds to the biomass

mainly by using amino and sulphydryl groups and have a more positive charge at low pH values, making them accessible to bind and reduce Au(III) to Au(0) (Gardea-Torresdey *et al.*, 2002b; Armendariz *et al.*, 2004). The capabilities of synthesizing nanoparticles will not be affected by the pH level, but it will have an influence on the size, shape and amount of particles produced (Armendariz *et al.*, 2004; Gericke & Pinches, 2006a; Altansukh *et al.*, 2008). pH can also be an important factor for the stability of aggregation and precipitation of the metal nanoparticles (Zheng *et al.*, 2002).

Nanoparticles, in particular the alkali metal and noble metals such as copper, silver, platinum and gold have a wide absorption range in the visible region of the electromagnetic spectrum. These metal nanoparticles exhibit very strong colours which are not seen in the bulk form or the atoms. Gold nanorods also have a very interesting property by enhancing fluorescence by a factor of 10^6 when compared with gold metal (Canizal *et al.*, 2001; Bönnemann & Nagabhushana, 2004). Size confinement of these metal particles will result in a change in their electronic properties and therefore changing their optical properties. This feature can be very important in electronic and opto-electronic properties and materials with third-order nonlinearity are very important for light-controlled phase and refractive index modulation in applications such as optical computing, real time holography, optical correlators and phase conjugators (Compton *et al.*, 2003).

Particles sizes and shapes can also be controlled by methods other than altering the synthesis conditions, such as post-physical and chemical treatments, including filtering, etching and flotation. These treatments are applied to samples dispersed in solution by surfactants where the ratio of surfactant to precursor is very important for controlling nanoparticles (Kasuya *et al.*, 2002; Pei *et al.*, 2007).

1.7 METHODS USED IN THE PRODUCTION OF NANOMATERIALS

Nanomaterials can be found in nature in large quantities, originating from combustion sources, such as traffic and forest fires, volcanic activity, atmospheric gas and due to microorganisms that function at almost nanoscale level. However, researchers are aiming to create novel nanomaterials in bigger amounts and within a more constant size

range. These materials can be produced, using several different physical, chemical and biological techniques and approaches such as top-down or bottom-up. Top-down is where nanoparticles are produced from larger structures or bulk material using ultrafine grinders, laser or vaporization, followed by cooling down and being stabilized by protecting agents. Bottom-up approaches arrange molecules in such a way that they form complex structures with new properties and applications, through reduction of the metals, electrochemical pathways or controlled decomposition of metastable organometallic compounds in solution (Aitken *et al.*, 2004; Bönnemann & Nagabhushana, 2004; Luther, 2004; Perez-Luna *et al.*, 2004; Doyle, 2006; Korbekandi *et al.*, 2009).

1.7.1 Physical & Chemical Methods

The oldest recognized method for the production of nanomaterials is the reduction of metal salts by adding a reducing agent, to produce nanoparticles in an aqueous suspension. Some of the reducing agents most commonly used include sodium citrate, $NaBH_4$, tannic acid, white phosphorus, hydrazine, hydrogen, carbon monoxide, hydroxylamine, ascorbic acid, alcohols, formamide and ethers (Perez-Luna *et al.*, 2004). The first report on chemical reduction was in 1857, on transition metals salts in the presence of stabilizing agents to produce zerovalent metal colloids in solution. A few years later, the first reproducible standard method was established, using sodium citrate as reducing agent (Faraday, 1857; Bönnemann & Nagabhushana, 2004). Ever since then, chemical reduction has become the most widely used method to synthesize nanomaterials (Bönnemann & Nagabhushana, 2004).

Top-down approaches takes place in an inert atmosphere or a vacuum, forming nanoparticles that are very reactive and that can easily form agglomerates. Methods in this approach include ultrasonic irradiation, high-energy ball milling, mechano-chemical processing, etching (chemical), electro-explosion (thermal/chemical), sonication, sputtering (kinetic) and laser-ablation (thermal) (Luther, 2004; Perez-Luna *et al.*, 2004; Korbekandi *et al.*, 2009).

Mechanical milling is very often used in powder metallurgy and mineral processing industries. Elemental or prealloyed powder mixtures are grinded, using equipment that can withstand high-energy compressive impact forces such as attrition and shaker mills, in a protective atmosphere. Electro-explosion supplies a very high current in a very short time period, using thin metallic wires in an inert or reactive gas. This will allow unusual temperatures to be achieved. The wires are changed into a plasma state that is controlled and compressed by the high fields obtained from the pulse. The wires are being heated to 20 000 – 30 000 degrees where the metals have unlimited resistivity that will stop the current flow. The electromagnetic field then disappears and a shock wave, in the ionised gas around the wire, is being created through the superheated metal plasma that expands with supersonic velocity. Metastable structures can then be stabilised through the tremendously fast cooling. This process can produce metallic powders of around 100 nanometres. Laser ablation focus pulsed light from an excimer laser onto a solid target in a vacuum chamber, boiling off a cloud of energetic atoms of the target material. The cloud is being captured by a substrate and will obtain a thin film deposit of the target material (Luther, 2004).

Bottom-up approaches include methods such as crystallization, sol-gel processing, aerosol based processes, spinning, supercritical fluid synthesis, chemical vapour deposition (CVD), plasma or flame spraying synthesis, laser pyrolysis, atomic or molecular condensation, using of templates and self-assembly. Sol-gel is used to prepare colloidal nanoparticles from liquid phase and takes place at low temperatures, allowing easy shaping and embedding. CVD activates a chemical reaction between the substrate surface and a gaseous precursor. The activation can be either through temperature (thermal CVD) or plasma enhanced CVD (PECVD). For atomic or molecular condensation, a bulk material is being heated in a vacuum, producing a stream of vaporised and atomic material. This is then directed to a chamber with an inert or reactive gas atmosphere. Collision of the gas molecules and the metals atoms will cause rapid cooling of the metal atoms, resulting in condensation and nanoparticle formation. Metal oxide nanoparticles are formed when the reactive gas used are oxygen. Any substance with standard nanosized pores or empty spaces can be used as a template for nanoparticle production and in self-assembly the conditions such as pH, temperature and solute concentrations are controlled to form self-assembled nanoparticles (Luther, 2004; Doyle, 2006; Korbekandi *et al*., 2009).

1.7.2 Biological Methods

Due to the vast interest in nanotechnology, development thereof is taking place at a very fast rate and millions of tons of nanomaterials are being produced yearly. These nanomaterials are becoming more and more important in everyday life; however the negative effect they have on the environment and public health from being produced with toxic and harmful chemicals is a big environmental concern. Most of the current chemical methods used for retrieving precious metals and producing nanoparticles are seen as unfriendly towards the environment and mostly produce only spherical nanoparticles. To overcome this problem, researchers are moving towards the use of clean, nontoxic, harmless and environmentally friendly biological methods or "green" chemistry (Gamez *et al*., 1999; Ahmad *et al*., 2003a; Ahmad *et al*., 2003b; Ahmad *et al*., 2003c; Bhattacharya & Gupta, 2005; Gericke & Pinches, 2006b; Mandal *et al*., 2006; Riddin *et al*., 2006; He *et al*., 2007; He *et al*., 2008; Chen *et al*., 2008; Castro *et al*., 2009; Korbekandi *et al*., 2009).

For the methods to be "green", all the reagents used, including the reducing reagent, the reaction medium and the capping reagent should be environmentally friendly and methods used for nanoparticle production includes making use of plant extracts, β-d-glucose as the reducing reagent and starch as the capping reagent, using polysaccharide as both a reducing and a stabilizing agent and other biochemical reagents, such as NAD(P)H cofactors, dopamine, L-DOPA, adrenaline, and noradrenaline (Chen *et al*., 2008; Castro *et al*., 2009).

Alternatively, as described previously, the use of microorganisms for producing nanomaterials has become a new and exciting, environmentally friendly approach. Both prokaryotic and eukaryotic organisms, including actinomycetes, bacteria, fungi and yeasts have been successfully used. This bioreduction of metal particles is seen as an organism's mechanism for survival against toxic metal ions and takes place *via* an active or passive process or a combination of the two (Ahmad *et al*., 2003a; Ahmad *et al*., 2003b; Ahmad *et al*., 2003c; Bhattacharya & Gupta, 2005; Riddin *et al*., 2006; Castro *et al*., 2009). This is not unexpected, since it is known that both unicellular and multicellular organisms are able to produce intracellular or extracellular inorganic materials. Microorganisms such as bacteria, fungi and yeast have been extensively used in metal

bioremediation; however, it is only in recent times that microorganisms have been used as potential environmentally friendly nanofactories (Ahmad *et al*., 2003a; Ahmad *et al*., 2003b; Ahmad *et al*., 2003c; Bhattacharya & Gupta, 2005; Das *et al*., 2009; Korbekandi *et al*., 2009).

This approach, called biomimetics or material science and engineering through biology, is expected to produce novel and complex structural nanomaterials with unexpected properties when compared with the conventional methods used (Bhattacharya & Gupta, 2005; Das *et al*., 2009). When microorganisms, and especially bacteria, are exposed to severe environmental conditions, it is important for their survival that they have the ability to control and defend against those stresses such as metal toxicity. These defence mechanisms include efflux systems, alterations of solubility and toxicity by changing the redox state of the metal ions, extracellular complexation or precipitation of the metals intracellularly, usually by formation of metal sulphides, biosorption, bioaccumulation and the lack of specific metal transport systems. These abilities are being used in several essential applications, such as bioleaching, bioremediation, microbial corrosion, biomineralization and nanoparticle synthesis (Ahmad *et al*., 2002; Bhattacharya & Gupta, 2005; Bhainsa & D'Souza, 2006; Korbekandi *et al*., 2009).

A wide range of microorganisms has been used in the synthesis of nanoparticles (some of which can be seen in table 1.3). Among these microorganisms, bacteria have gained the most interest due to the major advantages that they are simple to handle and work with and they can be easily modified, using genetic engineering techniques for overexpression of specific enzymes. Although much of the recent attention in nanoparticle production was focussed on eukaryotes, in particular fungi because they secrete large amounts of proteins therefore increasing productivity, and they are relative easy to work with, genetic manipulation of eukaryotic organisms for overexpression of specific enzymes used in nanomaterial synthesis is more complex and often more difficult than that in prokaryotes (Bhattacharya & Gupta, 2005; Mandal *et al*., 2006; Korbekandi *et al*., 2009).

Table 1.3: Several of the microorganisms used in the synthesis of nanoparticles and the different types of metal nanoparticles which they can produce (Adapted from Mandal *et al.*, 2006).

Microorganisms	**Type of Nanoparticle**
Bacteria	
• *Bacillus subtilis*	Gold
• *Shewanella algae*	Gold
• *Pseudomonas stutzeri*	Silver
• *Lactobacillus*	Gold, Silver, Au-Ag alloy
• *Clostridium thermoaceticum*	Cadmium sulphide
• *Klebsiella aerogenes*	Cadmium sulphide
• *Escherichia coli*	Cadmium sulphide, silver
• *Desulfobacteriaceae*	Zinc sulphide
• *Thermoanaerobacter ethanolicus*	Magnetite
• *Magnetospirillium magnetotacticum*	Magnetite
• *Thermomonospora* sp.	Gold
• *Rhodococcus*	Gold
• *Chlorella vulgaris*	Gold
• *Phaeodactylum tricornutum*	Cadmium sulphide
• *Plectonema boryanum* UTEX 485	Palladium, platinum, silver
• *Shewanella oneidensis*	Vanadium
• *Vibrio cholerae*	Silver
• *Pseudomonas aeruginosa*	Silver
• *Salmonella typhus Phoma* sp. 3.2883	Silver
• *Staphylococcus aureus*	Silver
Yeast	
• *Candida glabrata*	Cadmium sulphide
• *Torulopsis* sp.	Lead sulphide
• *Schizosaccharomyces pombe*	Cadmium sulphide
• MKY3 (a silver-tolerant yeast strain)	Silver
Fungi	
• *Verticillium*	Gold, silver
• *Fusarium oxysporum*	Gold, silver, Au-Ag alloy, cadmium sulphide zirconia, platinum
• *Colletotrichum* sp.	Gold
• *Aspergillus fumigatus*	Silver

1.8 APPLICATIONS IN NANOTECHNOLOGY

One of the outstanding features of nanotechnology is that it is multidisciplinary (as can be seen in table 1.4), showing a number of applications for nanomaterials in several sectors. Nanotechnology research has gained a great deal of attention, due to the possibility of developing a vast range of materials, designed for specific uses and behaving much differently at this scale from when they are in larger form, giving these materials new and unique properties and applications (Bhat, 2003).

Nanotechnology research in the medical field has been expected to bring innovative advances in diagnostics and therapeutics, molecular biology and bioengineering. Nanoparticles can be used in medicine as nano-carriers in drug delivery with new potential for drug synthesis and utilization, medical implants, artificial bones and tissues and cancer treatment (Krumov *et al.*, 2009). Photodynamic cancer treatment is the destruction of cancer cells by cytotoxic laser generated atomic oxygen. Special dye, used to create the atomic oxygen, is being taken in by the cancer cells and not the healthy cells. The cells are then exposed to laser radiation and only the cancer cells will be destroyed (Salata, 2004).

From an industrial approach, the most important non-biological application fields for nanoparticles are the information technologies and electronics. Nanoparticles are already being used in information storage technologies, as components in modern audio and videotapes, compact discs and in chemical and optical computers. The semiconductor nanoparticles are used for the production of better batteries, catalysts, solar, and fuel cells. In material science and coating technology, nanoparticles are used for the creation of enhanced ceramics, insulators and polymers, ensuing stronger and lighter materials, wear-resistant tires, durable coatings, and flame-retardant plastics. In the food industry, nanoparticles are used for “intelligent packaging” that include sensors for detection of food deterioration, detecting gasses present in packaged food, allowing better gas transfer through the package layers and give information on the status of frozen foods. Nanomaterials can also be used to adsorb and remove sequester pollutants from water, ensuring clean water for human consumption, agriculture and industrial processing (Doyle, 2006; Krumov *et al.*, 2009).

Table 1.4: Several applications in which nanomaterials are being used (Adapted from Bhat, 2003; Luther, 2004).

Automotive/Aerospace Industry	**Chemical Industry**	**Engineering**	**Electronic Industry**
• Lightweight construction • Painting (fillers, base coat, clear coat) • Catalysts • Tires (fillers) • Sensors • Coatings for windscreen and car bodies	• Fillers for paint systems • Coating systems based on nanocomposites • Impregnation of papers • Switchable adhesives • Magnetic fluids • Catalytic convertors • Catalysts	• Wear protection for tools and machines (anti blocking coatings, scratch resistant coatings on plastic parts, etc.) • Lubricant-free bearings	• Information processing, storage and transmission (MRAM, GMR-HD) • Displays (OLED, FED) • Laser diodes • Glass fibres • Optical switches • Filters (IR-blocking) • Conductive, antistatic coatings • Computers
Construction	**Medicine**	**Textile/Fabrics/Non-wovens**	**Energy**
• Construction materials • Thermal insulation • Flame retardants • Surface-functionalised building materials for wood, floors, stone, facades, tiles, roofs tiles, etc. • Façade coatings • Groove mortar	• Drug delivery systems • Active agents • Medical rapid tests • Prostheses and implants • Antimicrobial agents and coatings • Agents in cancer therapy • Gene monitoring • Bio-detection of pathogens	• Surface-processed textiles • Smart clothes	• Fuel cells • Solar cells • Batteries • Capacitors • Conversion • Storage • Distribution
Cosmetics	**Food and Drinks**	**Household**	**Sports/Outdoor**
• Sun protection • Lipsticks • Skin creams • Tooth paste	• Package materials • Storage life sensors • Additives • Clarification of fruit juices • Processing • Cleaning and disinfection	• Ceramic coatings for irons • Odours catalysts • Cleaner for glass, ceramic, floor and windows	• Ski wax • Antifogging of glasses/goggles • Antifouling coatings for ships/boats • Reinforced tennis rackets and balls
Environment Remediation	**Optical**	**Defence Technologies**	**Nano Applications**
• Pollution abatement • Waste water treatment • Bioremediation • Bioaccumulation • Biosorption • Bioleaching • Biomineralization • Microbial corrosion	• Flat panel displays • Novel display systems	• Smart textiles for uniforms	• Nanoscience • Nanomaterials • Nanotechnology

Gold and gold alloys have been widely used in the electronics and semiconductor industries and are the largest industrial use of gold, requiring 200-300 tonnes each year. Gold has outstanding properties, such as high corrosion resistance, the ability to form metallurgical bonds by soldering or cold welding, ease of fabrication and good electrical and thermal conductivity. These properties make it available in the electronics industry for applications such as contact and connector coatings, high melting point solders, solderable surface coatings for printed circuit boards (PCBs) or component leads, gold bonding wires, thick film inks, and sputtering targets. Where consistency is a major product quality, gold is the material of preference. Gold has also very promising properties in its use as a catalyst in chemical processing, pollution control and fuel cell applications and in the biomedical applications (Corti *et al*., 2003).

1.9 CONCLUSIONS

Metal nanoparticles are synthesized with a variety of metals to produce particles that differ in shape, size and dispersity. These nanoparticles have unique properties that have been extensively characterized and can be used in different applications. Nanoparticles are synthesized chemically and biologically, but without much success in controlling particle formation and obtaining monodisperse nanoparticles through the use of biological methods. However, biological methods are safer to use for public health and they are environmentally friendly, therefore, to be able to control the nanoparticle formation process, it is important to understand the mechanism of nanoparticle formation.

Nanotechnology has become an important discipline, drawing attention and creating interest in several applications and is believed to one day replace most of the existing technologies that are being used today. It is multidisciplinary with already a number of applications for nanomaterials in several sectors, based on its unique properties, but in many fields, nanotechnology is still in the early development stage of full commercial exploitation. Research into application structure types are extended daily and as a result, the next few years will be crucial as applications of nanomaterials in the industry are most likely to be increased. Therefore methods used for the production of these

nanomaterials have to be selected with great care, keeping in mind the safety of the environment and the public, and especially concerning human health.

REFERENCES

- **Ahmad, A., Mukherjee, P., Mandal, D., Senapati, S., Khan, M.I., Kumar, R. and Sastry, M.** (2002) Enzyme Mediated Extracellular Synthesis of CdS Nanoparticles by the Fungus, *Fusarium oxysporum*. *J. Am. Chem. Soc.* **124**:12108-12109.

- **Ahmad, A., Mukherjee, P., Senapati, S., Mandal, D., Khan, M.I., Kumar, R. and Sastry, M.** (2003a) Extracellular Biosynthesis of Silver Nanoparticles using the Fungus *Fusarium oxysporum*. *Colloids and Surfaces B: Biointerfaces.* **28**:313-318.

- **Ahmad, A., Senapati, S., Khan, M.I., Kumar, R. and Sastry, M.** (2003b) Extracellular Biosynthesis of Monodisperse Gold Nanoparticles by a Novel Extremophilic Actinomycete, *Thermomonospora* sp. *Langmuir.* **19**:3550-3553.

- **Ahmad, A., Senapati, S., Khan, M.I., Kumar, R., Ramani, R., Srinivas, V. and Sastry, M.** (2003c) Intracellular Synthesis of Gold Nanoparticles by a Novel Alkalotolerant Actinomycete, *Rhodococcus* species. *Nanotechnology.* **14**:824-828.

- **Aitken, R.J., Creely, K.S. and Tran, C.L.** (2004) Nanoparticles: An Occupational Hygiene Review. *Health and Safety Executive Research Report 274.* Riccarton. Edinburgh. *HSE Books.* London.

- **Altansukh, B., Yao, J. and Wang, D.** (2008) Synthesis and Characterization of Gold Nanorods by a Seeding Growth Method. *Journal of Nanoscience and Nanotechnology.* **8**:1-4.

- **Amoruso, S., Ausanio, G., de Lisio, C., Iannotti, V., Vitiello, M., Wang, X. and Lanotte, L.** (2005) Synthesis of Nickel Nanoparticles and Nanoparticles Magnetic Films by Femtosecond Laser Ablation in Vacuum. *Applied Surface Science.* **247**:71-75.

- **Armendariz, V., Gardea-Torresdey, J.L., Jose-Yacaman, M., Gonzalez, J., Herrera, I. and Parsons, J.G.** (2002) Gold Nanoparticle Formation by Oat and Wheat Biomasses. *Waste Research Technology – Proceedings of 2002 Conference on Application of Waste Resources.* Kansas City. Missouri. United States of America. 224-232.

- **Armendariz, V., Herrera, I., Peralta-Videa, J.R., Jose-Yacaman, M., Troiania, H., Santiago, P. and Gardea-Torresday, J.L.** (2004) Size Controlled Gold Nanoparticle Formation by *Avena sativa* Biomass: Use of Plants in Nanobiotechnology. *Journal of Nanoparticle Research.* **6**:377-382.

- **Bhainsa, K.C. and D'Souza, S.F.** (2006) Extracellular Biosynthesis of Silver Nanoparticles using the Fungus *Aspergillus fumigatus*. *Colloids and Surfaces B: Biointerfaces.* **47**:160-164.

- **Bhat, J.S.A.** (2003) Heralding a New Future – Nanotechnology? *Current Science.* **85**:147-154.

- **Bhattacharya, D. and Gupta, R.K.** (2005) Nanotechnology and Potential of Microorganisms. *Critical Reviews in Biotechnology*. **25**:199-204.

- **Bondi, J.F., Oyler, K.D., Ke, X., Schiffer, P. and Schaak, R.E.** (2009) Chemical Synthesis of Air-Stable Manganese Nanoparticles. *J. Am. Chem. Soc.* **131**:9144-9145.

- **Bönnemann, H. and Nagabhushana, K.S.** (2004) Chemical Synthesis of Nanoparticles. *Encyclopedia of Nanoscience and Nanotechnology.* **1**:777-813.

- **Canizal, G., Ascencio, J.A., Gardea-Torresdey, J. and José-Yacamán, M.** (2001) Multiple Twinned Gold Nanorods Grown by Bio-reduction Techniques. *Journal of Nanoparticle Research.* **3**:475-481.

- **Carpentier, W., Sandra, K., De Smet, I., Brigé, A., De Smet, L. And Van Beeumen, J.** (2003) Microbial Reduction and Precipitation of Vanadium by *Shewanella oneidensis*. *Applied and Environmental Microbiology*. **69**:3636-3639.

- **Castro, L., Blázquez, M.L., Ballester, A., González, F. and Muñoz, J.A.** (2009) Extracellular Biosynthesis of Gold Nanoparticles using Sugar Beet Pulp. *Poster.* Barcelona. Spain.

- **Chakraborty, N., Banerjee, A., Lahiri, S., Panda, A., Ghosh, A.N. and Pal, R.** (2009) Biorecovery of Gold using Cyanobacteria and an Eukaryotic Alga with Special Reference to Nanogold Formation – a Novel Phenomenon. *J. Appl. Phycol.* **21**:145-152.

- **Chen, J., Wang, J., Zhang, X. and Jin, Y.** (2008) Microwave-Assisted Green Synthesis of Silver Nanoparticles by Carboxymethyl Cellulose Sodium and Silver Nitrate. *Materials Chemistry and Physics.* **108**:421-424.

- **Chen, Y., Peng, D., Lin, D. and Luo, X.** (2007) Preparation and Magnetic Properties of Nickel Nanoparticles *via* the Thermal Decomposition of Nickel Organometallic Precursor in Alkylamines. *Nanotechnology.* **18**:505703-505708.

- **Chou, K. and Huang, K.** (2001) Studies on the Chemical Synthesis of Nanosized Nickel Powder and its Stability. *Journal of Nanoparticle Research.* **3**:127-132.

- **Compton, D., Cornish, L. and Van Der Lingen, E.** (2003) The Third Order Nonlinear Optical Properties of Gold Nanoparticles in Glasses, Part I. *Gold Bulletin.* **36**:10-16.

- **Corti, C.W., Holliday, R.J. and Thompson, D.T.** (2003) The Unique Properties of Gold for Nanoscale Technologies and Fabrication. *International Technology, World Gold Council.* London.

- **Das, S.K., Das, A.R. and Guha, A.K.** (2009) Gold Nanoparticles: Microbial Synthesis and Application in Water Hygiene Management. *Langmuir.* **25**:8192-8199.

- **Dos Santos Jr., D.S., Alvarez-Puebla, R.A., Oliveira Jr., O.N. and Aroca, R.F.** (2005) Controlling the Size and Shape of Gold Nanoparticles in Fulvic Acid Colloidal Solutions and their Optical Characterization using SERS. *J. Mater. Chem.* **15**:3045-3049.

- **Doyle, M.E.** (2006) Nanotechnology: A Brief Literature Review. *Food Research Institute Briefings.*

- **Dresco, P.A., Zaitsev, V.S., Gambino, R.J. and Chu, B.** (1999) Preparation and Properties of Magnetite and Polymer Magnetite Nanoparticles. *Langmuir.* **15**:1945-1951.

- **Faraday, M.** (1857) Experimental Relations of Gold (and Other Metals) to Light. *Philos. Trans. R. Soc.* **147**:145-181.

- **Fu, L., Dravid, V.P. and Johnson, D.L.** (2001) Self-assembled (SA) Bilayer Molecular Coating on Magnetic Nanoparticles. *Applied Surface Science.* **181**:173-178.

- **Furlong, D.N., Launikonis, A. and Sasse, W.H.F.** (1984) Colloidal Platinum Sols: Preparation, Characterization and Stability Towards Salt. *J. Chem. Soc. Faraday. Trans. 1.* **80**:571-588.

- **Gamez, G., Dokken, K., Tiemann, K.J., Herrera, I., Yacaman, M.J., Renner, M.W., Furenlid, L.R. and Gardea-Torresdey, J.L.** (1999) Spectroscopic Studies of Gold(III) Binding to Alfalfa Biomass. *Proceedings of the 1999 Conference on Hazardous Waste Research. "Gateways to Environmental Solutions.* Manhattan. Kansas. United States of America. 78-90.

- **Gardea-Torresdey, J.L., Gomez, E., Peralta-Videa, J.R., Parsons, J.G., Troiani, H. and Jose-Yacaman, M.** (2003) Alfalfa Sprouts: A Natural Source for the Synthesis of Silver Nanoparticles. *Langmuir.* **19**:1357-1361.

- **Gardea-Torresdey, J.L., Parsons, J.G., Gomez, E., Peralta-Videa, J., Troiani, H.E., Santiago, P. and José-Yacamán, M.** (2002a) Formation and Growth of Au Nanoparticles Inside Live Alfalfa Plants. *Nano Letters.* **2**:397-401.

- **Gardea-Torresdey, J.L., Tiemann, K.J., Gamez, G., Dokken, K., Tehuacanero, S. and José-Yacamán, M.** (1999) Gold Nanoparticles Obtained by Bio-precipitation from Gold(III) Solution. *Journal of Nanoparticle Research.* **1**:397-404.

- **Gardea-Torresdey, J.L., Tiemann, K.J., Parsons, J.G., Gamez, G. and José-Yacamán, M.** (2002b) Characterization of Trace Level Au(III) Binding to Alfalfa Biomass. *Adv. Environ. Res.* **6**:313-323.

- **Gericke, M. and Pinches, A.** (2006a) Biological Synthesis of Metal Nanoparticles. *Hydrometallurgy.* **83**:132-140.

- **Gericke, M. and Pinches, A.** (2006b) Microbial Production of Gold Nanoparticles. *Gold Bulletin.* **39**:22-28.

- **He, S., Guo, Z., Zhang, Y., Zhang, S., Wang, J. and Gu, N.** (2007) Biosynthesis of Gold Nanoparticles using the Bacteria *Rhodopseudomonas capsulata*. *Materials Letters.* **61**:3984-3987.

- **He, S., Zhang, Y., Guo, Z. and Gu, N.** (2008) Biological Synthesis of Gold Nanowires Using Extract of *Rhodopseudomonas capsulata*. *Biotechnol. Prog.* **24**:476-480.

- **Hou, Y., Kondoh, H., Ohta, T. and Gao, S.** (2005) Size-Controlled Synthesis of Nickel Nanoparticles. *Applied Surface Science.* **241**:218-222.

- http://www.britishbiocell.co.uk.

- http://www.discovernano.northwestern.edu/whatis/index_html/howsmall_html.

- http://www.news.wustl.edu/news/Pages/20401.aspx.

- http://www.plasmachem.com.

- **Huang, H. and Yang, X.** (2005) One-step, Shape Control Synthesis of Gold Nanoparticles Stabilized by 3-thiopheneacetic acid. *Colloids and Surfaces A: Physicochem. Eng. Aspects.* **255**:11-17.

- **Husseiny, M.I., Abd El-Aziz, M., Badr, Y. and Mahmoud, M.A.** (2007) Biosynthesis of Gold Nanoparticles using *Pseudomonas aeruginosa*. *Spectrochimica Acta Part A.* **67**:1003-1006.

- **Inasawa, S., Masakazu, S. and Seiichiro, K.** (2003) Size Controlled Formation of Gold Nanoparticles using Photochemical Growth and Photothermal Size Reduction by 308 nm Laser Pulses. *Jpn. J. Appl. Phys.* **42**:6705-6712.

- **Karamushka, V.I. and Gadd, G.M.** (1999) Interaction of *Saccharomyces cerevisiae* with Gold: Toxicity and Accumulation. *Bio Metals.* **12**:289-294.

- **Karn, B.P. and Bergeson, L.L.** (2009) Green Nanotechnology: Straddling Promise and Uncertainty. *Natural Resources & Environment.* **24**:9-14.

- **Kashefi, K., Tor, J.M., Nevin, K.P. and Lovley, D.R.** (2001) Reductive Precipitation of Gold by Dissimilatory Fe(III)-Reducing Bacteria and Archaea. *Applied and Environmental Microbiology.* **67**:3275-3279.

- **Kasuya, A., Milczarek, G., Dmitruk, I., Barnakov, Y., Czajka, R., Perales, O., Liu, X., Tohji, K., Jeyadevan, B., Shinoda, K., Ogawa, T., Arai, T., Hihara, T. and Sumiyama, K.** (2002) Size- and Shape-controls and Electronic Functions of Nanometre-scale Semiconductors and Oxides. *Colloids and Surfaces A: Physicochemical and Engineering Aspects.* **202**:291-296.

- **Kim, Y.H., Lee, D.K., Jo, B.G., Jeong, J.H. and Kang, Y.S.** (2006) Synthesis of Oleate Capped Cu Nanoparticles by Thermal Decomposition. *Colloids and Surfaces A: Physicochem. Eng. Aspects.* **284-285**:364-368.

- **Klaus, T., Joerger, R., Olsson, E. and Granqvist, C.** (1999) Silver-based Crystalline Nanoparticles, Microbially Fabricated. *PNAS.* **96**:13611-13614.

- **Konishi, Y., Ohno, K., Saitoh, N., Nomura, T., Nagamine, S., Hishida, H., Takahashi, Y. and Uruga, T.** (2007a) Bioreductive Depostition of Platinum Nanoparticles on the Bacterium *Shewanella algae*. *Journal of Biotechnology.* **128**:648-653.

- **Konishi, Y., Tsukiyama, T., Tachimi, T., Saitoh, N., Nomura, T. and Nagamine, S.** (2007b) Microbial Deposition of Gold Nanoparticles by the Metal-Reducing Bacterium *Shewanella algae*. *Electrochimica Acta.* **53**:186-192.

- **Korbekandi, H., Iravani, S. and Abbasi, S.** (2009) Production of Nanoparticles using Organisms. *Critical Reviews in Biotechnology.* **29**:279-306.

- **Krumov, N., Perner-Nochta, I., Oder, S., Gotcheva, V., Angelov, A. and Posten, C.** (2009) Production of Inorganic Nanoparticles by Microorganisms. *Chem. Eng. Technol.* **32**:1026-1035.

- **Lee, E.P., Chen, J., Yin, Y., Campbell, C.T. and Xia, Y.** (2006) Pd-Catalyzed Growth of Pt Nanoparticles or Nanowires as Dense Coatings on Polymeric and Ceramic Particulate Supports. *Adv. Mater.* **18**:3271-3274.

- **Lengke, M.F., Fleet, M.E. and Southam, G.** (2006a) Morphology of Gold Nanoparticles Synthesized by Filamentous Cyanobacteria from Gold(I)-Thiosulfate and Gold(III)-Chloride Complexes. *Langmuir.* **22**:2780-2787.

- **Lengke, M.F., Fleet, M.E. and Southam, G.** (2006b) Synthesis of Platinum Nanoparticles by Reaction of Filamentous Cyanobacteria with Platinum(IV)-Chloride Complex. *Langmuir.* **22**:7318-7323.

- **Lengke, M.F., Fleet, M.E. and Southam, G.** (2007a) Biosynthesis of Silver Nanoparticles by Filamentous Cyanobacteria from a Silver(I) Nitrate Complex. *Langmuir.* **23**:2694-2699.

- **Lengke, M.F., Fleet, M.E. and Southam, G.** (2007b) Synthesis of Palladium Nanoparticles by Reaction of Filamentous Cyanobacterial Biomass with a Palladium(II) Chloride Complex. *Langmuir.* **23**:8982-8987.

- **Luther, W.** (2004) Industrial Application of Nanomaterials – Chances and Risks. *Future Technologies.* **54**:1-112.

- **Maliszewska, I., Szewczyk, K. and Waszak, K.** (2009) Biological Synthesis of Silver Nanoparticles. *Journal of Physics: Conference Series.* **146**:012025.

- **Mandal, D., Bolander, M.E., Mukhopadhyay, D., Sarkar, G. and Mukherjee, P.** (2006) The Use of Microorganisms for the Formation of Metal Nanoparticles and their Application. *Appl. Microbiol. Biotechnol.* **69**:485-492.

- **Mandal, M., Ghosh, S.K., Kundu, S., Esumi, K. and Pal, T.** (2002) UV Photoactivation for Size and Shape Controlled Synthesis and Coalescence of Gold Nanoparticles in Micelles. *Langmuir.* **18**:7792-7797.

- **Masala, O. and Seshadri, R.** (2004) Synthesis Routes for Large Volumes of Nanoparticles. *Annu. Rev. Mater. Res.* **34**:41-81.

- **Miyazaki, A., Balint, I. and Nakano, Y.** (2003) Morphology Control of Platinum Nanoparticles and their Catalytic Properties. *Journal of Nanoparticle Research.* **5**:69-80.

- **Moon, J., Roh, Y., Lauf, R.J., Vali, H., Yeary, L.W. and Phelps, T.J.** (2007) Microbial Preparation of Metal-Substituted Magnetite Nanoparticles. *Journal of Microbiological Methods.* **70**:150-158.

- **Mukherjee, P., Ahmad, A., Mandal, D., Senapati, S., Sainkar, S.R., Khan, M.I., Parishcha, R., Ajaykumar, P.V., Alam, M., Kumar, R. and Sastry, M.** (2001a) Fungus-Mediated Synthesis of Silver Nanoparticles and their Immobilization in the Mycelial Matrix: A Novel Biological Approach to Nanoparticle Synthesis. *Nano Letters.* **1**:515-519.

- **Mukherjee, P., Ahmad, A., Mandal, D., Senapati, S., Sainkar, S.R., Khan, M.I., Ramani, R., Parishcha, R., Ajaykumar, P.V., Alam, M., Sastry, M. and Kumar, R.** (2001b) Bioreduction of $AuCl_4^-$ Ions by the Fungus, *Verticillium* sp. and Surface Trapping of the Gold Nanoparticles Formed. *Angew. Chem. Int. Ed.* **40**:3585-3588.

- **Mukherjee, P., Senapati, S., Mandal, D., Ahmad, A., Khan, M.I., Kumar, R. and Sastry, M.** (2002) Extracellular Synthesis of Gold Nanoparticles by the Fungus *Fusarium oxysporum*. *ChemBioChem.* **5**:461-463.

- **Mulholland, G.W. and Bauer, B.J.** (2000) Nanometre Calibration Particles: What is Available and What is Needed? *Journal of Nanoparticle Research.* **2**:5-15.

- **Nair, B. and Pradeep, T.** (2002) Coalescence of Nanoclusters and Formation of Submicron Crystallites Assisted by *Lactobacillus* Strains. *Crystal Growth and Design.* **2**:293-298.

- **Narayanan, R. and El-Sayed, M.A.** (2004) Shape-Dependant Catalytic Activity of Platinum Nanoparticles in Colloidal Solution. *Nano Letters.* **4**:1343-1348.

- **Okuda, M., Iwahori, K., Yamashita, I. and Yoshimura, H.** (2003) Fabrication of Nickel and Chromium Nanoparticles using the Protein Cage of Apoferritin. *Biotechnology and Bioengineering.* **84**:187-194.

- **Pang, S., Wang, L., Li, G. and Zhang, Z.** (2007) Preparation of Manganese and their Derivate Compounds by arc Plasma Method. *Surface & Coatings Technology.* **201**:5451-5453.

- **Panigrahi, S., Praharaj, S., Basu, S., Ghosh, S.K., Jana, S., Pande, S., Vo-Dinh, T., Jiang, H. and Pal, T.** (2006) Self-Assembly of Silver Nanoparticles: Synthesis, Stabilization, Optical Properties, and Application in Surface-Enhanced Raman Scattering. *J. Phys. Chem. B.* **110**:13436-13444.

- **Pedersen, D.B. and Wang, S.** (2007) Surface Plasmon Resonance Spectra of 2.8 ± 0.5 nm Diameter Copper Nanoparticles in Both Near and Far Fields. *J. Phys. Chem. C.* **111**:17493-17499.

- **Pei, L., Mori, K. and Adachi, M.** (2004) Formation Process of Two-Dimensional Networked Gold Nanowires by Citrate Reduction of $AuCl_4^-$ and the Shape Stabilization. *Langmuir.* **20**:7837-7843.

- **Pei, W., Fu, Y., Kumada, H., Wang, T., Hasegawa, T., Washiya, T., Saito, H. and Ishio, S.** (2007) Influence of Synthetic Conditions on Iron Oxide Nanoparticles. *Phys. Stat. Sol. A.* **204**:4017-4020.

- **Perez-Luna, V.H., Aslan, K. and Betala, P.** (2004) Colloidal Gold. *Encyclopedia of Nanoscience and Nanotchnology.* **2**:27-49.

- **Rao, C.N.R. and Cheetham, A.K.** (2001) Science and Technology of Nanomaterials: Current Status and Future Prospects. *J. Mater. Chem.* **11**:2887-2894.

- **Riddin, T.L., Gericke, M. and Whiteley, C.G.** (2006) Analysis of the Inter- and Extracellular Formation of Platinum Nanoparticles by *Fusarium oxysporum* f. sp. *Lycopersici* using Response Surface Methodology. *Nanotechnology.* **17**:3482-3489.

- **Sadowski, Z., Maliszewska, I.H., Grochowalska, B., Polowczyk, I. and Koźlecki, T.** (2008) Synthesis of Silver Nanoparticles using Microorganisms. *Materials Science-Poland.* **26**:419-424.

- **Salata, O.V.** (2004) Applications of Nanoparticles in Biology and Medicine. *Journal of Nanobiotechnology.* **2**:3-6.

- **Sargent, J.** (2010) Nanotechnology: A Policy Primer. *Congressional Research Service – Report for Congress.*

- **Sastry, M., Ahmad, A., Khan, M.I. and Kumar, R.** (2003) Biosynthesis of Metal Nanoparticles using Fungi and Actinomycete. *Current Science.* **85**:162-170.

- **Sau, T.K., Pal, A., Jana, N.R., Wang, Z.L. and Pal, T.** (2001) Size Controlled Synthesis of Gold Nanoparticles using Photochemically Prepared Seed Particles. *Journal of Nanoparticle Research.* **3**:257-261.

- **Scott, D., Toney, M. and Muzikár, M.** (2008) Harnessing the Mechanism of Glutathione Reductase for Synthesis of Active Site Bound Metallic Nanoparticles and Electrical Connection to Electrodes. *J. Am. Chem. Soc.* **130**:865-874.

- **Shankar, S.S., Rai, A., Ahmad, A. and Sastry, M.** (2004) Rapid Synthesis of Au, Ag, and Bimetallic Au Core-Ag Shell Nanoparticles using Neem (*Azadirachta indica*) leaf broth. *Journal of Colloid and Interface Science.* **275**:496-502.

- **Shao, P., Ji, G and Chen, P.** (2005) Gold Nanotube Membranes: Preparation, Characterization and Application for Enantioseparation. *Journal of Membrane Science.* **255**:1-11.

- **Silberglitt, R.** (2004) Nanomaterials: New Trends. *Encyclopedia of Nanoscience and Nanotchnology.* **1**:2451-2463.

- **Šlouf, M., Kužel, R. and Matěj, Z.** (2006) Preparation and Characterization of Isometric Gold Nanoparticles with Pre-calculated Size. *Z. Kristallogr. Suppl.* **23**:319-324.

- **Song, J.Y. and Kim, B.S.** (2009) Rapid Biological Synthesis of Silver Nanoparticles using Plant Leaf Extracts. *Bioprocess. Biosyst. Eng.* **32**:79-84.

- **Sridevi, D. and Rajendran, K.V.** (2009) Preparation of ZnO Nanoparticles and Nanorods by using CTAB Assisted Hydrothermal Method. *International Journal of Nanotechnology and Applications.* **3**:43-48.

- **Sun, Y. and Xia, Y.** (2002) Shape-Controlled Synthesis of Gold and Silver Nanoparticles. *Science.* **298**:2176-2179.

- **Swami, A., Kumar, A. and Sastry, M.** (2003) Formation of Water-Dispersible Gold Nanoparticles using a Technique Based on Surface-Bound Interdigitated Bilayers. *Langmuir.* **19**:1168-1172.

- **Tojo, C.** (1997) Preparation of Nanoparticles in Microemulsions: A Monte Carlo Study of the Influence of the Synthesis Variables. *Langmuir.* **13**:4527-4534.

- **Varshney, R., Mishra, A.N., Bhadauria, S. and Gaur, M.S.** (2009) A Novel Microbial Route to Synthesize Silver Nanoparticles using Fungus *Hormoconis resinae*. *Digest Journal of Nanomaterials and Biostructures.* **4**:349-355.

- **Yang, W., Ma, Y., Tang, J. and Yang, X.** (2007) "Green Synthesis" of Monodisperse Pt Nanoparticles and their Catalytic Properties. *Colloids and Surfaces A: Physicochem. Eng. Aspects.* **302**:628-633.

- **Zheng, J., Stevenson, M.S., Hikida, R.S. and Gregory Van Patten, P.** (2002) Influence of pH on Dendrimer-Protected Nanoparticles. *J. Phys. Chem. B.* **106**:1252-1255.

- **Zweers, M.L.T., Grijpma, D.W., Engbers, G.H.M. and Feijen, J.** (2003) The Preparation of Monodisperse Biodegradable Polyester Nanoparticles with a Controlled Size. *Inc. J. Biomed. Mater. Res. Part B: Appl. Biomater.* **66B**:559-566.

CHAPTER 2

INTRODUCTION TO PRESENT STUDY

2.1 INTRODUCTION

Nanotechnology aims at understanding the basic principles of biological functional units as well as creating extremely small elements at nanoscale in a controlled way with technical materials and interfaces. As far as the synthesis of nanoparticles is concerned, a number of chemical methods exist in the literature that uses toxic chemicals in the synthesis protocol. This raises great concern for health environmental reasons. Another drawback of chemical synthesis is that the nanoparticles produced are normally spherical and to increase the applications for nanoparticles the shapes that can be produced should include non-spherical forms (Scott *et al.,* 2008; Karn & Bergeson, 2009).

Metal nanoparticles are of great interest because of their unique physical and chemical properties. In particular, gold particles at nanoscale have a wide variety of applications, as the material properties at nanoscale differ from that of the bulk form. These differences can be due to an increase in relative surface area and an increase in the dominance of quantum effects. These changes subsequently influence the optical, magnetic and electronic properties of the material. The unique properties of gold at nanoscale results in the application of gold in diverse areas, such as catalysis, biolabelling, nonlinear optical devices and optical recording media, colours and coatings, as well as the biomedical sector (Sun & Xia, 2002; Inasawa *et al*., 2003; Lengke *et al*., 2007).

Several micro-organisms have been found to produce nanoparticles of different shapes and sizes with better monodispersity, and the microbial interaction with metals will also supply eco-friendly methods for nanoparticle production (Bhattacharya & Gupta, 2005; Mandal *et al*., 2006). For tailor-made nanoparticle synthesis, the possibility of optimizing

the size and shape of nanoparticles has been tested. Temperature, pH and other conditions were varied and nanoparticles with exciting new shapes were produced, but with limited success in controlling the shapes to obtain monodisperse nanoparticles and especially when biological methods were used in the synthesis protocol (Korbekandi *et al.*, 2009).

2.2 AIMS OF THIS STUDY

Thermus scotoductus SA-01, a thermophilic bacterium, isolated from a deep gold mine at a depth of 3.2 km, with ambient rock temperature of 60ºC, was used for purification of a gold(III) reducing and nanoparticle synthesizing protein. This discovery, done by van Marwijk, (2009), revealed that gold nanoparticles could be produced by a peptide-binding protein. The interaction of the protein purified from *Thermus scotoductus* SA-01, as well as the protein expressed in *Escherichia coli*, was studied and characterized. Physico-chemical conditions were varied, but throughout the characterization, several parameters remained unclear in order to exert control, on not only the reduction, but also the final nanoparticle production. With this specific protein identified for nanoparticle formation, it is important to understand the conditions for nanoparticle formation, being able to control and direct synthesis as well as having sufficient amount of nanoparticles for evaluation and possibly commercial interest.

The research reported in this dissertation focuses on the characterization of a thermophilic protein from *Thermus scotoductus* SA-01 which is responsible for the reduction of gold(III), as well as the formation of gold nanoparticles. This protein, previously identified as an ABC transporter, peptide-binding protein, was expressed in *Escherichia coli*, a mesophilic expression host, with and without the addition of a Histidine-Tag (His-Tag). This was done to determine if the His-Tag influences the folding of the protein, which in turn could influence the nanoparticle formation, but also allows for easy purification of the proteins. This protein was also expressed in *Thermus thermophilus*, a thermophilic expression host, to compare the influence of the expression hosts on the protein folding and nanoparticle formation. These comparisons were done by varying different parameters and evaluated by using transmission electron microscopy (TEM), energy dispersive X-ray spectrometry (EDX), selected-area electron

diffraction (SAED) and measuring the surface plasmon resonance (SPR) band, to illustrate the effect on particle morphology and to propose a mechanism for this process. Only about 40% of the *Thermus thermophilus* genes will be accessible through cloning and expression screening in *Escherichia coli* and when thermostable enzymes are cloned into mesophilic organisms, differences in codon usage or improper folding of the proteins at low temperatures may prevent the expected activities or the desired amounts of the proteins to be obtained (Hidalgo *et al.*, 2004; Moreno *et al.*, 2005; Turner *et al.*, 2007). Thus, expression in a thermophilic host might exert more control over dispersity in nanoparticle formation.

REFERENCES

- **Bhattacharya, D. and Gupta, R.K.** (2005) Nanotechnology and Potential of Microorganisms. *Critical Reviews in Biotechnology*. **25**:199-204.

- **Hidalgo, A., Betancor, L., Moreno, R., Zafra, O., Cava, F., Fernández-Lafuente, R., Guisán, J.M. and Berenguer, J.** (2004) *Thermus thermophilus* as a Cell Factory for the Production of a Thermophilic MN-Dependant Catalase which Fails to be Synthesized in an Active Form in *Escherichia coli*. *Applied and Environmental Microbiology.* **70**:3839-3844.

- **Inasawa, S., Masakazu, S. and Seiichiro, K.** (2003) Size Controlled Formation of Gold Nanoparticles using Photochemical Growth and Photothermal Size Reduction by 308 nm Laser Pulses. *Jpn. J. Appl. Phys.* **42**:6705-6712.

- **Karn, B.P. and Bergeson, L.L.** (2009) Green Nanotechnology: Straddling Promise and Uncertainty. *Natural Resources & Environment.* **24**:9-14.

- **Korbekandi, H., Iravani, S. and Abbasi, S.** (2009) Production of Nanoparticles using Organisms. *Critical Reviews in Biotechnology.* **29**:279-306.

- **Lengke, M.F., Fleet, M.E. and Southam, G.** (2007) Biosynthesis of Silver Nanoparticles by Filamentous Cyanobacteria from a Silver(I) Nitrate Complex. *Langmuir.* **23**:2694-2699.

- **Mandal, D., Bolander, M.E., Mukhopadhyay, D., Sarkar, G. and Mukherjee, P.** (2006) The Use of Microorganisms for the Formation of Metal Nanoparticles and their Application. *Appl. Microbiol. Biotechnol.* **69**:485-492.

- **Moreno, R., Haro, A., Castellanos, A. and Berenguer, J.** (2005) High-Level Overproduction of His-Tagged *Tth* DNA Polymerase in *Thermus thermophilus*. *Applied and Environmental Microbiology.* **71**:591-593.

- **Scott, D., Toney, M. and Muzikár, M.** (2008) Harnessing the Mechanism of Glutathione Reductase for Synthesis of Active Site Bound Metallic Nanoparticles and Electrical Connection to Electrodes. *J. Am. Chem. Soc.* **130**:865-874.

- **Sun, Y. and Xia, Y.** (2002) Shape-Controlled Synthesis of Gold and Silver Nanoparticles. *Science.* **298**:2176-2179.

- **Turner, P., Mamo, G. and Karlsson, E.N.** (2007) Potential and Utilization of Themophiles and Thermostable Enzymes in Biorefining. *Microbial Cell Factories.* **6**:9-31.

- **Van Marwijk, J.** (2009) Biological Synthesis of Gold Nanoparticles by *Thermus scotoductus* SA-01. *PhD. Thesis.* University of the Free State. Bloemfontein. South Africa.

CHAPTER 3

EXPRESSION AND CHARACTERIZATION OF AN ABC TRANSPORTER, PEPTIDE-BINDING PROTEIN FROM *THERMUS SCOTODUCTUS* SA-01 IN A MESOPHILIC HOST

3.1 INTRODUCTION

The synthesis of nanoparticles with different chemical compositions, sizes and shapes have become an important part of nanotechnology, however a number of chemical methods that are used in the synthesis protocol are not environmentally friendly and are expensive procedures to use (Sastry *et al*., 2003; Scott *et al.,* 2008; Karn & Bergeson, 2009; Korbekandi *et al*., 2009). Researchers are increasingly making use of biological systems and microorganisms in nanoscience and nanotechnology to develop environmentally friendly methods for nanoparticle production as greener alternatives. These microorganisms have unique potential in the environmental outcome of toxic metals by using several mechanisms for conversion between soluble and insoluble forms and in the production of nanoparticles with different shapes and sizes (Gadd, 2000; Korbekandi *et al*., 2009).

Metal nanoparticles, and in particular gold, being the most stable of the metal nanoparticles, have unique physical and chemical properties and a wide variety of uses, as the material properties at nanoscale differ from that of the bulk form (Daniel & Astruc, 2004; Chen *et al*., 2006). These differences can be due to an increase in relative surface area and these changes then influence the optical, magnetic and electronic properties of the material (Mulholland & Bauer, 2000; Bönnemann & Nagabhushana, 2004; Luther, 2004; Riddin *et al*., 2006; He *et al*., 2008). The unique properties of gold at nanoscale are being used in diverse areas, such as catalysis, biolabeling, nonlinear optical devices and optical recording media, colours and coatings, as well as the biomedical sector, however, worldwide, gold are predominantly used for the making of

jewellery. Therefore by using the properties of gold at the nanoscale, it can result in the use of gold beyond only jewellery to increase its applications in the industry (Butterman & Amey III, 2005).

Microorganisms have been extensively used in biotechnological applications, such as heavy metal bioremediation, biosorption, bioleaching and oxidoreduction of various toxic metals, but a recent addition to these applications is the formation of nanoparticles. These microorganisms can be prokaryotic bacteria, to more complicated eukaryotic fungi and yeast; furthermore, biologically synthesized nanoparticles are generally more polydisperse when compared with chemical methods. (Beveridge & Murray, 1980; Wakatsuki, 1995; Southam & Beveridge, 1996; Gadd, 2000; Tsuruta, 2004; Korbekandi *et al*., 2009). Most of the methods that are used for the production of nanoparticles are still in the development phase and needs to be improved to overcome problems experienced, such as shape and size, size distribution, stability and aggregation of nanoparticles and control of crystal growth. Researchers are aiming to control nanoparticle properties and production through the optimization of a number of parameters, such as temperature, pH, exposure time, biomass, and substrate concentration. These parameters may however influence the growth conditions of the organisms, their cellular activities and enzymatic processes (Korbekandi *et al*., 2009).

A recent discovery by van Marwijk, (2009) revealed that *Thermus scotoductus* SA-01 has the ability to reduce heavy metals with the subsequent formation of nanoparticles. In this case soluble gold(III) was reduced to insoluble elemental gold. This thermophilic bacterium was isolated by Kieft *et al*., (1999) from groundwater samples from Mponeng (a deep South African gold mine in the Witwatersrand Supergroup operated by AngloGold Ashanti) at a depth of 3.2 km, with ambient rock temperature of 60ºC and it was later described by Balkwill *et al*., (2004) as *Thermus scotoductus*. Van Marwijk, (2009) also revealed that *Thermus scotoductus* SA-01 has several membrane proteins as well as several cytoplasmic proteins that participate in the gold reduction and nanoparticle formation process. One of these thermophilic proteins was purified and after N-terminal sequencing, the protein was identified as an ABC transporter, peptide-binding protein. This protein was overexpressed in the mesophilic expression host, *Escherichia coli*, and initial characterization was done. Particles were produced that

differ in size, shape, amount and distribution but the control of these particles were not optimal, in fact, very little control was possible with the purified and expressed protein.

This chapter describes the overexpression of the ABC transporter, peptide-binding protein, identified in *Thermus scotoductus* SA-01, in the mesophilic expression host, *Escherichia coli* and subsequent characterization of gold reduction and nanoparticle formation.

3.2 MATERIALS AND METHODS

3.2.1 Bacterial Strains and Culture Conditions

All bacterial strains used for cloning and expression can be seen in table 3.1. *Thermus scotoductus* SA-01 (ATCC 700910) was cultured from a 20% glycerol stock (maintained at -80ºC) on a complex, organic medium, TYG [5 $g.L^{-1}$ tryptone (Biolab); 3 $g.L^{-1}$ yeast extract (Biolab); 1 $g.L^{-1}$ glucose (Saarchem) and 18 $g.L^{-1}$ bacteriological agar (Biolab), pH 7.0], and incubated for 24 hours at 65ºC. A loop full of the growth was then used to prepare the pre-inoculum in 50 ml TYG broth in a 250 ml Erlenmeyer flask and incubated at 65ºC, with aeration (200 rpm) for ± 8 hours (until the mid-exponential growth phase was reached). The pre-inoculum (10 ml) was added to 90 ml TYG broth in a 500 ml Erlenmeyer flask to prepare the inoculum, and incubated at 65ºC, with aeration (200 rpm) for again ± 8 hours to reach the mid-exponential growth phase.

Escherichia coli TOP10 (Invitrogen) were used as a host for cloning of the protein and *E. coli* BL21(DE3) (Lucigen) were used as a host for expression of the protein at 37ºC. These strains were grown in Luria-Bertani (LB) medium [10 $g.L^{-1}$ tryptone (Biolab); 5 $g.L^{-1}$ yeast extract (Biolab) and 10 $g.L^{-1}$ NaCl (Saarchem), pH 7.0] (Sambrook *et al.*, 1989), at 37ºC with aeration (200 rpm). Ampicillin (100 $\mu g.ml^{-1}$) or kanamycin (30 $\mu g.ml^{-1}$) was added when required.

3.2.2 Plasmids

All plasmids used for cloning and expression studies are described in table 3.1. Plasmid pGEM®-T Easy (Promega) were used for sub-cloning of the gene into *E. coli* and plasmids pET-22b(+) and pET-28b(+) (Novagen) were used to express the gene in *E. coli* BL21(DE3). The pET-22b(+) vector was used for expression without any His-Tags by cloning into the vector between the *Eco*RI and *Nde*I sites and contains an ampicillin resistance gene (Figure 3.1). The pET-28b(+) vector was used for expression with a N-terminal His-Tag by cloning into the vector between the *Eco*RI and *Nde*I sites and contains a kanamycin resistance gene (Figure 3.2).

Table 3.1: Bacterial strains and plasmids used for cloning and expression in a mesophilic host.

Strain or plasmid	Description	Reference
Strain		
• *Thermus scotoductus* SA-01		ATCC 700910
• *Escherichia coli* TOP10	One Shot Top10 chemically Competent cells	Invitrogen
• *Escherichia coli* BL21 (DE3)	*E. coli* EXPRESS BL21(DE3) Chemically competent cells	Lucigen
Plasmid		
• pGEM®-T Easy	Amp^r, T7 and SP6 promoter, *Lac*Z, ori, 3018 bp	Promega
• pET-22b(+)	Amp^r, T7 promoter and Terminator, *Lac*I, ORI ColE1 5493 bp	Novagen
• pET-28b(+)	Kan^r, T7 promoter and Terminator, *Lac*I, N-terminal His-Tag, ORI ColE1, Thrombin configuration 5368 bp	Novagen

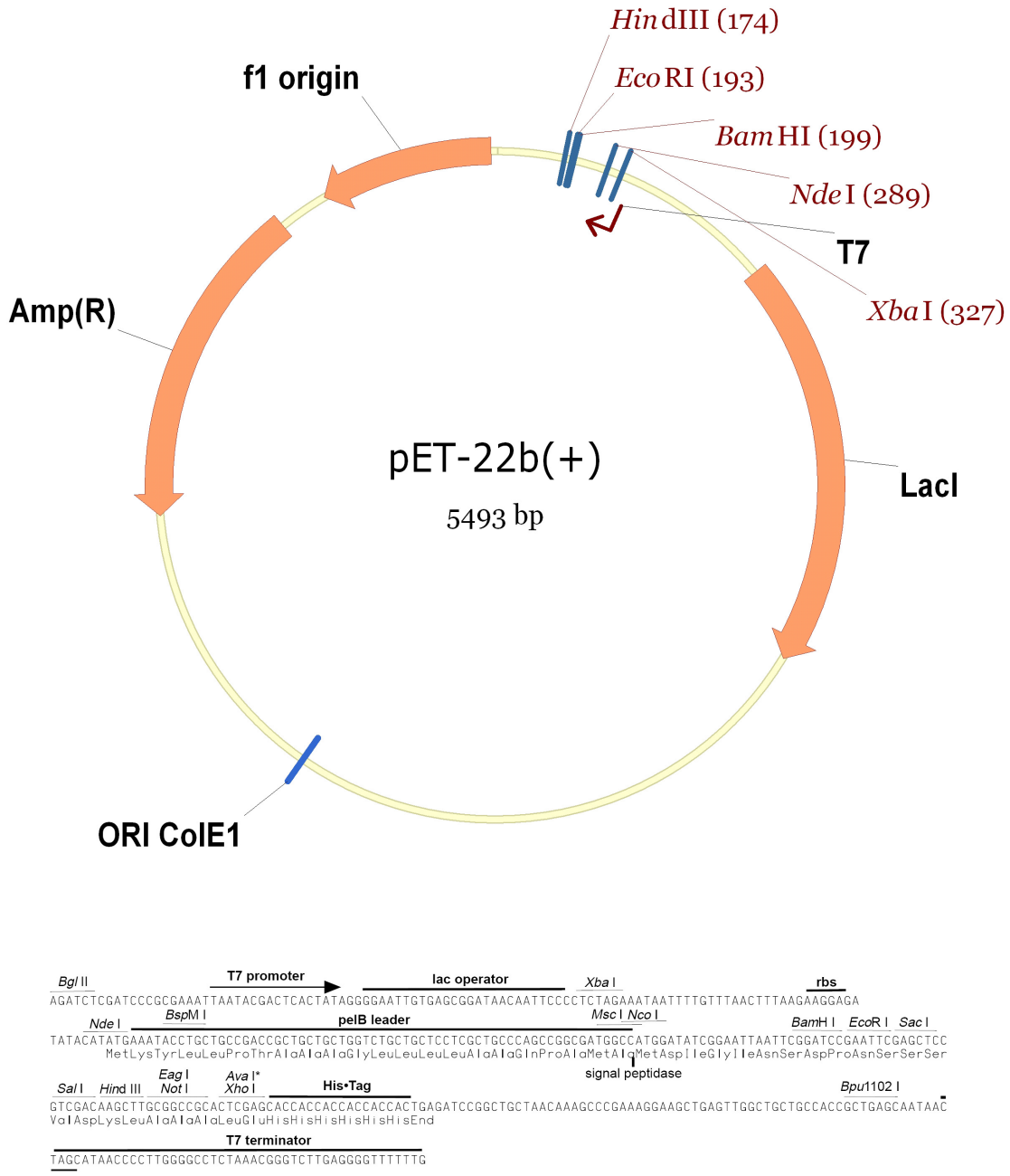

Figure 3.1: Vector map of pET-22b(+), indicating the ampicillin resistance gene, the ColE1 origin of plasmid replication, the *Lac*I coding site and the multiple cloning site under the T7 promoter. Sequence of the pET-22b(+) cloning region, showing the *Eco*RI and *Nde*I sites where the gene was inserted to yield a construct with no His-Tag.

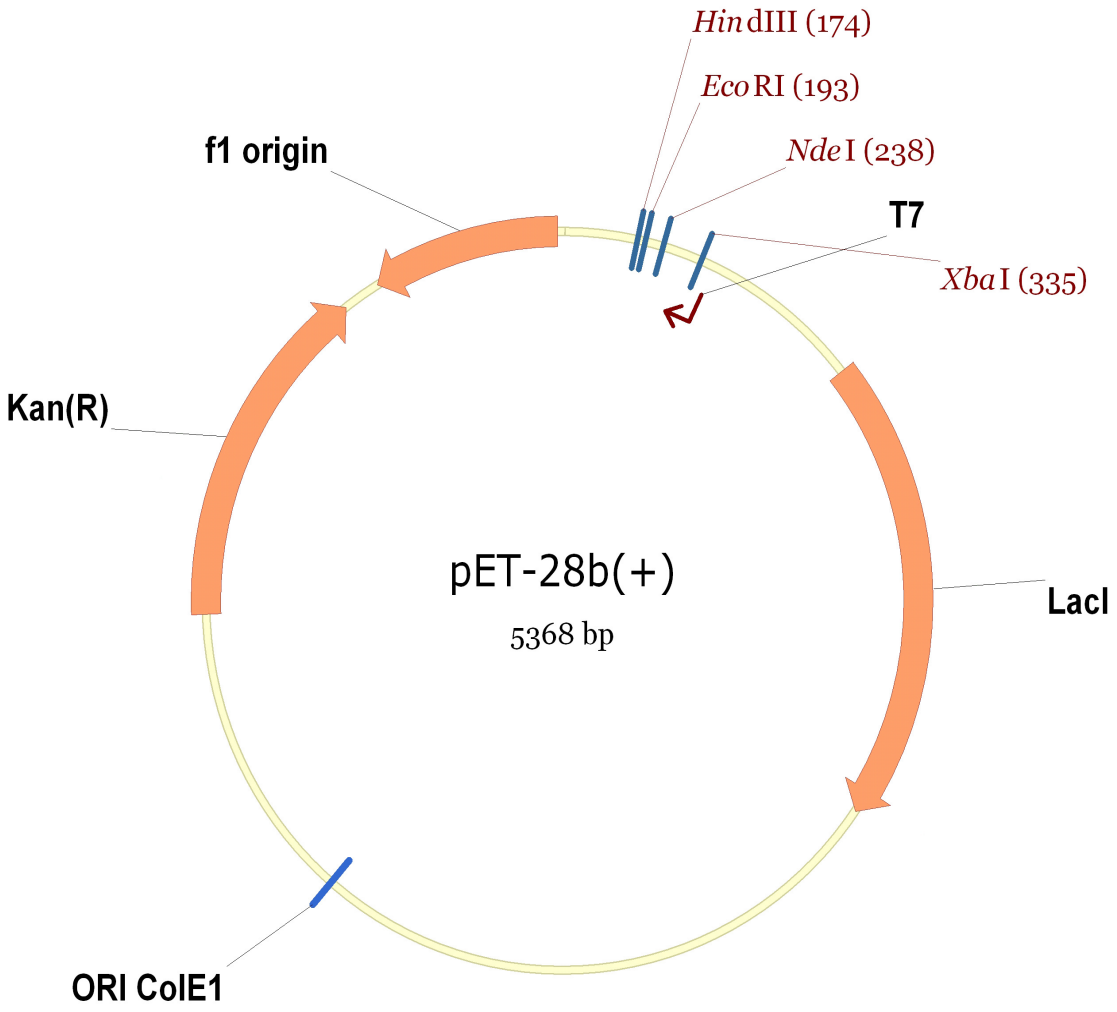

Figure 3.2: Vector map of pET-28b(+), indicating the kanamycin resistance gene, the ColE1 origin of plasmid replication, the *Lac*I coding site and the multiple cloning site under the T7 promoter. Sequence of the pET-28b(+) cloning region, showing the ribosome binding site, the thrombin cleavage site fusion and the *Eco*RI and *Nde*I sites where the gene was inserted to yield a construct with a N-terminal His-Tag.

3.2.3 Genomic DNA Isolation

Genomic DNA (gDNA) was isolated from *T. scotoductus* SA-01, using an adapted SDS-proteinase K method of Towner, (1991). Cells were harvested from the mid-exponential growth phase using centrifugation (3000 *x g*; 10 minutes; 4ºC) and washed in TE-buffer [10 mM Tris-HCl; 1 mM ethylene diaminetetraacetic acid (EDTA), pH 8.0]. The cell pellet was resuspended in resuspension buffer [50 mM Tris-HCl (pH 8.0), containing 0.7 mM sucrose] in a 6.4 ml:1 g (wet weight) ratio. Lysozyme was added to a final concentration of 3.2 $mg.ml^{-1}$ and placed on ice for 5 minutes. EDTA (68 mM final concentration) and sodium dodecyl sulphate (SDS) (1% final concentration) were added, the sample was mixed gently and again placed on ice for 5 minutes. 10 ml digestion buffer [1% SDS; 50 mM Tris-HCl (pH 8.0); 0.1 M EDTA; 0.2 M NaCl and 0.5 $mg.ml^{-1}$ proteinase K] was added to the mixture for every 0.5 g cells (wet weight) and incubated overnight with gentle shaking at 55℃. pH calibrated phenol (the pH of the upper aqueous phase must be less than 7.2) was added (1 x sample volume) to the sample and mixed for 3 hours at room temperature. The sample was centrifuged (4000 *x g;* 10 minutes; room temperature) to separate the aqueous and organic phases. The aqueous phase was transferred to a new tube and 1x sample volume phenol:chloroform:isoamyl alcohol [25:24:1 (v/v/v)] was added and mixed by inverting. The sample was centrifuged (4000 *x g;* 10 minutes; room temperature) and the aqueous phase transferred to a new tube. This was placed on ice for 5 minutes and 1:10 (v/v) 5 M NaCl (pH 5.7) and 10 ml high purity, ice cold ethanol (EtOH) was added. The precipitated DNA was spooled from the suspension and placed in a 1.5 ml tube. The spooled DNA was washed two times with 70% ethanol (1 ml) and centrifuged (12 000 rpm; 1 minute; 4℃). The resulting DNA pellet was air dried and dissolved in 50 mM Tris-HCl buffer (pH 8), by incubation for 1 hour at 50℃. RNase A was added to a final concentration of 20 $\mu g.ml^{-1}$ and incubated at 37ºC for 1 hour. The DNA integrity was evaluated using agarose gel electrophoresis. All of the agarose gels used in this study consisted of 1% agarose in TAE buffer (0.04 M Tris-HCl; 1 mM EDTA, pH 8.0 and 0.021 mM glacial acetic acid) with 0.6 $\mu g.ml^{-1}$ ethidium bromide (EtBr). gDNA (10 µl) was added to 2 µl loading dye (Fermentas) before separated in the gel at 5.6 $V.cm^{-1}$ for 60 minutes. Either MassRuler™ DNA ladder or GeneRuler™ DNA ladder (Fermentas) was used to determine the size of the bands visualized under a high frequency UV source (ChemiDoc XRS Gel Documentation

system with Quantity One V4.5 software, BIO-RAD). The concentration of the DNA was determined, using the NanoDrop® Spectrophotometer ND-1000.

3.2.4 Polymerase Chain Reaction

All primers used for cloning and expression studies can be seen in table 3.2. Polymerase chain reaction (PCR) was done on the gDNA isolated from *T. scotoductus* SA-01, to amplify the complete ABC transporter, peptide-binding gene. The PCR was performed in a total reaction volume of 50 µl, using a Thermal Cycler (PxE 0.2, Thermo Electron Corporation). The oligonucleotide primers used (Primers 1 and 2, Table 3.2) were designed to yield constructs that included the leader peptide and contained no His-Tag when expressed in pET-22b(+) and a N-terminal His-Tag when expressed with the pET-28b(+) vector (Table 3.3). This was done to determine the influence (if any) of the His-Tag on gold reduction and nanoparticle formation.

The reaction mixture consisted out of 5 µl Super-Therm reaction buffer (10x), 5 µl $MgCl_2$ (25 mM), 5 µl dNTPs (10 mM), Super-Therm polymerase (2.5 U), 1 µl of both the forward (ABC_F_Nde) and reverse (ABC_R_Eco) primers (10 µM each) (Table 3.2), 50 $ng.\mu l^{-1}$ template and sterile double distilled water (ddH_2O) filled to the reaction volume.

Table 3.2: Oligonucleotide primers used for PCR amplification and sequencing. Underlined sequences indicate the introduced restriction sites for *Nde*I and *Eco*RI in primers 1 and 2 respectively.

Primer	Nucleotide sequence	Tm (ºC)
1. ABC_F_Nde	5'- CAT ATG AGA AAA GTA GGC AAG CTG GCT G -3'	59.5
2. ABC_R_Eco	5'- GAA TTC TTA CTT GAC GGA AAG AGC GTA C -3'	57.4
3. ABC_Int_F	5'- AGG ATG CGG AGA GGC TC -3'	56.9
4. ABC_Int_R	5'- CGC TGG ATG TAG TCG TCG -3'	55.4
5. T7 Terminator	5'- GCT AGT TAT TGC TCA GCG G -3'	53.4
6. T7 Promoter	5'- TAA TAC GAC TCA CTA TAG GG -3'	47.5

Reaction conditions consisted of an initial denaturing step at 95ºC for 5 minutes, followed by 30 cycles of denaturing at 95ºC (30 seconds), annealing at 55ºC (40 seconds) and elongation at 72ºC (2.5 minutes). A final elongation step of 10 minutes at 72ºC was added to ensure complete elongation of the amplified product. The DNA was visualized on a 1% agarose gel as described in section 3.2.3. Purification of the PCR product was achieved by excising the desired band (± 1.9 kb) from the agarose gel, using a non-UV transilluminator (Dark Reader™ transilluminator DR-45M, Clare Chemical Research) and extracted using the BioSpin Gel Extraction Kit (BioFlux), as per manufacturer's instructions.

Table 3.3: Constructs obtained when using a combination of primers 1 and 2 with the pET-22b(+) and pET-28b(+) vectors respectively.

Primers	**pET22b(+)**	**pET28b(+)**
1 & 2*	- N-terminal His-Tag - C-terminal His-Tag + Leader peptide	+ N-terminal His-Tag - C-terminal His-Tag + Leader peptide

* Numbers correspond to primer numbers indicated in Table 3.2.

3.2.5 Ligation into pGEM®-T Easy

The ± 1.9 kb PCR product, purified from the agarose gel, was ligated into the pGEM®-T Easy Vector system (Promega), as per manufacturer's instructions. The ligation reaction was performed in a total reaction volume of 10 µl and consisted out of 2x Rapid Ligation Buffer (5 µl), pGEM®-T Easy Vector (2.5 ng), PCR product (3 µl) and T4 DNA Ligase (0.3 Weiss units). The ligation reactions were incubated overnight at 4ºC.

3.2.6 Preparation of *Escherichia coli* TOP10 and BL21(DE3) Competent Cells

Competent *E. coli* One Shot TOP10 (Invitrogen) and *E. coli* EXPRESS BL21(DE3) (Lucigen) cells were prepared according to the method described by Hanahan, (1983) with modifications. Flasks containing Psi broth (5 $g.L^{-1}$ yeast extract (Biolab), 20 $g.L^{-1}$ tryptone (Biolab), 5 $g.L^{-1}$ magnesium sulphate (Saarchem), pH 7.6 with KOH) were

inoculated with 1 ml of an overnight culture and grown at 37℃, with aeration (200 rpm) until an absorbance of 0.6 at 600 nm was reached. Cells were placed on ice for 30 minutes and centrifuged (3 000 *x g*; 10 minutes; 4℃) to collect cells. Cells were resuspended in 40 ml TfbI buffer (30 mM potassium acetate; 100 mM rubidium chloride; 10 mM calcium chloride and 15% glycerol, pH 5.8) and incubated on ice for 15 minutes. Cells were collected through centrifugation (3 000 *x g*; 10 minutes; 4℃) and resuspended in 4 ml TfbII buffer (10 mM MOPS-NaOH; 75 mM calcium chloride; 10 mM rubidium chloride and 15% glycerol, pH 6.5). The cell suspensions were incubated on ice for 10 minutes, aliquoted and snap frozen in liquid nitrogen followed by storage at -80℃ until used.

3.2.7 Transformation into *Escherichia coli* TOP10

A stock (50 µl) of the *E. coli* One Shot TOP10 competent cells was removed from the -80ºC and allowed to thaw on ice. The ligated plasmid reactions (5 µl) were added to the cells and incubated on ice for 30 minutes. This was also done for a negative control, containing no plasmid and positive controls [for both pET-22b(+) and pET-28b(+)], containing empty plasmid. The cell suspension was heat shocked for 40 seconds at 42ºC and immediately placed back in ice-water for 2 minutes. 250 µl SOC medium (20 $g.L^{-1}$ tryptone; 5 $g.L^{-1}$ yeast extract; 0.01 M NaCl; 0.0025 M KCl; 0.01 M $MgCl_2$; 0.01 M $MgSO_4$ and 0.02 M glucose) was added to the transformation reactions and incubated for 60 minutes at 37ºC, with gentle shaking. Different volumes were plated out on separate LB plates, containing ampicillin (60 $\mu g.ml^{-1}$), isopropyl β-D-1-thiogalactopyranoside (IPTG, 9.6 $\mu g.ml^{-1}$) and 5-bromo-4-chloro-3-indolyl-beta-D-galactopyranosidehosphate (X-Gal 40 $\mu g.ml^{-1}$) and incubated overnight at 37ºC to verify DNA ligation using blue/white selection.

3.2.8 Evaluation of the Insert Size

To evaluate the ligated insert sizes, 10 single white colonies were separately inoculated into 5 ml LB medium, containing ampicillin (60 $\mu g.ml^{-1}$) and incubated overnight at 37ºC with aeration (200 rpm). Plasmids were isolated using the BioSpin Plasmid DNA Extraction Kit (BioFlux), as per manufacturer's instructions. Double digestion was done

on the plasmids, using the restriction enzymes *Eco*RI and *Nde*I (Fermentas). The digestion reaction was performed in a total reaction volume of 50 µl and consisted out of 10 µl purified plasmid, 5 µl buffer O, 2.5 µl of each restriction enzyme and sterile ddH_2O filled to the reaction volume. The reaction mixture was incubated at 37ºC for 3 hours, after which the enzymes were heat activated at 65ºC for 20 minutes. The restriction digestions were visualized on a 1% agarose gel as described in section 3.2.3. Purification of the insert was achieved by excising the desired band (± 1.9 kb) from the agarose gel, using a non-UV transilluminator (Dark Reader™ transilluminator DR-45M, Clare Chemical Research) and extracted using the BioSpin Gel Extraction Kit (BioFlux), as per manufacturer's instructions.

3.2.9 Preparation of the pET-22b(+) and pET-28b(+) Expression Plasmids

pET-22b(+) and pET-28b(+) (Novagen) was used as expression vectors in *E. coli*. The vectors were propagated by transforming 2 µl into *E. coli* One Shot TOP10 competent cells as described in section 3.2.7. Selective pressure was maintained by using LB plates containing 100 $\mu g.ml^{-1}$ ampicillin [pET-22b(+)] or 30 $\mu g.ml^{-1}$ kanamycin [pET-28b(+)]. Single white colonies were separately inoculated into 5 ml LB medium, containing the required antibiotic and incubated overnight at 37ºC with aeration (200 rpm). Plasmids were isolated using the BioSpin Plasmid DNA Extraction Kit (BioFlux), as per manufacturer's instructions. Double digestion was done on the plasmids, using the restriction enzymes *Eco*RI and *Nde*I (Fermentas), as described in section 3.2.8. The restriction digestions were visualized on a 1% agarose gel as described in section 3.2.3. Purification of the plasmid was achieved by excising the desired bands (± 5.5 kb) from the agarose gel, using a non-UV transilluminator (Dark Reader™ transilluminator DR-45M, Clare Chemical Research) and extracted using the BioSpin Gel Extraction Kit (BioFlux), as per manufacturer's instructions.

The ± 1.9 kb insert, purified from the agarose gel, was separately ligated into the pET-22b(+) and pET-28b(+) expression vectors. The ligation reaction was performed in a total reaction volume of 20 µl and consisted out of 10x Rapid Ligation Buffer (1 µl), pET-22b(+)/pET-28b(+) vector (6 µl), insert (5 µl), T4 DNA Ligase (0.3 Weiss units) and sterile ddH_2O filled to the reaction volume. The ligation reactions were incubated overnight at 4ºC. The ligated plasmid reactions (5 µl) were transformed into *E. coli* One

Shot TOP10 competent cells as described in section 3.2.7. Selective pressure was maintained by using LB plates, containing 100 µg.ml^{-1} ampicillin [pET-22b(+)] or 30 µg.ml^{-1} kanamycin [pET-28b(+)].

3.2.10 Evaluation of the Insert Size

To evaluate the ligated insert sizes, 10 single white colonies for each vector, were separately inoculated into 5 ml LB medium, containing 100 µg.ml^{-1} ampicillin [pET-22b(+)] or 30 µg.ml^{-1} kanamycin [pET-28b(+)] and incubated overnight at 37ºC with aeration (200 rpm). Plasmids were isolated using the BioSpin Plasmid DNA Extraction Kit (BioFlux), as per manufacturer's instructions. Double digestion was done on the plasmids, using the restriction enzymes *Eco*RI and *Nde*I (Fermentas), as described in section 3.2.8. The restriction digestions were visualized on a 1% agarose gel as described in section 3.2.3. Purification of the insert was achieved by excising the desired band (± 1.9 kb) from the agarose gel, using a non-UV transilluminator (Dark Reader™ transilluminator DR-45M, Clare Chemical Research) and extracted using the BioSpin Gel Extraction Kit (BioFlux), as per manufacturer's instructions.

3.2.11 Sequencing

The purified inserts were sequenced for confirmation of the nucleotide composition of the ABC transporter, peptide-binding gene. Sanger sequencing was done using the ABI Prism® Big Dye™ Terminator Cycle Sequencing Ready Reaction Kit V.3.1 (Applied Biosystems), as per manufacturer's instructions. The primers used in the sequence reaction can be seen in table 3.2, (Primers 3 – 6). The reaction was performed in a total volume of 10 µl and consisted out of 0.5 µl premix, 2 µl dilution buffer, 1 µl primer (3.2 pmol.µl^{-1}), template (200-500 ng.µl^{-1}) and sterile ddH_2O filled to the reaction volume. Reaction conditions consisted of an initial denaturing step at 96ºC for 1 minute, followed by 25 cycles of denaturing at 96ºC (10 seconds), annealing at 50ºC (5 seconds) and elongation at 60ºC (4 minutes).

The PCR product was purified, using an EDTA/EtOH precipitation protocol for sequencing cleanup, as per manufacturer's instructions. The sequencing reaction

volume was adjusted to 20 µl and added to 5 µl EDTA with 60 µl absolute ethanol and mixed for 5 seconds before allowing precipitating for 15 minutes at room temperature. The mixture was then centrifuged (20 000 *x g;* 10 minutes; 4ºC) and the supernatant was removed through aspiration, without disturbing the pellet. 70% ethanol (60 µl) was added to the pellet and centrifuged again (20 000 *x g;* 5 minutes; 4ºC). The supernatant was again removed through aspiration and the pellet was dried for 5 minutes, using a Concentrator 5301 (Eppendorf). The samples were stored in the dark at 4ºC until used.

Sequencing reactions were done with a 3130*xl* Genetic Analyzer, HITACHI (Applied Biosystems). The data was analyzed and contigs were formed, using ContigExpress (Vector NTI Suite 9). Analyzed sequences were used to search the Genbank Database (NCBI, 2009) and alignments were done using ClustalW2 (EBI, 2009).

3.2.12 Transformation into *Escherichia coli* BL21 (DE3)

The ligated plasmid reactions (5 µl) were transformed into *E. coli* EXPRESS BL21(DE3) competent cells as described in section 3.2.7. Selective pressure was maintained by using LB plates, containing 100 $\mu g.ml^{-1}$ ampicillin [pET-22b(+)] or 30 $\mu g.ml^{-1}$ kanamycin [pET-28b(+)].

3.2.13 Expression and Fractionation of the ABC Transporter, Peptide-Binding Protein

Positive clones for the constructs in pET-22b(+) and pET-28b(+) were identified through selection on LB plates containing 100 $\mu g.ml^{-1}$ ampicillin [pET-22b(+)] or 30 $\mu g.ml^{-1}$ kanamycin [pET-28b(+)] and inoculated into LB medium with the required antibiotic. Cells were incubated at 37ºC with aeration (200 rpm) until an OD_{600} of approximately 0.8 - 1 was reached. IPTG was added as inducer to a final concentration of 1 mM and cells was again incubated at 37ºC with aeration (200 rpm), for an additional four hours and samples were collected every two hours for SDS-PAGE analysis. Cells were harvested through centrifugation (5500 rpm; 15 minutes; 4ºC) and washed using 50 mM phosphate buffer (pH 7.4). The same was done with empty pET-22b(+) and pET-28b(+) vectors that was used as negative controls.

Harvested cells were dissolved in 60 ml phosphate buffer (50 mM, pH 7.4) and complete EDTA free protease inhibitor cocktail was added. Cells were broken by using a One Shot Constant Cell disruption system and the unbroken cells and debris were removed through centrifugation (6000 rpm; 15 minutes, 4ºC). The soluble fraction (cytoplasm) was separated from the insoluble fraction (membranes) through ultracentrifugation (30 000 rpm; 90 minutes, 4ºC). Van Marwijk, (2009) revealed that the activity was found in the soluble fraction and therefore the supernatant was used for further experiments.

3.2.14 Purification of the ABC Transporter, Peptide-Binding Protein

3.2.14.1 Expression in pET-22b(+)

The soluble fraction for expression in pET-22b(+) was heat shocked for 90 minutes at 70ºC. The denatured proteins were separated from the thermal stable proteins (supernatant), by centrifugation (12000 *x g*; 30 minutes; 4℃). The supernatant was concentrated to 3 ml using an Amicon stirrer with a 30 kDa MWCO membrane (Osmonics Inc.). The 3 ml concentrated sample was loaded onto a size-exclusion, Sephacryl S200HR (Gel-filtration) column (2.5 x 63 cm, Sigma) equilibrated with 50 mM phosphate buffer (pH 7.4), containing 50 mM NaCl. Proteins were eluted using the same buffer at a flow speed of 0.5 $ml.min^{-1}$. Fractions were collected for protein concentrations, SDS-PAGE analysis and characterization. Before characterization, all the fractions that contained the correct protein and showed gold reduction activity (as described in section 3.2.15.3), were pooled and dialysed overnight with 50 mM phosphate buffer (pH 7.4), using SnakeSkin® Pleated Dialysis Tubing with a 10 kDa MWCO membrane (Thermo Scientific), to remove the NaCl.

3.2.14.2 Expression in pET-28b(+)

The soluble fraction for expression in pET-28b(+) was loaded onto a 5 ml Nickel NTA (HisTrapFF) column (Amersham Biosciences) and unbound proteins eluted at a flow speed of 5 $ml.min^{-1}$ with 20 mM phosphate buffer (pH 7.4), containing 20 mM imidazole and 0.5 M NaCl. Bound proteins were subsequently eluted in the same buffer using a linear gradient (100 ml) of imidazole up to 0.5 M. Fractions were collected for SDS-

PAGE analysis, pooled and concentrated to 3 ml using an Amicon stirrer with a 30 kDa MWCO membrane (Osmonics Inc.). The 3 ml concentrated sample was loaded onto a size-exclusion, Sephacryl S200HR (Gel-filtration) column (2.5 x 63 cm, Sigma) equilibrated with 50 mM phosphate buffer (pH 7.4), containing 50 mM NaCl. Proteins were eluted using the same buffer at a flow speed of 0.5 $ml.min^{-1}$. Fractions were collected for protein concentrations, SDS-PAGE analysis and characterization. Before characterization, all the fractions that contained the correct protein and showed gold reduction activity (as described in section 3.2.15.3), were pooled and dialysed overnight with 50 mM phosphate buffer (pH 7.4), using SnakeSkin® Pleated Dialysis Tubing with a 10 kDa MWCO membrane (Thermo Scientific), to remove the NaCl.

3.2.15 Characterization of the ABC Transporter, Peptide-Binding Protein in *Escherichia coli*

Unless otherwise mentioned, all characterization steps were carried out on the protein expressed in both the pET-22b(+) and pET-28b(+) vectors.

3.2.15.1 SDS-PAGE Analysis

The homogeneity of the proteins present in each fraction was determined by sodium dodecyl sulphate polyacrylamide gel electrophoresis (SDS-PAGE) analysis. A 10% separating gel and 4% stacking gel was used to determine the relative molecular mass (Mr) of each of the resulting proteins by comparing their electrophoretic mobility with a commercially available SDS-PAGE molecular weight standard (Precision Plus Protein™ Standards, Unstained, BIO-RAD). SDS-PAGE analysis was done using the Hoefer SE 200 Mighty Small miniature slab gel electrophoresis unit (Hoefer Scientific Instruments). SDS-PAGE analysis was performed as described by Laemmli, (1970) and the protein band detection was done by Coomassie staining (Fairbanks *et al.,* 1971).

3.2.15.2 Protein Concentrations

Protein concentrations of the fractions were determined using the Micro BCA™ Protein Assay Kit (PIERCE) (Smith *et al.,* 1985). This assay is a detergent-compatible

formulation based on bicinchoninic acid (BCA) for the colorimetric detection and quantitation of total protein. The working reagent (WR) solution was prepared by mixing 50 parts of reagent A with 1 part of reagent B (50:1, reagent A:B). 1 ml of the WR was added to 50 µl of the sample (20:1, WR:sample) and incubated at 60ºC for 30 minutes. After incubation, the samples were left to cool to room temperature and the absorbance was measured at 562 nm, using a Spectronic® Genesys™ 5 spectrophotometer. The total protein concentration was determined using a standard curve that was constructed in the same way, but on a series of dilutions from a 2 $mg.ml^{-1}$ bovine serum albumin (BSA) stock (Figure 3.3).

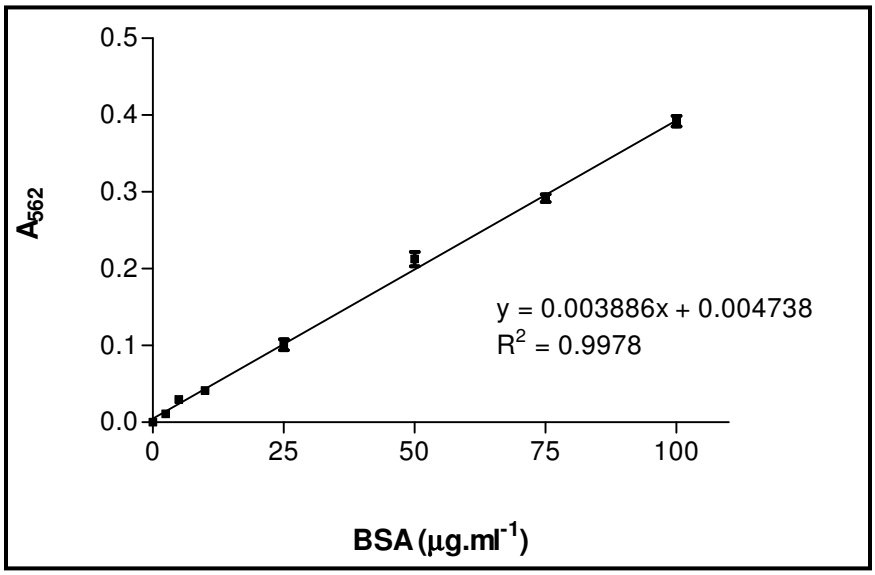

Figure 3.3: Standard curve for the Micro BCA™ protein assay kit (PIERCE) at 60ºC, using BSA as protein standard. Error bars indicate standard deviations and are smaller than the symbols used.

3.2.15.3 Gold Reduction Assay

All the activity tests on the different fractions collected in section 3.2.14, as well as the effect on gold reduction and nanoparticle formations, tested with different parameters in sections 3.2.15.9 – 3.2.16 were done using the gold reduction assay. This assay was developed by van Marwijk, (2009) through modifications of the nitrate assay from Showe & DeMoss, (1968).

To determine if the protein solutions had gold(III) reducing and nanoparticles production capabilities, van Marwijk, (2009) adapted the nitrate assay, by adding 100 µl purified protein (100 $\mu g.ml^{-1}$) to the following reaction mixture: 100 µl phosphate buffer (50 mM; pH 7.4), 100 µl gold(III) ($HAuCl_4$; 20 mM), 100 µl methyl viologen (1 µM) and 500 µl ddH_2O. The reaction was started by adding 100 µl sodium dithionite (46 µM), dissolved in sodium hydrogen carbonate (100 µM), to the reaction mixture. After slowly inverting the mixture it was incubated at 65°C for 24 hours, the reaction was stopped by shaking the tube to oxidize the remaining dithionite and reduced methyl viologen. The formation of a pink/purple to blue colour indicated gold reduction and nanoparticle production (Showe & DeMoss, 1968; Lazarides & Schatz, 2000). For every sample tested, a blank reaction was prepared in the same way, but using an additional 100 µl phosphate buffer (50 mM; pH 7.4) instead of the protein. The pH was confirmed before and after the assay to be approximately between 7. 2 – 7.6.

3.2.15.4 Surface Plasmon Resonance

From literature it is known that gold nanoparticles exhibit pink-purple colours, which arises due to excitation of surface plasmon vibrations in the gold nanoparticles (Figure 3.4). UV-Vis spectroscopy can be used to record this distinct band in the visible electronic spectrum, known as the surface plasmon resonance (SPR) band of the gold nanoparticles (Figure 3.5). The surface plasmon is a quantized plasma oscillation taking place at the surface of the gold particle, giving a distinctive peak location at maximal absorbance (*A*) and peak width. The SPR wavelength and width depend on the particle diameter and any increase in the average diameter of the particles, results in a red shift of the SPR wavelength together with a decrease in maximal *A*. Therefore particles characterized by interparticle distances larger than the average particle diameter appears red and when the interparticle distance in aggregates decreases to less than approximately the average particle diameter, the colour changes to blue (Figure 3.4) (Englebienne, 1998; Mukherjee *et al.*, 2002; Husseiny *et al.*, 2007; Del Fatti *et al.*, 2008).

To verify gold reduction and nanoparticle formation, UV-Vis wave scans in the range of 300-800 nm was done on all the parameters tested in sections 3.2.15.9 – 3.2.16 and spectrums were obtained using a SpectraMax M2 UV-Vis Scanner (Labotec), to

evaluate the plasmon band associated with gold-nanoparticles. The SPR was used to determine which samples were subjected to downstream analysis.

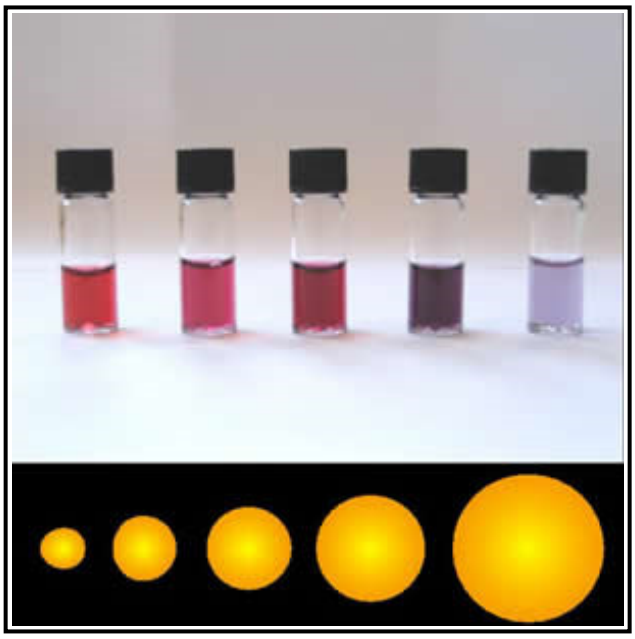

Figure 3.4: An increase in the size of nanoparticles results in a change of colour, from pink, to purple, to blue, due to the surface plasmon vibrations of the gold nanoparticles (Taken from http://www.webexhibits.org).

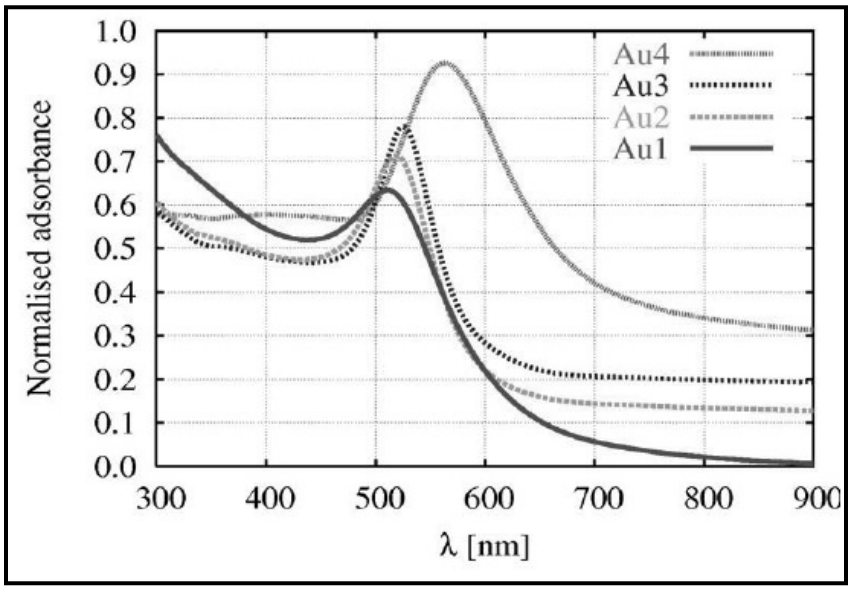

Figure 3.5: UV-Vis spectra of colloidal gold. An increase in the size of nanoparticles results in a shift to bigger wavelengths and forming bigger peaks. Au1 will represent the pink colour in Figure 3.4 and Au4 to the blue colour (Taken from Šlouf *et al.*, 2006).

3.2.15.5 Transmission Electron Microscopy

Transmission electron microscopy (TEM) analysis was done on specific samples, selected *via* SPR analysis, from the gold reduction and nanoparticle formations, tested with different parameters in sections 3.2.15.9 – 3.2.16. This was carried out on Formvar carbon-coated 200-mesh copper grids, by placing a drop of the sample, washed and resuspended in sterile ddH_2O, on the grid and removed after two minutes, using filter paper. The grid was allowed to air-dry before TEM analysis. Electron micrographs of the gold nanoparticles were taken with either a JEOL TEM 1010, 60 kV or 200 kV Philips CM 20 TEM, by the University of Ghent (Ghent, Belgium) and NMMU (Port Elizabeth, South Africa) respectively. TEM was done to evaluate the size and morphology of the nanoparticles.

3.2.15.6 Energy Dispersive X-ray Spectrometry and Selected-Area Electron Diffraction

Energy dispersive X-ray spectrometry (EDX) and selected-area electron diffraction (SAED) analysis was done on specific samples, selected *via* SPR analysis, from the gold reduction and nanoparticle formations, tested with different parameters in sections 3.2.15.9 – 3.2.16. This was used to identify the chemical composition of the particles present in the samples and their relative amounts, and was done using an EDAX DX4 energy dispersive X-ray spectrometry system, coupled to a 200 kV Philips CM 20 TEM, by the NMMU (Port Elizabeth, South Africa).

3.2.15.7 Nanotrac Particle Size Analyzer

Only three samples were analyzed, using a Microtrac-Nanotrac 251 Ultra particle size analyzer with a 1 nm – 6.5 µm measurement range. Data were analyzed, using the Microtrac Flex 10.5.4 software. These samples were analyzed in Germany, with the courtesy of Swiss Lab (Pty) Ltd (Midrand, Johannesburg, South Africa). The Nanotrac was used to determine the size and size distribution of the particles present in the samples.

3.2.15.8 Scanning Auger Nanoprobe

Only one sample from the protein expressed in pET-28b(+) was analyzed, using the PHI 700 Scanning Auger Nanoprobe, courtesy of the Department of Physics from the University of the Free State (Bloemfontein, South Africa). The nanoprobe used a 25 kV 20 nA electron beam, together with scanning electron microscopy (SEM) to identify the elements in the sample and to give an idea about the shape and size of the particles present in the sample.

3.2.15.9 The Effect of Methyl Viologen Concentrations on Gold Reduction and Nanoparticle Formation

The effect of different methyl viologen concentrations on gold reduction and nanoparticle formation was evaluated with the gold reduction assay as described in section 3.2.15.3, by keeping the sodium dithionite concentration constant and varying the methyl viologen concentrations from 0 – 4.6 µM. Methyl viologen was used as an intermediate by accepting electrons from sodium dithionite to form a free radical which in turn then acts as an electron donor and reducing agent. In the absence of sodium dithionite, methyl viologen acted as an electron donor and reducing agent. UV-Vis spectrums were obtained as described in section 3.2.15.4 and selected samples were subjected for TEM, EDX and SAED analysis as described in sections 3.2.15.5 and 3.2.15.6 respectively.

3.2.15.10 The Effect of Sodium Dithionite Concentrations on Gold Reduction and Nanoparticle Formation

The effect of different sodium dithionite concentrations on gold reduction and nanoparticle formation was evaluated with the gold reduction assay as described in section 3.2.15.3, by keeping the methyl viologen concentration constant and varying the sodium dithionite concentrations from 0 – 6 µM. Sodium dithionite was used as an electron donor and reducing agent. UV-Vis spectrums were obtained as described in section 3.2.15.4 and selected samples were subjected for TEM, EDX and SAED analysis as described in sections 3.2.15.5 and 3.2.15.6 respectively.

3.2.15.11 The Effect of Protein Concentrations on Gold Reduction and Nanoparticle Formation

The effect of protein concentrations on gold reduction and nanoparticle formation was evaluated with the gold reduction assay as described in section 3.2.15.3, but by using protein concentrations varying from 0 – 50 $\mu g.ml^{-1}$. Protein concentrations were determined as described in section 3.2.15.2. UV-Vis spectrums were obtained as described in section 3.2.15.4 and selected samples were subjected for TEM, EDX and SAED analysis as described in sections 3.2.15.5 and 3.2.15.6 respectively.

3.2.15.12 The Effect of Denatured Protein on Gold Reduction and Nanoparticle Formation

The effect of denatured protein on gold reduction and nanoparticle formation was evaluated with the gold reduction assay as described in section 3.2.15.3. The protein was denatured through boiling for 3 hours and all three the electron donors from section 3.2.15.17 were used. UV-Vis spectrums were obtained as described in section 3.2.15.4 and selected samples were subjected for TEM, EDX and SAED analysis as described in sections 3.2.15.5 and 3.2.15.6 respectively.

3.2.15.13 The Effect of Exposure Time on Gold Reduction and Nanoparticle Formation

The effect of exposure time on gold reduction and nanoparticle formation was evaluated with the gold reduction assay as described in section 3.2.15.3, but by incubation with different time intervals, ranging from 30 minutes to 48 hours. UV-Vis spectrums were obtained as described in section 3.2.15.4 and selected samples were subjected for TEM, EDX and SAED analysis as described in sections 3.2.15.5 and 3.2.15.6 respectively.

3.2.15.14 The Effect of $HAuCl_4$ Concentrations on Gold Reduction and Nanoparticle Formation

The effect of different gold(III) concentrations, using $HAuCl_4$ as the gold(III) source, on gold reduction and nanoparticle formation was evaluated with the gold reduction assay as described in section 3.2.15.3, but by using gold(III) concentrations varying from 0 – 10 mM. UV-Vis spectrums were obtained as described in section 3.2.15.4 and selected samples were subjected for TEM, EDX and SAED analysis as described in sections 3.2.15.5 and 3.2.15.6 respectively.

3.2.15.15 The Effect of Temperature on Gold Reduction and Nanoparticle Formation

The effect of temperature on gold reduction and nanoparticle formation was evaluated with the gold reduction assay as described in section 3.2.15.3, but by incubating the samples at a temperature range between 30 and 85°C. UV-Vis spectrums were obtained as described in section 3.2.15.4 and selected samples were subjected for TEM, EDX and SAED analysis as described in sections 3.2.15.5 and 3.2.15.6 respectively.

3.2.15.16 The Effect of pH on Gold Reduction and Nanoparticle Formation

The effect of pH on gold reduction and nanoparticle formation was evaluated with the gold reduction assay as described in section 3.2.15.3, but by using specific buffers, ranging from pH 3.6 to 9.0. Acetate was used for the acidic pH range, phosphate buffer for the neutral pH range and borax for the alkaline pH range. UV-Vis spectrums were obtained as described in section 3.2.15.4 and selected samples were subjected for TEM, EDX and SAED analysis as described in sections 3.2.15.5 and 3.2.15.6 respectively.

3.2.15.17 The Effect of Different Disulphide Bond Reducing Agents on Gold Reduction and Nanoparticle Formation

The effect of different disulphide bond reducing agents on gold reduction and nanoparticle formation was evaluated with the gold reduction assay as described in section 3.2.15.3, but by using 46 µM of various electron donors, including sodium dithionite, dithiothreitol (DTT) and β-mercaptoethanol. UV-Vis spectrums were obtained as described in section 3.2.15.4 and selected samples were subjected for TEM, EDX and SAED analysis as described in sections 3.2.15.5 and 3.2.15.6 respectively.

3.2.16 Mechanism Hypothesis

Van Marwijk, (2009) hypothesized that the mechanism for gold reduction takes place *via* reduction of a surface exposed disulphide bond, since the ABC transporter, peptide-binding protein contains a disulphide bond (Figure 3.6). Gold reduction and nanoparticle formation can either take place *via* chemical reduction or the dithionite can reduce the disulphide bond resulting in a reduced protein which in turns reduces the gold to elemental gold. When the gold is reduced and nanoparticles are formed, a change in colour will take place, as described in section 3.2.15.4. If the latter one is true, iodoacetic acid, which is a sulphydryl blocking agent, can then be added, preventing the disulphide bond to become reduced, thereby preventing the protein to become reduced and therefore no reduction of gold should take place, giving no change in colour when the gold reduction assay is used.

Scott *et al.* (2008) has demonstrated a similar mechanism, involving reduction *via* a disulphide bond exchange reaction to produce metallic nanoparticles. They found the *E. coli* enzyme, glutathione reductase, catalyses the NADPH-dependant reduction of oxidized glutathione through a disulphide bond exchange reaction, involving two active site cysteine residues to form gold nanoparticles at the active site that are tightly bound through the catalytic cysteines.

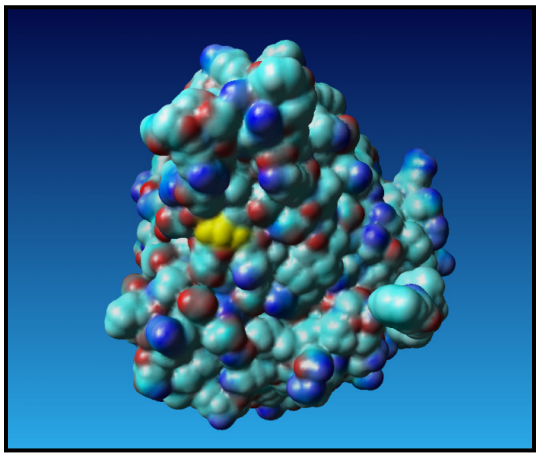

Figure 3.6: Homology model of the *T. scotoductus* ABC transporter, peptide-binding protein. The surface exposed disulphide bond, hypothesized to be involved in the gold reduction and nanoparticle formation process, can be seen in yellow (Taken from van Marwijk, (2009).

To test the hypothesis, the effect of the sulphydryl blocking agent, iodoacetic acid, on all three the electron donors from section 3.2.15.17 were tested for gold reduction and nanoparticle formation with the gold reduction assay as described in section 3.2.15.3. UV-Vis spectrums were obtained as described in section 3.2.15.4 and selected samples were subjected for TEM analysis as described in section 3.2.15.5.

3.3 RESULTS AND DISCUSSIONS

3.3.1 Selection of the ABC Transporter, Peptide-Binding Protein

Van Marwijk, (2009) revealed that *Thermus scotoductus* SA-01 has several membrane proteins as well as several cytoplasmic proteins that participate in the gold reduction and nanoparticle formation process. Finally she completed her PhD studies on one of the cytoplasmic proteins, since it showed the highest ability to reduce gold(III). This protein was purified and after N-terminal sequencing thereof, identified as an ABC transporter, peptide-binding protein from *Thermus thermophilus* (YP_144900). This gene sequence was aligned to the ABC transporter, peptide-binding protein in the *T. scotoductus* SA-01 genome database that was constructed through pyrosequencing by Gounder, (2009) and showed 100% alignment.

In order to determine if there are other proteins available in the *T. scotoductus* SA-01 genome that can be used to control the nanoparticle formation process, the ABC transporter, peptide-binding protein from *T. thermophilus* (YP_144900) was compared with the *T. scotoductus* SA-01 genome database from Gounder, (2009). Comparison was done with both the N-terminal sequence and the protein name on an annotation basis.

Several other peptide-binding proteins were found in the *T. scotoductus* SA-01 genome database that may also have the ability to reduce gold and form nanoparticles, like the ABC transporter, peptide-binding protein; however none other proteins were found with the same size or that had 100% alignment with the N-terminal sequence of the ABC transporter, peptide-binding protein from van Marwijk, (2009), therefore this peptide-binding protein was used in downstream experiments. The gene was found to be 1881 base pairs in size; the protein had a molecular weight of 70.6 kDa with a pI of 9.54 and is not part of an operon.

3.3.2 Genomic DNA Isolation and Polymerase Chain Reaction

Genomic DNA (gDNA) (2047 ng.µl^{-1}) was isolated from *T. scotoductus* SA-01, using a modified SDS-proteinase K method, as described in section 3.2.3 (Figure 3.7A).

The ABC transporter, peptide-binding gene was amplified for cloning and expression studies as described in section 3.2.4, using primers 1 and 2 (Table 3.2), to obtain an amplicon of ± 1.9 kb (Figure 3.7B). This yielded constructs that included the leader peptide and contained no His-Tag when expressed in pET-22b(+) and a N-terminal His-Tag when expressed wit the pET-28b(+) vector (Table 3.3).

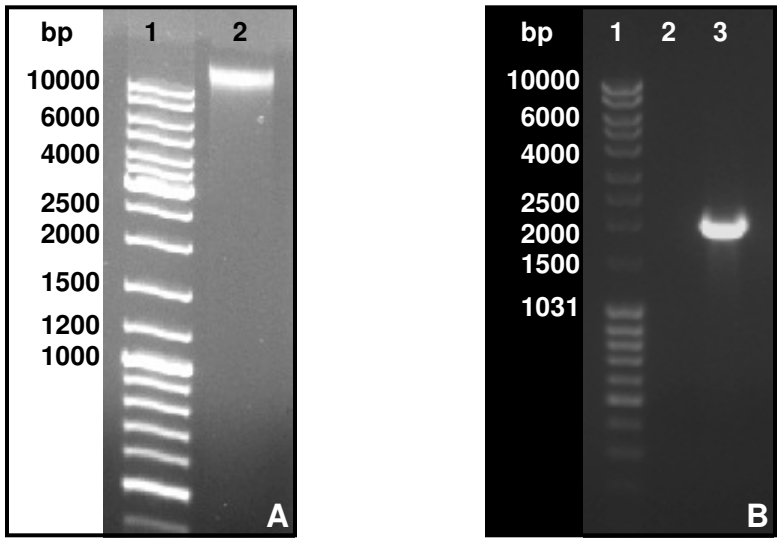

Figure 3.7: (A) Genomic DNA isolated from *T. scotoductus* SA-01 (Lane 2) with the GeneRuler™ DNA ladder (Lane 1). (B) The amplified ABC transporter, peptide-binding gene of ± 1.9 kb, using primers 1 and 2 (Lane 3), negative control (Lane 2) and the MassRuler™ DNA ladder (Lane 1).

3.3.3 Cloning into pGEM®-T Easy

The ± 1.9 kb PCR product, purified from the agarose gel, was ligated into the pGEM®-T Easy Vector system, as described in section 3.2.5. The ligated plasmid reactions were transformed into *Escherichia coli* One Shot TOP10 competent cells, as described in section 3.2.7. Plasmids were isolated from 10 clones and the insert sizes were evaluated by double digestion with the restriction enzymes *Eco*RI and *Nde*I, as

described in section 3.2.8. RFLP, confirming the insert of the ABC transporter, peptide-binding gene into the pGEM®-T Easy Vector system, can be seen in figure 3.8. Clone 4 (Lane 5; Figure 3.8) was chosen for downstream experiments.

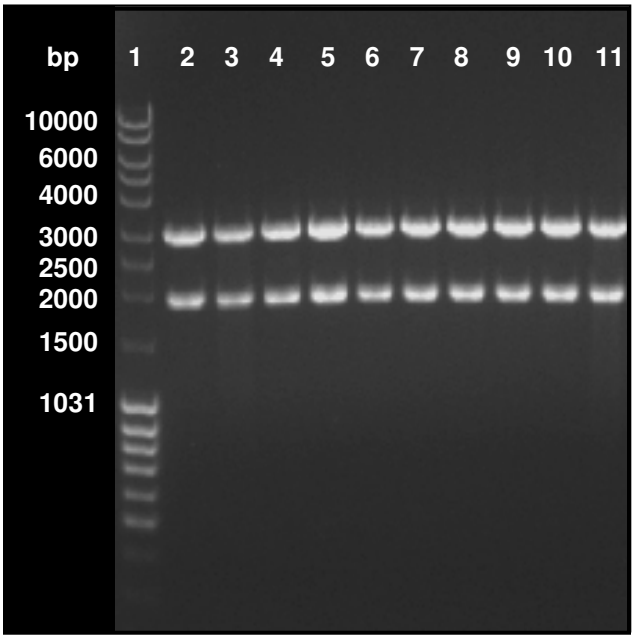

Figure 3.8: The amplified ABC transporter, peptide-binding gene of ± 1.9 kb, using primers 1 and 2, inserted into the pGEM®-T Easy Vector system of ± 3 kb (Lanes 2 - 11) and the MassRuler™ DNA ladder (Lane 1).

3.3.4 Cloning into pET-22b(+) and pET-28b(+)

The pET-22b(+) and pET-28b(+) vectors were propagated in *E. coli* One Shot TOP10 competent cells as described in section 3.2.9. Plasmids were isolated and the insert sizes were evaluated by double digestion with the restriction enzymes, *Eco*RI and *Nde*I, as described in section 3.2.8, to yield compatible cohesive ends. RFLP, confirming the empty, digested pET-22b(+) and pET-28b(+) vectors, can be seen in figure 3.9A.

The ± 1.9 kb insert, purified from the agarose gel, was ligated into the pET-22b(+) and pET-28b(+) vectors, as described in section 3.2.9. The ligated plasmid reactions were transformed into *E. coli* One Shot TOP10 competent cells, as described in section 3.2.9. Plasmids were isolated from 10 clones for each vector and the insert sizes were evaluated by double digestion with the restriction enzymes *Eco*RI and *Nde*I, as

described in section 3.2.8. RFLP, confirming the insertion of the ABC transporter, peptide-binding gene into the pET-22b(+) and pET-28b(+) vectors, can be seen in figure 3.9B. Clones 7 and 9 (Lanes 8 and 21; Figure 3.9B) were chosen for pET-22b(+) and pET-28b(+) respectively for downstream experiments.

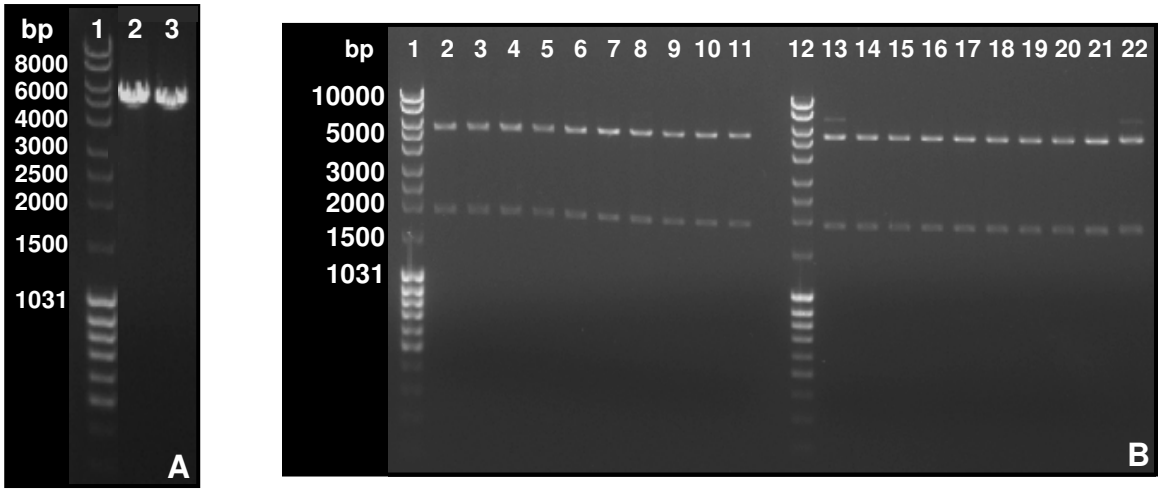

Figure 3.9: (A) The empty, digested pET-22b(+) and pET-28b(+) vectors (Lanes 2 and 3 respectively), and the MassRuler™ DNA ladder (Lane 1). (B) The ABC transporter, peptide-binding gene of ± 1.9 kb, inserted into pET-22b(+) of ± 5.5 kb (Lanes 2 - 11) and inserted into pET-28b(+) of ± 5.5 kb (Lanes 13 - 22) and the MassRuler™ DNA ladder (Lanes 1 and 12).

The two selected clones were sequenced for confirmation of the nucleotide composition of the ABC transporter, peptide-binding gene, as described in section 3.2.11. The data was analyzed and contigs were formed, using ContigExpress (Vector NTI Suite 9). Analyzed sequences were used to search the Genbank Database, using BLAST (NCBI, 2009) and alignments were done using ClustalW (EBI, 2009). Sequence results of the inserts showed 100% identity to ABC transporter, peptide-binding gene of *T. scotoductus* SA-01 (Figure 3.10) and were confirmed with BLAST analysis to be an ABC transporter, peptide-binding protein. The results for both clone 7 in pET-22b(+) and clone 9 in pET-28b(+) were identical and therefore only the alignment from clone 9 in pET-28b(+) is shown here as a representation.

*T.scot*SA01	ATGAGAAAAGTAGGCAAGCTGGCTGTATTCGGTTTAGCCGCCCTGGGCTTGGCCCTGGCG
9/pET-28	ATGAGAAAAGTAGGCAAGCTGGCTGTATTCGGTTTAGCCGCCCTGGGCTTGGCCCTGGCG
*T.scot*SA01	GGGCCCCAGGACAACAGCCTGGTCATAGGGGCTTCGCAGGAGCCCCGGGTTCTGGCGGGG
9/pET-28	GGGCCCCAGGACAACAGCCTGGTCATAGGGGCTTCGCAGGAGCCCCGGGTTCTGGCGGGG
*T.scot*SA01	GACTTCCTAAGCATCATCTCCAACCAGTCCATCAAGTTGGAGATCGAGCAGTACCTCTTC
9/pET-28	GACTTCCTAAGCATCATCTCCAACCAGTCCATCAAGTTGGAGATCGAGCAGTACCTCTTC
*T.scot*SA01	GCCCCCCTCATCGGTTTCAACGCCAACAGCGAAAACTTTCCCGTGCTGGTCACCGAGGTG
9/pET-28	GCCCCCCTCATCGGTTTCAACGCCAACAGCGAAAACTTTCCCGTGCTGGTCACCGAGGTG
*T.scot*SA01	CCCACCCGGCAAAACGGGCGTTTGCGGGTGACGGACATCGGCGGGGGCAAGAAGCGCTTG
9/pET-28	CCCACCCGGCAAAACGGGCGTTTGCGGGTGACGGACATCGGCGGGGGCAAGAAGCGCTTG
*T.scot*SA01	GAGATGGACCTCACCATCCGGCCCGATGCCCGCTGGTCCGACGGCAAGCCCATCACCACC
9/pET-28	GAGATGGACCTCACCATCCGGCCCGATGCCCGCTGGTCCGACGGCAAGCCCATCACCACC
*T.scot*SA01	GAGGATGTGGCCTTCTACTACGAGGTGGGCAAGGCCAAGGGGATGCCGGTGCTCAACCCG
9/pET-28	GAGGATGTGGCCTTCTACTACGAGGTGGGCAAGGCCAAGGGGATGCCGGTGCTCAACCCG
*T.scot*SA01	GACTACTGGGAGCGGGTGAACCTCCGGGTCAGGGACGCCCGCAACTTCACCGTGATCTTT
9/pET-28	GACTACTGGGAGCGGGTGAACCTCCGGGTCAGGGACGCCCGCAACTTCACCGTGATCTTT
*T.scot*SA01	GAGCCCGCCTACTACTACGACACCTACGGCGGCACCTACGGCTCCCCCATCGGCTACGCT
9/pET-28	GAGCCCGCCTACTACTACGACACCTACGGCGGCACCTACGGCTCCCCCATCGGCTACGCT
*T.scot*SA01	CCCAAGCACATCATGGGCGCCGAGTGGGAGAAGGTGAAAGCGGCGGCCCGGAACCTGGAT
9/pET-28	CCCAAGCACATCATGGGCGCCGAGTGGGAGAAGGTGAAAGCGGCGGCCCGGAACCTGGAT
*T.scot*SA01	CCCGATAAGGATGCGGAGAGGCTCAACGAGCTCTACCGCAACTTCTTCCTCAAGTTCGCC
9/pET-28	CCCGATAAGGATGCGGAGAGGCTCAACGAGCTCTACCGCAACTTCTTCCTCAAGTTCGCC
*T.scot*SA01	ACTCCCCAGGCCCTAAACCGGGGAGCCATGGTCTACTCGGGGGCCTTCAAGCTGCGGCGC
9/pET-28	ACTCCCCAGGCCCTAAACCGGGGAGCCATGGTCTACTCGGGGGCCTTCAAGCTGCGGCGC
*T.scot*SA01	TGGGTGCCGGGGAACTCCATTGAGATGGAGCGGAACCCCAACTTCCCCATCAAGCCCGAG
9/pET-28	TGGGTGCCGGGGAACTCCATTGAGATGGAGCGGAACCCCAACTTCCCCATCAAGCCCGAG
*T.scot*SA01	GGTGGGGAGAGCCGGTACGTGCAGAGGGTGGTCTACCGCTTCATCCAGAACACCAACTCC
9/pET-28	GGTGGGGAGAGCCGGTACGTGCAGAGGGTGGTCTACCGCTTCATCCAGAACACCAACTCC
*T.scot*SA01	CTCCTGGTGGCCGTCCTGGGCGGGAGCATTGACGCCACCTCCAGCGTCTCCCTCACCTTT
9/pET-28	CTCCTGGTGGCCGTCCTGGGCGGGAGCATTGACGCCACCTCCAGCGTCTCCCTCACCTTT
*T.scot*SA01	GACCAAGGCCGTAGCCGCCAGCTCACCTCCCGGGCCCCTGGCCGCTTTGACATCTGGTTC
9/pET-28	GACCAAGGCCGTAGCCGCCAGCTCACCTCCCGGGCCCCTGGCCGCTTTGACATCTGGTTC
*T.scot*SA01	GTGCCCGGGGCCATCTGGGAGCACATTGACGTCAACAAGTTTGAGAACTGCCAGGCGGTC
9/pET-28	GTGCCCGGGGCCATCTGGGAGCACATTGACGTCAACAAGTTTGAGAACTGCCAGGCGGTC
*T.scot*SA01	CGCGACTTGGGCCTGAACGACGTCCGCACCCGTCGGGCCCTCCTCCACGCTCTGAACCGC
9/pET-28	CGCGACTTGGGCCTGAACGACGTCCGCACCCGTCGGGCCCTCCTCCACGCTCTGAACCGC
*T.scot*SA01	GAGGGGTTGGTCAAGGCCTTCTTTGACGGCCTCCAGCCCGTGGCCCACACCTGGATCGCC
9/pET-28	GAGGGGTTGGTCAAGGCCTTCTTTGACGGCCTCCAGCCCGTGGCCCACACCTGGATCGCC
*T.scot*SA01	CCCGTCAACCCCCTCTTCAACCCCAATGTGCGGAAGTACGAGTTTGACCTGAAGAAGGCG
9/pET-28	CCCGTCAACCCCCTCTTCAACCCCAATGTGCGGAAGTACGAGTTTGACCTGAAGAAGGCG
*T.scot*SA01	GAGGCGCTCTTGGCGGAGATGGGCTGGAGGAAGGGGCCGGACGGCATCCTTCAGCGCACC
9/pET-28	GAGGCGCTCTTGGCGGAGATGGGCTGGAGGAAGGGGCCGGACGGCATCCTTCAGCGCACC

```
T.scotSA01      GTGGGTGGCCGCACCGTGCGCTTTGAGATTGAGTTCGTCACCACCGCGGGCAACGCTATC
9/pET-28        GTGGGTGGCCGCACCGTGCGCTTTGAGATTGAGTTCGTCACCACCGCGGGCAACGCTATC

T.scotSA01      CGGGAGCGCACCCAGCAGTTCTTCGCCGAGGACCTGAAGAAGATCGGCATCGCCGTCAAG
9/pET-28        CGGGAGCGCACCCAGCAGTTCTTCGCCGAGGACCTGAAGAAGATCGGCATCGCCGTCAAG

T.scotSA01      ATCAATAACGCCCCCAGCGCCGTGGTCTTCGCCGACGACTACATCCAGCGGGCCAGCGAG
9/pET-28        ATCAATAACGCCCCCAGCGCCGTGGTCTTCGCCGACGACTACATCCAGCGGGCCAGCGAG

T.scotSA01      TGCAAGTGGACCGGGCTGTTTGAGTTCGCTTGGGTTTCCAACCTGGCCGAGGATGGCTCC
9/pET-28        TGCAAGTGGACCGGGCTGTTTGAGTTCGCTTGGGTTTCCAACCTGGCCGAGGATGGCTCC

T.scotSA01      CTCTTCCAGTACAAGAACCTGAACACCGGGGCCATCATGGTGCCCACCAAGGAGAACAAC
9/pET-28        CTCTTCCAGTACAAGAACCTGAACACCGGGGCCATCATGGTGCCCACCAAGGAGAACAAC

T.scotSA01      TACCAGGGGCAGAACATCGGCGGCTGGCGCAACGACGAGTTTGACCGTCTGACGAGCCAG
9/pET-28        TACCAGGGGCAGAACATCGGCGGCTGGCGCAACGACGAGTTTGACCGTCTGACGAGCCAG

T.scotSA01      GGTGTCCTGGAGTTTGACGAGGCCAGGCGGAAGCAGCTCTTCTGGAGGGCCCAGGAGATC
9/pET-28        GGTGTCCTGGAGTTTGACGAGGCCAGGCGGAAGCAGCTCTTCTGGAGGGCCCAGGAGATC

T.scotSA01      TGGGCCGAGGAGCTGCCTGCCTTGCCCCTCTACTTCCGCGCTAACCCCTACGTGGTGCGG
9/pET-28        TGGGCCGAGGAGCTGCCTGCCTTGCCCCTCTACTTCCGCGCTAACCCCTACGTGGTGCGG

T.scotSA01      AAGGGCCTGGTCAACTACGTGGCCAGCGCTTACGCGGGCGGCTACGGTTACCCCGGCTGG
9/pET-28        AAGGGCCTGGTCAACTACGTGGCCAGCGCTTACGCGGGCGGCTACGGTTACCCCGGCTGG

T.scotSA01      AACGCTTGGGAGATCGGCTGGGAGAGCCGCGGCGCCGTGAAGAAGTGGGACCAGGCGAAG
9/pET-28        AACGCTTGGGAGATCGGCTGGGAGAGCCGCGGCGCCGTGAAGAAGTGGGACCAGGCGAAG

T.scotSA01      TACGCTCTTTCCGTCAAGTAA
9/pET-28        TACGCTCTTTCCGTCAAGTAA
```

Figure 3.10: Sequence alignments of the ABC transporter, peptide-binding gene from *T. scotoductus* SA-01 and clone 9 in pET-28b(+), showing 100% identity.

3.3.5 Expression of the ABC Transporter, Peptide-Binding Protein

The two selected clones [clone 7 in pET-22b(+) and clone 9 in pET-28b(+)] were used for overexpression of the ABC transporter, peptide-binding protein, as described in section 3.2.13. After induction with IPTG, samples were withdrawn at 0 hours; 2 hours and 4 hours. These cells were harvested and washed as described in section 3.2.13 and subjected for SDS-PAGE analysis (Figure 3.11), as described in section 3.2.15.1. The overexpressed protein was detected at ± 70 kDa in size and both pET-22b(+) and pET-28b(+) gave high levels of expression, without significant differences in expression levels and activity.

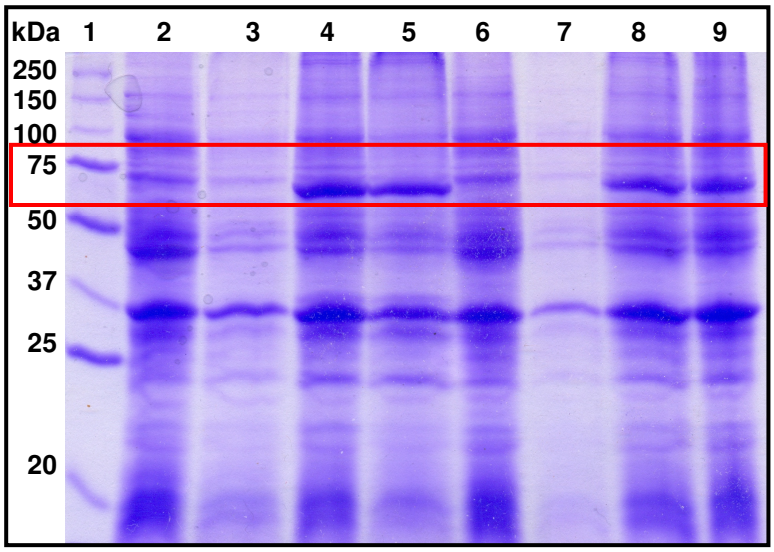

Figure 3.11: Overexpression of the ABC transporter, peptide-binding protein of ± 70 kDa. Lane 1 represents the Precision Plus Protein™ Standard. Lanes 2 and 6 are the negative control's 4 hours of pET-22b(+) and pET-28b(+) respectively. Lanes 3 – 5 are the overexpressed clone 7 in pET-22b(+) 0 hours; 2 hours and 4 hours respectively. Lanes 7 – 9 are the overexpressed clone 9 in pET-28b(+) 0 hours; 2 hours and 4 hours respectively.

3.3.6 Purification of the ABC Transporter, Peptide-Binding Protein

3.3.6.1 Expression in pET-22b(+)

After fractionation, as described in section 3.2.13, the soluble fraction for expression in pET-22b(+) was used for purification purposes, using a size-exclusion, Sephacryl S200HR (Gel-filtration) column (2.5 x 63 cm, Sigma), as described in section 3.2.14.1. An elution profile (Figure 3.12A) was obtained and used to select fractions for SDS-PAGE analysis (Figure 3.12B) and activity assessments (Figure 3.12C), as described in sections 3.2.15.1 and 3.2.15.3 respectively. Fractions that contained the protein of expected size (± 70 kDa) and showed gold reduction activity were pooled and dialysed overnight with 50 mM phosphate buffer (pH 7.4) to remove the NaCl. This purified protein, containing no His-Tags, was used for downstream experiments.

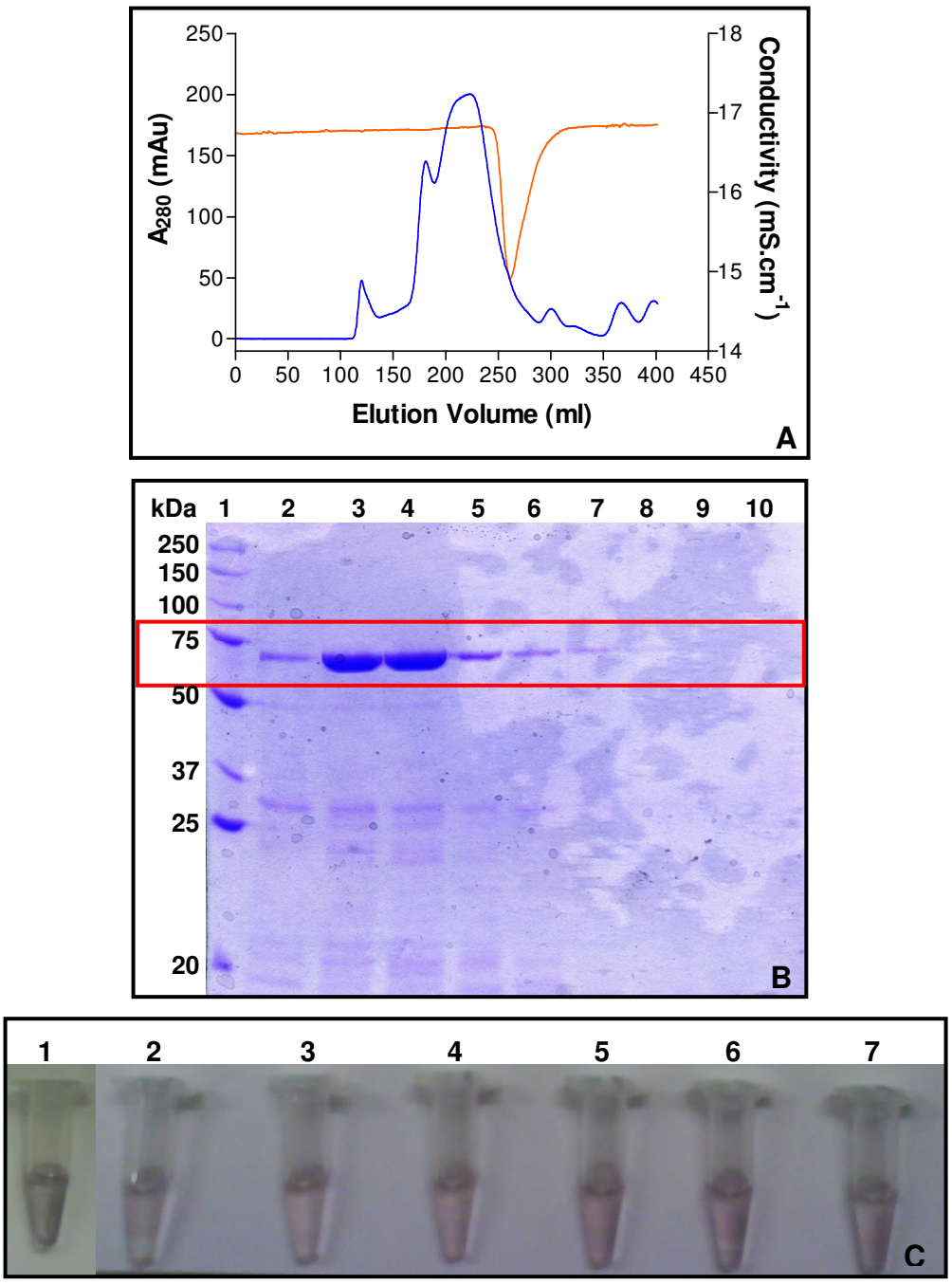

Figure 3.12: Purification of clone 7 in pET-22b(+), with the Sephacryl S200HR (Gel-filtration) column. (A) Elution profile obtained, showing the protein eluted between ± 150 and 200 ml [A_{280} ( ); Conductivity ( )]. (B) SDS-PAGE with lane 1 representing the Precision Plus Protein™ Standard and lanes 2 – 10 the fractions selected from the elution profile to determine which fractions contained the ± 70 kDa protein. (C) Activity determinations with tube 1 representing the blank reaction, containing no protein and showing a black colour and tubes 2 – 7 are the fractions in B (lanes 2 – 7), showing a pink/purple colour, which proved that the protein has gold reduction activity.

3.3.6.2 Expression in pET-28b(+)

After fractionation, as described in section 3.2.13, the soluble fraction for expression in pET-28b(+) was initially purified, using a 5 ml Nickel NTA (HisTrapFF) column (Amersham Biosciences), as described in section 3.2.14.2. An elution profile (Figure 3.13A) was obtained and used to select fractions for SDS-PAGE analysis (Figure 3.13B) and activity assessments (Figure 3.13C), as described in sections 3.2.15.1 and 3.2.15.3 respectively.

Fractions that contained the protein of expected size (± 70 kDa) and showed gold reduction activity, were pooled, concentrated and further purified, using a size-exclusion, Sephacryl S200HR (Gel-filtration) column (2.5 x 63 cm, Sigma), as described in section 3.2.14.2. An elution profile (Figure 3.14A) was obtained and used to select fractions for SDS-PAGE analysis (Figure 3.14B) and activity assessments (Figure 3.14C), as described in sections 3.2.15.1 and 3.2.15.3 respectively. Fractions that again contained the protein of expected size (± 70 kDa) and showed gold reduction activity were pooled and dialysed overnight with 50 mM phosphate buffer (pH 7.4) to remove the NaCl. This purified protein, containing an N-terminal His-Tag, was used for downstream experiments.

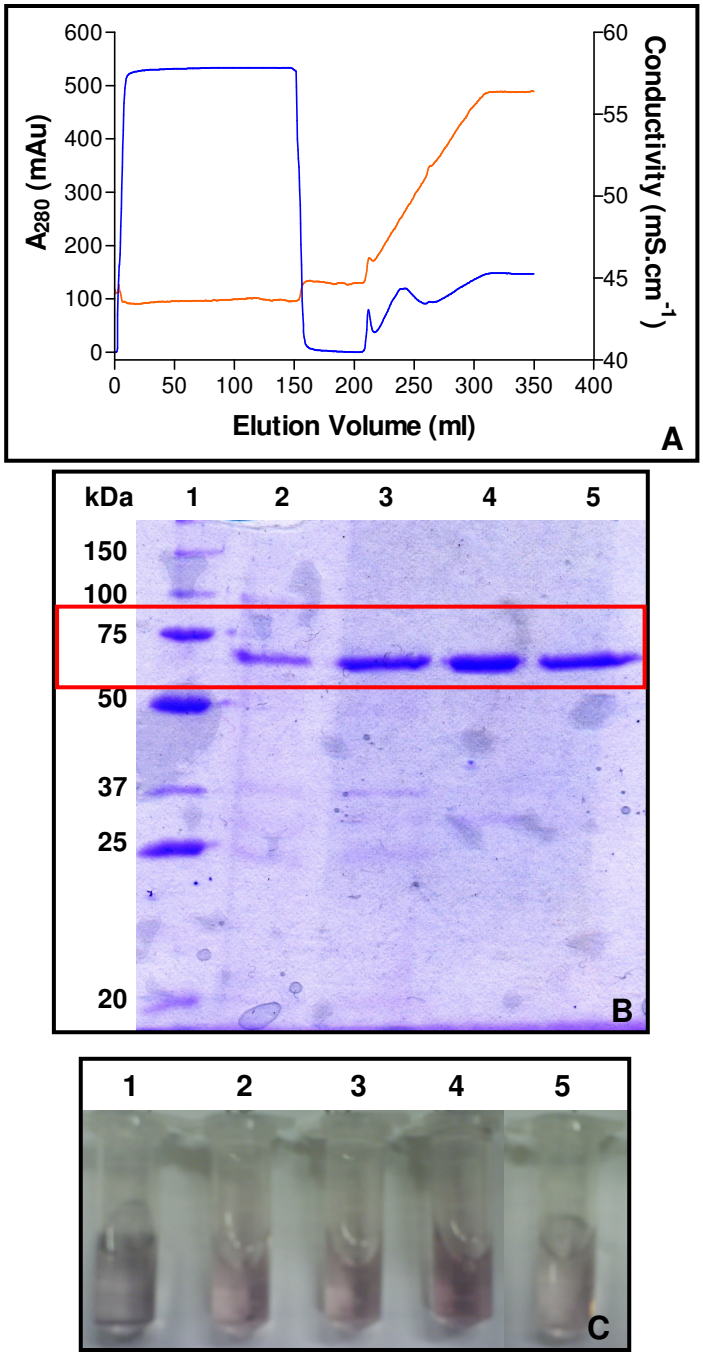

Figure 3.13: Purification of clone 9 in pET-28b(+), with the Nickel NTA (HisTrapFF) column. (A) Elution profile obtained, showing the protein eluted between ± 200 and 220 ml [A_{280} ( ); Conductivity ( )]. (B) SDS-PAGE with lane 1 representing the Precision Plus Protein™ Standard and lanes 2 – 5 the fractions selected from the elution profile to determine which fractions contained the ± 70 kDa protein. (C) Activity determinations with tube 1 representing the blank reaction, containing no protein and showing a black colour and tubes 2 – 5 are the fractions in B (lanes 2 – 5), showing a pink/purple colour, which proved that the protein has gold reduction activity.

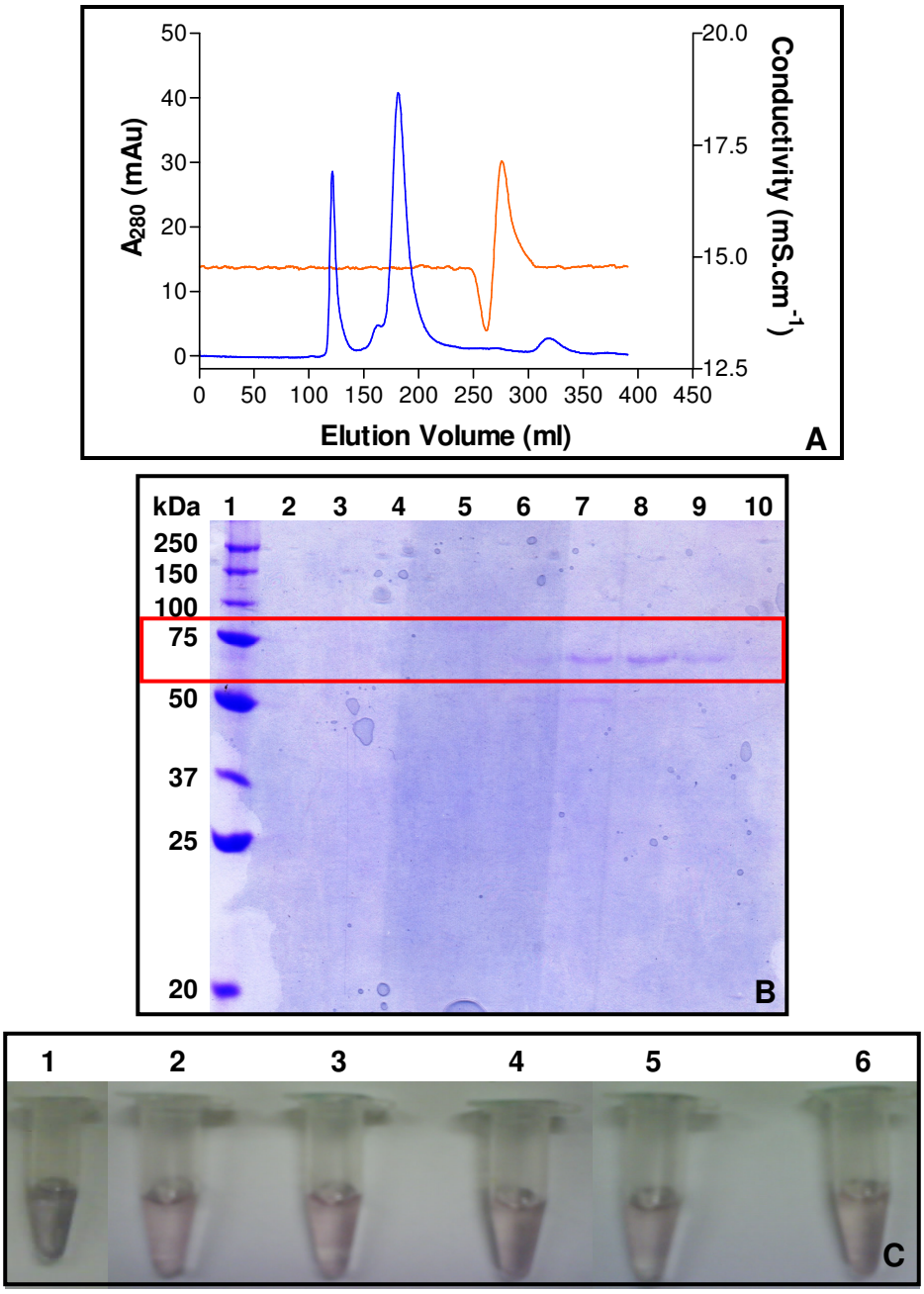

Figure 3.14: Purification of clone 9 in pET-28b(+), with the Sephacryl S200HR (Gel-filtration) column. (A) Elution profile obtained, showing the protein eluted between ± 150 and 200 ml [A_{280} ( ); Conductivity ( )]. (B) SDS-PAGE with lane 1 representing the Precision Plus Protein™ Standard and lanes 2 – 10 the fractions selected from the elution profile to determine which fractions contained the ± 70 kDa protein. (C) Activity determinations with tube 1 representing the blank reaction, containing no protein and showing a blackish colour and tubes 2 – 6 are the fractions in B (lanes 6 – 10), showing a pink/purple colour, which proved that the protein has gold reduction activity.

3.3.7 Characterization of the ABC Transporter, Peptide-Binding Protein in *Escherichia coli*

The results revealed no specific differences between the protein expressed in pET-22b(+), containing no His-Tags and the protein expressed in pET-28b(+), containing an N-terminal His-Tag. If there are differences, these will be highlighted. This indicated that the His-Tag had no influence on the gold reduction and nanoparticle formation process and only results for the protein expressed in pET-28b(+) will be shown here as a representation. Furthermore, only results that had shown significant differences will be discussed.

In all characterization steps, the protein mediated reduction and nanoparticle formation reactions were done, using protein at a starting concentration of 100 $\mu g.ml^{-1}$, except for when the effect of protein concentrations on gold reduction and nanoparticle formation were tested. All protein concentrations were determined with the Micro BCA™ Protein Assay Kit (PIERCE), as described in section 3.2.15.2. A blank reaction was made for each parameter tested, containing additional buffer instead of the protein. This was done to compensate for chemical reduction that might occur, but also to demonstrate the differences in nanoparticle formations from the protein reactions, proving the significant role of the protein in the nanoparticle formation process. All gold reduction and nanoparticle formation experiments were done with the gold reduction assay, as described in section 3.2.15.3. In all the experiments, gold reduction and nanoparticle formation is displayed in figures and please note that protein reactions can be seen with an odd number and their respective blank reactions with an even number. The SPR band was recorded for all the samples from each parameter, to verify gold reduction and nanoparticle formation. This was done through UV-Vis wave scans in the range of 300-800 nm, as described in section 3.2.15.4.

As discussed in sections 1.2.5 and 3.2.15.4, it is known in literature that gold nanoparticles differ in colour, from yellow/orange to red/pink to purple to blue, depending on particle size and that these differences in colour occur due to excitation of surface plasmon vibrations in the gold nanoparticles. Therefore, samples subjected for TEM and EDX analysis, were selected simply based on the SPR obtained through UV-Vis spectra

and visual observations in the colour obtained through the gold reduction assay, and was done as described in sections 3.2.15.5 and 3.2.15.6 respectively. Furthermore, the samples that were subjected for SAED, Nanotrac and Nanoprobe analysis, as described in sections 3.2.15.6; 3.2.15.7 and 3.2.15.8 respectively, were only tested for additional confirmation of the size, shape and elemental analysis and only a few samples for these analyses were randomly selected.

3.3.7.1 The Effect of Methyl Viologen Concentrations on Gold Reduction and Nanoparticle Formation

The effect of methyl viologen concentrations on gold reduction and nanoparticle formation was tested at 0 µM; 1.5 µM; 2.5 µM; 3.5 µM and 4.5 µM final concentrations respectively, to determine the influence of methyl viologen as well as the optimum concentration for nanoparticle formation with the best defined shapes. When comparing the reactions through the visual assay (Figure 3.15) and the SPR, obtained through UV-Vis spectra (Figure 3.16), nanoparticle formation took place at all the different concentrations and can be seen due to a change in the absorbance around 540 – 560 nm in the protein reactions (Figure 3.16A) with no change in the respective blank reactions (Figure 3.16B). At 0 µM methyl viologen (Tubes 1 and 2), gold reduction still took place and might be due to the sodium dithionite acting as a reducing agent in the absence of methyl viologen, as discussed in figure 3.19.

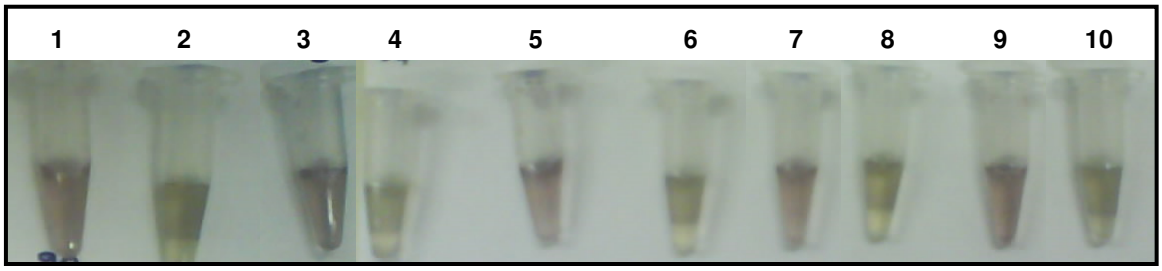

Figure 3.15: The different colours obtained through the gold reduction assay at varying methyl viologen concentrations, indicating gold nanoparticle formation. The odd numbers (1 – 9) indicate protein reactions for 0 µM; 1.5 µM; 2.5 µM; 3.5 µM and 4.5 µM respectively and the even numbers (2 – 10) the corresponding blank reactions.

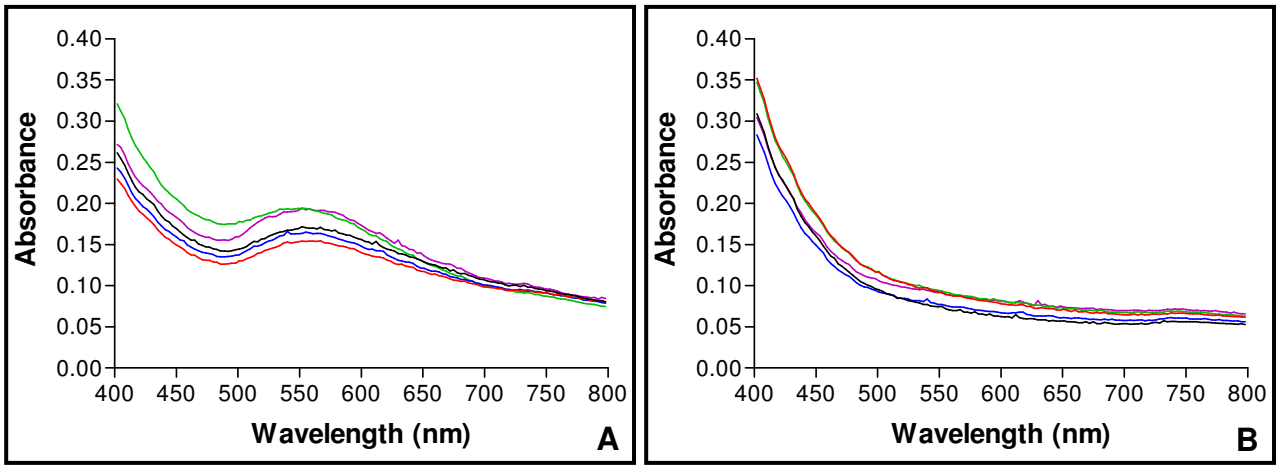

Figure 3.16: UV-Vis absorption spectra of the surface plasmon resonance recorded for the different methyl viologen concentrations, indicating gold nanoparticle production through a change in the absorbance around 540 - 560 nm. (A) The protein reactions and (B) the corresponding blank reactions. [0 µM (▬); 1.5 µM (▬); 2.5 µM (▬); 3.5 µM (▬); 4.5 µM (▬)].

The TEM micrographs (Figure 3.17) confirmed that nanoparticles formed at all the concentrations, and they were mostly spherical. No real differences were obtained with the various methyl viologen concentrations.

EDX was done on all the samples and the nanoparticles were confirmed to be gold, as can be seen in figure 3.18.

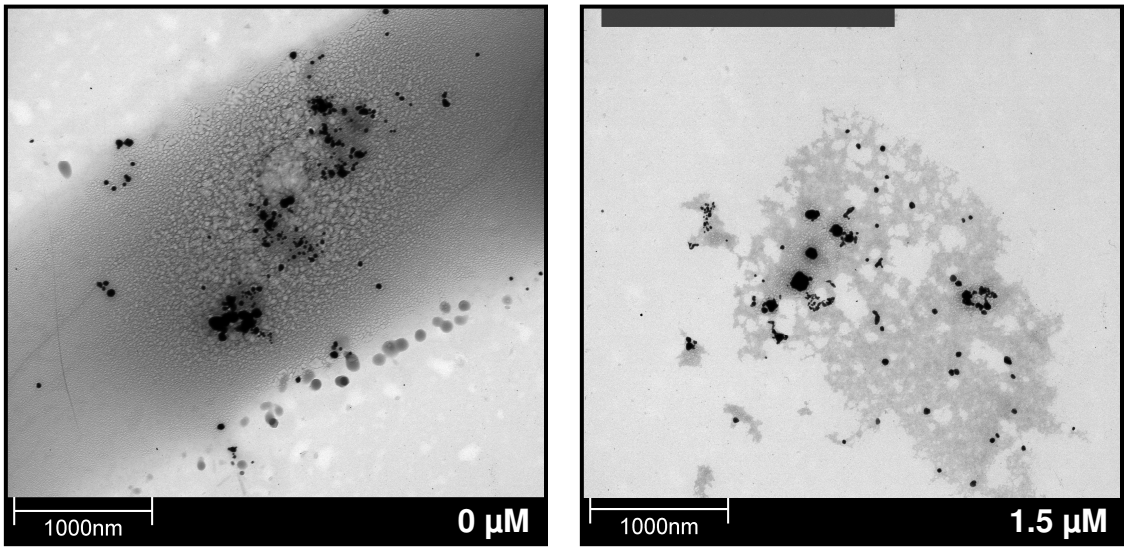

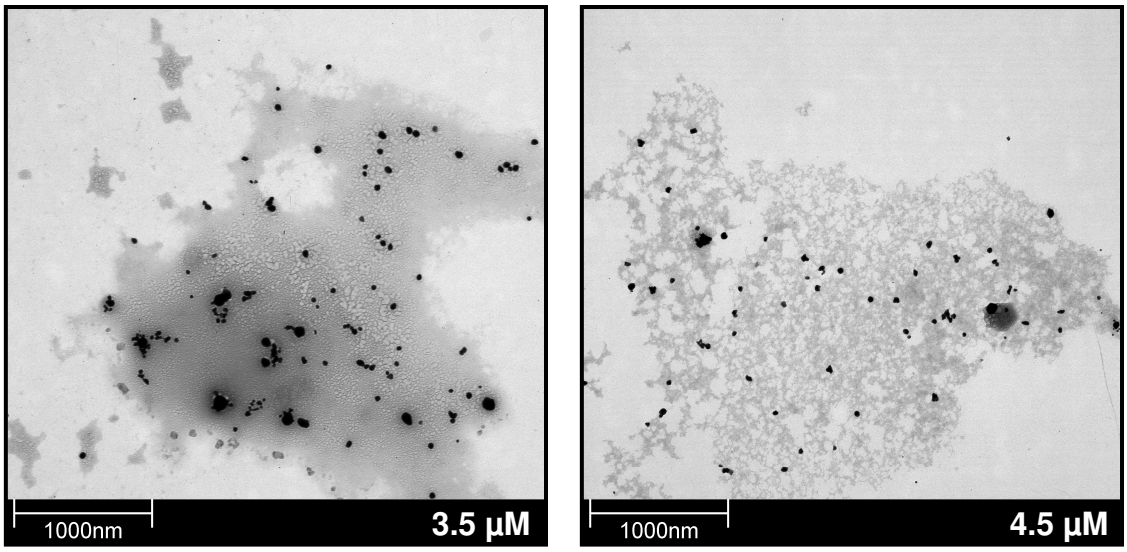

Figure 3.17: TEM micrographs for the different methyl viologen concentrations, indicating the shapes, sizes and amounts of gold nanoparticles obtained. All scale bars are equal to 1000 nm.

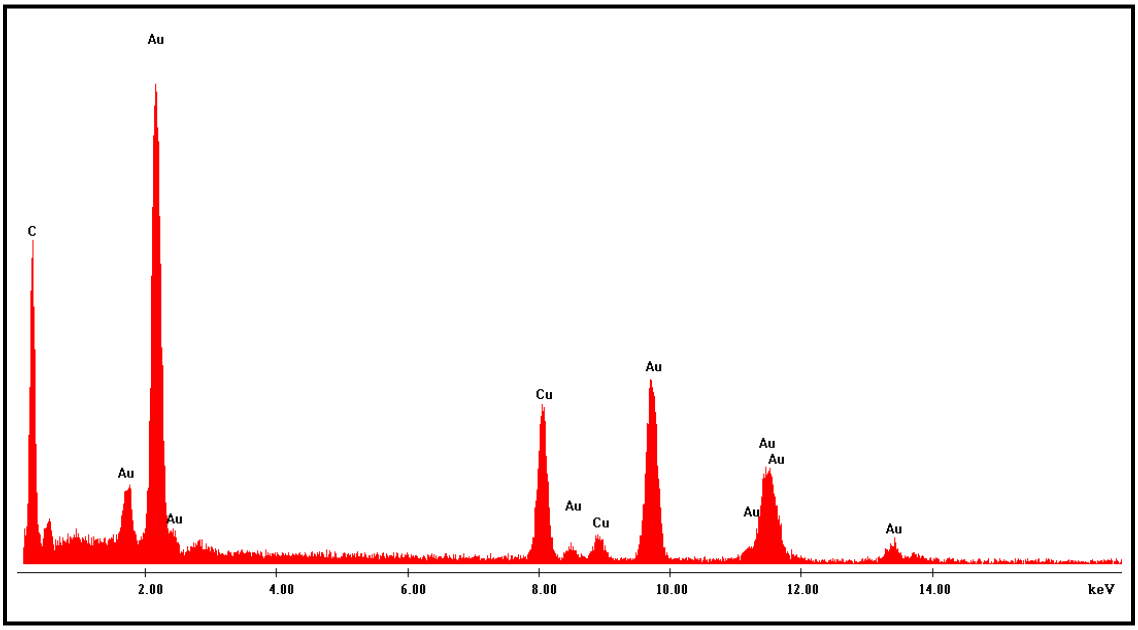

Figure 3.18: EDX spectrum recorded for the nanoparticles produced at different methyl viologen concentrations, showing a typical pattern for all the samples and indicates that the nanoparticles are gold.

From this it can be concluded that the methyl viologen concentration does not influence the formation of nanoparticles and in fact is not needed when producing nanoparticles with the gold reduction assay. When using the nitrate reduction assay, as mentioned in section 3.2.15.3, methyl viologen, together with sodium dithionite, plays a crucial role in

the reduction of nitrate to nitrite, but have no function in reducing gold(III) to gold(0). This proposed mechanism, for nitrate reduction, can be explained as follows: Sodium dithionite ($Na_2S_2O_4$) can be obtained from sodium bisulphite ($NaHSO_3$) as can be seen in reaction A, and can react with methyl viologen in one of two ways (Figure 3.19).

$$2\ NaHSO_3 + Zn \rightarrow Na_2S_2O_4 + Zn(OH)_2 \qquad (A)$$

Methyl viologen (MV^{2+}) can react with sodium dithionite *via* an ion exchange reaction, to from MV^0 (Reaction 1), or it can accept electrons from sodium dithionite to form a free radical ion ($MV\bullet^+$) (Reaction 2). The second reaction is more likely to occur and when $MV\bullet^+$ is formed, it will reduce nitrate to nitrite, as can be seen in reaction B.

$$NO_3^- + 2\ MV\bullet^+ + 2\ H^+ \rightarrow NO_2^- + 2\ MV^{2+} + H_2O \qquad (B)$$

The nitrite will then react with the sulphanilamide, present in the nitrate reduction assay, to form diazonium salt. From this it can be seen that both sodium dithionite and methyl viologen is needed to reduce nitrate to nitrite, in the nitrate reduction assay.

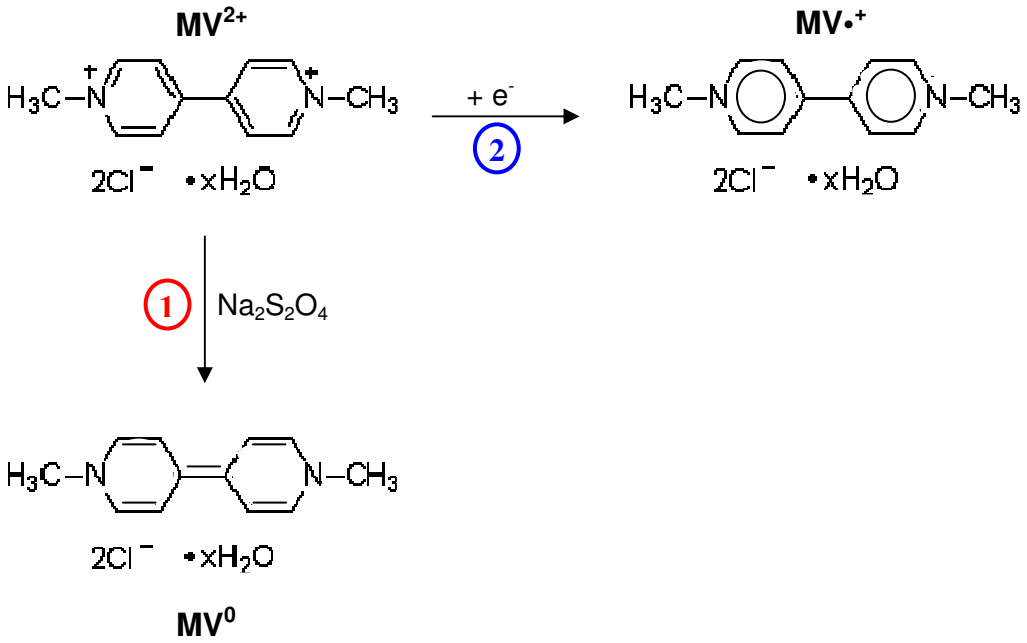

Figure 3.19: Methyl viologen (MV^{2+}) either reacts with sodium dithionite *via* an ion exchange reaction, to form MV^0, in reaction 1 or it can accept electrons from sodium dithionite to form the free radical ion ($MV\bullet^+$), in reaction 2.

For the gold reduction assay, in the presence of both methyl viologen and sodium dithionite, the same proposed mechanism are used for the reduction of gold(III) to gold(0), but it was found that methyl viologen had no effect on gold reduction and nanoparticle formation and that nanoparticles were obtained without methyl viologen present and within the presence of sodium dithionite alone. The reaction for gold reduction with only sodium dithionite present in the assay can be explained as follows: Sodium dithionite ($Na_2S_2O_4$) are oxidized with molecular oxygen to form bisulphite ($NaHSO_3$) (The reverse of reaction A). During this reaction, two hydrogen ions (H^+) will be released which will cleave the surface exposed disulphide bond (S-S) of the protein to yield a reduced protein (SH-SH). According to the mechanism hypothesis, discussed in section 3.2.16, this reduced protein will then reduce gold(III) to gold(0) and will result in the formation of nanoparticles.

3.3.7.2 The Effect of Sodium Dithionite Concentrations on Gold Reduction and Nanoparticle Formation

The effect of sodium dithionite concentrations on gold reduction and nanoparticle formation was tested at 0 µM; 1 µM; 2 µM; 3 µM; 4 µM; 5 µM and 6 µM final concentrations respectively, to determine the influence of sodium dithionite as well as the optimum concentration for nanoparticle formation with the best defined shapes. When comparing the reactions through the visual assay (Figure 3.20) and the SPR, obtained through UV-Vis spectra (Figure 3.21), nanoparticle formation took place at all the different concentrations and can be seen due to a change in the absorbance around 540 – 560 nm in the protein reactions (Figure 3.21A) with no change in the respective blank reactions (Figure 3.21B). At 0 µM sodium dithionite (Tubes 1 and 2), gold reduction still took place and might be due to the methyl viologen acting as an additional electron donor and reducing agent in the absence of sodium dithionite, but indicating more chemical reduction. At 6 µM (Tubes 13 and 14), nanoparticle formation was also obtained, but when compared with the blank reaction, it was mostly due to chemical reduction, since a change in absorbance was also obtained with the blank reaction. Dithionite is a strong reducing agent and therefore it should not be used in too high concentrations, to prevent chemical reduction taking place at a faster rate.

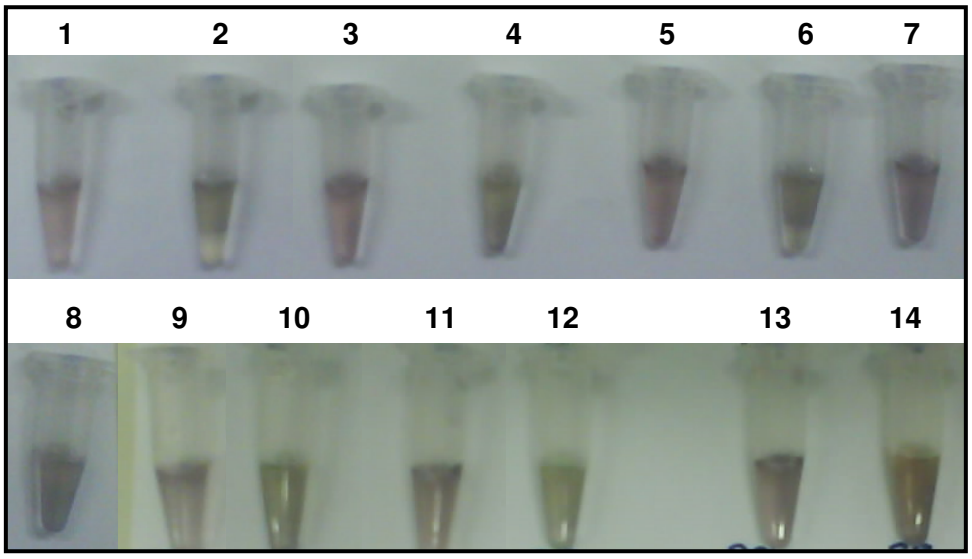

Figure 3.20: The different colours obtained through the gold reduction assay at varying sodium dithionite concentrations, indicating gold nanoparticle formation. The odd numbers (1 – 13) indicate protein reactions for 0 µM; 1 µM; 2 µM; 3 µM; 4 µM; 5 µM and 6 µM respectively and the even numbers (2 – 14) the corresponding blank reactions.

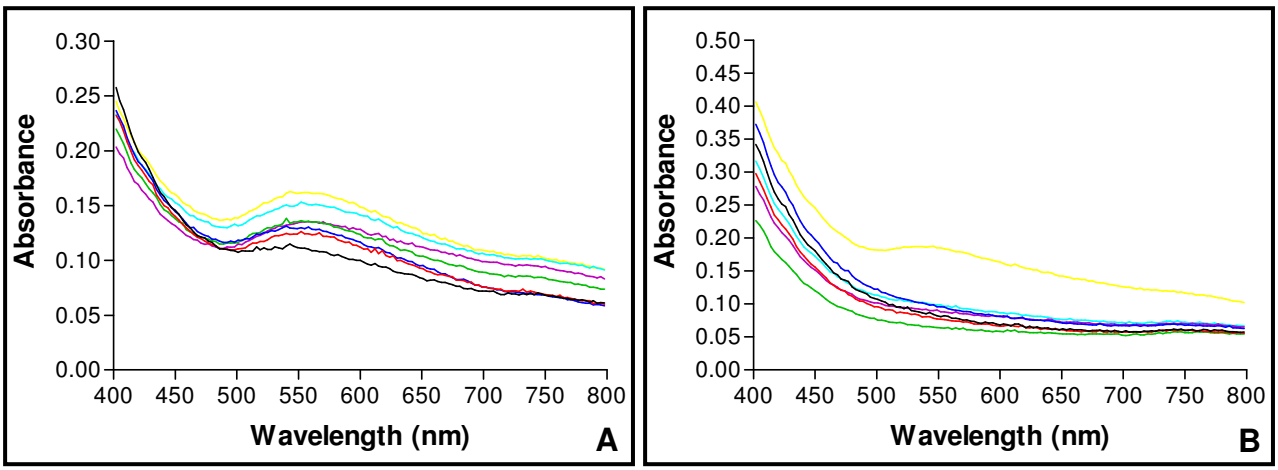

Figure 3.21: UV-Vis absorption spectra of the surface plasmon resonance recorded for the different sodium dithionite concentrations, indicating gold nanoparticle production through a change in the absorbance around 540 - 560 nm. (A) The protein reactions and (B) the corresponding blank reactions. [0 µM (—); 1 µM (—); 2 µM (—); 3 µM (—); 4 µM (—); 5 µM (—); 6 µM (—)].

The TEM micrographs (Figure 3.22) confirmed that nanoparticles formed at all the concentrations and they were mostly spherical. At 6 µM, the particles were noticeably

bigger, and may be due to the chemical reduction that took place, resulting in a faster reaction rate with bigger particles, as discussed in sections 1.6 and 3.3.7.7. Other than the increase in size at higher concentrations, no real differences were obtained with the various sodium dithionite concentrations.

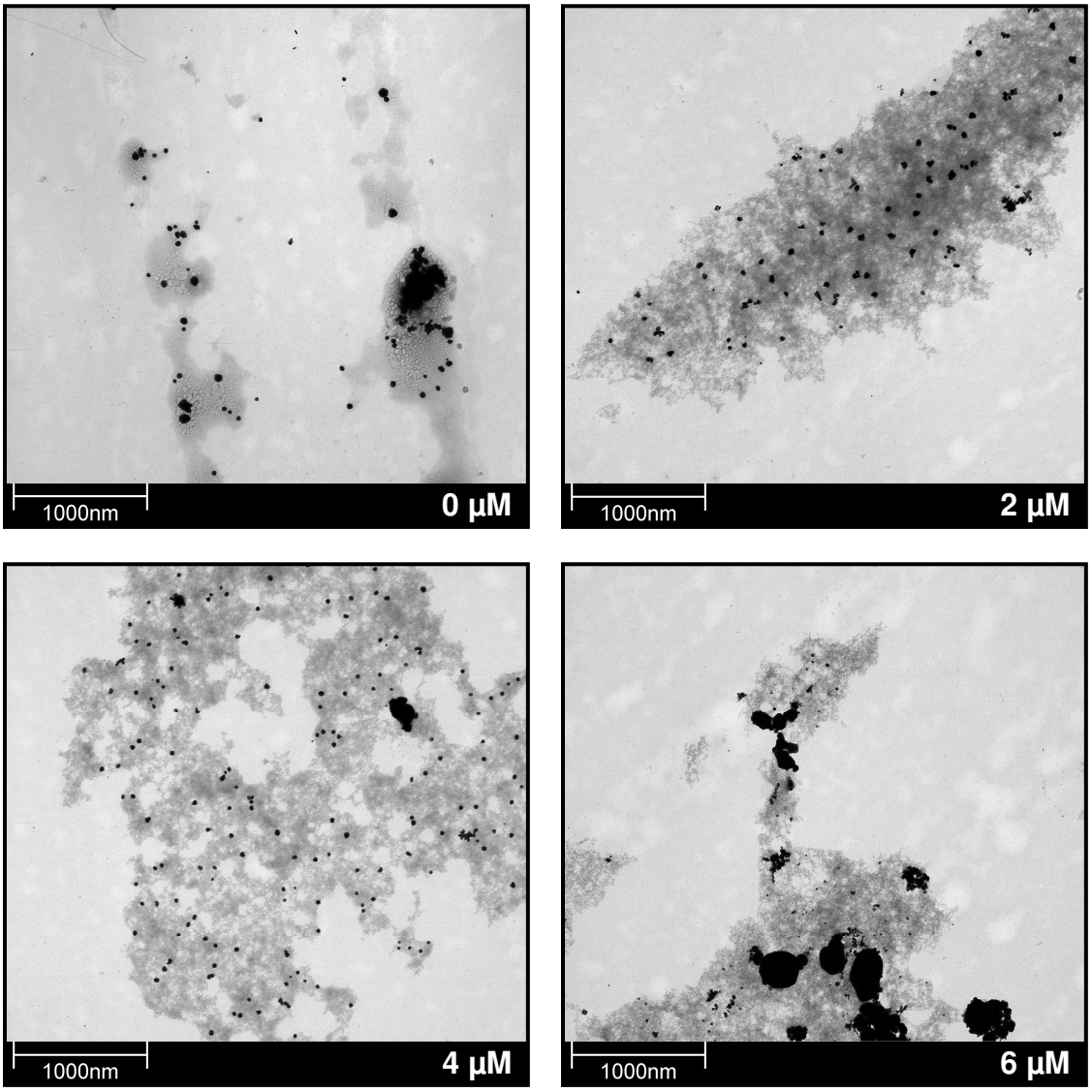

Figure 3.22: TEM micrographs for the different sodium dithionite concentrations, indicating the shapes, sizes and amounts of gold nanoparticles obtained. All scale bars are equal to 1000 nm.

EDX was done on all the samples and the nanoparticles were confirmed to be gold, as can be seen in figure 3.23.

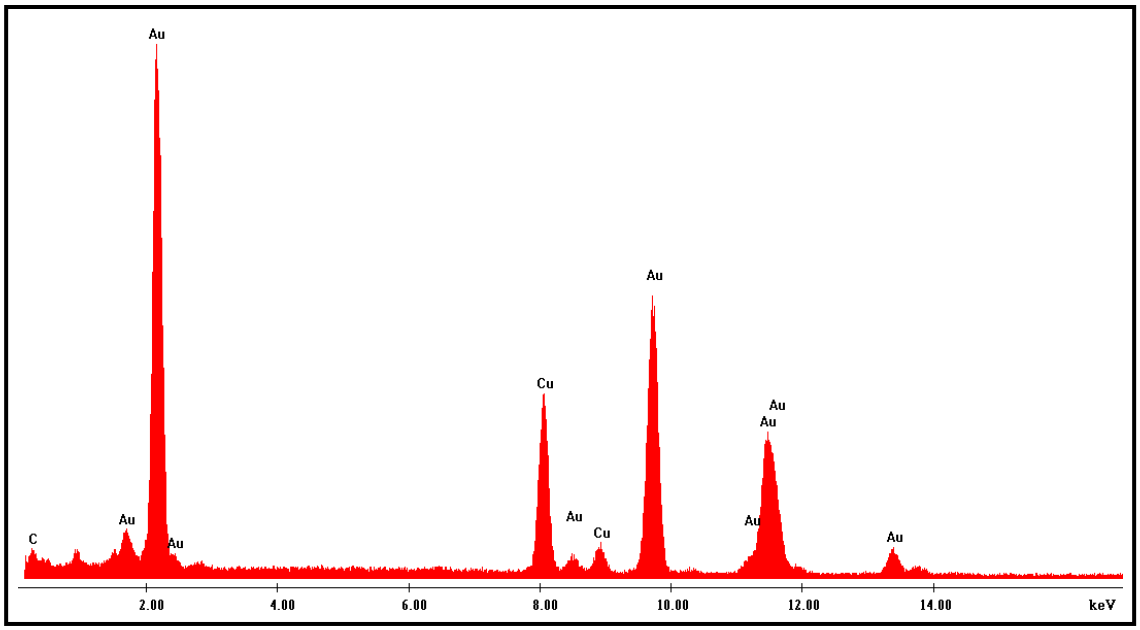

Figure 3.23: EDX spectrum recorded for the nanoparticles produced at different sodium dithionite concentrations, showing a typical pattern for all the samples and indicates that the nanoparticles are gold.

From this it can be concluded that an increase in sodium dithionite concentration does not influence the formation of nanoparticles, unless too high concentrations are used, then the particles become bigger, due to the interference of chemical reduction. Although particles were obtained when no sodium dithionite was added, the amount of particles were less and might be formed *via* purely chemical reduction with methyl viologen present in the solution. Therefore sodium dithionite is needed in the reaction for the protein to play a role in the gold reduction and nanoparticle formation process. The mechanisms of sodium dithionite and methyl viologen in the gold reduction and nitrate reduction assays are discussed in section 3.3.7.1.

3.3.7.3 The Effect of Protein Concentrations on Gold Reduction and Nanoparticle Formation

The effect of protein concentrations on gold reduction and nanoparticle formation was tested at 0 $\mu g.ml^{-1}$; 10 $\mu g.ml^{-1}$; 20 $\mu g.ml^{-1}$; 30 $\mu g.ml^{-1}$; 40 $\mu g.ml^{-1}$ and 50 $\mu g.ml^{-1}$ final protein concentrations respectively, to determine the optimum protein concentration for nanoparticle formation with the best defined shapes. When comparing the reactions

through the visual assay (Figure 3.24) and the SPR, obtained through UV-Vis spectra (Figure 3.25), nanoparticle formation took place at protein concentrations from 10 µg.ml^{-1} to 50 µg.ml^{-1} (Tubes 3 – 12). Nanoparticle formations can be seen through a change in the absorbance around 540 – 560 nm in the protein reactions (Figure 3.25A) with no change in the respective blank reactions (Figure 3.25B). At 30 µg.ml^{-1} to 50 µg.ml^{-1} (Tubes 7 – 12), bigger nanoparticles were expected and can be seen due to the high absorbance values. Clear differences in the blank reactions could be detected as well, except for 0 µg.ml^{-1} (Tubes 1 and 2), which had no protein present and was purely chemical reduction. This suggests that when no protein is present and only chemical reduction is taking place, the reaction rate is faster, and as discussed in sections 1.6 and 3.3.7.7, the rate of reduction can influence the type of particle formed. At 0 µg.ml^{-1}, no indication of any particles at all was obtained, again illustrating that the nanoparticle formation process is not only a chemical reaction, but is actually mediated by the protein.

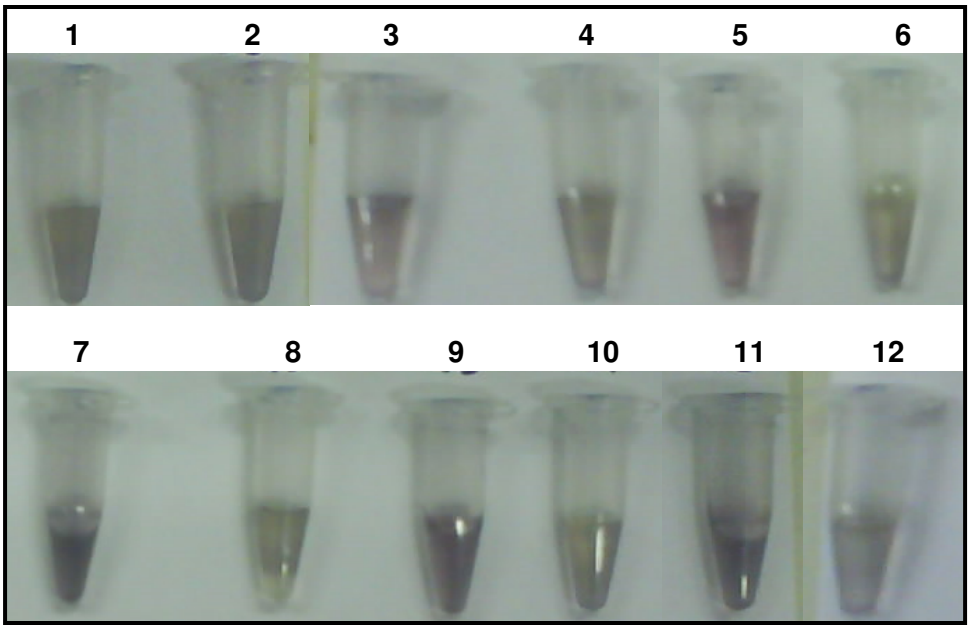

Figure 3.24: The different colours obtained through the gold reduction assay at varying protein concentrations, indicating gold nanoparticle formation. The odd numbers (1 – 11) indicate protein reactions for 0 µg.ml^{-1}; 10 µg.ml^{-1}; 20 µg.ml^{-1}; 30 µg.ml^{-1}; 40 µg.ml^{-1} and 50 µg.ml^{-1} respectively and the even numbers (2 – 12) the corresponding blank reactions.

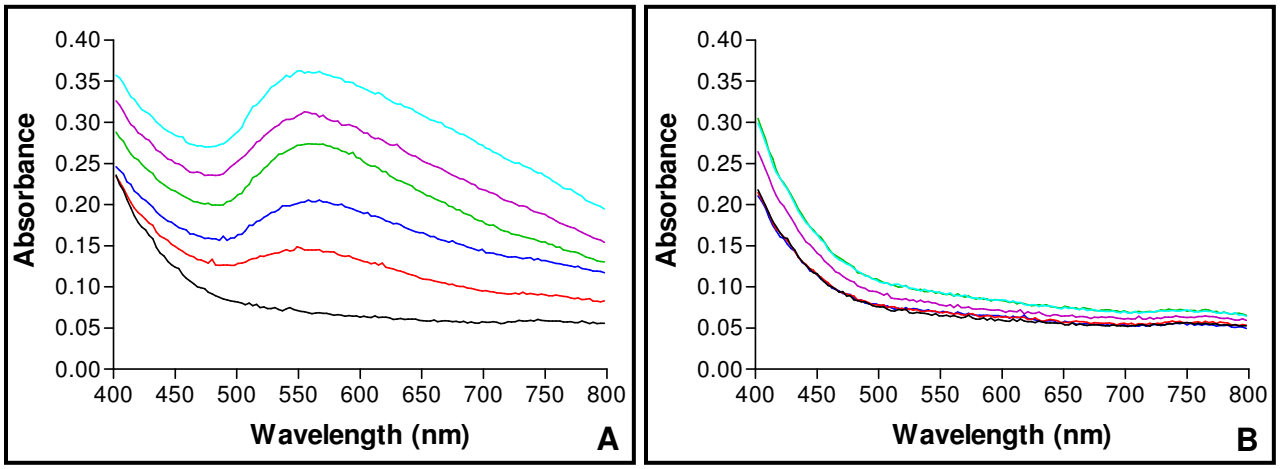

Figure 3.25: UV-Vis absorption spectra of the surface plasmon resonance recorded for the different protein concentrations, indicating gold nanoparticle production through a change in the absorbance around 540 - 560 nm. (A) The protein reactions and (B) the corresponding blank reactions. [0 $\mu g.ml^{-1}$ ( ); 10 $\mu g.ml^{-1}$ ( ); 20 $\mu g.ml^{-1}$ ( ); 30 $\mu g.ml^{-1}$ ( ); 40 $\mu g.ml^{-1}$ ( ); 50 $\mu g.ml^{-1}$ ( )].

The TEM micrographs (Figure 3.26) confirmed that all the particles formed are in the nano size range, but are not completely monodispersed. More particles were obtained at the higher protein concentrations, but with better controlled shapes and the majority of the particles were spherical. At 50 $\mu g.ml^{-1}$, the thin sheets with bend contours were again obtained.

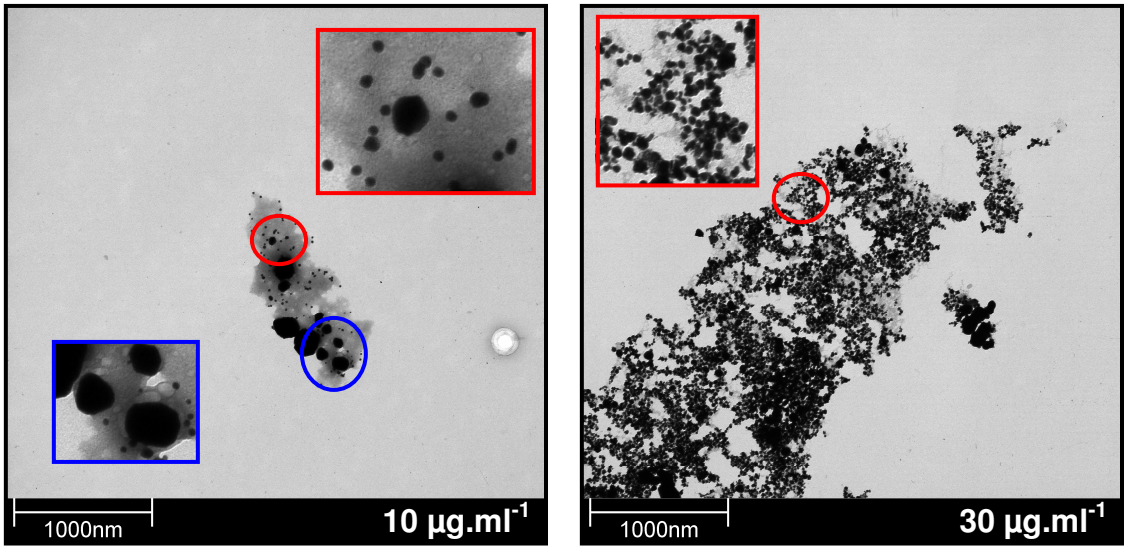

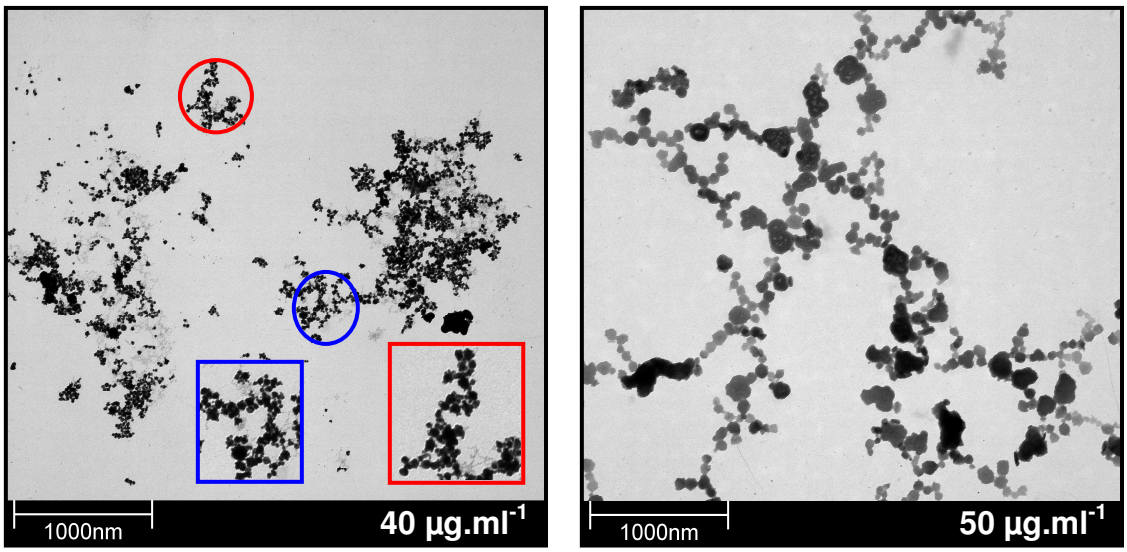

Figure 3.26: TEM micrographs for the different protein concentrations, indicating the shapes, sizes and amounts of gold nanoparticles obtained. All scale bars are equal to 1000 nm.

EDX was done on all the samples and the nanoparticles were confirmed to be gold, as can be seen in figure 3.27.

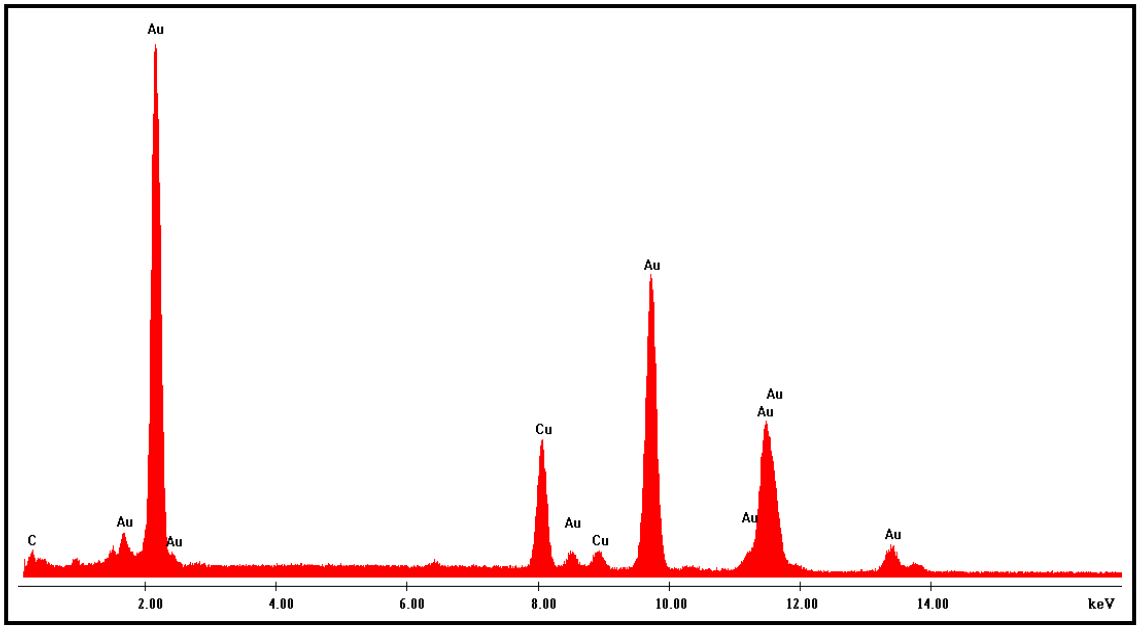

Figure 3.27: EDX spectrum recorded for the nanoparticles produced at different protein concentrations, showing a typical pattern for all the samples and indicates that the nanoparticles are gold.

From this it can be concluded that an increase in the protein concentration, results in an increase in the amount of particles obtained, but the protein concentration did not affect the shape of the particles. Therefore, it might be possible to obtain more nanoparticles, with controlled shapes, at higher protein concentrations. These findings agree with the physico-chemical properties of nanoparticles as discussed in section 1.6.

3.3.7.4 The Effect of Denatured Protein on Gold Reduction and Nanoparticle Formation

The effect of denatured protein on gold reduction and nanoparticle formation was tested with protein that was boiled for 3 hours to become denatured and inactive and sodium dithionite, dithiothreitol (DTT) and β-mercaptoethanol were used as electron donors and reducing agents respectively. When comparing the reactions through the visual assay (Figure 3.28) and the SPR, obtained through UV-Vis spectra (Figure 3.29), insignificant changes were observed with all three components, indicating that in comparison with the activity obtained in section 3.3.7.9 where folded protein was used, gold reduction and nanoparticle formation was not very effective when the protein is not active. This can be seen through the absence of any changes in the absorbance 540 – 560 nm in the protein reactions (Figure 3.29A) and in the respective blank reactions (Figure 3.29B). The slight change in colour is due to purely chemical reduction and proves that the protein has to be present in an active form and the disulphide bond should be reduced for nanoparticle formation to take place.

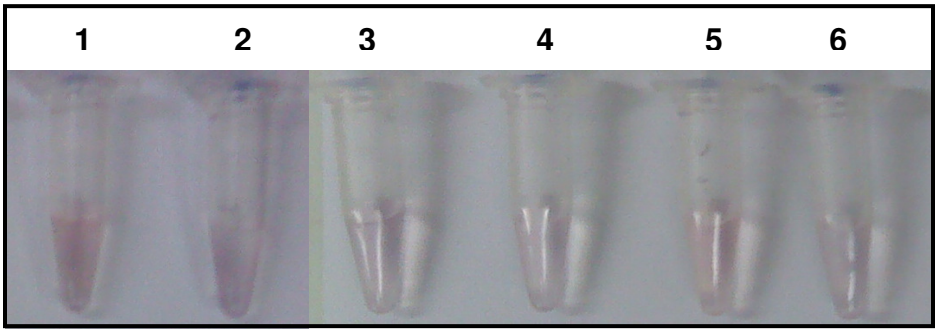

Figure 3.28: The different colours obtained through the gold reduction assay with denatured protein and various electron donors, indicating gold nanoparticle formation. The odd numbers (1 – 5) indicate protein reactions for sodium dithionite; dithiothreitol and β-mercaptoethanol respectively and the even numbers (2 – 6) the corresponding blank reactions.

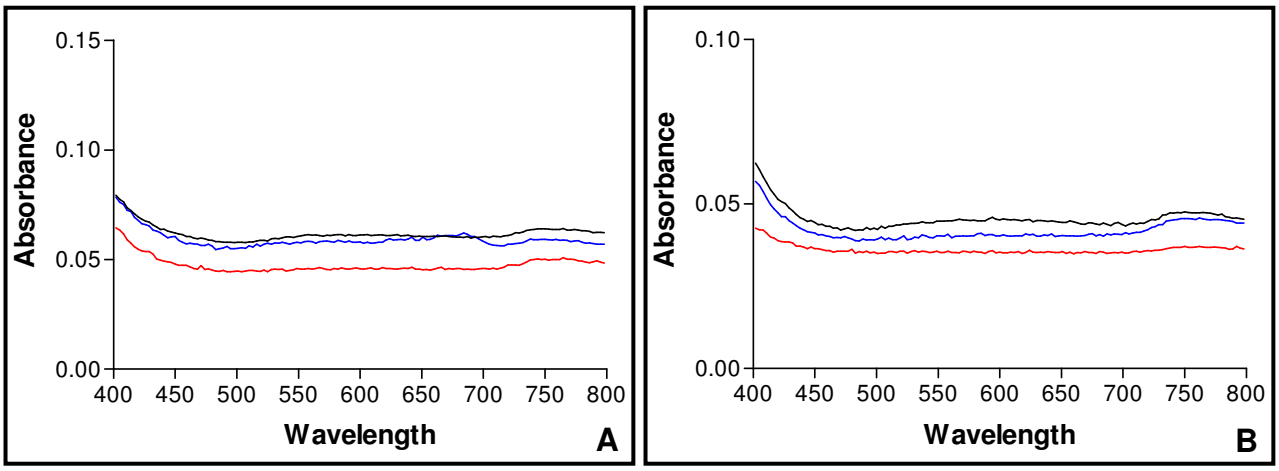

Figure 3.29: UV-Vis absorption spectra of the surface plasmon resonance recorded for the denatured protein and various electron donors, indicating insignificant nanoparticle production through no change in the absorbance around 540 - 560 nm. (A) Protein reactions with the different electron donors and (B) the corresponding blank reactions. [Sodium dithionite (▬); Dithiothreitol (▬); β-mercaptoethanol (▬)].

The TEM micrographs (Figure 3.30) confirmed that no significant nanoparticle formation was obtained with all three the electron donors.

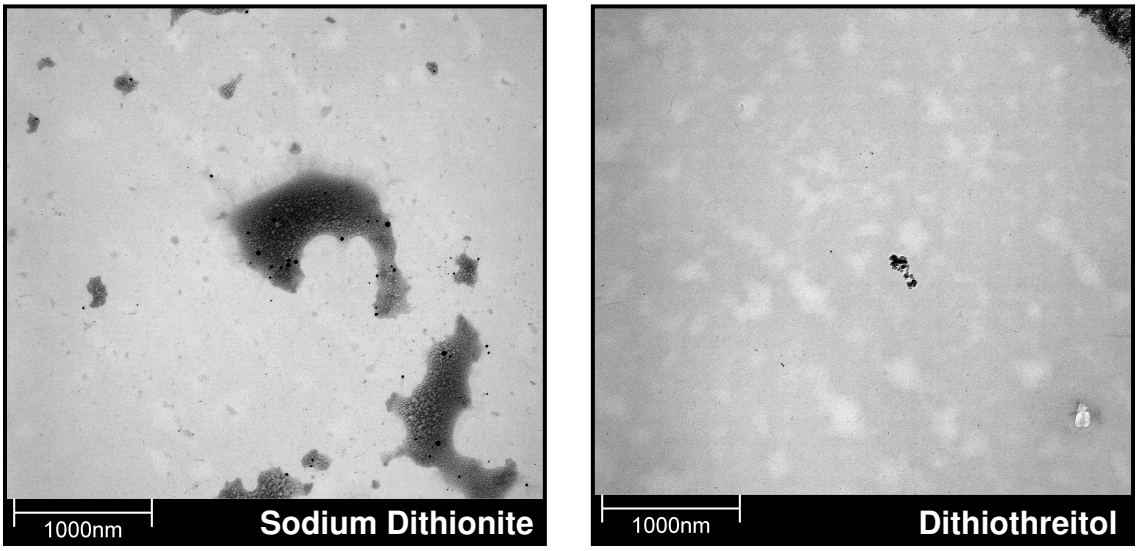

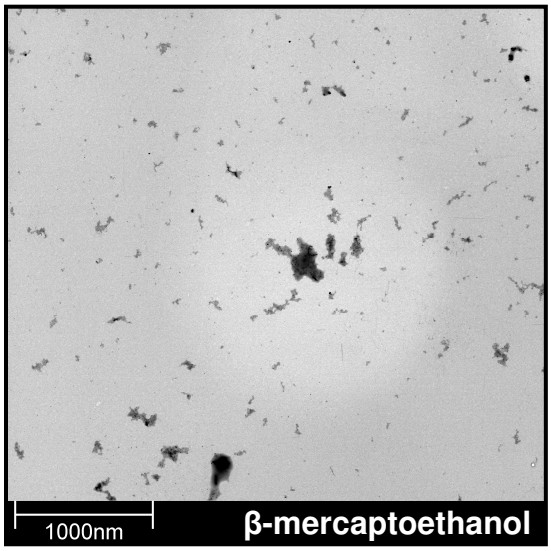

Figure 3.30: TEM micrographs of gold nanoparticles for the denatured protein with different electron donors, indicating the shapes, sizes and amounts of gold nanoparticles obtained. All scale bars are equal to 1000 nm.

From this it can be concluded that chemical reduction does take place when using the gold reduction assay, but when comparing the results obtained in this section with those from section 3.3.7.9, a clear difference was obtained, indicating that the presence of the folded protein play a significant role in gold reduction and nanoparticle formation, yielding a level of control over the rate of the process and as discussed before in sections 1.6 and 3.3.7.7, the rate of particle formation can influence the type of particle formed.

3.3.7.5 The Effect of Exposure Time on Gold Reduction and Nanoparticle Formation

The effect of exposure time on gold reduction and nanoparticle formation was tested through incubation for several time intervals. This included 30 minutes; 1 hour; 2 hours; 4 hours; 6 hours; 8 hours; 10 hours; 12 hours; 24 hours and 48 hours respectively, to determine the optimum incubation time for nanoparticle formation with the best defined shapes. When comparing the reactions through the visual assay (Figure 3.31) and the SPR, obtained through UV-Vis spectra (Figure 3.32), nanoparticle formation started at 8 hours (Tubes 11 and 12), with optimum formation at 12 – 24 hours (Tubes 15 - 18).

Nanoparticle formations can be seen through a change in the absorbance around 540 – 560 nm in the protein reactions (Figure 3.32A) with no change in the respective blank reactions (Figure 3.32B). Too much chemical reduction took place at 48 hours (Tubes 19 and 20) and no real difference in the blank reaction was obtained, indicating that control is not exerted after 24 hours *via* the protein. At 30 minutes – 6 hours (Tubes 1 – 10), only an insignificant change in the absorbance was obtained, indicating that nanoparticle formation was very slow and not very effective, if any at all, although a change in the colour of the blank reaction could be seen from 2 hours (Tube 6). This may again be, as discussed in sections 1.6 and 3.3.7.7, due to the presence of the protein slowing down the reaction rate and without the protein in the blank reactions, purely chemical reduction is taking place as a faster rate, hence an earlier change in colour could be detected in the blank reactions.

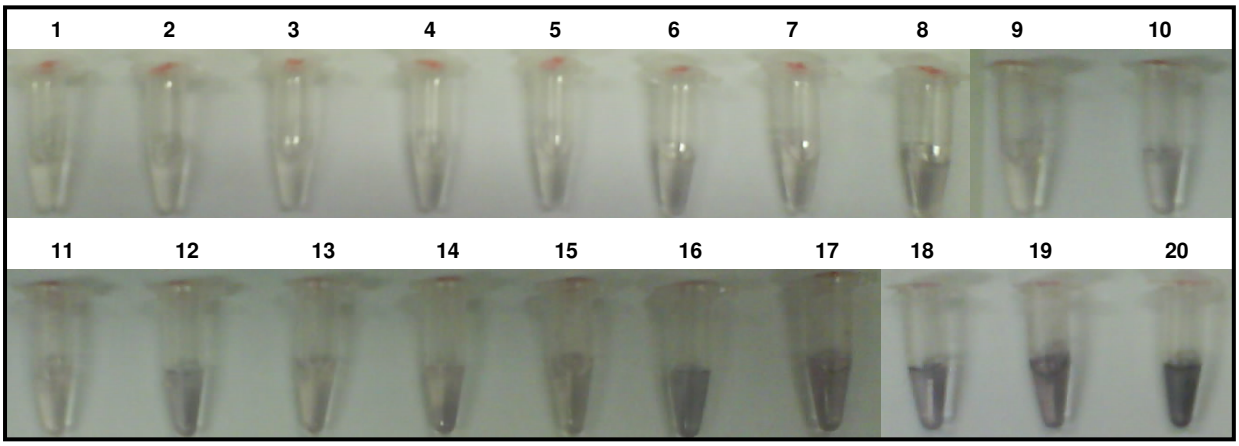

Figure 3.31: The different colours obtained through the gold reduction assay at various exposure times, indicating gold nanoparticle formation. The odd numbers (1 – 19) indicate protein reactions for 30 minutes; 1 hour; 2 hours; 4 hours; 6 hours; 8 hours; 10 hours; 12 hours; 24 hours and 48 hours respectively and the even numbers (2 – 20) the corresponding blank reactions.

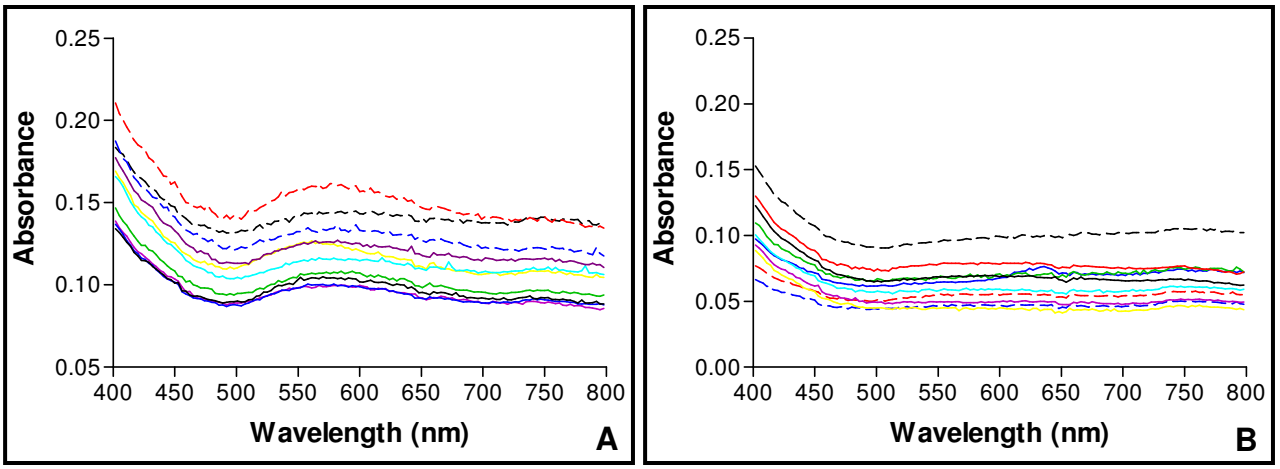

Figure 3.32: UV-Vis absorption spectra of the surface plasmon resonance recorded for the different exposure times, indicating gold nanoparticle production through a change in the absorbance around 540 - 560 nm. (A) The protein reactions and (B) the corresponding blank reactions. [30 minutes ( ); 1 hour ( ); 2 hours ( ); 4 hours ( ); 6 hours ( ); 8 hours ( ); 10 hours ( ); 12 hours ( ); 24 hours ( ); 48 hours ( )].

The TEM micrographs (Figure 3.33) confirmed that particles were indeed formed at each exposure time, and that all the particles are in the nano size range, but not monodispersed. Although the SPR showed an increase in the absorbance values, the TEM suggests uncontrolled nanoparticle formation at incubation times longer than 24 hours. At 30 minutes, only a few particles were obtained but with longer exposure times, the particles became notably more and bigger. The particles obtained were almost completely spherical and only at 12 and 24 hours a few triangular shapes were obtained. At 48 hours, the particles were noticeably bigger and mostly with no shape definition.

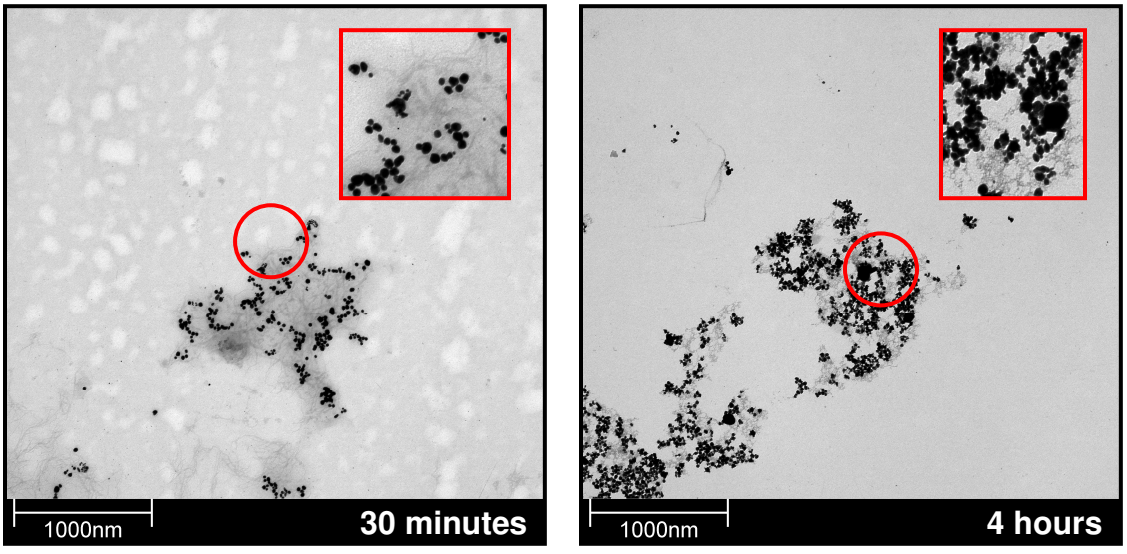

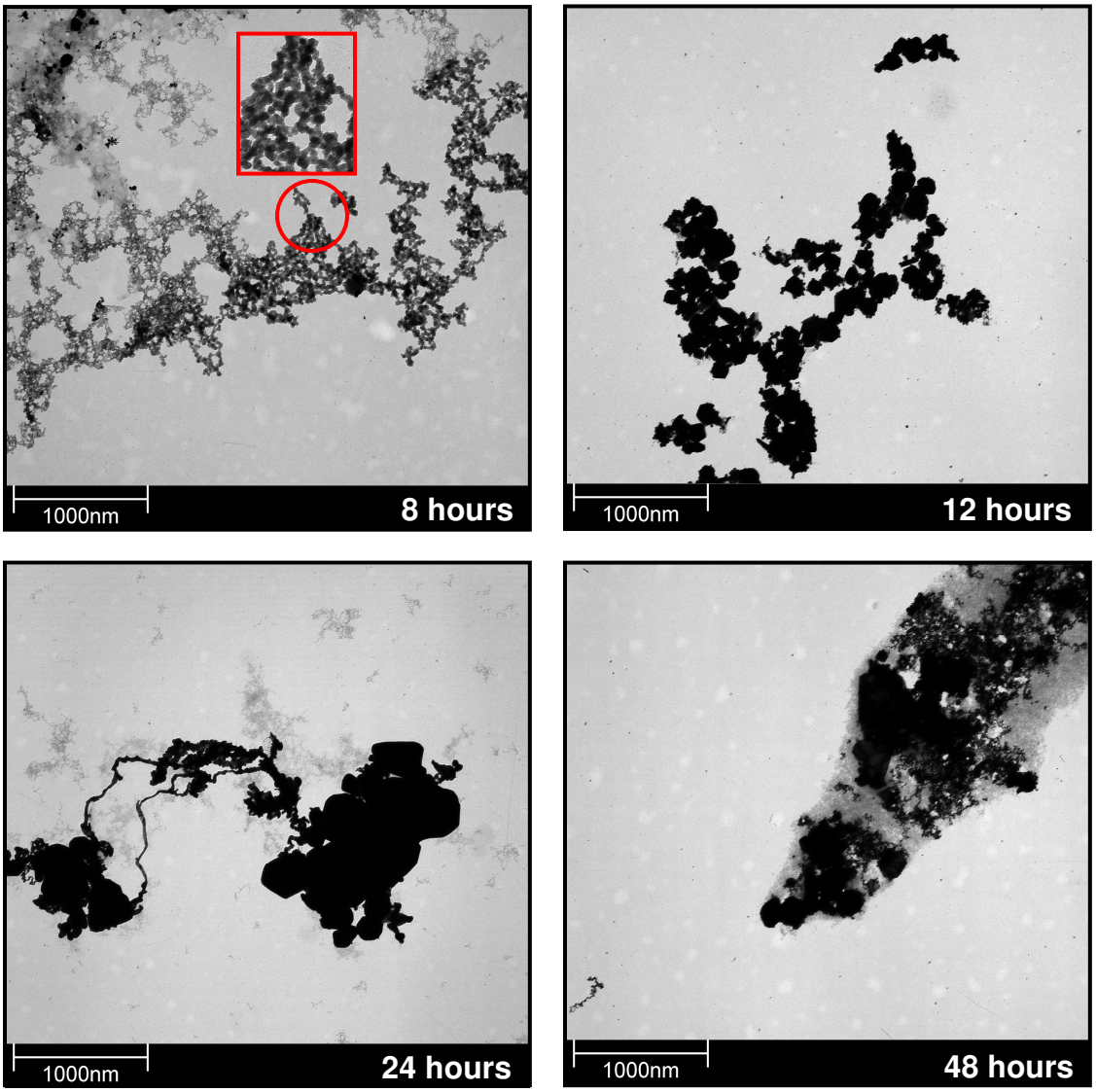

Figure 3.33: TEM micrographs for the different exposure times, indicating the shapes, sizes and amounts of gold nanoparticles obtained. All scale bars are equal to 1000 nm.

EDX was done on all the samples and the nanoparticles were confirmed to be gold, as can be seen in figure 3.34.

From this it can be concluded that at shorter exposure times, the particles obtained are smaller and fewer were formed, but increases in both size and amount with longer exposure times. At too long exposure times, the particles will become too big and out of the nano size range and also less shape definition or incomplete shapes were obtained. If particles were to be exposed for longer incubation times, this should be done at lower temperatures, as discussed in sections 1.6 and 3.3.7.7, to obtain better defined particles.

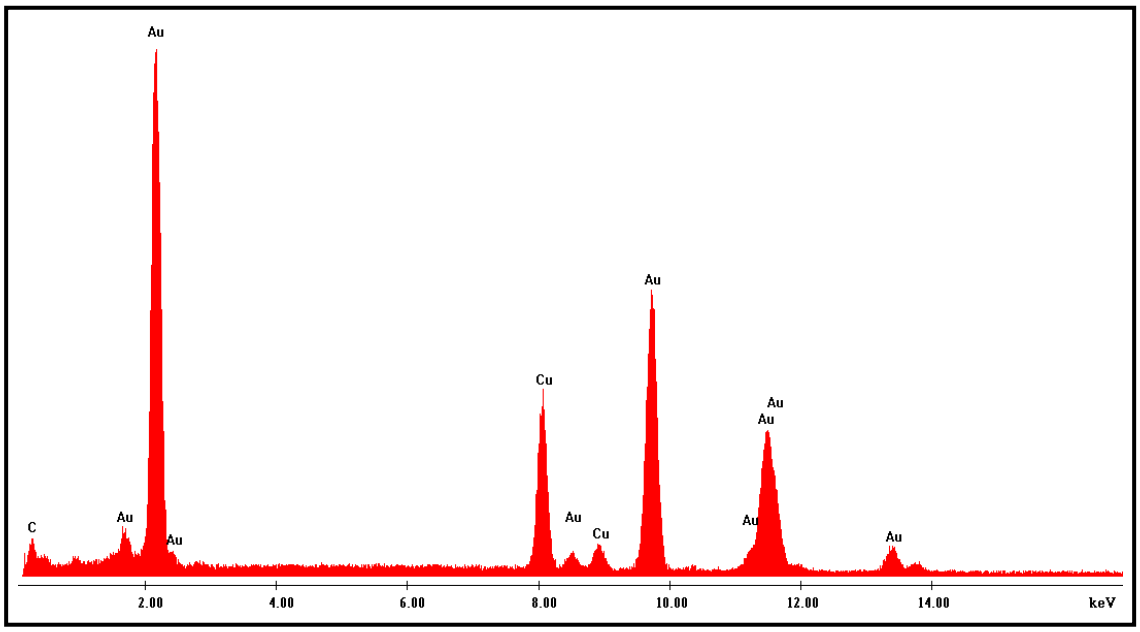

Figure 3.34: EDX spectrum recorded for the nanoparticles produced at different exposure times, showing a typical pattern for all the samples and indicates that the nanoparticles are gold.

3.3.7.6 The Effect of $HAuCl_4$ Concentrations on Gold Reduction and Nanoparticle Formation

The effect of gold(III) concentrations on gold reduction and nanoparticle formation was tested at 0 mM; 0.5 mM; 1.0 mM; 2.0 mM; 5.0 mM; 7.5 mM and 10 mM final concentrations of $HAuCl_4$ respectively, to determine the optimum gold(III) concentration for nanoparticle formation with the best defined shapes. When comparing the reactions through the visual assay (Figure 3.35) and the SPR, obtained through UV-Vis spectra (Figure 3.36), optimum nanoparticle formation took place from 0.5 mM to 2 mM (Tubes 3 – 8). Nanoparticle formations can be seen through a change in the absorbance around 540 – 560 nm in the protein reactions (Figure 3.36A) with no change in the respective blank reactions (Figure 3.36B). At 0 mM gold (Tubes 1 and 2), no reaction took place, indicating no interference by any of the assay components that could have influenced nanoparticle formations. At 5.0 mM (Tubes 9 and 10), big particles were expected, due to the reaction containing particles that had already precipitated out of solution and can be seen in a shift in the wavelength, giving a change in absorbance around 640 – 650

nm. At 5.0 mM to 10 mM (Tubes 11 – 14) no change in absorbance was detected, indicating particles most likely not in the nano size range anymore.

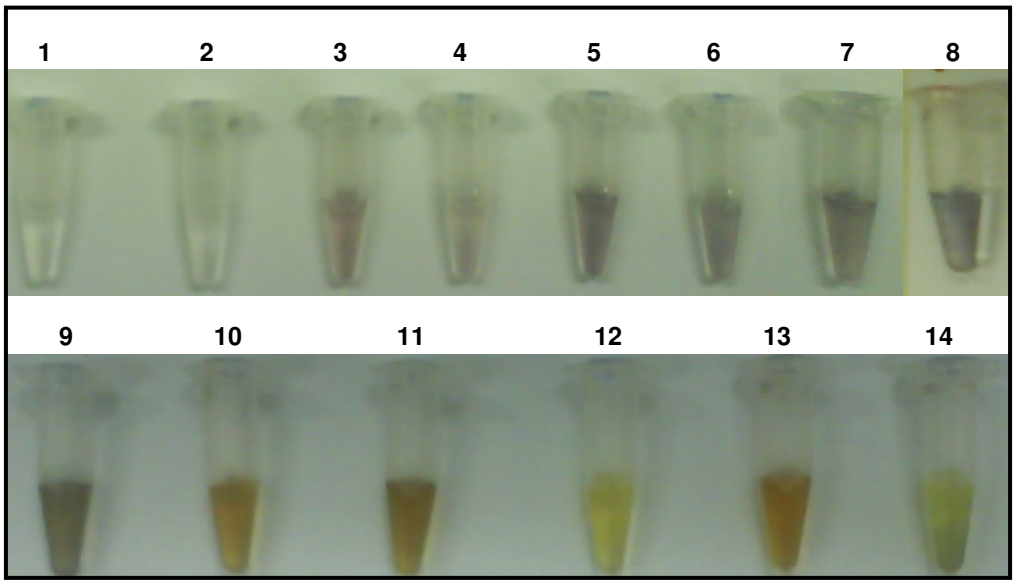

Figure 3.35: The different colours obtained through the gold reduction assay at varying $HAuCl_4$ concentrations, indicating gold nanoparticle formation. The odd numbers (1 – 13) indicate protein reactions for 0 mM; 0.5 mM; 1.0 mM; 2.0 mM; 5.0 mM; 7.5 mM and 10 mM respectively and the even numbers (2 – 14) the corresponding blank reactions.

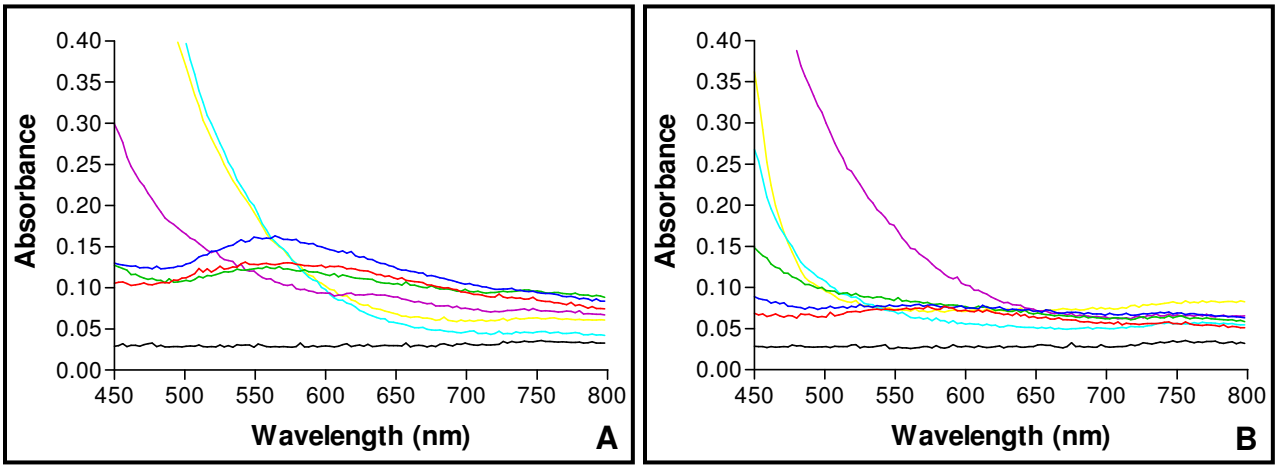

Figure 3.36: UV-Vis absorption spectra of the surface plasmon resonance recorded for the different $HAuCl_4$ concentrations, indicating gold nanoparticle production through a change in the absorbance around 540 - 560 nm. (A) The protein reactions and (B) the corresponding blank reactions. [0 mM ( ); 0.5 mM ( ); 1.0 mM ( ); 2.0 mM ( ); 5.0 mM ( ); 7.5 mM ( ); 10 mM ( )].

The TEM micrographs (Figure 3.37) confirmed no interference from the assay components at 0 mM. At 5.0 mM, the particles were much bigger and very close to the limits of the nano size range and at 10.0 mM, the particles were out of the nano size range. Only between 0.5 mM and 2.0 mM, nanoparticles were obtained. Several shapes and sizes were formed, with mostly spherical at 0.5 mM and 2.0 mM and several triangular shaped nanoparticles at 1.0 mM, but they were not completely monodispersed. At 2.0 mM, the thin sheets with bend contours were again obtained.

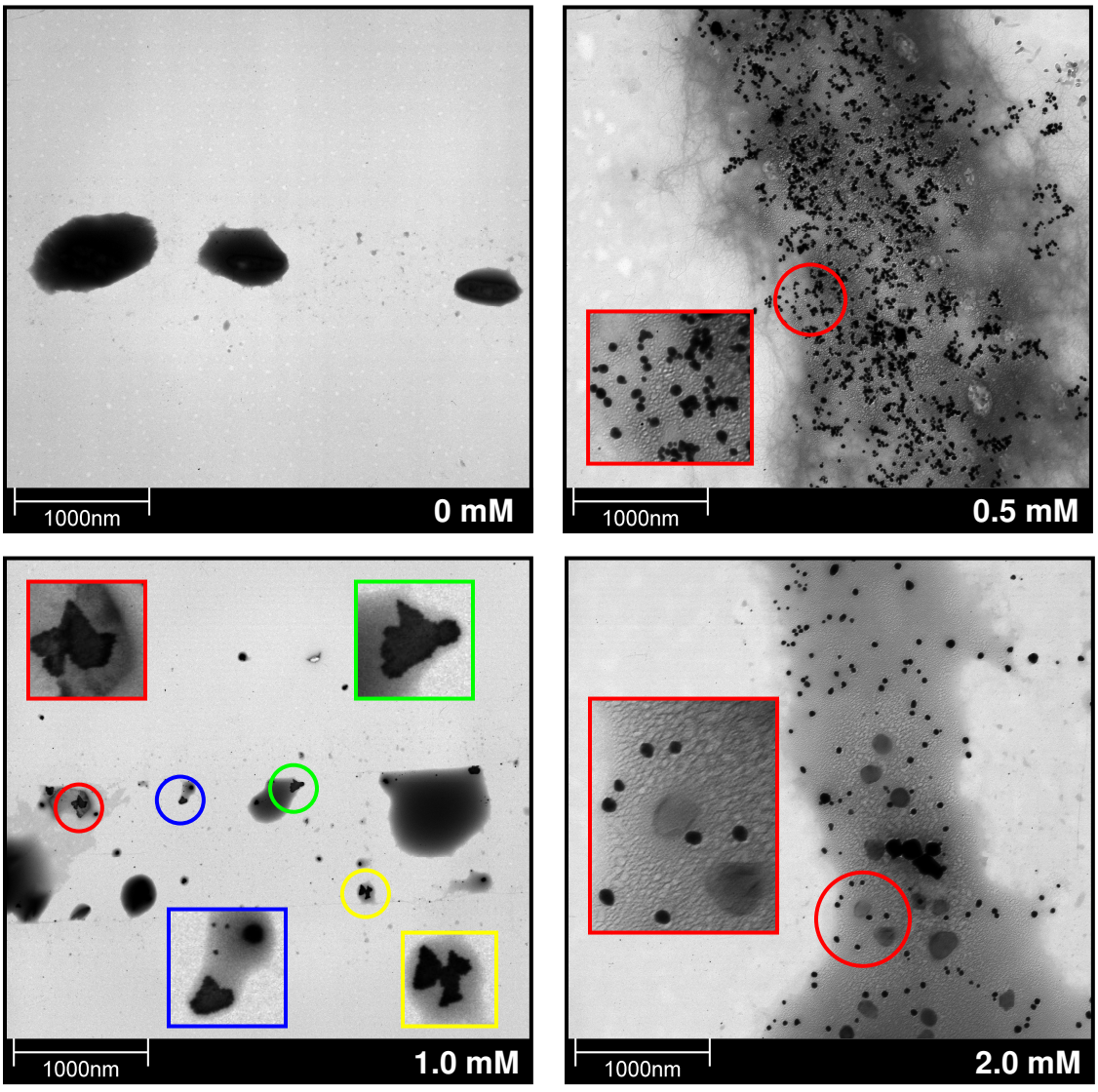

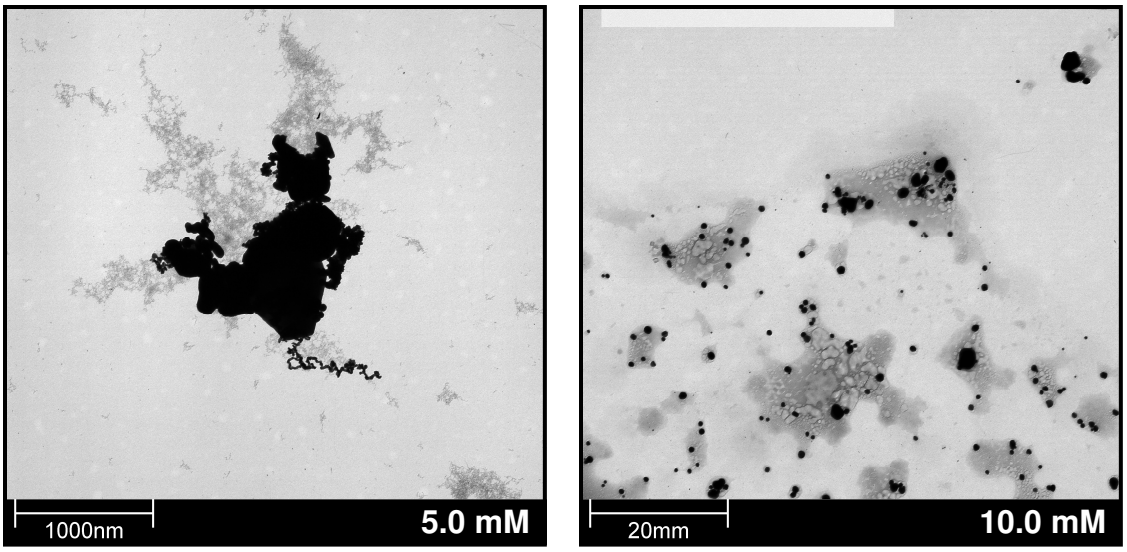

Figure 3.37: TEM micrographs for the different $HAuCl_4$ concentrations, indicating the shapes, sizes and amounts of gold nanoparticles obtained. Scale bars in 0 mM – 5.0 mM are equal to 1000 nm and in 10.0 mM the scale bar is equal to 20 mm.

EDX was done on all the samples and the nanoparticles were confirmed to be gold, as can be seen in figure 3.38.

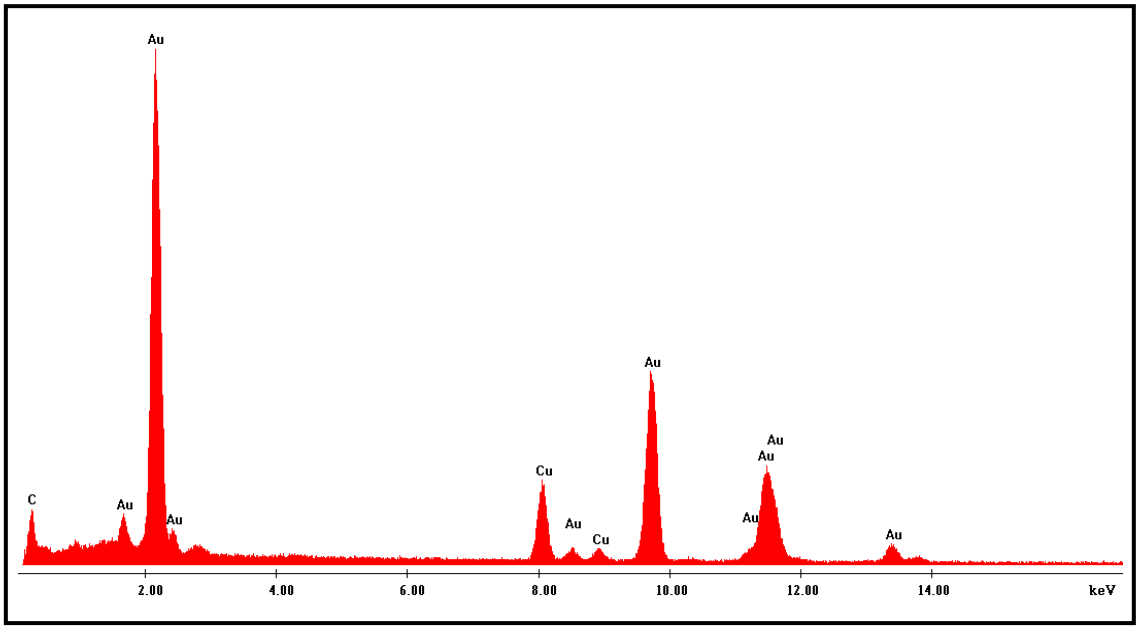

Figure 3.38: EDX spectrum recorded for the nanoparticles produced at different $HAuCl_4$ concentrations, showing a typical pattern for all the samples and indicates that the nanoparticles are gold.

From this, it can be seen that the optimum gold concentration for nanoparticle formation is around 1.0 mM. At this concentration, the particles obtained had the best defined shapes. At higher concentrations, particle formation has grown past shape depositing control. An increase in the gold(III) concentration, results in an increase in particle size and if the gold(III) concentration is too high, the particles are out of the nano size range. Therefore, it might be possible to obtain more nanoparticles with better defined shapes at lower gold(III) concentrations. Furthermore, if the protein aids not only in gold reduction but also nanoparticle formation, it might be a plausible explanation for the differences in the stoichiometry, therefore leading to uncontrolled particle formation at higher concentrations. These findings agree with the physico-chemical properties of nanoparticles as discussed in section 1.6.

3.3.7.7 The Effect of Temperature on Gold Reduction and Nanoparticle Formation

The effect of temperature on gold reduction and nanoparticle formation was tested through incubation at 30ºC; 37ºC; 42ºC; 55ºC; 65ºC and 85ºC respectively, to determine the optimum temperature for nanoparticle formation with the best defined shapes. When comparing the reactions through the visual assay (Figure 3.39) and the SPR, obtained through UV-Vis spectra (Figure 3.40), nanoparticle formation started at 55ºC (Tubes 7 and 8), with optimum formation at 65ºC (Tubes 9 and 10) and excessive chemical reduction at 85ºC (Tubes 11 and 12). At 55ºC the protein reaction gave a light pink colour, signifying the formation of nanoparticles, with a clear difference in the black colour of the blank reaction, indicating chemical reduction and if any particles were formed, they would be notably bigger. At 65ºC the protein reaction gave a dark pink colour, with again a clear difference in the blank reaction, proving it to be the optimum temperature to produce gold nanoparticles. This might be due to the optimum growth temperature for *T. scotoductus* SA-01 also being 65ºC. At 85ºC, no differences were obtained in the colours with the protein reaction and the blank reaction, suggesting that excessive chemical reduction took place at a faster rate, giving too much interference since the protein was not active anymore and did not play a significant role. The dark purple/black colours indicate that nanoparticles were produced, but they should be bigger particles. Nanoparticle formations can be seen through a change in the absorbance around 540 – 550 nm in the protein reactions (Figure 3.40A) with no change

in the respective blank reactions (Figure 3.40B). At 30ºC – 42ºC (Tubes 1 – 6), no colour formation was obtained, indicating that nanoparticle formation was exceptionally slow and not very effective but a change in the absorbance (Figure 3.40A), although at low values, indicate that some nanoparticles were in fact obtained, however not very significantly. Even though chemical reduction was observed through the visual assay for 55ºC – 85ºC, no change in the absorbance was detected for the blank reactions, indicating purely chemical reduction and no nanoparticle formation.

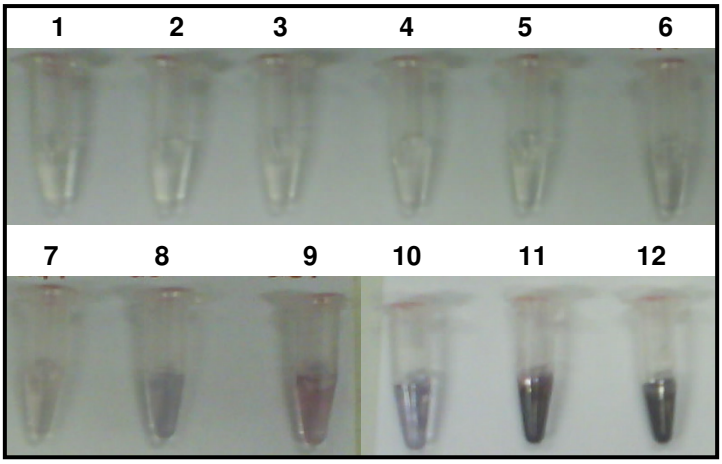

Figure 3.39: The different colours obtained through the gold reduction assay at varying temperatures, indicating gold nanoparticle formation. The odd numbers (1 – 11) indicate protein reactions for 30ºC; 37ºC; 42ºC; 55ºC; 65ºC and 85ºC respectively and the even numbers (2 – 12) the corresponding blank reactions.

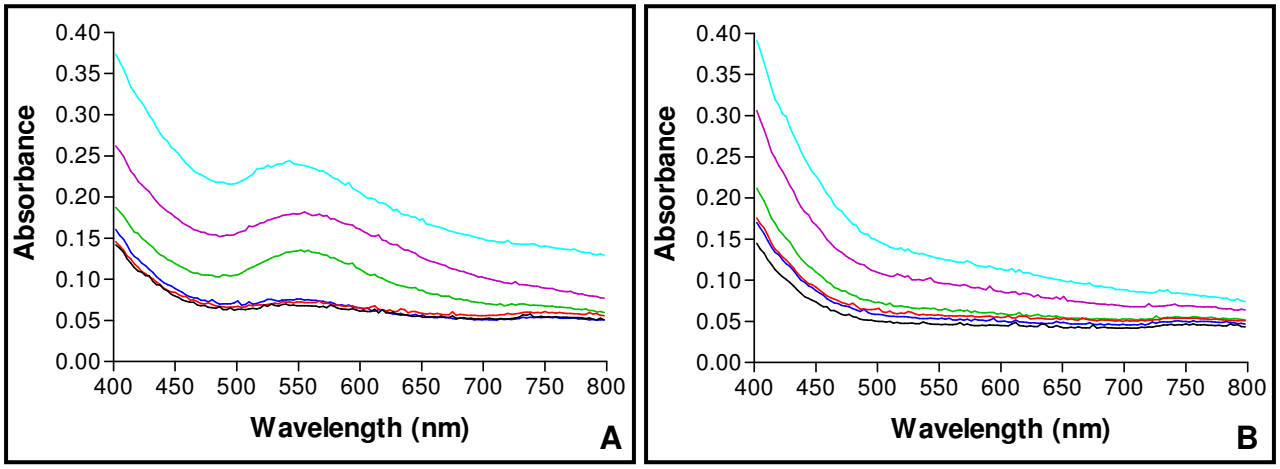

Figure 3.40: UV-Vis absorption spectra of the surface plasmon resonance recorded for the different temperatures, indicating gold nanoparticle production through a change in the absorbance around 540 - 550 nm. (A) The protein reactions and (B) the corresponding blank reactions. [30ºC ( ); 37ºC ( ); 42ºC ( ); 55ºC ( ); 65ºC ( ); 85ºC ( )].

The TEM micrographs (Figure 3.41) confirmed that particles were indeed formed at each temperature, and that all the particles are in the nano size range, but not monodisperse. At 30ºC, the particles were noticeably smaller and almost completely spherical. At 37ºC and 42ºC, particles were still very small, but different, well defined shapes were obtained, including rods, triangles and diamond shapes. At 55ºC, an increase can be seen in the size and amount of the particles, but still with defined shapes. At 65ºC, the particle size kept on increasing and although shapes like rods and triangles could still be detected; several particles with less shape definition were also present. The particles obtained at 85ºC were noticeably bigger and mostly particles with less shape definition or incomplete shapes were obtained. This again indicates that smaller but more controlled nanoparticle formation takes place at lower temperatures with slower reaction rates.

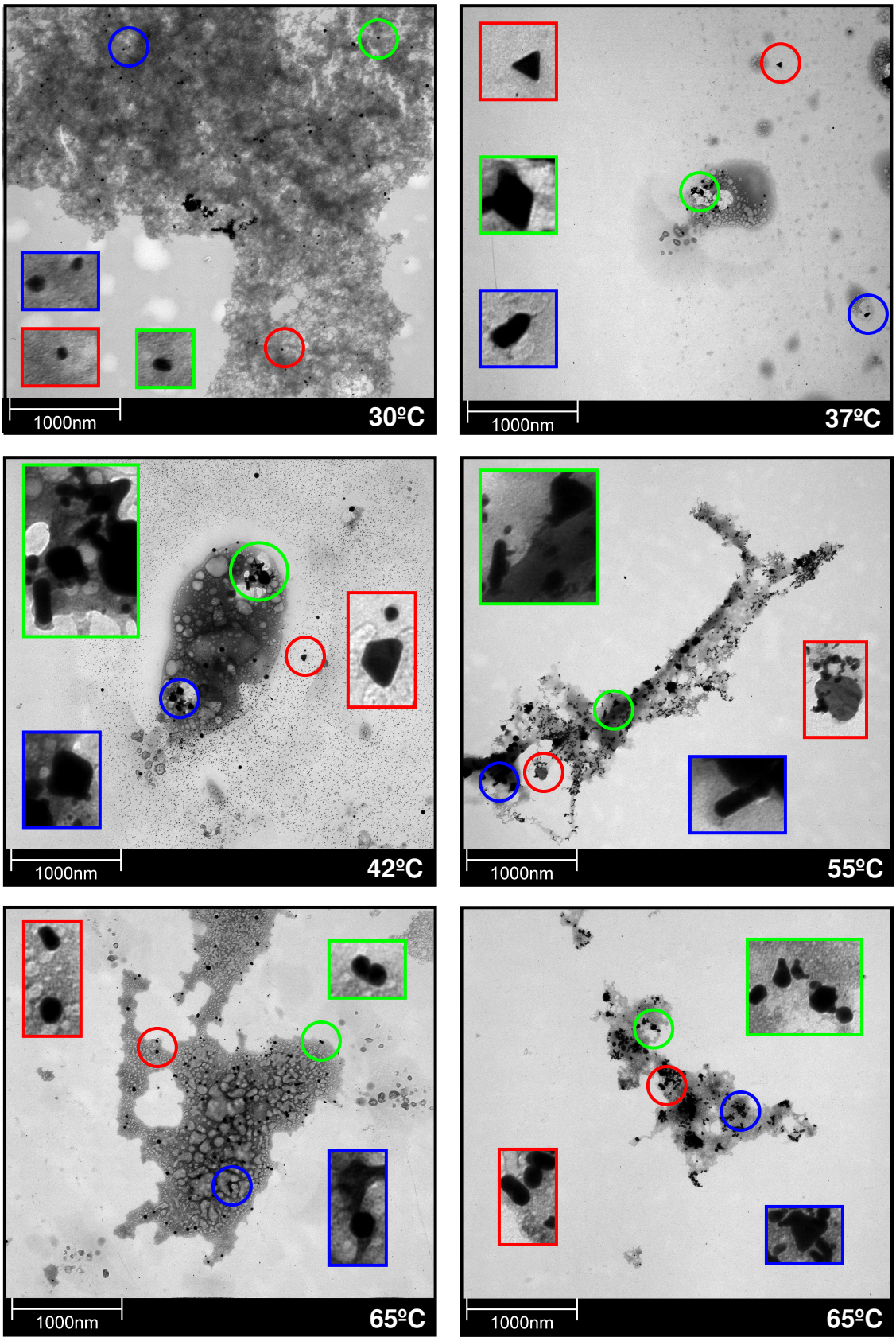
1000nm
30ºC
1000nm
37ºC
1000nm
42ºC
1000nm
55ºC
1000nm
65ºC
1000nm
65ºC

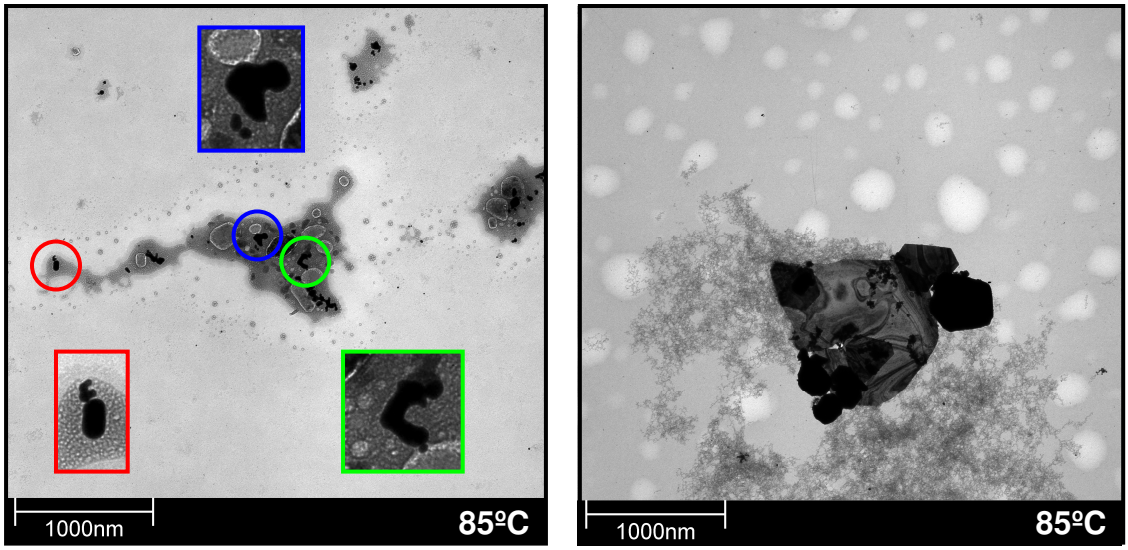

Figure 3.41: TEM micrographs for the different temperatures, indicating the shapes, sizes and amounts of gold nanoparticles obtained. All scale bars are equal to 1000 nm.

EDX was done on all the samples and the nanoparticles were confirmed to be gold, as can be seen in figure 3.42. In all the figures with EDX spectra from here onwards, the carbon and copper detected in the samples is due to the TEM grids, since analysis was done on Formvar carbon-coated 200-mesh copper grids (Section 3.2.15.5).

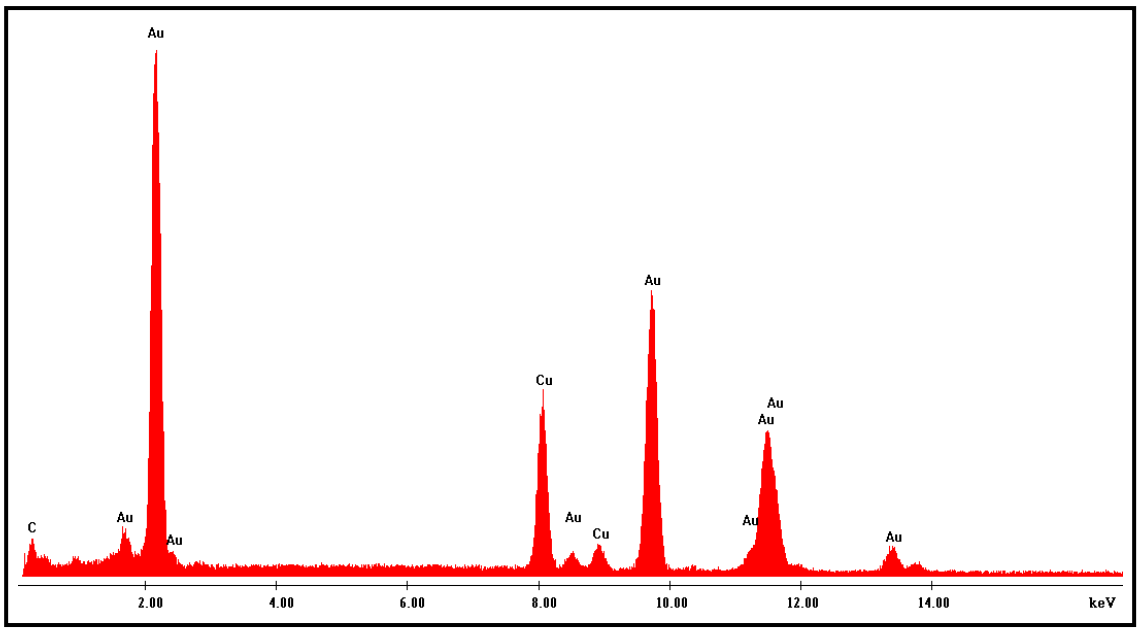

Figure 3.42: EDX spectrum recorded for the nanoparticles produced at different temperatures, showing a typical pattern for all the samples and indicates that the nanoparticles are gold.

From this it can be concluded that at lower temperatures the particles obtained are smaller and fewer were formed, but with better defined shapes and with no chemical reduction taking place. This may be due to the nanoparticle formation process taking place at a slower rate, yielding a measure of control over this process to form particles that are well shaped and clearly defined. At higher temperatures, the process is taking place much faster and chemical reduction can be detected, yielding unusual shapes or not giving enough time to form defined particles and the reaction is finished before the particle was completely formed. These findings agree with the physico-chemical properties of nanoparticles as discussed in section 1.6 and coincide with Gericke & Pinches, (2006) who stated that the rate of particle formation can be correlated with the incubation temperature where an increase in temperature will allow faster particle formation and the rate of reduction can influence the type of particle formed. Therefore, it might be possible to obtain more nanoparticles with better defined shapes through incubation at lower temperatures, but for longer time intervals.

3.3.7.8 The Effect of pH on Gold Reduction and Nanoparticle Formation

The effect of pH on gold reduction and nanoparticle formation was tested at pH values of 3.6; 5.5; 7.5 and 9.0 respectively, to determine the optimum pH for nanoparticle formation with the best defined shapes. When comparing the reactions through the visual assay (Figure 3.43) and the SPR, obtained through UV-Vis spectra (Figure 3.44), nanoparticles were formed at all pH values, with optimum formation at pH 5.5 - 9.0 (Tubes 3 - 8). Nanoparticle formations can be seen through a change in the absorbance around 540 – 550 nm in the protein reactions (Figure 3.44A) with no change in the respective blank reactions (Figure 3.44B). At pH 3.6 (Tubes 1 and 2) very small nanoparticles were formed, indicated by the yellow colour, but no change in the absorbance was observed, indicating ineffective particle formation. At pH 5.5 and 9.0 (Tubes 3 and 7 respectively), the biggest nanoparticles were formed, because of the purple colours and significant changes in the absorbance readings, again with clear differences in the blank reactions (Tubes 4 and 8).

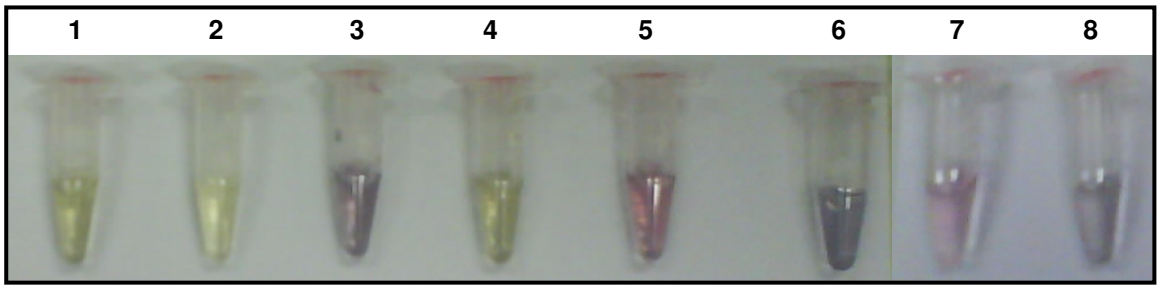

Figure 3.43: The different colours obtained through the gold reduction assay at varying pH values, indicating gold nanoparticle formation. The odd numbers (1 – 7) indicate protein reactions for pH 3.6; 5.5; 7.5 and 9.0 respectively and the even numbers (2 – 8) the corresponding blank reactions.

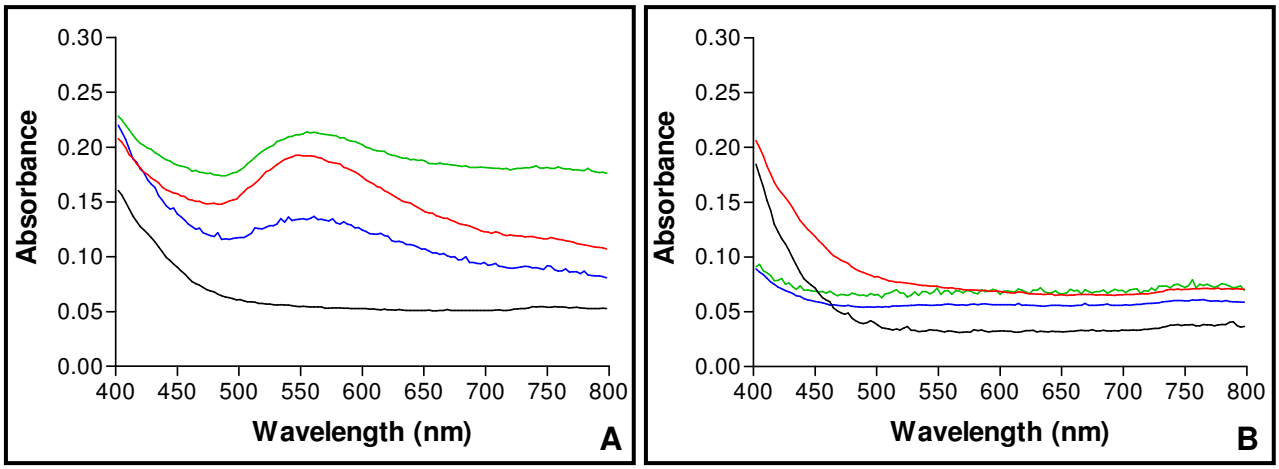

Figure 3.44: UV-Vis absorption spectra of the surface plasmon resonance recorded for the different pH values, indicating gold nanoparticle production through a change in the absorbance around 540 - 550 nm. (A) The protein reactions and (B) the corresponding blank reactions. [pH 3.6 (—); pH 5.5 (—); pH 7.5 (—); pH 9.0 (—)].

The TEM micrographs (Figure 3.45) confirmed that particles were formed at each pH value, and that all the particles are in the nano size range, but not monodisperse. At pH 3.6, the particles were very small and mostly attached to each other, forming a herringbone structure but no distinctive shapes were formed. At pH 5.5, the particles were bigger, but with the herringbone structure again present. No well defined, complete shapes were obtained either. At pH 7.5, the particles were again smaller, but several well defined triangles were obtained. Other nanoparticles that were formed at this pH, included spherical and rod like shapes. Bigger particles were again obtained at pH 9.0 and also included several well defined triangles, with spherical and rod like

shapes. At pH 7.5, several very thin sheets with bend contours were obtained. Although these particles have a higher transparency, they were confirmed through SAED and EDX analysis to be gold nanoparticles and have simply a thinner appearance. Similar particles were found by Lengke *et al.*, (2007) and Narayanan & El-Sayed, (2004), as can be seen in figures 1.3 and 1.7 respectively and due to the extremely small sizes of these particles with a large surface to volume ratio, they might have more unique physical and chemical properties at this scale that differs considerably from when they are used in larger form and this may result in an even bigger increase in applications. This indicates at lower pH values, good nanoparticle formation, but herringbone structures can be obtained, whereas better shape definition can be obtained at higher pH values.

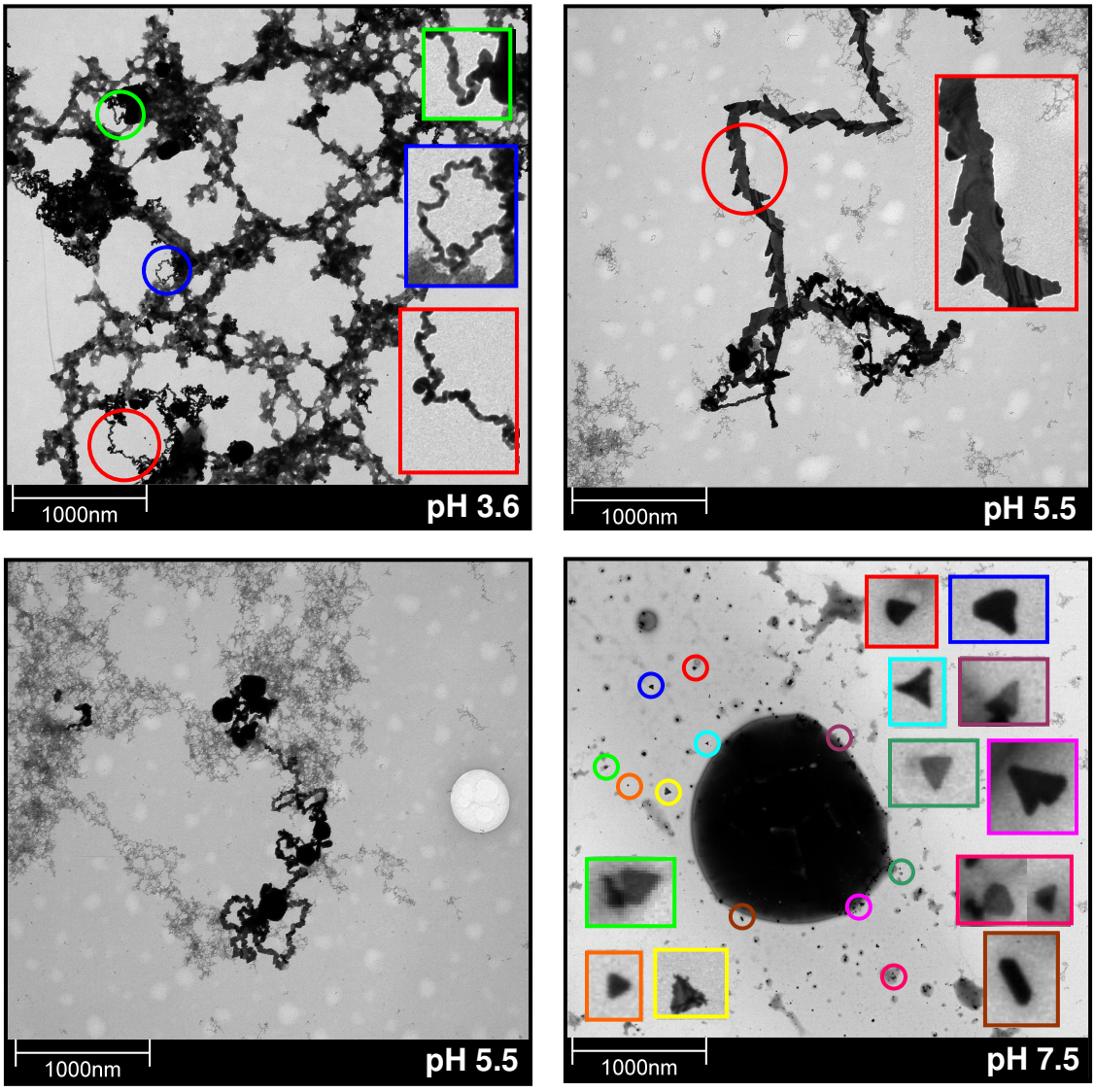

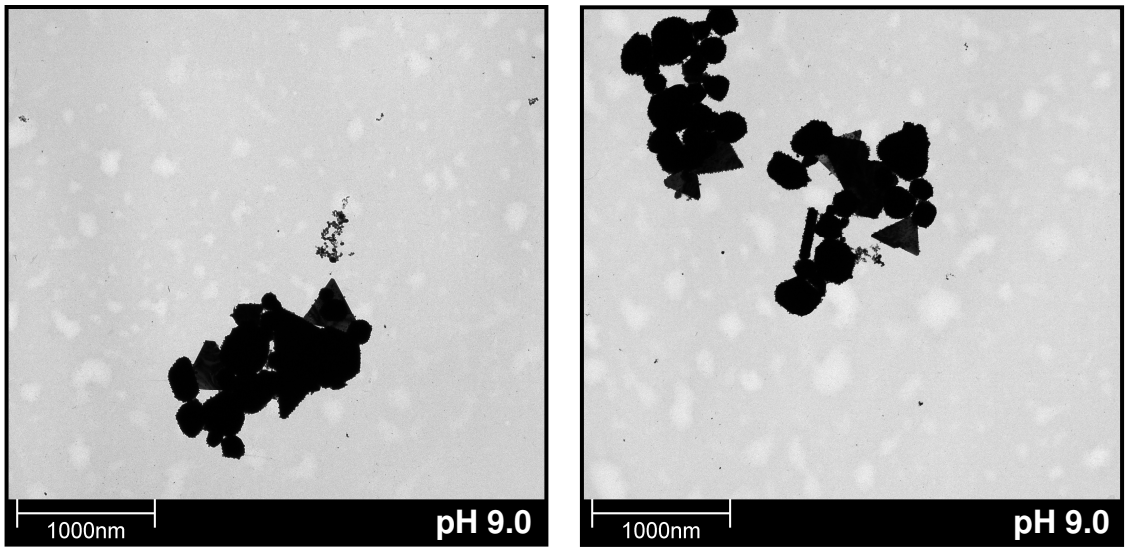

Figure 3.45: TEM micrographs for the different pH values, indicating the shapes, sizes and amounts of gold nanoparticles obtained. All scale bars are equal to 1000 nm.

SAED was performed on the nanoparticles from pH 9.0 and EDX was done on all the samples and the nanoparticles were confirmed to be gold, as can be seen in figure 3.46 and figure 3.47 respectively. In figure 3.46B the micro-diffraction pattern for gold can be seen.

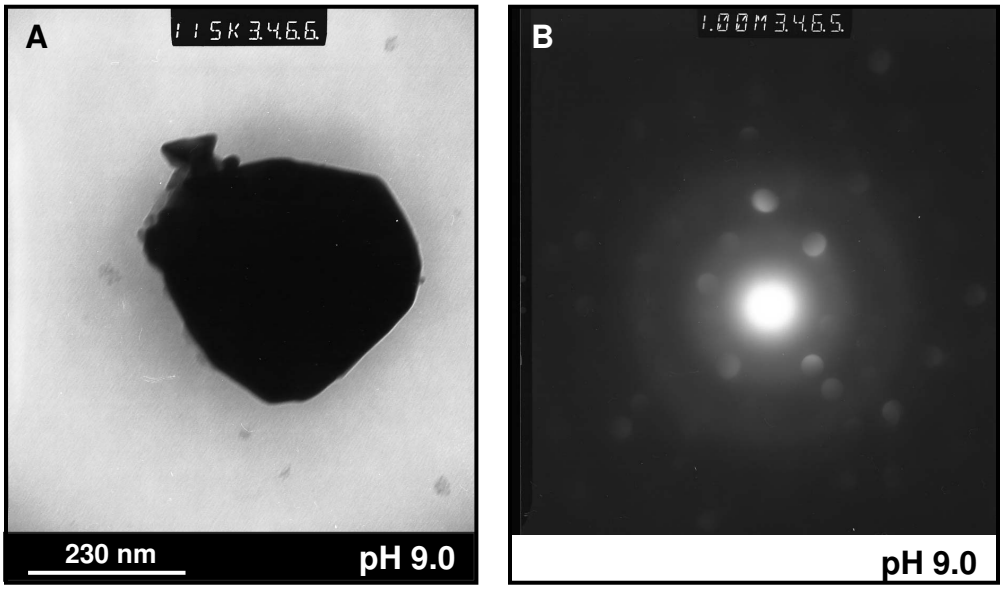

Figure 3.46: (A) TEM micrograph of a gold nanoparticle with (B) corresponding selected-area electron micro-diffraction pattern for pH 9.0. The scale bar in A is equal to 230 nm.

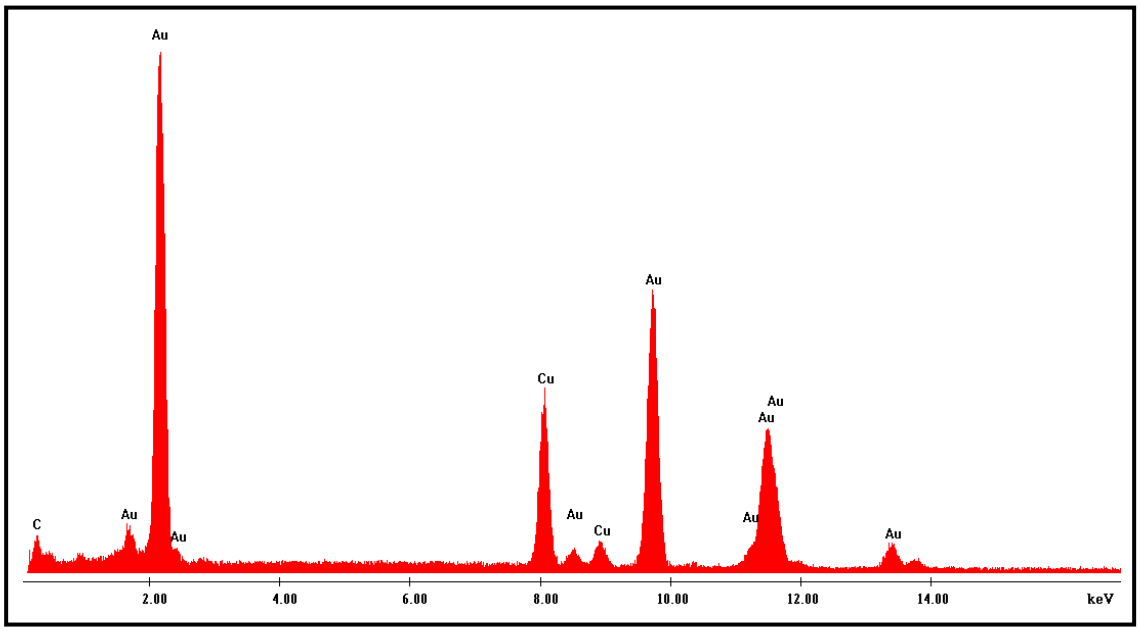

Figure 3.47: EDX spectrum recorded for the nanoparticles produced at different pH values, showing a typical pattern for all the samples and indicates that the nanoparticles are gold.

From this it can be concluded that bigger, but better defined gold nanoparticles are obtained at pH values closer to the pI of the protein, which is 9.54. Therefore, it might be possible to obtain more nanoparticles with better defined shapes at higher pH values. These findings agree with the physico-chemical properties of nanoparticles as discussed in section 1.6, that the shape and size of nanoparticles can be controlled by changing the pH of the reaction and the reaction kinetics strongly depend on the pH of the solution.

Nanotrac particle size analyses were performed on pH 7.5 and pH 9.0, for additional confirmation of the size and size distribution of the gold nanoparticles (Section 3.2.15.7). The average size percentage can be seen in table 3.4, indicating that the overall sizes for pH 9.0 are bigger than those of pH 7.5. For pH 7.5, 70% of the particles are smaller than 100 nm (100.6 nm), with only 30% bigger than 100 nm and 95% are smaller than 148.8 nm. For pH 9.0, only 10% of the particles are smaller than 100 nm (99.1 nm), with 90% bigger than 100 nm and 95% smaller than 124.6 nm.

Table 3.4: The average size percentage of the nanoparticles present at (A) pH 7.5 and (B) pH 9.0.

A

% Tile	Size (µm)	Size (nm)
10	0.0215	21.5
20	0.0381	38.1
30	0.0549	54.9
40	0.0687	68.7
50	0.0800	80.0
60	0.0902	90.2
70	0.1006	100.6
80	0.1130	113.0
90	0.1314	131.4
95	0.1488	148.8

B

% Tile	Size (µm)	Size (nm)
10	0.0991	99.1
20	0.1032	103.2
30	0.1058	105.8
40	0.1082	108.2
50	0.1104	110.4
60	0.1127	112.7
70	0.1151	115.1
80	0.1178	117.8
90	0.1210	121.0
95	0.1246	124.6

The size distribution can be seen in table 3.5 and figure 3.48, with pH 7.5 having a more extensive distribution than pH 9.0. For pH 7.5, 99.66% of the particles are smaller than 204.4 nm; 71.43% are smaller than 102.2 nm; 27.62% are smaller than 51.1 nm and only 3.14% are smaller than 10.74 nm. For pH 9.0, 100% of the particles are smaller than 144.5 nm; 91.55% are smaller than 121.5 nm and only 16.21% are smaller than 102.2 nm. From this it can be concluded that the overall sizes of the particles are bigger at pH 9.0, even though a few bigger ones were obtained at pH 7.5 and the particles are more monodisperse in size at pH 9.0 than at pH 7.5.

Table 3.5: Size distribution of the nanoparticles present at (A) pH 7.5 and (B) pH 9.0.

A

Size (nm)	% Channel	% Passed
289.0	0.00	100.00
243.0	0.34	100.00
204.4	1.60	99.66
171.9	3.95	98.06
144.5	8.68	94.11
121.5	14.00	85.43
102.2	15.70	71.43
85.9	12.79	55.73
72.3	8.99	42.94
60.8	6.33	33.95
51.1	4.83	27.62
43.0	3.98	22.79
36.1	3.40	18.81
30.4	2.92	15.41
25.55	2.50	12.49
21.48	2.14	9.99
18.06	1.82	7.85
15.19	1.56	6.03
12.77	1.33	4.47
10.74	1.14	3.14
9.03	0.98	2.00
7.60	0.87	1.02
6.39	0.15	0.15
5.37	0.00	0.00

B

Size (nm)	% Channel	% Passed
171.9	0.00	100.00
144.5	8.45	100.00
121.5	75.34	91.55
102.2	16.21	16.21
85.9	0.00	0.00

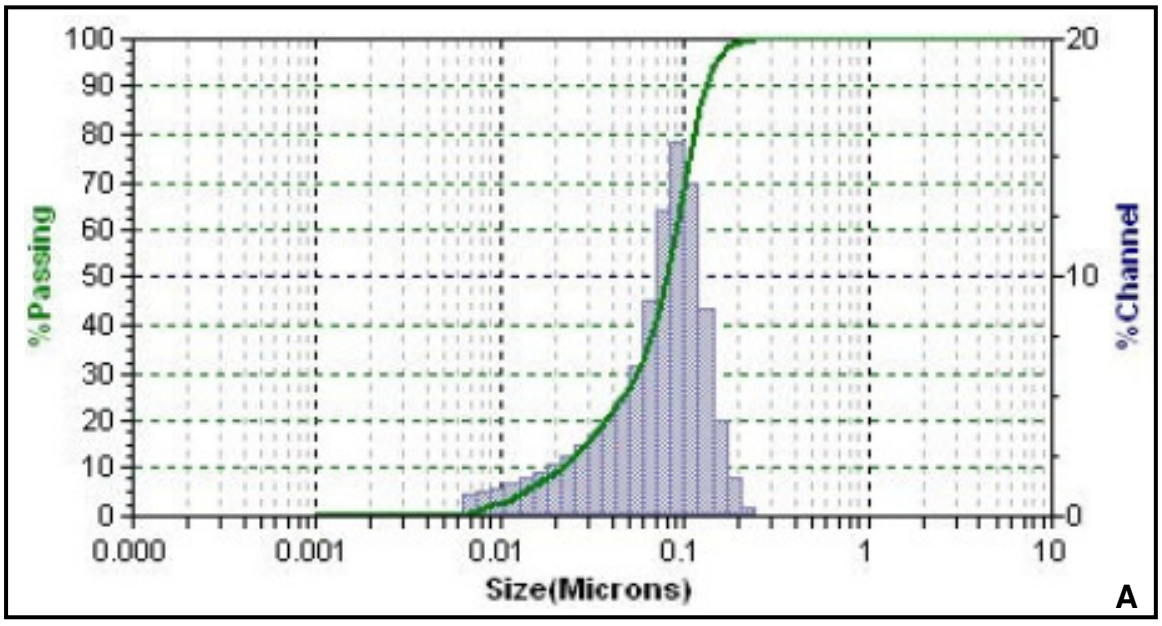

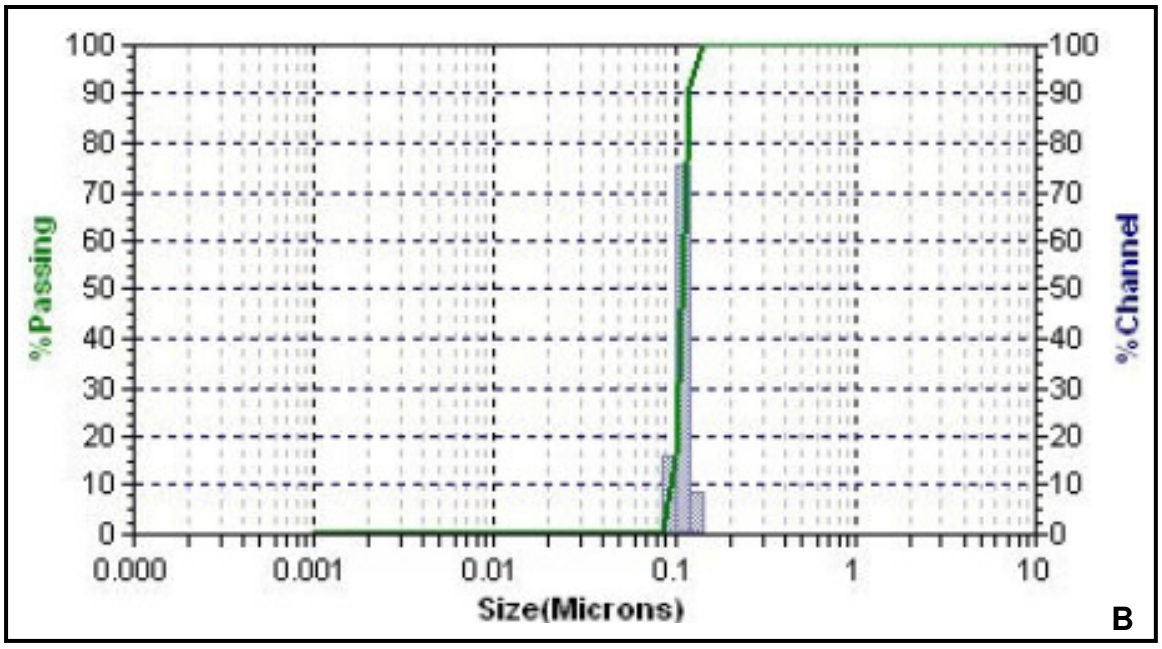

Figure 3.48: Size distribution for the gold nanoparticles obtained at (A) pH 7.5 and (B) pH 9.0.

Scanning Auger Nanoprobe analyses were performed on particles formed at pH 7.5, for additional confirmation of the size and elemental composition (Section 3.2.15.8). SEM images were obtained (Figure 3.49), showing different shapes of nanoparticles obtained and also confirming that the particles were in the nano size range. Selected-area elemental spectrums (Figure 3.50) and elemental map tests (Figure 3.51) were used to confirm that the particles obtained were gold. Several particles were analyzed, all with similar results.

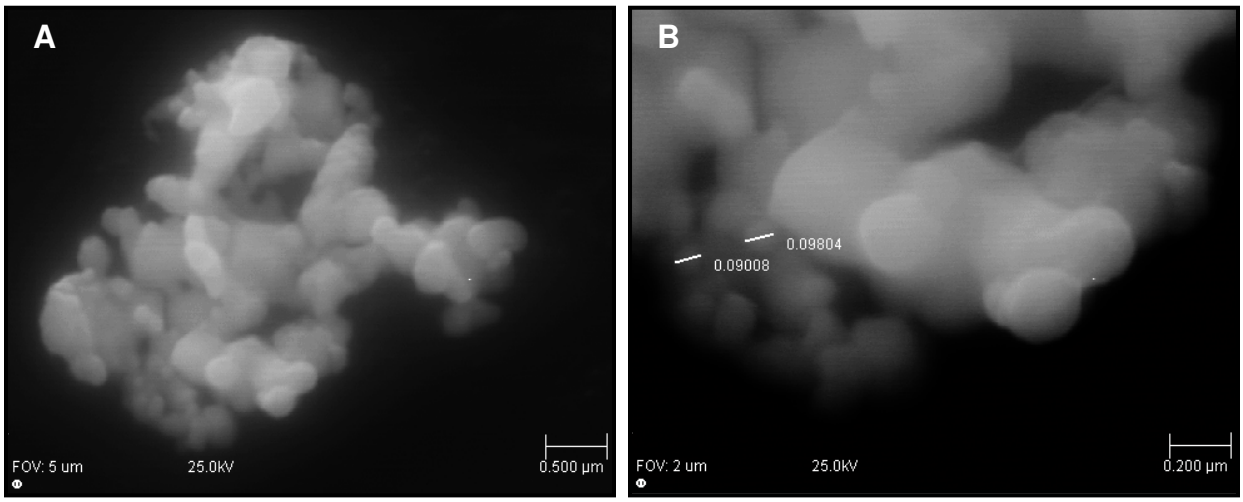

Figure 3.49: SEM micrographs for pH 7.5, indicating different shapes and sizes of gold nanoparticles obtained. Scale bars in A and B are equal to 500 nm and 200 nm, respectively.

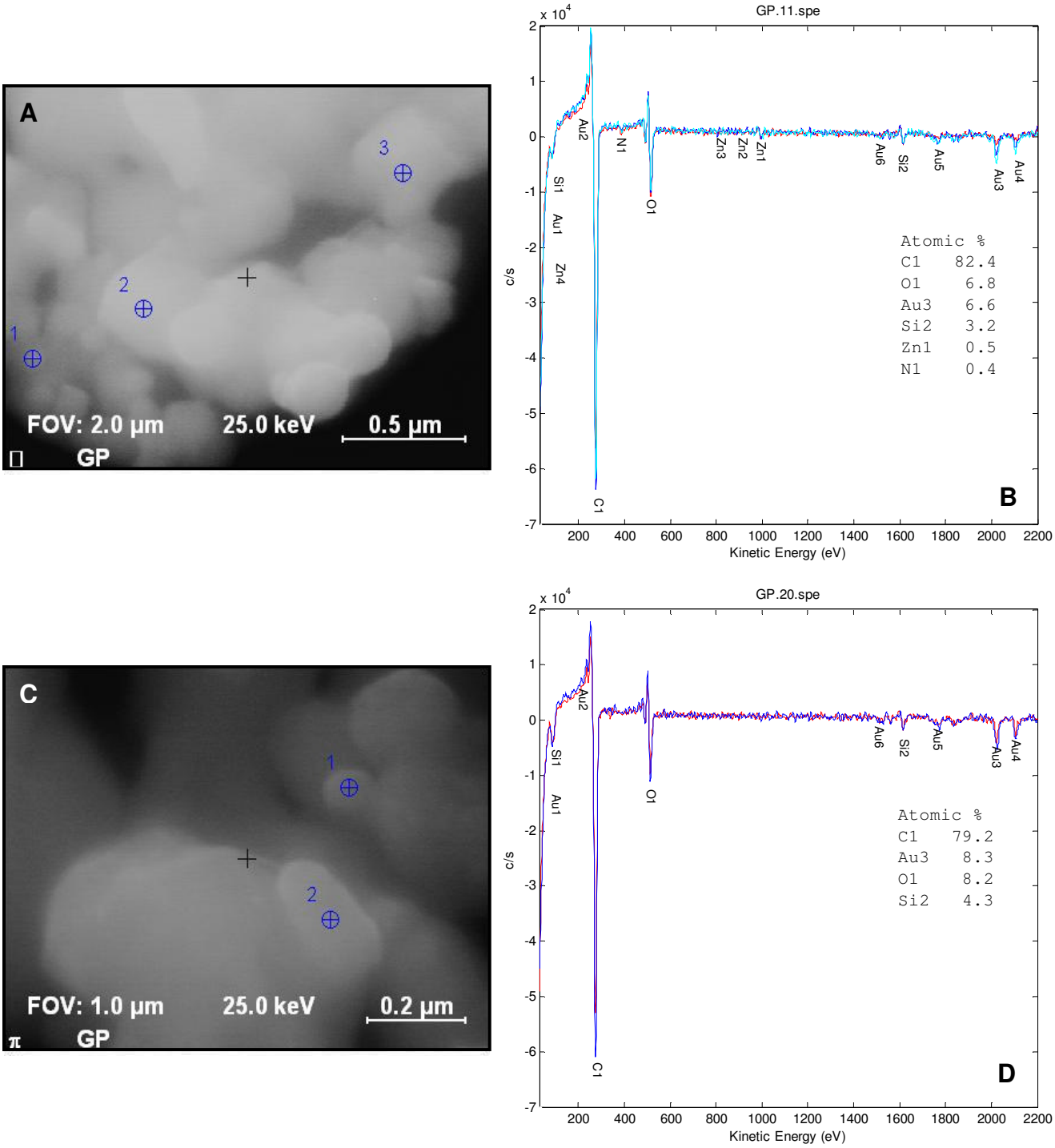

Figure 3.50: (A and C) SEM micrographs of gold nanoparticles with (B and D) corresponding selected-area Auger spectra, indicating the gold from the nanoparticles. [Area 1 (—); Area 2 (—); Area 3 (—)]. Scale bars in A and C are equal to 500 nm and 200 nm, respectively.

Samples to be analyzed with the Nanoprobe are mounted on carbon tape, therefore the large carbon peaks are present in the elemental spectrums and the oxygen was obtained from the proteins in the sample and due to the particle formation taking place aerobically. Elemental map tests were done for the presence of oxygen, carbon and gold in the selected areas in figure 3.50. This indicated that the gold was distributed all over the sample and confirmed that the particles were gold.

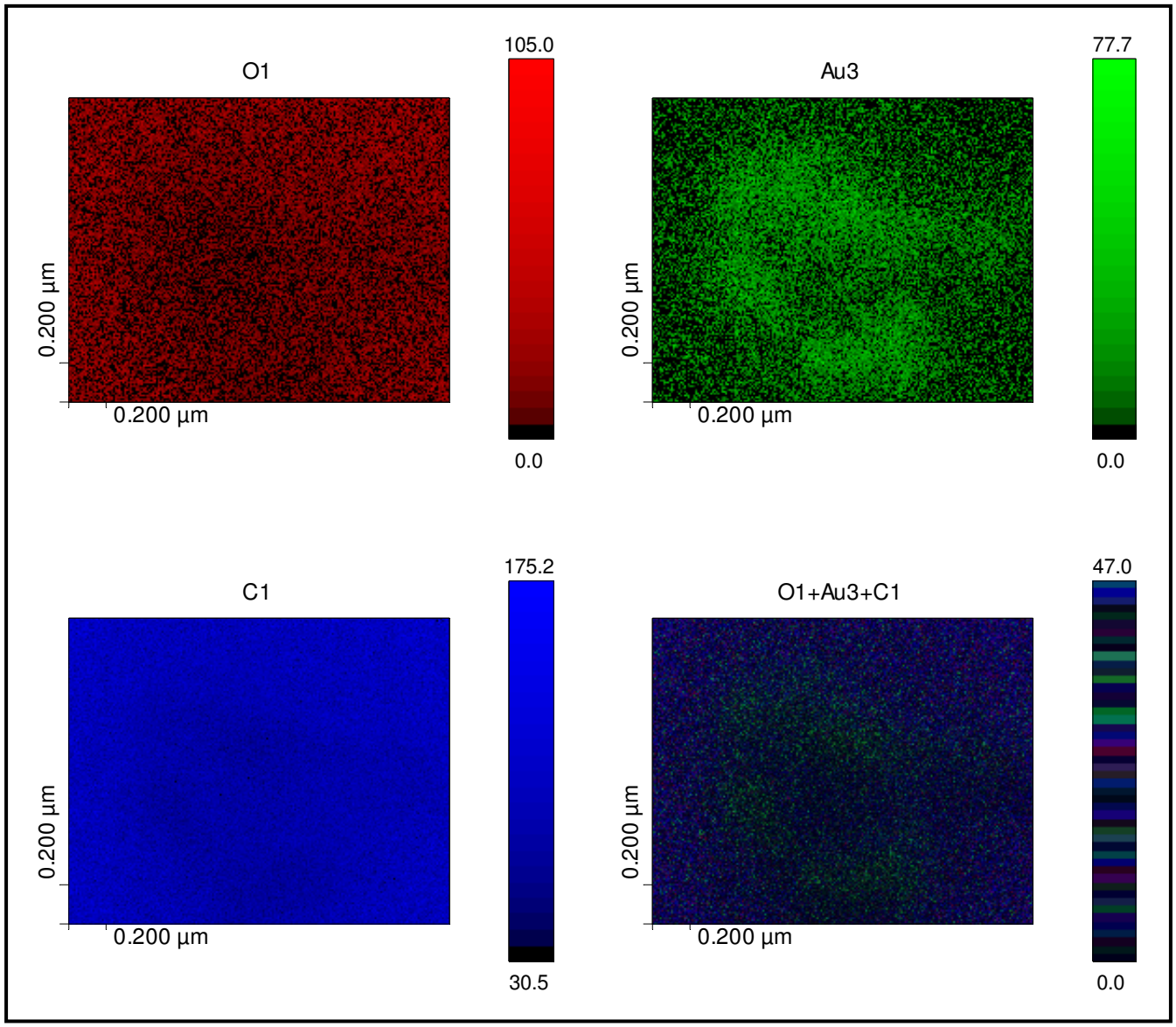

Figure 3.51: Elemental map tests done with ten frames, indicating the presence and distribution of the gold from the nanoparticles.

3.3.7.9 The Effect of Different Disulphide Bond Reducing Agents on Gold Reduction and Nanoparticle Formation

The effect of different disulphide bond reducing agents on gold reduction and nanoparticle formation was tested, using sodium dithionite, dithiothreitol (DTT) and β-mercaptoethanol as electron donors and reducing agents respectively. All three components were used without the addition of methyl viologen and the same principle applies for the mechanism of gold reduction and nanoparticle formation as discussed in section 3.3.7.1. When comparing the reactions through the visual assay (Figure 3.52) and the SPR, obtained through UV-Vis spectra (Figure 3.53), effective nanoparticle formation was obtained with all three components and can be seen due to a change in the absorbance around 540 – 580 nm in the protein reactions (Figure 3.53A) with no change in the respective blank reactions (Figure 3.53B). The blank reaction for sodium dithionite (Tube 2), gave a large amount of chemical reduction that was not obtained in the blank reactions for DTT and β-mercaptoethanol (Tubes 4 and 6 respectively). This is due to sodium dithionite being a very strong reducing agent as discussed in section 3.3.7.2. No other significant differences were obtained in the activity of the three components and since they are all disulphide bond reducing agents, the proposed mechanism hypothesis, as discussed in section 3.2.16, can be applied to all three these electron donors.

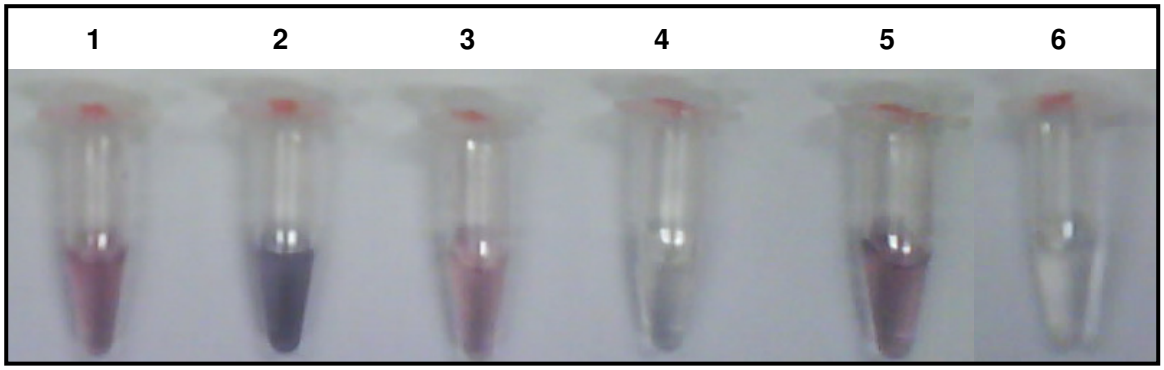

Figure 3.52: The different colours obtained through the gold reduction assay with various electron donors, indicating gold nanoparticle formation. The odd numbers (1 – 5) indicate protein reactions for sodium dithionite; dithiothreitol and β-mercaptoethanol respectively and the even numbers (2 – 6) the corresponding blank reactions.

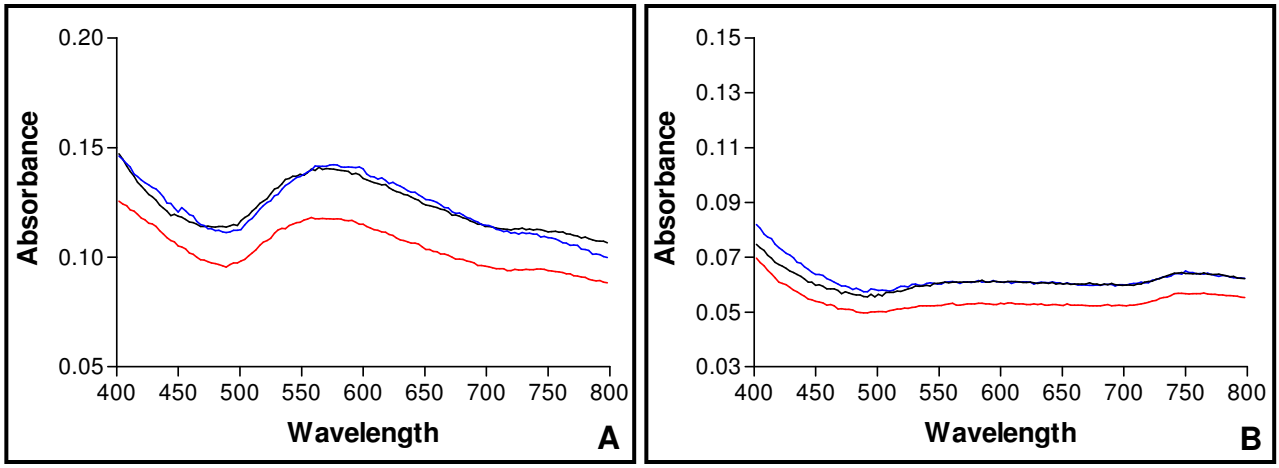

Figure 3.53: UV-Vis absorption spectra of the surface plasmon resonance recorded for the different electron donors, indicating gold nanoparticle production through a change in the absorbance around 540 - 580 nm. (A) The protein reactions and (B) the corresponding blank reactions. [Sodium dithionite (▬); Dithiothreitol (▬); β-mercaptoethanol (▬)].

The TEM micrographs (Figure 3.54) confirmed that particles were formed with all three electron donors and that all the particles are in the nano size range, with no real differences amongst the three components. Several hexagon and elongated hexagon shapes were obtained. SAED (Figure 3.54B) was performed on the sodium dithionite as electron donor and EDX (Figure 3.55) was done on all the samples and the nanoparticles were confirmed to be gold. In figure 3.54B the micro-diffraction pattern for gold can be seen.

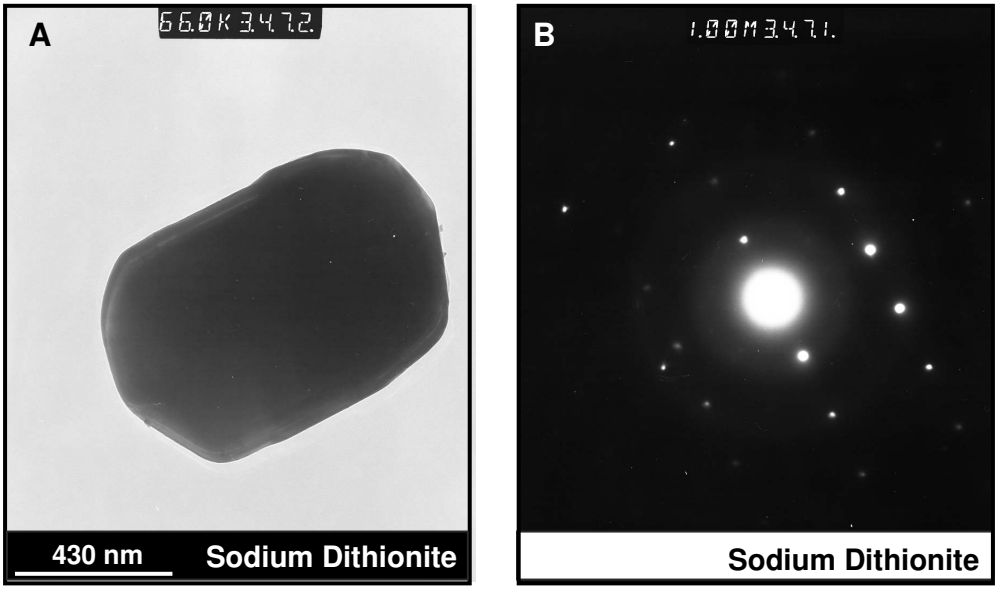

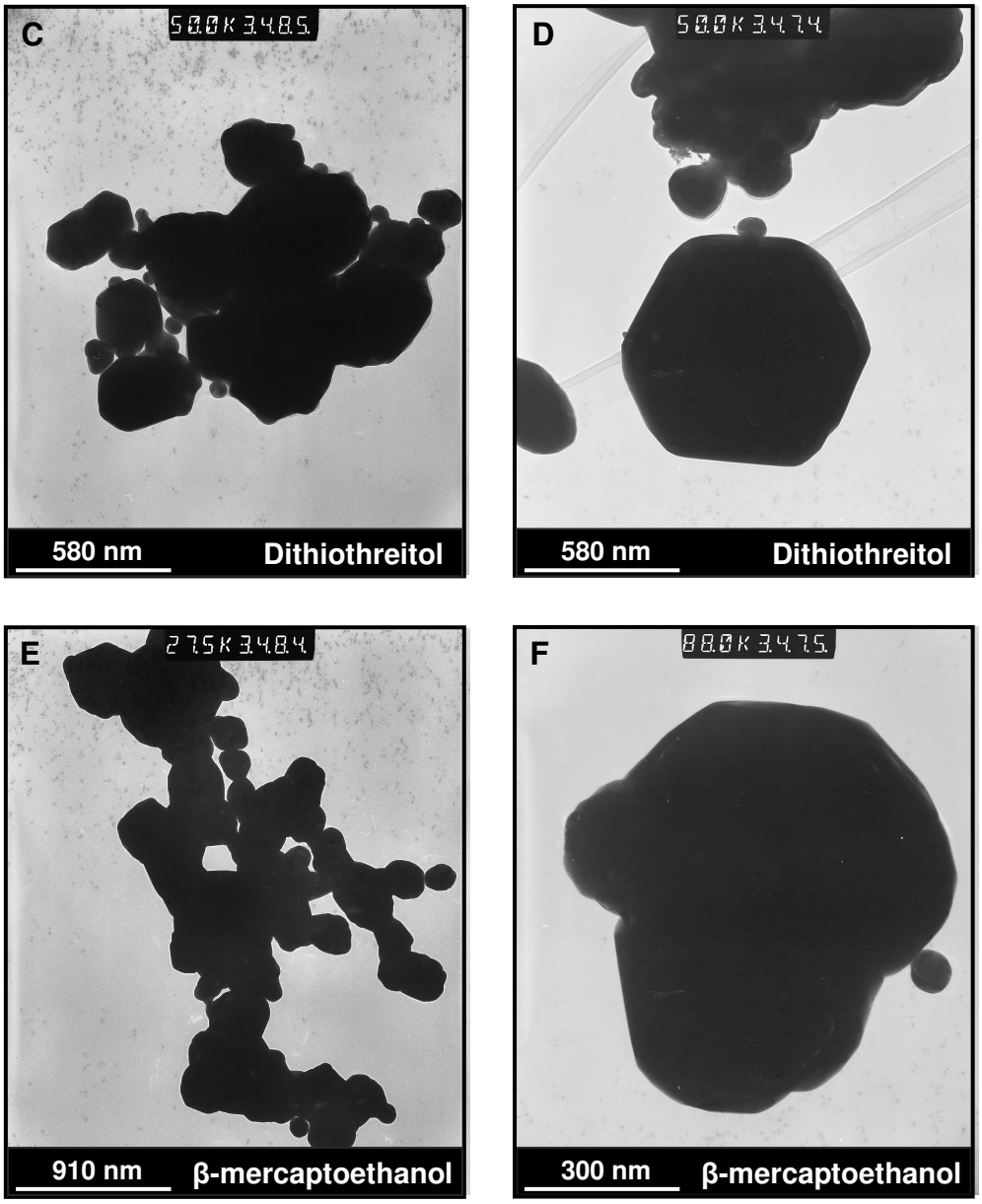

Figure 3.54: (A) TEM micrograph of a gold nanoparticle with (B) corresponding selected-area electron micro-diffraction pattern for sodium dithionite as electron donor. (C and D) TEM micrographs for dithiothreitol and (E and F) TEM micrographs for β-mercaptoethanol, indicating the shapes, sizes and amounts of gold nanoparticles obtained. The scale bars in A, C, D, E and F are equal to 430 nm; 580 nm; 580 nm; 910 nm and 300 nm respectively.

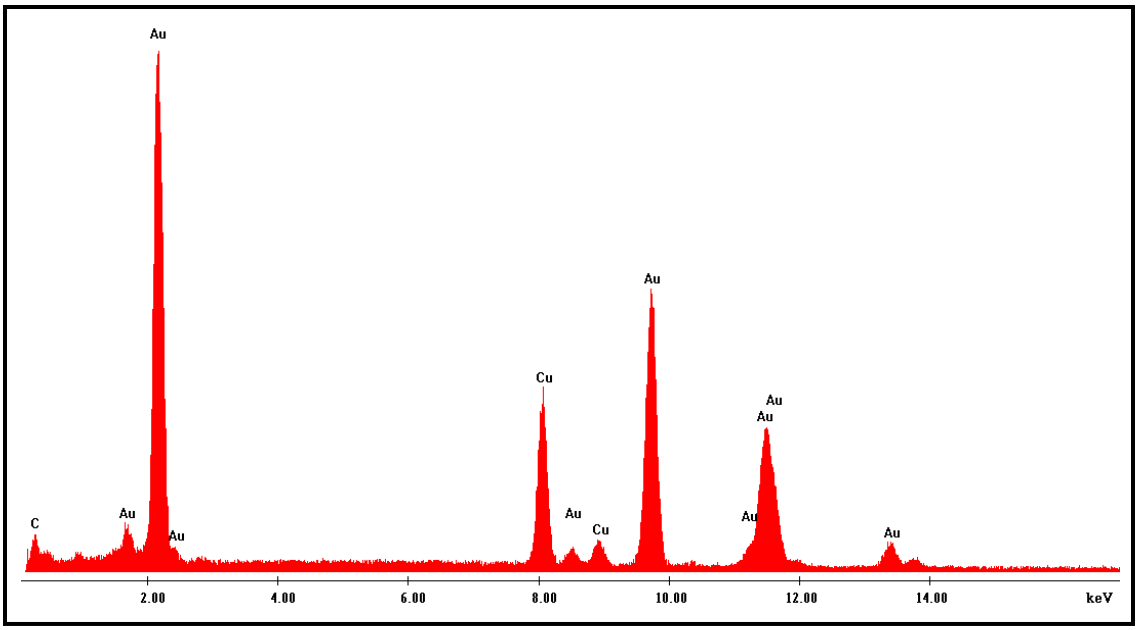

Figure 3.55: EDX spectrum recorded for the nanoparticles produced with different electron donors, showing a typical pattern for all the samples and indicates that the nanoparticles are gold.

From this it can be concluded that the different electron donors and reducing agents did not influence nanoparticle formation, since they all function as described in section 3.2.16. However, with sodium dithionite, more chemical reduction was obtained than with the other two components.

Nanotrac particle size analyses were performed on the sodium dithionite as the electron donor, for additional confirmation of the size and size distribution of the gold nanoparticles. The average size percentage can be seen in table 3.6, indicating that all the particles are bigger than 100 nm, but smaller than 130 nm. 50 % of the particles are smaller than 111.7 nm and 95 % are smaller than 125.3 nm.

Table 3.6: The average size percentage of the nanoparticles present with sodium dithionite as the electron donor.

% Tile	Size (µm)	Size (nm)
10	0.1029	102.9
20	0.1054	105.4
30	0.1077	107.7
40	0.1097	109.7
50	0.1117	111.7
60	0.1139	113.9
70	0.1160	116.0
80	0.1187	118.7
90	0.1215	121.5
95	0.1253	125.3

The size distribution can be seen in table 3.7 and figure 3.56, with sodium dithionite as the electron donor. 100% of the particles are smaller than 171.9 nm; 90.08% are smaller than 121.5 nm and only 7.33% are smaller than 102.2 nm.

Table 3.7: Size distribution of the nanoparticles present with sodium dithionite as the electron donor.

Size (nm)	% Channel	% Passed
171.9	0.00	100.00
144.5	9.92	100.00
121.5	82.75	90.08
102.2	7.33	7.33
85.9	0.00	0.00

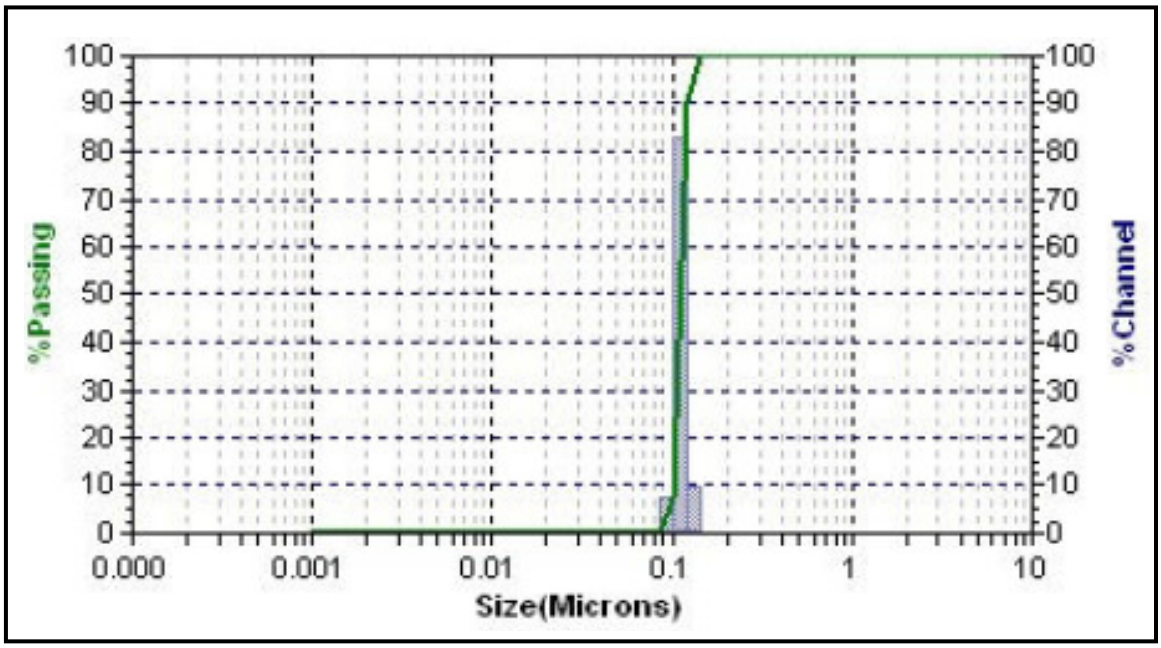

Figure 3.56: Size distribution for the gold nanoparticles obtained with sodium dithionite as the electron donor.

3.3.8 Mechanism Hypothesis

The mechanism hypothesis, as discussed in section 3.2.16, was verified by testing the effect of the sulphydryl blocking agent, iodoacetic acid, on sodium dithionite, dithiothreitol (DTT) and β-mercaptoethanol for gold reduction and nanoparticle formation. When comparing the reactions through the visual assay (Figure 3.57) and the SPR, obtained through UV-Vis spectra (Figure 3.58), no significant change in colour was observed with all three the components, indicating that no gold reduction and nanoparticle formation took place. This can be seen through the absence of any changes in the absorbance around 540 – 560 nm in the protein reactions with the electron donors (Figure 3.58A), and in the respective blank reactions (Figure 3.58B).

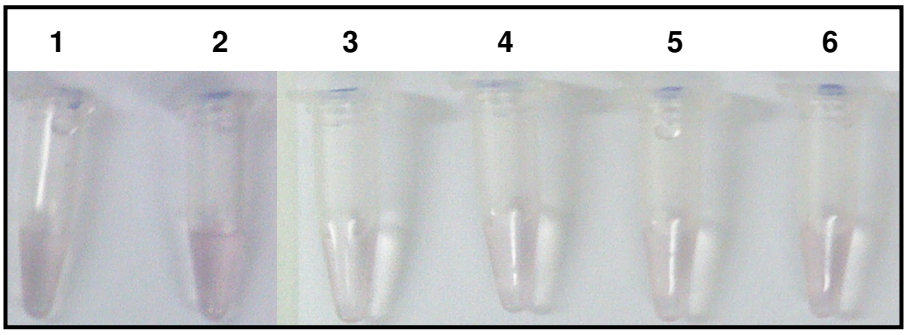

Figure 3.57: No significant change in colour obtained through the gold reduction assay with iodoacetic acid and the various electron donors, indicating negative nanoparticle formation. The odd numbers (1 – 5) indicate protein reactions for sodium dithionite; dithiothreitol and β-mercaptoethanol respectively and the even numbers (2 – 6) the corresponding blank reactions.

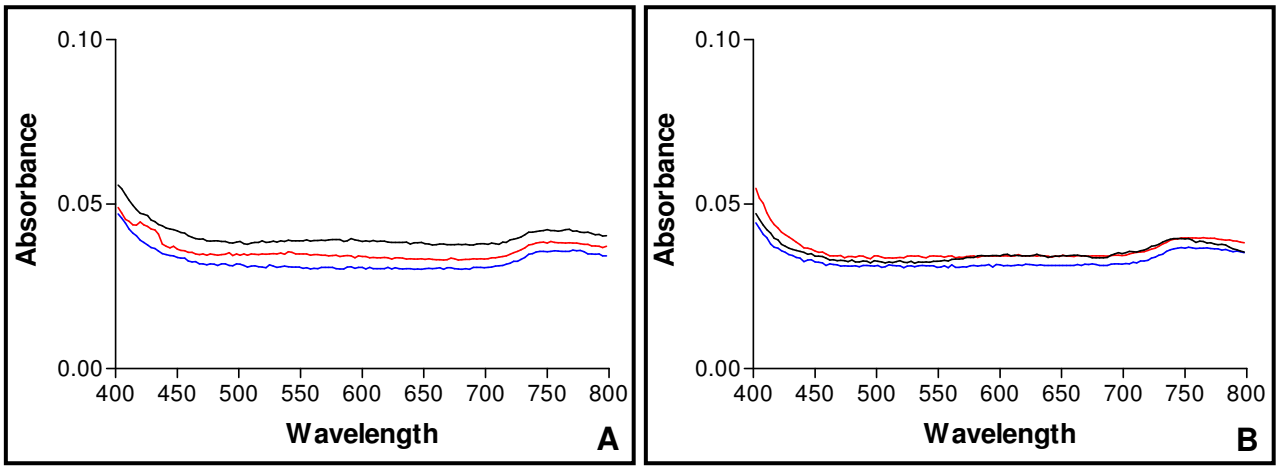

Figure 3.58: UV-Vis absorption spectra of the surface plasmon resonance recorded for the iodoacetic acid with the various electron donors, indicating no nanoparticle production through no change in the absorbance around 540 - 560 nm. (A) Protein reactions with the different electron donors and (B) the corresponding blank reactions. [Sodium dithionite ( ); Dithiothreitol ( ); β-mercaptoethanol ( )].

The TEM micrographs (Figure 3.59) confirmed that no significant nanoparticle formation was obtained with all three the electron donors in the presence of iodoacetic acid.

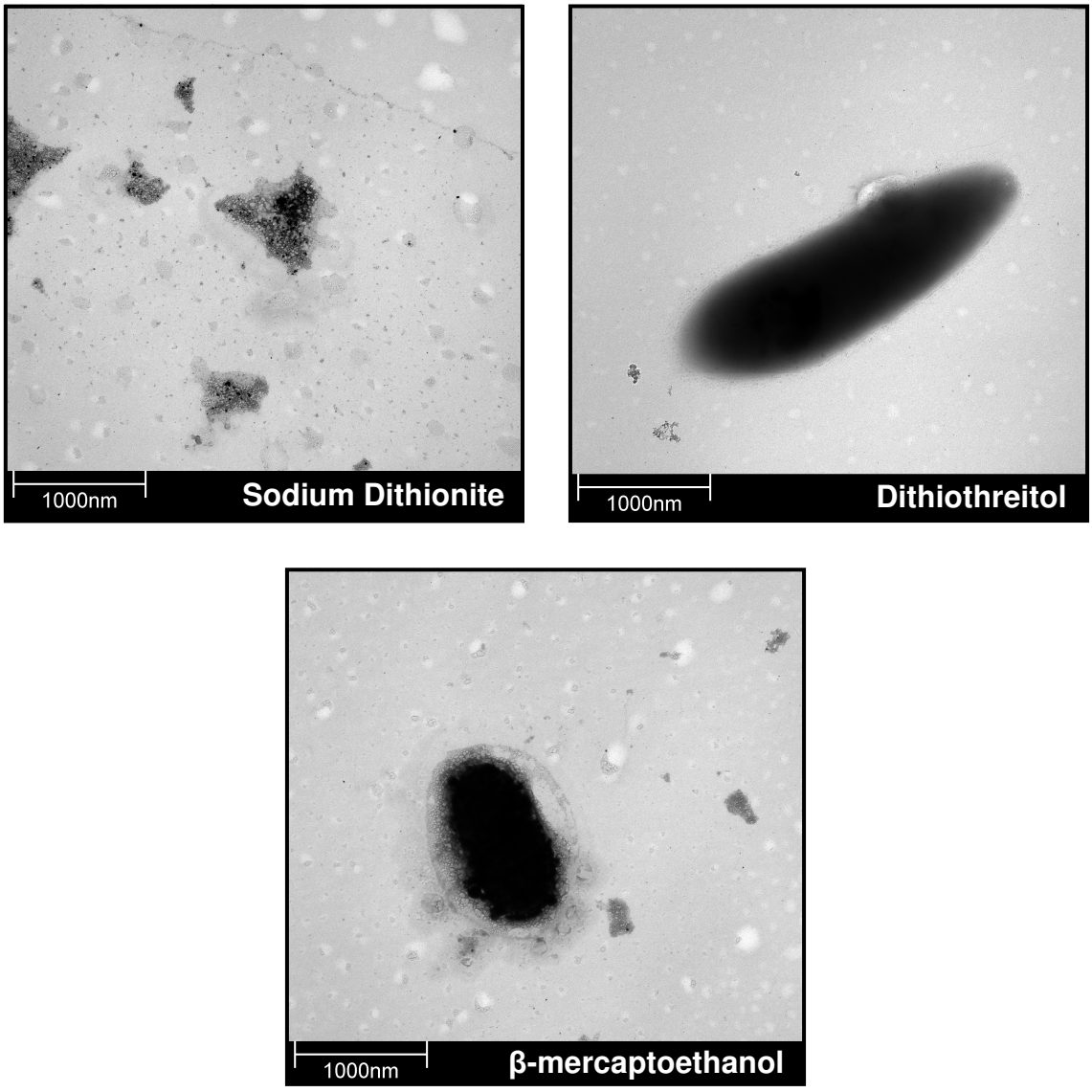

Figure 3.59: TEM micrographs of gold nanoparticles for iodoacetic acid with the different electron donors, no formation of gold nanoparticles. All scale bars are equal to 1000 nm.

From this it can be concluded that the hypothesis of Van Marwijk, (2009) might be true, since no indication if nanoparticle formation was obtained at all when iodoacetic acid was added as a sulphydryl blocking agent. Furthermore, no colour formation was obtained; indicating that gold reduction did not take place and therefore the disulphide bond was not reduced and the protein could not produce gold nanoparticles.

3.4 CONCLUSIONS

The ABC transporter, peptide-binding protein from *Thermus scotoductus* SA-01 was successfully cloned and overexpressed in the mesophilic host, *Escherichia coli*. Expressed protein was obtained in high levels and was effectively purified, with and without the N-terminal His-Tag. Characterization studies showed that the His-Tag had no significant influence on the gold reduction and nanoparticle formation process, since no real differences were obtained in the characterization with or without the His-Tag.

The ABC transporter, peptide-binding protein was also successful in the reduction of gold(III) to gold(0) and in the formation of gold nanoparticles, at various parameters. Nanoparticles of different shapes, sizes and distributions were obtained, but these particles were not monodisperse at most parameters tested, the majority were spherical particles. Nanoparticle formation was dependant on environmental parameters but control of the process was not complete. Chemical reduction did have an influence in some instances, but overall it could be seen that the presence of the protein played a significant role in slowing down the reaction rate, yielding a level of control over the nanoparticles produced and ensuring a more environmentally friendly, biological process for the production of gold nanoparticles. It was proved that methyl viologen is not needed in the gold reduction assay to obtain nanoparticles, since it only aids in chemical reduction and that only sodium dithionite, used as a reducing agent, is needed.

For the mechanism hypothesis, it was confirmed that when reduction of the disulphide bond was blocked with a sulphydryl blocking agent, no gold reduction and nanoparticle formation was obtained, proving that the hypothesis might be true and that gold reduction and nanoparticle formation takes place through reduction of the disulphide bond.

Overall, the best nanoparticles were obtained at temperatures closer to the optimum growth temperature of *T. scotoductus* SA-01, at pH values closer to the pI of the protein and at lower gold(III) concentrations, proving that if the protein aids not only in gold reduction but also nanoparticle formation, it might be a plausible explanation for the differences in the stoichiometry, therefore leading to uncontrolled particle formation at higher concentrations.

REFERENCES

- **Balkwill, D.L., Kieft, T.L., Tsukuda, T., Kostandarithes, H.M., Onstott, T.C., Macnaughton, S., Bownas, J. and Fredrickson, J.K.** (2004) Identification of Iron-Reducing *Thermus* Strains as *Thermus scotoductus*. *Extremophiles.* **8**:37-44.

- **Beveridge, T.J. and Murray, R.G.E.** (1980) Sites of Metal Deposition in the Cell Wall of *Bacillus subtilis*. *Journal of Bacteriology.* **141**:876-887.

- **Bönnemann, H. and Nagabhushana, K.S.** (2004) Chemical Synthesis of Nanoparticles. *Encyclopedia of Nanoscience and Nanotechnology.* **1**:777-813.

- **Butterman, W.C. and Amey III, E.B.** (2005) Mineral Commodity Profiles - Gold. *USGS. Open-File Report 02-303.*

- **Chen, H., Wang, Y., Wang, Y., Dong, S. and Wang, E.** (2006) One-Step Preparation and Characterization of PDDA-Protected Gold Nanoparticles. *Polymer.* **47**:763-766.

- **Daniel, M. and Astruc, D.** (2004) Gold Nanoparticles: Assembly, Supramolecular Chemistry, Quantum-Size-Related Properties, and Applications toward Biology, Catalysis, and Nanotechnology. *Chem. Rev.* **104**:293-346.

- **Del Fatti, N., Christofilos, D. and Vallée, F.** (2008) Optical Response of a Single Gold Nanoparticle. *Gold Bulletin.* **41**:147-158.

- **Englebienne, P.** (1998) Use of Colloidal Gold Surface Plasmon Resonance Peak Shift to Infer Affinity Constants from the Interactions between Protein Antigens and Antibodies Specific for Single or Multiple Epitopes. *Analyst.* **123**:1599-1603.

- **Fairbanks, G., Steck, T.L. and Wallach, D.F.H.** (1971) Electrophoretic Analysis of the Major Polypeptides of the Human Erythrocyte Membrane. *Biochemistry.* **10**:2606-2617.

- **Gadd, G.M.** (2000) Bioremedial Potential of Microbial Mechanisms of Metal Mobilization and Immobilization. *Current Opinion in Biotechnology.* **11**:271-279.

- **Gericke, M. and Pinches, A.** (2006) Biological Synthesis of Metal Nanoparticles. *Hydrometallurgy.* **83**:132-140.

- **Gounder, K.** (2009) Genome sequencing of the Extremophile *Thermus scotoductus* SA-01 and Expression of Selected Genes. *PhD. Thesis.* University of the Free State. Bloemfontein. South Africa.

- **Hanahan, D.** (1983) Studies on Transformation of *E. coli* with Plasmid. *Journal of Molecular Biology.* **166**:557-580.

- **He, S., Zhang, Y., Guo, Z. and Gu, N.** (2008) Biological Synthesis of Gold Nanowires Using Extract of *Rhodopseudomonas capsulata*. *Biotechnol. Prog.* **24**:476-480.

- **Husseiny, M.I., Abd El-Aziz, M., Badr, Y. and Mahmoud, M.A.** (2007) Biosynthesis of Gold Nanoparticles using *Pseudomonas aeruginosa*. *Spectrochimica Acta Part A.* **67**:1003-1006.

- **Karn, B.P. and Bergeson, L.L.** (2009) Green Nanotechnology: Straddling Promise and Uncertainty. *Natural Resources & Environment.* **24**:9-14.

- **Kieft, T.L., Fredrickson, J.K., Onstott, T.C., Gorby, Y.A., Kostandarithes, H.M., Bailey, T.J., Kennedy, D.W., Li, S.W., Plymale, A.E., Spadoni, C.M. and Gray, M.S.** (1999) Dissimilatory Reduction of Fe(III) and Other Electron Acceptors by a *Thermus* isolate. *Applied and Environmental Microbiology.* **65**:1214-1221.

- **Korbekandi, H., Iravani, S. and Abbasi, S.** (2009) Production of Nanoparticles using Organisms. *Critical Reviews in Biotechnology.* **29**:279-306.

- **Laemmli, U.K.** (1970) Cleavage of Structural Proteins during the Assembly of the Head of Bacteriophage T4. *Nature.* **227**:680-685.

- **Lazarides, A.A. and Schatz, G.C.** (2000) DNA-Linked Metal Nanosphere Materials: Structural Basis for the Optical Properties. *Journal of Physical Chemistry B*. **104**:460-467.

- **Lengke, M.F., Fleet, M.E. and Southam, G.** (2007) Biosynthesis of Silver Nanoparticles by Filamentous Cyanobacteria from a Silver(I) Nitrate Complex. *Langmuir.* **23**:2694-2699.

- **Luther, W.** (2004) Industrial Application of Nanomaterials – Chances and Risks. *Future Technologies.* **54**:1-112.

- **Mukherjee, P., Senapati, S., Mandal, D., Ahmad, A., Khan, M.I., Kumar, R. and Sastry, M.** (2002) Extracellular Synthesis of Gold Nanoparticles by the Fungus *Fusarium oxysporum*. *ChemBioChem.* **5**:461-463.

- **Mulholland, G.W. and Bauer, B.J.** (2000) Nanometre Calibration Particles: What is Available and what is Needed? *Journal of Nanoparticle Research.* **2**:5-15.

- **Narayanan, R. and El-Sayed, M.A.** (2004) Shape-Dependant Catalytic Activity of Platinum Nanoparticles in Colloidal Solution. *Nano Letters.* **4**:1343-1348.

- **Riddin, T.L., Gericke, M. and Whiteley, C.G.** (2006) Analysis of the Inter- and Extracellular Formation of Platinum Nanoparticles by *Fusarium oxysporum* f. sp. *Lycopersici* using Response Surface Methodology. *Nanotechnology*. **17**:3482-3489.

- **Sambrook, J., Fritsch, E.F. and Maniatis, T.** (1989) Molecular Cloning: A Laboratory Manual. *Cold Spring Harbour Laboratory Press.* Cold Spring Harbour.

- **Sastry, M., Ahmad, A., Khan, M.I. and Kumar, R.** (2003) Biosynthesis of Metal Nanoparticles using Fungi and Actinomycete. *Current Science.* **85**:162-170.

- **Scott, D., Toney, M. and Muzikár, M.** (2008) Harnessing the Mechanism of Glutathione Reductase for Synthesis of Active Site Bound Metallic Nanoparticles and Electrical Connection to Electrodes. *J. Am. Chem. Soc.* **130**:865-874.

- **Showe, M.K. and DeMoss, J.A.** (1968) Localization and Regulation of Synthesis of Nitrate Reductase in *Escherichia coli. Journal of Bacteriology*. **95**:1305-1313.

- **Šlouf, M., Kužel, R. and Matěj, Z.** (2006) Preparation and Characterization of Isometric Gold Nanoparticles with Pre-calculated Size. *Z. Kristallogr. Suppl.* **23**:319-324.

- **Smith, P.K., Krohn, R.I., Hermanson, G.T., Mallia, A.K., Gartner, F.H., Provenzano, M.D., Fujimoto, E.K., Goeke, N.M., Olson, B.J. and Klenk, D.C.** (1985) Measurement of Protein using Bicinchoninic Acid. *Analytical Biochemistry.* **150**:76-85.

- **Southam, G. and Beveridge, T.J.** (1996) The Occurrence of Sulphur and Phosphorus within Bacterially Derived Crystalline and Pseudocrystalline Octahedral Gold Formed *in vitro*. *Geochimica et Cosmochimica Acta.* **60**:4369-4376.

- **Towner, P.** (1991) Isolation of DNA by SDS-Proteinase K Treatment. *In* T.A. Brown (Ed.). *Essential Molecular Biology. A Practical Approach.* **1**:52-53. Oxford University Press. United Kingdom.

- **Tsuruta, T.** (2004) Biosorption and Recycling of Gold using Various Microorganisms. *J. Gen. Appl. Microbiol.* **50**:221-228.

- **Van Marwijk, J.** (2009) Biological Synthesis of Gold Nanoparticles by *Thermus scotoductus* SA-01. *PhD. Thesis.* University of the Free State. Bloemfontein. South Africa.

- **Wakatsuki, T.** (1995) Metal Oxidoreduction by Microbial Cells. *Journal of Industrial Microbiology.* **14**:169-177.

- **Web Exhibits.** What Causes the Colours of Metals like Gold? http://www.webexhibits.org/causesofcolour/9.html.

CHAPTER 4

EXPRESSION AND CHARACTERIZATION OF AN ABC TRANSPORTER, PEPTIDE-BINDING PROTEIN FROM *THERMUS SCOTODUCTUS* SA-01 IN A THERMOPHILIC HOST

4.1 INTRODUCTION

Structural and functional modifications of model enzymes and enzymes used in industrial applications need to be very stable at elevated temperatures. To achieve these properties, thermostable enzymes are used in many applied studies. Production of these thermostable enzymes is usually accomplished through heterologous expression in a mesophilic host, normally *Escherichia coli* and *Bacillus subtilis*, which allows for its rapid purification through the thermal denaturation of the host's mesophilic enzymes. There are however several drawbacks and limitations in this process, because a number of thermostable enzymes require cofactors, appropriate posttranslational processing, active chaperones and high temperatures to fold correctly and/or cannot be overproduced in an active form in a mesophilic host (Bruins *et al.*, 2001; Hidalgo *et al.*, 2004; Moreno *et al.*, 2005; Averhoff, 2006; Turner *et al.*, 2007). To overcome these limitations, genetic tools have been developed that allows the overexpression of biotechnologically important thermophilic proteins through the use of thermophilic hosts (Lasa *et al.*, 1992; De Grado *et al.*, 1999; Bruins *et al.*, 2001; Moreno *et al.*, 2003; Hidalgo *et al.*, 2004; Moreno *et al.*, 2005; Averhoff, 2006; Turner *et al.*, 2007).

The microorganism most acquiescent to genetic manipulation is the thermophile, *Thermus*. *Thermus thermophilus* HB8 and HB27 are displaying high natural transformation frequencies and are therefore amenable to genetic manipulation. It is suggested that between all the *Thermus* strains, *Thermus thermophilus* HB27 is the most favourable recipient for DNA transfer studies and the transformation protocol

developed by Koyama et al., (1986) has been used for transfer of chromosomal and plasmid DNA and is still effectively the standard protocol for DNA transfer in *Thermus* (Averhoff, 2006).

This chapter describes the expression of the ABC transporter, peptide-binding protein, identified in *Thermus scotoductus* SA-01, in the thermophilic expression host, *Thermus thermophilus* HB27 and subsequent characterization of gold reduction and nanoparticle formation.

4.2 MATERIALS AND METHODS

4.2.1 Bacterial Strains and Culture Conditions

All bacterial strains used for cloning and expression studies can be seen in table 4.1. *Thermus scotoductus* SA-01 was cultured as described in section 3.2.1.

Escherichia coli TOP10 (Invitrogen) were used as a host for cloning purposes and were cultured as described in section 3.2.1.

Thermus thermophilus HB27 (ATCC BAA-163) was used as a host for expression of the protein at 60 – 70ºC and was kindly provided by Prof. J. Berenguer (CBMSO, Universidad Autónoma de Madrid, Spain). *T. thermophilus* HB27 was cultured from a 20% glycerol stock (maintained at -80ºC) as described in section 3.2.1, using *Thermus* broth [8 $g.L^{-1}$ tryptone (Biolab); 4 $g.L^{-1}$ yeast extract (Biolab); 3 $g.L^{-1}$ NaCl (Saarchem), pH 7.0 with 2 M NaOH] (Ramírez-Arcos *et al.*, 1998) as the growth medium. Bleomycin (3 $\mu g.ml^{-1}$) or kanamycin (30 $\mu g.ml^{-1}$) was added when required.

4.2.2 Plasmids

All plasmids used for cloning and expression studies are described in table 4.1. Plasmids pGEM®-T Easy (Promega), pET-22b(+) and pET-28b(+) (Novagen) were used for cloning of the gene into *E. coli* as described in chapter 3. Plasmids pWUR (Brouns *et al.*, 2005) and pMK184 (De Grado *et al.*, 1999) were used to clone and express the gene in *T. thermophilus* HB27 and was kindly provided by Prof. J. Berenguer (CBMSO, Universidad Autónoma de Madrid, Spain). The pWUR vector contains a bleomycin resistance gene (Figure 4.1) and the pMK184 vector contains a kanamycin resistance gene and is a modification of the pMK18 vector (De Grado *et al.*, 1999), where two of the three *Bam*HI restrictions sites were removed (Figure 4.2).

Table 4.1: Bacterial strains and plasmids used for cloning and expression in a thermophilic host.

Strain or plasmid	Description	Reference
Strain		
• *Thermus scotoductus* SA-01		ATCC 700910
• *Thermus thermophilus* HB27		ATCC BAA-163
• *Escherichia coli* TOP10	One Shot Top10 chemically Competent cells	Invitrogen
Plasmid		
• pGEM®-T Easy	Amp^r, T7 and SP6 promoter, *Lac*Z, ori, 3018 bp	Promega
• pET-22b(+)	Amp^r, T7 promoter and Terminator, *Lac*I, ori, 5493 bp	Novagen
• pET-28b(+)	Kan^r, T7 promoter and Terminator, *Lac*I, N-terminal His-Tag, ori, 5368 bp Thrombin configuration	Novagen
• pWUR	$Bleo^r$, PslpA and Plac promoters, RepA, ori*Eco*, 4404 bp	Brouns *et al.*, 2005
• pMK184	Kan^r, PslpA and Plac promoters, a-*lac*Z, RepA, ori*Eco*, 5043 bp	De Grado *et al.*, 1999

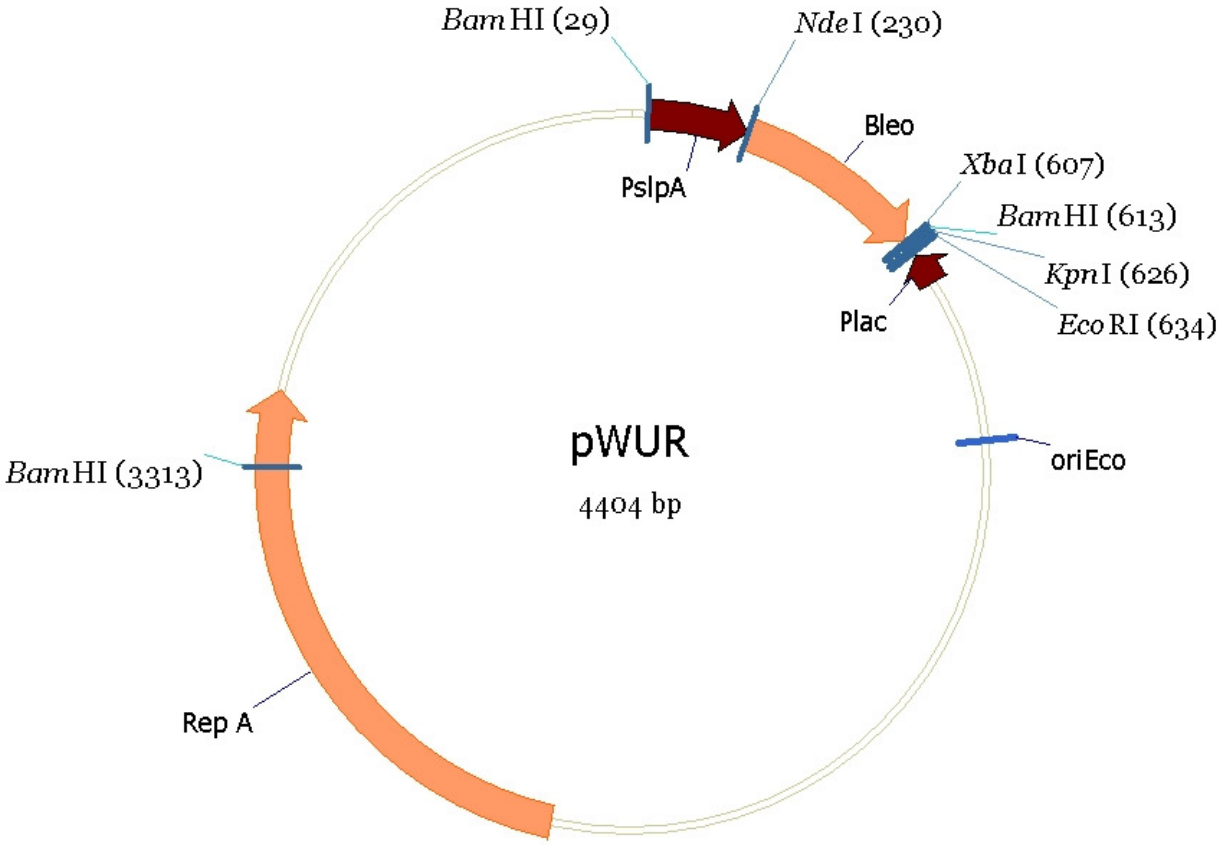

Figure 4.1: Vector map of pWUR, indicating the bleomycin resistance gene, the ori*Eco* origin for replication in *E. coli*, minimal replicon (RepA) for replication in *Thermus* sp. and the multiple cloning site under the PslpA and Plac promoters, showing the *Eco*RI and *Xba*I sites where the gene was inserted.

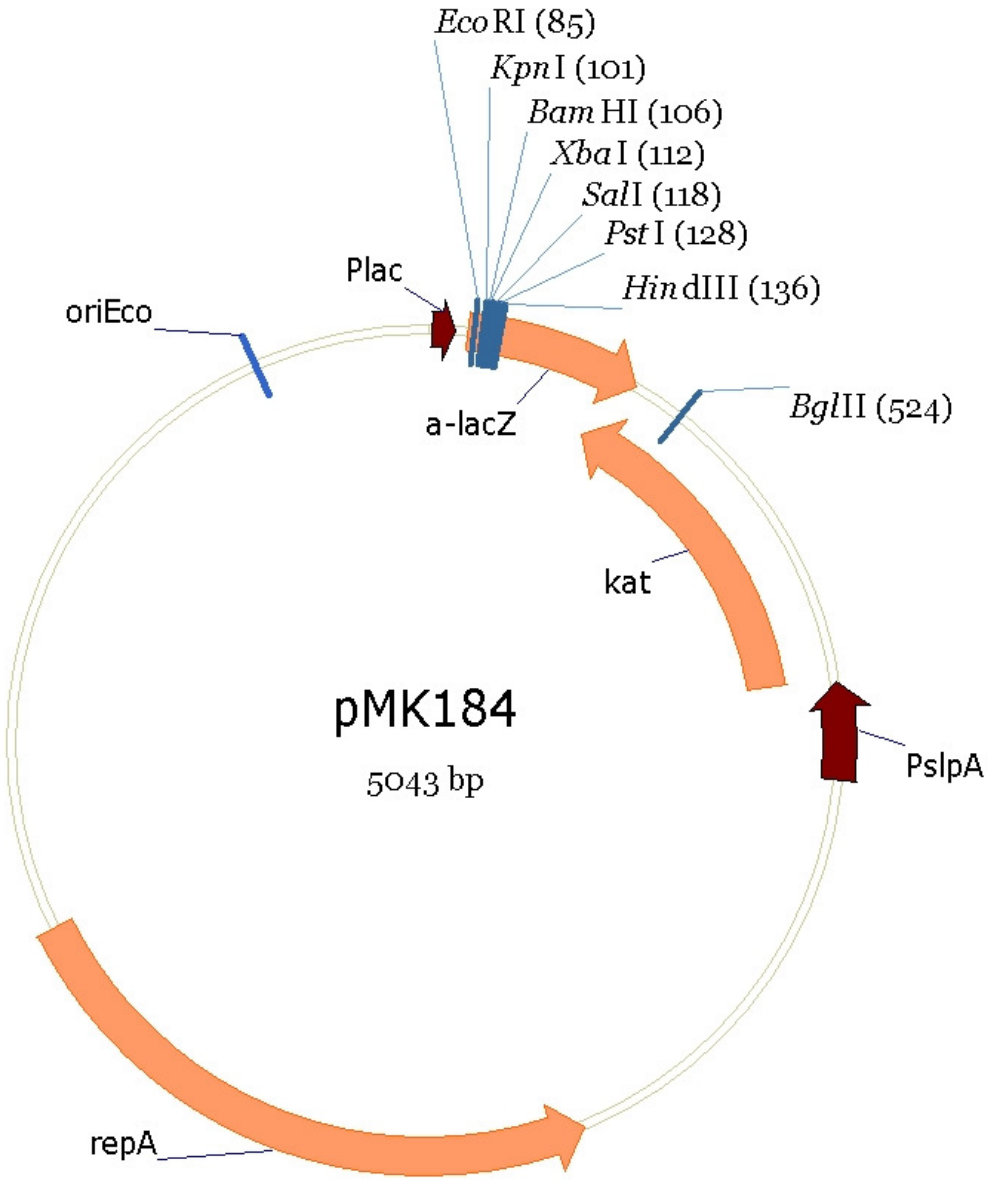

Figure 4.2: Vector map of pMK184, indicating the kanamycin resistance gene, the ori*Eco* origin for replication in *E. coli*, the a-*lac*Z coding site, minimal replicon (RepA) for replication in *Thermus* sp. and the multiple cloning site under the PslpA and Plac promoters, showing the *Eco*RI and *Xba*I sites where the gene was inserted.

4.2.3 Genomic DNA Isolation

Genomic DNA (gDNA) was isolated from *T. scotoductus* SA-01 according to the method described in section 3.2.3 by Towner, (1991), with modifications.

4.2.4 Polymerase Chain Reaction

All primers used for cloning and expression studies can be seen in table 4.2. Polymerase chain reaction (PCR) was done on the gDNA isolated from *T. scotoductus* SA-01, to amplify the complete ABC transporter, peptide-binding gene. The PCR was done as described in section 3.2.4. The oligonucleotide primers used (Primers 1, 2, 5 and 6, Table 4.2) were designed to yield constructs that either included or excluded the leader peptide, the C-terminal and/or the N-terminal His-Tag when cloned in pET-22b(+) and pET-28b(+) (Table 4.3), when different combinations of these primers were used. This was done to determine the influence (if any) of the His-Tag and the leader peptide on gold reduction and nanoparticle formation. The His-Tags were also added for purification purposes.

Table 4.2: Oligonucleotide primers used for PCR amplification and sequencing. Underlined sequences indicate the introduced restriction sites for *Nde*I in primers 1 and 5 and *Eco*RI in primers 2 and 6 respectively.

Primer	**Nucleotide sequence**	**Tm (ºC)**
1. ABC_F_Nde	5'- CAT ATG AGA AAA GTA GGC AAG CTG GCT G -3'	59.5
2. ABC_R_Eco	5'- GAA TTC TTA CTT GAC GGA AAG AGC GTA C -3'	57.4
3. ABC_Int_F	5'- AGG ATG CGG AGA GGC TC -3'	56.9
4. ABC_Int_R	5'- CGC TGG ATG TAG TCG TCG -3'	55.4
5. ABC_2F_-LP	5'- CAT ATG GGG CCC CAG GAC AAC AGC -3'	64.1
6. ABC_C-His-1R	5'- GAA TTC GCC TTG ACG GAA AGA GCG TAC TT -3'	62.1
7. T7 Terminator	5'- GCT AGT TAT TGC TCA GCG G -3'	53.4
8. T7 Promoter	5'- TAA TAC GAC TCA CTA TAG GG -3'	47.5
9. ABC_pWUR_R	5'- CCG GCT CGT ATG TTG TGT GG -3'	58.5
10. ABC_pWUR_F	5'- AAC TGC GTG CAC TTC GTG G -3'	58.8
11. ABC_pMK184_R	5'- GCG ATT AAG TTG GGT AAC G -3'	51.2
12. ABC_pMK184_F	5'- CTT TAT GCT TCC GGC TCG -3'	53.6

Table 4.3: Constructs obtained when using a combination of primers 1, 2, 5 and 6 with the pET-22b(+) and pET-28b(+) vectors respectively.

Primers	**pET22b(+)**	**pET28b(+)**
1 & 6*	- N-terminal His-Tag + C-terminal His-Tag + Leader peptide	+ N-terminal His-Tag + C-terminal His-Tag + Leader peptide
2 & 5*	- N-terminal His-Tag - C-terminal His-Tag - Leader peptide	+ N-terminal His-Tag - C-terminal His-Tag - Leader peptide
5 & 6*	- N-terminal His-Tag + C-terminal His-Tag - Leader peptide	+ N-terminal His-Tag + C-terminal His-Tag - Leader peptide

* Numbers correspond to primer numbers indicated in Table 4.2.

4.2.5 Ligation into pGEM®-T Easy

The ± 1.9 kb PCR products, purified from the agarose gel, were ligated into the pGEM®-T Easy Vector system (Promega), as described in section 3.2.5.

4.2.6 Preparation of *Escherichia coli* TOP10 Competent Cells

Competent *E. coli* One Shot TOP10 (Invitrogen) cells were prepared according to the method described in section 3.2.6 by Hanahan, (1983), with modifications.

4.2.7 Transformation into *Escherichia coli* TOP10

The ligated plasmid reactions (5 µl) were transformed into the *E. coli* One Shot TOP10 competent cells as described in section 3.2.7 and the ligated insert sizes were evaluated, using double digestion as described in section 3.2.8.

4.2.8 Ligation into pET-22b(+) and pET-28b(+)

The pET-22b(+) and pET-28b(+) vectors were propagated and double digested as described in section 3.2.9. The ± 1.9 kb PCR products, purified from the agarose gel, were ligated into the pET-22b(+) and pET-28b(+) vectors and transformed into *E. coli* One Shot TOP10 competent cells, as described in section 3.2.9. After ligation into these pET vectors, only three of the constructs were used (Table 4.4) for downstream experiments.

Table 4.4: Constructs used for downstream experiments, after ligation in the pET-22b(+) and pET-28b(+) vectors respectively.

Primers	pET22b(+)	pET28b(+)
1 & 6*	- N-terminal His-Tag + C-terminal His-Tag + Leader peptide	
2 & 5*		+ N-terminal His-Tag - C-terminal His-Tag - Leader peptide
5 & 6*	- N-terminal His-Tag + C-terminal His-Tag - Leader peptide	

* Numbers correspond to primer numbers indicated in Table 4.2.

4.2.9 Evaluation of the Insert Size and Sequencing

To evaluate the ligated insert sizes, 10 single white colonies for each construct, were separately inoculated into 5 ml LB medium, containing 100 $\mu g.ml^{-1}$ ampicillin [pET-22b(+)] or 30 $\mu g.ml^{-1}$ kanamycin [pET-28b(+)] and incubated overnight at 37ºC with aeration (200 rpm). Plasmids were isolated using the BioSpin Plasmid DNA Extraction Kit (BioFlux), as per manufacturer's instructions. Double digestion was done on the plasmids, using the restriction enzymes *Eco*RI and *Xba*I (Fermentas). The digestion reaction was performed in a total reaction volume of 50 µl and consisted out of 10 µl purified plasmid, 5 µl buffer Tango, 2.5 µl *Eco*RI, 5 µl *Xba*I and sterile ddH_2O filled to the reaction volume. The reaction mixture was incubated at 37ºC for 3 hours, after which the enzymes were heat activated at 65ºC for 20 minutes. The restriction digestions were visualized on a 1% agarose gel as described in section 3.2.3. Purification of the insert was achieved by excising the desired band (± 1.9 kb) from the agarose gel, using a non-UV transilluminator (Dark Reader™ transilluminator DR-45M, Clare Chemical Research) and extracted using the BioSpin Gel Extraction Kit (BioFlux), as per manufacturer's instructions.

The purified inserts were sequenced for confirmation of the nucleotide composition of the ABC transporter, peptide-binding gene. Sanger sequencing was done as described in section 3.2.11, using primers 3, 4, 7 and 8 (Table 4.2).

4.2.10 Preparation of the pWUR and pMK184 Expression Plasmids

pWUR (Brouns *et al.*, 2005) and pMK184 (De Grado *et al.*, 1999) was used as expression vectors in *T. thermophilus* HB27. The vectors were propagated by transforming 2 µl into *E. coli* One Shot TOP10 competent cells, as described in section 3.2.7. Selective pressure was maintained by using LB plates containing 3 $\mu g.ml^{-1}$ bleomycin (pWUR) or 30 $\mu g.ml^{-1}$ kanamycin (pMK184). Single white colonies were separately inoculated into 5 ml LB medium, containing the required antibiotic and incubated overnight at 37ºC with aeration (200 rpm). Plasmids were isolated using the BioSpin Plasmid DNA Extraction Kit (BioFlux), as per manufacturer's instructions. Double digestion was done on the plasmids, using the restriction enzymes *Eco*RI and *Xba*I (Fermentas), as described in section 4.2.9. The restriction digestions were visualized on a 1% agarose gel as described in section 3.2.3. Purification of the insert was achieved by excising the desired band (± 4.5 - 5 kb) from the agarose gel, using a non-UV transilluminator (Dark Reader™ transilluminator DR-45M, Clare Chemical Research) and extracted using the BioSpin Gel Extraction Kit (BioFlux), as per manufacturer's instructions.

The ± 1.9 kb inserts, purified from the agarose gel, for each of the three different constructs (Table 4.4) were ligated separately into the pWUR and pMK184 expression vectors. The ligation reaction was performed in a total reaction volume of 10 µl and consisted out of 10x Rapid Ligation Buffer (1 µl), pWUR/pMK184 vector (2 µl), insert (6 µl), T4 DNA Ligase (0.3 Weiss units). The ligation reactions were incubated overnight at 4ºC. The ligated plasmid reactions (5 µl) were transformed into *E. coli* One Shot TOP10 competent cells as described in section 3.2.7. Selective pressure was maintained by using LB plates, containing 3 $\mu g.ml^{-1}$ bleomycin (pWUR) or 30 $\mu g.ml^{-1}$ kanamycin (pMK184).

4.2.11 Evaluation of the Insert Size and Sequencing

To evaluate the ligated insert sizes, 10 single white colonies for each construct in both vectors, were separately inoculated into 5 ml LB medium, containing 3 $\mu g.ml^{-1}$ bleomycin (pWUR) or 30 $\mu g.ml^{-1}$ kanamycin (pMK184) and incubated overnight at 37ºC with aeration (200 rpm). Plasmids were isolated using the BioSpin Plasmid DNA Extraction Kit (BioFlux), as per manufacturer's instructions. Double digestion was done on the plasmids, using the restriction enzymes *Eco*RI and *Xba*I (Fermentas), as described in section 4.2.9. The restriction digestions were visualized on a 1% agarose gel as described in section 3.2.3. Purification of the insert was achieved by excising the desired band (± 1.9 kb) from the agarose gel, using a non-UV transilluminator (Dark Reader™ transilluminator DR-45M, Clare Chemical Research) and extracted using the BioSpin Gel Extraction Kit (BioFlux), as per manufacturer's instructions.

The purified inserts were again sequenced for confirmation of the nucleotide composition of the ABC transporter, peptide-binding gene. Sanger sequencing was done as described in section 3.2.11, using primers 9 - 12 (Table 4.2).

4.2.12 Transformation into *Thermus thermophilus* HB27

Transformation was done according to the method described by Koyama *et al.*, (1986) with modifications. *T. thermophilus* HB27 was inoculated from a 20% glycerol stock (stored at -80ºC) into 10 ml *Thermus* broth and incubated overnight at 70ºC, with aeration (200 rpm). The overnight grown culture (500 µl) was inoculated into fresh, pre-warmed at 70ºC, 10 ml *Thermus* broth and incubated at 70ºC, with aeration (200 rpm) for ± 3 hours or until an absorbance of 0.8 at 600 nm (until the mid-exponential growth phase was reached). During inoculation, both the growing culture and the fresh medium were kept at 70ºC, to prevent a temperature drop and give the cells a temperature shock. The purified inserts (10 µl) for each construct in both the pWUR and pMK184 vectors were added to a tube and heated at 70ºC. This was also done for a negative control, containing no plasmid and positive controls (for both pMK184 and pWUR), containing empty plasmid. The reinoculated culture (700 µl) were added to the plasmid and incubated at 70ºC for 3 hours, with aeration (200 rpm). Again, both the plasmid and the culture were kept at 70ºC while working. Different volumes were plated out on

separate pre-warmed *Thermus* broth plates and selective pressure was maintained by using LB plates, containing 3 $\mu g.ml^{-1}$ bleomycin (pWUR) or 30 $\mu g.ml^{-1}$ kanamycin (pMK184) and incubated at both 60ºC for 48 hours and 70ºC for 24 hours.

4.2.13 Expression and Fractionation of the ABC Transporter, Peptide-Binding Protein

The growth on the incubated plates from the transformation in section 4.2.12 were again plated out onto fresh *Thermus* broth plates and incubated at 65ºC, to obtain single colonies. Once single colonies were obtained, these were inoculated into 5 ml *Thermus* broth containing the required antibiotic and incubated overnight at 65ºC, with aeration (200 rpm). The overnight grown culture (500 µl) was again inoculated into 5 ml *Thermus* broth, containing the required antibiotic and incubated 65ºC, with aeration (200 rpm) until an absorbance of 0.4 - 0.8 at 600 nm was reached. The cells were harvested and fractionated as described in section 3.2.13. Samples were collected for analysis, during each step since harvesting.

4.2.14 Purification of the ABC Transporter, Peptide-Binding Protein

4.2.14.1 Expression in pWUR and pMK184

The soluble fraction for expression in pWUR and pMK184 was purified using a Nickel NTA (HisTrapFF) column (Amersham Biosciences), as described in section 3.2.14.2.

4.2.15 Characterization of the ABC Transporter, Peptide-Binding Protein in *Thermus thermophilus* HB27

Unless otherwise mentioned, all characterization steps were carried out on the protein expressed in both the pWUR and pMK184 vectors.

4.2.15.1 SDS-PAGE and Western Blot Analysis

The homogeneity of the proteins present in each fraction was determined by sodium dodecyl sulphate polyacrylamide gel electrophoresis (SDS-PAGE) analysis as described by Laemmli, (1970) in section 3.2.15.1. The protein band detection was done by either Coomassie staining (Fairbanks *et al.,* 1971) or Silver staining (Rabilloud *et al.*, 1988). To confirm the presence of the protein, Western blot analysis was done, using a Hybond ECL, nitrocellulose membrane (Amersham Life Science). Transfer of the protein from a SDS-PAGE to the membrane was done as per manufacturer's instructions and using a Mini Trans-Blot Cell (BIO-RAD) with the PageRuler™ Prestained Protein Ladder (Fermentas) as the molecular weight standard. Blocking and incubation with the antibody was done, using the SuperSignal® West HisProbe™ Kit (PIERCE), as per manufacturer's instructions. The blot was developed onto a Medical X-ray film 100 NIF CP-G Plus (AGFA), using Developer G153 (AGFA) and Rapid Fixer G354 (AGFA).

4.2.15.2 Protein Concentrations

Protein concentrations of the fractions were determined using the Micro BCA™ Protein Assay Kit (PIERCE) (Smith *et al.,* 1985), as described in section 3.2.15.2.

4.2.15.3 Gold Reduction Assay

All the activity tests on the different fractions collected in section 4.2.14, as well as the effect on gold reduction and nanoparticle formations, tested with different parameters in sections 4.2.15.7 – 4.2.16 were done using the gold reduction assay as described in section 3.2.15.3, but using incubation temperatures of both 65ºC and 85ºC.

4.2.15.4 Surface Plasmon Resonance

To verify gold reduction and nanoparticle formation, UV-Vis wave scans in the range of 300-800 nm was done on all the parameters tested in sections 4.2.15.7 – 4.2.16 and spectrums were obtained using a SpectraMax M2 UV-Vis Scanner (Labotec), to evaluate the plasmon band associated with gold-nanoparticles. This was done as

described in section 3.2.15.4. The SPR was used to determine which samples were subjected to downstream analysis.

4.2.15.5 Transmission Electron Microscopy

Transmission electron microscopy (TEM) analysis was done on specific samples, selected *via* SPR analysis, from the gold reduction and nanoparticle formations, tested with different parameters in sections 4.2.15.7 – 4.2.16. TEM was done to evaluate the size and morphology of the nanoparticles as described in section 3.2.15.5. Electron micrographs of the gold nanoparticles were taken with either a JEOL TEM 1010, 60 kV or 200 kV Philips CM 20 TEM, by the University of Ghent (Ghent, Belgium) and NMMU (Port Elizabeth, South Africa) respectively.

4.2.15.6 Energy Dispersive X-ray Spectrometry and Selected-Area Electron Diffraction

Energy dispersive X-ray spectrometry (EDX) and selected-area electron diffraction (SAED) analysis was done on specific samples, selected *via* SPR analysis, from the gold reduction and nanoparticle formations, tested with different parameters in sections 4.2.15.7 – 4.2.16. This was used to identify the chemical composition of the particles present in the samples and their relative amounts, and was done using an EDAX DX4 energy dispersive X-ray spectrometry system, coupled to a 200 kV Philips CM 20 TEM, by the NMMU (Port Elizabeth, South Africa).

4.2.15.7 The Effect of the Assay Components (Sodium Dithionite and Methyl Viologen) on Gold Reduction and Nanoparticle Formation

The effect of sodium dithionite and methyl viologen on gold reduction and nanoparticle formation was evaluated with the gold reduction assay as described in section 4.2.15.3, by eliminating the sodium dithionite from the assay and keeping the methyl viologen concentration constant or by eliminating the methyl viologen from the assay and keeping the sodium dithionite concentration constant or by keeping both the sodium dithionite

and methyl viologen concentrations constant. Sodium dithionite was used as an electron donor and reducing agent. Methyl viologen was used as an intermediate by accepting electrons from sodium dithionite to form a free radical which in turn then acts as an electron donor and reducing agent. UV-Vis spectrums were obtained as described in section 3.2.15.4 and selected samples were subjected for TEM, EDX and SAED analysis as described in sections 3.2.15.5 and 3.2.15.6 respectively.

4.2.15.8 The Effect of Denatured Protein on Gold Reduction and Nanoparticle Formation

The effect of denatured protein on gold reduction and nanoparticle formation was evaluated with the gold reduction assay as described in section 4.2.15.3. The protein was denatured through boiling for 3 hours and all three the electron donors from section 4.2.15.12 were again used. UV-Vis spectrums were obtained as described in section 3.2.15.4 and selected samples were subjected for TEM, EDX and SAED analysis as described in sections 3.2.15.5 and 3.2.15.6 respectively.

4.2.15.9 The Effect of $HAuCl_4$ Concentrations on Gold Reduction and Nanoparticle Formation

The effect of different gold(III) concentrations, using $HAuCl_4$ as the gold(III) source, on gold reduction and nanoparticle formation was evaluated with the gold reduction assay as described in section 4.2.15.3, but by using gold(III) concentrations varying from 0 – 10 mM. UV-Vis spectrums were obtained as described in section 3.2.15.4 and selected samples were subjected for TEM, EDX and SAED analysis as described in sections 3.2.15.5 and 3.2.15.6 respectively.

4.2.15.10 The Effect of Temperature on Gold Reduction and Nanoparticle Formation

The effect of temperature on gold reduction and nanoparticle formation was evaluated with the gold reduction assay as described in section 4.2.15.3, but by incubating the

samples at a temperature range between 30 and 85℃. UV-Vis spectrums were obtained as described in section 3.2.15.4 and selected samples were subjected for TEM, EDX and SAED analysis as described in sections 3.2.15.5 and 3.2.15.6 respectively.

4.2.15.11 The Effect of pH on Gold Reduction and Nanoparticle Formation

The effect of pH on gold reduction and nanoparticle formation was evaluated with the gold reduction assay as described in section 4.2.15.3, but by using specific buffers, ranging from pH 3.6 to 9.0. Acetate was used for the acidic pH range, phosphate buffer for the neutral pH range and borax for the alkaline pH range. UV-Vis spectrums were obtained as described in section 3.2.15.4 and selected samples were subjected for TEM, EDX and SAED analysis as described in sections 3.2.15.5 and 3.2.15.6 respectively.

4.2.15.12 The Effect of Different Disulphide Bond Reducing Agents on Gold Reduction and Nanoparticle Formation

The effect of different disulphide bond reducing agents on gold reduction and nanoparticle formation was evaluated with the gold reduction assay as described in section 4.2.15.3, but by using 46 µM of various electron donors, including sodium dithionite, dithiothreitol (DTT) and β-mercaptoethanol. UV-Vis spectrums were obtained as described in section 3.2.15.4 and selected samples were subjected for TEM, EDX and SAED analysis as described in sections 3.2.15.5 and 3.2.15.6 respectively.

4.2.16 Mechanism Hypothesis

To test the hypothesis as described in section 3.2.16 by van Marwijk, (2009), the effect of the sulphydryl blocking agent, iodoacetic acid, on all three the electron donors from section 4.2.15.12 were tested for gold reduction and nanoparticle formation with the gold reduction assay as described in section 4.2.15.3. UV-Vis spectrums were obtained as described in section 3.2.15.4 and selected samples were subjected for TEM analysis as described in section 3.2.15.5.

4.3 RESULTS AND DISCUSSIONS

4.3.1 Genomic DNA Isolation and Polymerase Chain Reaction

Genomic DNA (gDNA) (2047 ng.µl^{-1}) was isolated from *Thermus scotoductus* SA-01, using a modified SDS-proteinase K method, as described in section 3.2.3 (Figure 4.3A).

The ABC transporter, peptide-binding gene was amplified for cloning and expression studies as described in section 4.2.4, using primers 1, 2, 5 and 6 (Table 4.2), to obtain amplicons of ± 1.9 kb (Figure 4.3B). This yielded constructs that either included or excluded the leader peptide, the C-terminal and/or the N-terminal His-Tag when cloned in pET-22b(+) and pET-28b(+) (Table 4.3), when different combinations of these primers were used. These constructs are from this point on referred to as construct 1 (Primers 1 and 6), construct 2 (Primers 2 and 5) and construct 3 (Primers 5 and 6).

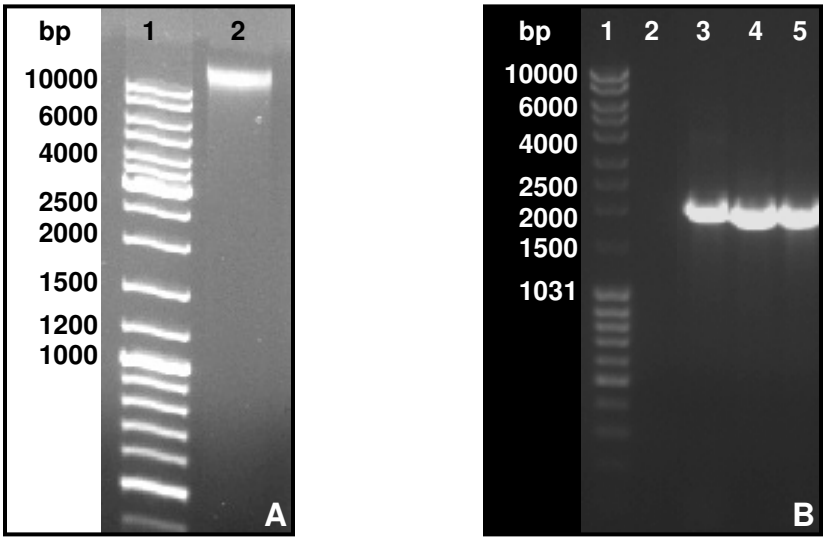

Figure 4.3: (A) Genomic DNA isolated from *T. scotoductus* SA-01 (Lane 2) with the GeneRuler^{TM} DNA ladder (Lane 1). (B) The amplified ABC transporter, peptide-binding gene of ± 1.9 kb for construct 1 (Lane 3); construct 2 (Lane 4) and construct 3 (Lane 5); negative control (Lane 2) and the MassRuler^{TM} DNA ladder (Lane 1).

4.3.2 Cloning into pGEM®-T Easy

The ± 1.9 kb PCR products, purified from the agarose gel, were ligated into the pGEM®-T Easy Vector system, as described in section 3.2.5. The ligated plasmid reactions were transformed into *Escherichia coli* One Shot TOP10 competent cells, as described in section 3.2.7. Plasmids were isolated from 10 clones for each construct and the insert sizes were evaluated by double digestion with the restriction enzymes *Eco*RI and *Nde*I, as described in section 3.2.8. RFLP, confirming the insert for all three the different constructs of the ABC transporter, peptide-binding gene into the pGEM®-T Easy Vector system, can be seen in figure 4.4. Clone 1 for construct 1 (Lane 2; Figure 4.4A); clone 5 for construct 2 (Lane 6; Figure 4.4B) and clone 3 for construct 3 (Lane 4; Figure 4.4C) were chosen for downstream experiments.

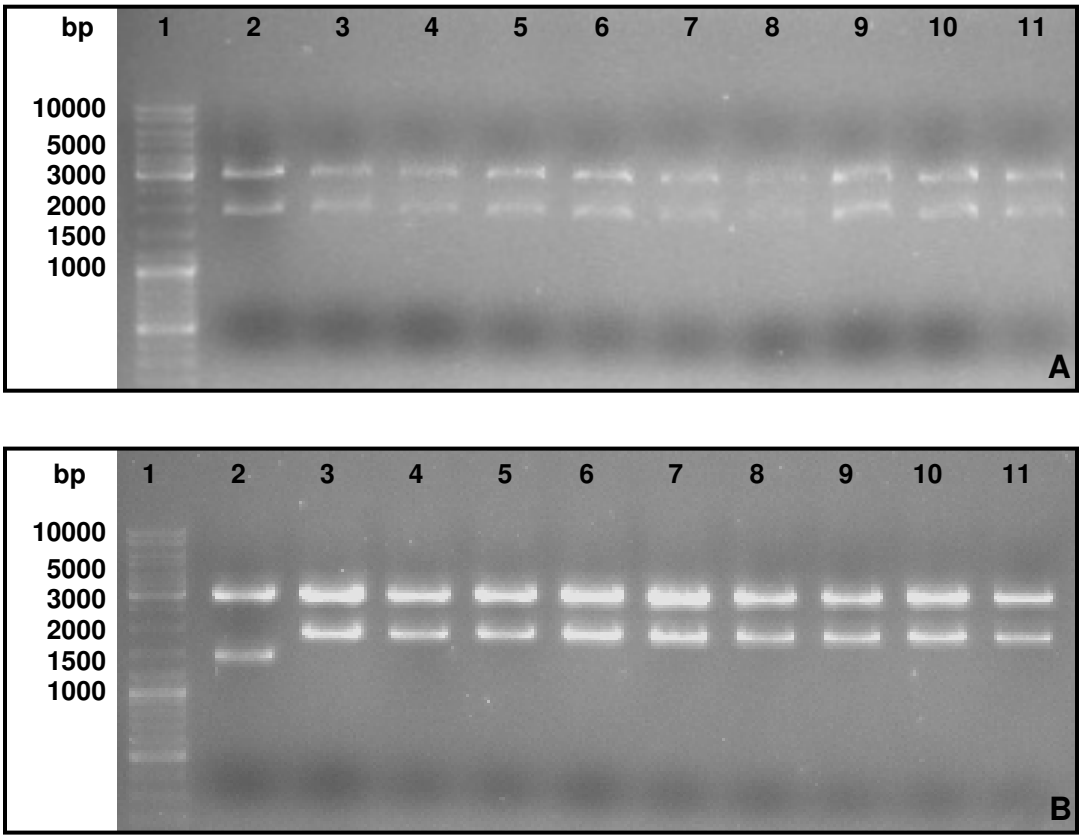

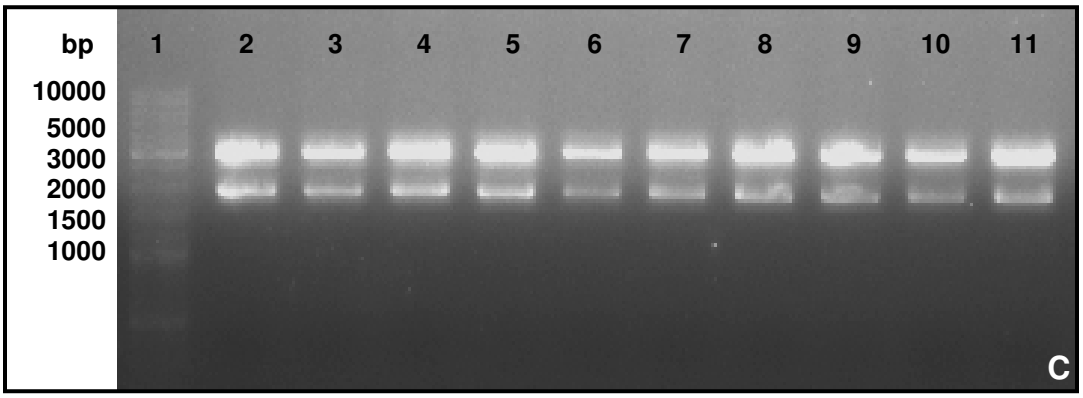

Figure 4.4: The amplified ABC transporter, peptide-binding gene of ± 1.9 kb, inserted into the pGEM®-T Easy Vector system of ± 3 kb, for (A) Construct 1 (Lanes 2 - 11) and the GeneRuler™ DNA ladder (Lane 1). (B) Construct 2 (Lanes 2 - 11) and the GeneRuler™ DNA ladder (Lane 1). (C) Construct 3 (Lanes 2 - 11) and the GeneRuler™ DNA ladder (Lane 1).

4.3.3 Cloning into pET-22b(+) and pET-28b(+)

The pET-22b(+) and pET-28b(+) vectors were propagated in *E. coli* One Shot TOP10 competent cells as described in section 3.2.9. Plasmids were isolated and the insert sizes were evaluated by double digestion with the restriction enzymes, *Eco*RI and *Nde*I, as described in section 3.2.8, to yield compatible cohesive ends. RFLP, confirming the empty, digested pET-22b(+) and pET-28b(+) vectors, can be seen in figure 4.5A.

The ± 1.9 kb inserts, purified from the agarose gel, were ligated into the pET-22b(+) and pET-28b(+) vectors, as described in section 3.2.9, to obtain the three constructs (Table 4.4). Clone 1 (Construct 1) and clone 3 (Construct 3) were ligated into pET-22b(+) and clone 5 (Construct 2) was ligated into pET-28b(+).

The ligated plasmid reactions were transformed into *E. coli* One Shot TOP10 competent cells, as described in section 3.2.9. Plasmids were isolated from 10 clones for each construct and the insert sizes were evaluated by double digestion with the restriction enzymes *Eco*RI and *Xba*I, as described in section 4.2.9. RFLP, confirming the insertion of the ABC transporter, peptide-binding gene into the pET-22b(+) or pET-28b(+) vectors for all three constructs, can be seen in figure 4.5B. One clone for each of the three constructs was selected for downstream experiments. The selected clones were clone 6

in pET-22b(+) (Construct 1; Lane 7; Figure 4.5B); clone 3 in pET-28b(+) (Construct 2; Lane 14; Figure 4.5B) and clone 1 in pET-22b(+) (Construct 3; Lane 23; Figure 4.5B)

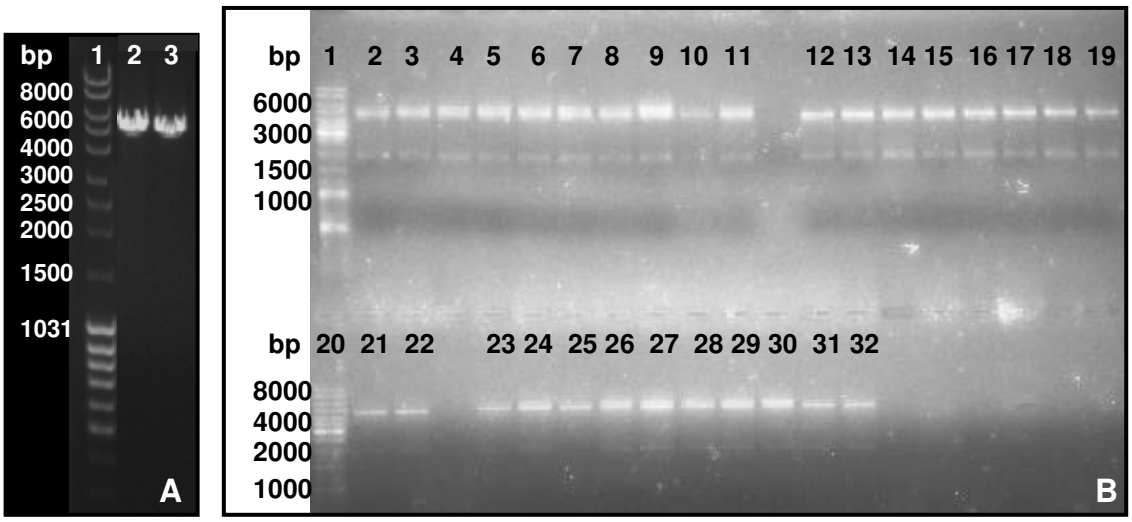

Figure 4.5: (A) The empty, digested pET-22b(+) and pET-28b(+) vectors (Lanes 2 and 3 respectively), and the MassRuler^{TM} DNA ladder (Lane 1). (B) The ABC transporter, peptide-binding gene of ± 1.9 kb, inserted into the pET vectors of ± 5.5 kb. Clone 1, inserted into pET-22b(+) (Lanes 2 - 11); clone 5, inserted into pET-28b(+) (Lanes 12 – 19, 21 and 22); clone 3, inserted into pET-22b(+) (Lanes 23 – 32) and the GeneRuler^{TM} DNA ladder (Lanes 1 and 20).

The three selected clones were sequenced for confirmation of the nucleotide composition of the ABC transporter, peptide-binding gene, as described in section 4.2.9. The data was analyzed and contigs were formed, using ContigExpress (Vector NTI Suite 9). Analyzed sequences were used to search the Genbank Database, using BLAST (NCBI, 2009) and alignments were done using ClustalW (EBI, 2009). Sequence results of the inserts showed 100% identity to ABC transporter, peptide-binding gene of *T. scotoductus* SA-01 (Figure 4.6) and were confirmed with BLAST analysis to be an ABC transporter, peptide-binding protein. The results for all three clones were identical and therefore only the alignment from clone 6 in pET-22b(+) (Construct 1) is shown here as a representation.

*T.scot*SA01	ATGAGAAAAGTAGGCAAGCTGGCTGTATTCGGTTTAGCCGCCCTGGGCTTGGCCCTGGCG
6/pET-22	ATGAGAAAAGTAGGCAAGCTGGCTGTATTCGGTTTAGCCGCCCTGGGCTTGGCCCTGGCG
*T.scot*SA01	GGGCCCCAGGACAACAGCCTGGTCATAGGGGCTTCGCAGGAGCCCCGGGTTCTGGCGGGG
6/pET-22	GGGCCCCAGGACAACAGCCTGGTCATAGGGGCTTCGCAGGAGCCCCGGGTTCTGGCGGGG
*T.scot*SA01	GACTTCCTAAGCATCATCTCCAACCAGTCCATCAAGTTGGAGATCGAGCAGTACCTCTTC
6/pET-22	GACTTCCTAAGCATCATCTCCAACCAGTCCATCAAGTTGGAGATCGAGCAGTACCTCTTC
*T.scot*SA01	GCCCCCCTCATCGGTTTCAACGCCAACAGCGAAAACTTTCCCGTGCTGGTCACCGAGGTG
6/pET-22	GCCCCCCTCATCGGTTTCAACGCCAACAGCGAAAACTTTCCCGTGCTGGTCACCGAGGTG
*T.scot*SA01	CCCACCCGGCAAAACGGGCGTTTGCGGGTGACGGACATCGGCGGGGGCAAGAAGCGCTTG
6/pET-22	CCCACCCGGCAAAACGGGCGTTTGCGGGTGACGGACATCGGCGGGGGCAAGAAGCGCTTG
*T.scot*SA01	GAGATGGACCTCACCATCCGGCCCGATGCCCGCTGGTCCGACGGCAAGCCCATCACCACC
6/pET-22	GAGATGGACCTCACCATCCGGCCCGATGCCCGCTGGTCCGACGGCAAGCCCATCACCACC
*T.scot*SA01	GAGGATGTGGCCTTCTACTACGAGGTGGGCAAGGCCAAGGGGATGCCGGTGCTCAACCCG
6/pET-22	GAGGATGTGGCCTTCTACTACGAGGTGGGCAAGGCCAAGGGGATGCCGGTGCTCAACCCG
*T.scot*SA01	GACTACTGGGAGCGGGTGAACCTCCGGGTCAGGGACGCCCGCAACTTCACCGTGATCTTT
6/pET-22	GACTACTGGGAGCGGGTGAACCTCCGGGTCAGGGACGCCCGCAACTTCACCGTGATCTTT
*T.scot*SA01	GAGCCCGCCTACTACTACGACACCTACGGCGGCACCTACGGCTCCCCCATCGGCTACGCT
6/pET-22	GAGCCCGCCTACTACTACGACACCTACGGCGGCACCTACGGCTCCCCCATCGGCTACGCT
*T.scot*SA01	CCCAAGCACATCATGGGCGCCGAGTGGGAGAAGGTGAAAGCGGCGGCCCGGAACCTGGAT
6/pET-22	CCCAAGCACATCATGGGCGCCGAGTGGGAGAAGGTGAAAGCGGCGGCCCGGAACCTGGAT
*T.scot*SA01	CCCGATAAGGATGCGGAGAGGCTCAACGAGCTCTACCGCAACTTCTTCCTCAAGTTCGCC
6/pET-22	CCCGATAAGGATGCGGAGAGGCTCAACGAGCTCTACCGCAACTTCTTCCTCAAGTTCGCC
*T.scot*SA01	ACTCCCCAGGCCCTAAACCGGGGAGCCATGGTCTACTCGGGGGCCTTCAAGCTGCGGCGC
6/pET-22	ACTCCCCAGGCCCTAAACCGGGGAGCCATGGTCTACTCGGGGGCCTTCAAGCTGCGGCGC
*T.scot*SA01	TGGGTGCCGGGGAACTCCATTGAGATGGAGCGGAACCCCAACTTCCCCATCAAGCCCGAG
6/pET-22	TGGGTGCCGGGGAACTCCATTGAGATGGAGCGGAACCCCAACTTCCCCATCAAGCCCGAG
*T.scot*SA01	GGTGGGGAGAGCCGGTACGTGCAGAGGGTGGTCTACCGCTTCATCCAGAACACCAACTCC
6/pET-22	GGTGGGGAGAGCCGGTACGTGCAGAGGGTGGTCTACCGCTTCATCCAGAACACCAACTCC
*T.scot*SA01	CTCCTGGTGGCCGTCCTGGGCGGGAGCATTGACGCCACCTCCAGCGTCTCCCTCACCTTT
6/pET-22	CTCCTGGTGGCCGTCCTGGGCGGGAGCATTGACGCCACCTCCAGCGTCTCCCTCACCTTT
*T.scot*SA01	GACCAAGGCCGTAGCCGCCAGCTCACCTCCCGGGCCCCTGGCCGCTTTGACATCTGGTTC
6/pET-22	GACCAAGGCCGTAGCCGCCAGCTCACCTCCCGGGCCCCTGGCCGCTTTGACATCTGGTTC
*T.scot*SA01	GTGCCCGGGGCCATCTGGGAGCACATTGACGTCAACAAGTTTGAGAACTGCCAGGCGGTC
6/pET-22	GTGCCCGGGGCCATCTGGGAGCACATTGACGTCAACAAGTTTGAGAACTGCCAGGCGGTC
*T.scot*SA01	CGCGACTTGGGCCTGAACGACGTCCGCACCCGTCGGGCCCTCCTCCACGCTCTGAACCGC
6/pET-22	CGCGACTTGGGCCTGAACGACGTCCGCACCCGTCGGGCCCTCCTCCACGCTCTGAACCGC
*T.scot*SA01	GAGGGGTTGGTCAAGGCCTTCTTTGACGGCCTCCAGCCCGTGGCCCACACCTGGATCGCC
6/pET-22	GAGGGGTTGGTCAAGGCCTTCTTTGACGGCCTCCAGCCCGTGGCCCACACCTGGATCGCC
*T.scot*SA01	CCCGTCAACCCCCTCTTCAACCCCAATGTGCGGAAGTACGAGTTTGACCTGAAGAAGGCG
6/pET-22	CCCGTCAACCCCCTCTTCAACCCCAATGTGCGGAAGTACGAGTTTGACCTGAAGAAGGCG
*T.scot*SA01	GAGGCGCTCTTGGCGGAGATGGGCTGGAGGAAGGGGCCGGACGGCATCCTTCAGCGCACC
6/pET-22	GAGGCGCTCTTGGCGGAGATGGGCTGGAGGAAGGGGCCGGACGGCATCCTTCAGCGCACC

```
T.scotSA01      GTGGGTGGCCGCACCGTGCGCTTTGAGATTGAGTTCGTCACCACCGCGGGCAACGCTATC
6/pET-22        GTGGGTGGCCGCACCGTGCGCTTTGAGATTGAGTTCGTCACCACCGCGGGCAACGCTATC

T.scotSA01      CGGGAGCGCACCCAGCAGTTCTTCGCCGAGGACCTGAAGAAGATCGGCATCGCCGTCAAG
6/pET-22        CGGGAGCGCACCCAGCAGTTCTTCGCCGAGGACCTGAAGAAGATCGGCATCGCCGTCAAG

T.scotSA01      ATCAATAACGCCCCCAGCGCCGTGGTCTTCGCCGACGACTACATCCAGCGGGCCAGCGAG
6/pET-22        ATCAATAACGCCCCCAGCGCCGTGGTCTTCGCCGACGACTACATCCAGCGGGCCAGCGAG

T.scotSA01      TGCAAGTGGACCGGGCTGTTTGAGTTCGCTTGGGTTTCCAACCTGGCCGAGGATGGCTCC
6/pET-22        TGCAAGTGGACCGGGCTGTTTGAGTTCGCTTGGGTTTCCAACCTGGCCGAGGATGGCTCC

T.scotSA01      CTCTTCCAGTACAAGAACCTGAACACCGGGGCCATCATGGTGCCCACCAAGGAGAACAAC
6/pET-22        CTCTTCCAGTACAAGAACCTGAACACCGGGGCCATCATGGTGCCCACCAAGGAGAACAAC

T.scotSA01      TACCAGGGGCAGAACATCGGCGGCTGGCGCAACGACGAGTTTGACCGTCTGACGAGCCAG
6/pET-22        TACCAGGGGCAGAACATCGGCGGCTGGCGCAACGACGAGTTTGACCGTCTGACGAGCCAG

T.scotSA01      GGTGTCCTGGAGTTTGACGAGGCCAGGCGGAAGCAGCTCTTCTGGAGGGCCCAGGAGATC
6/pET-22        GGTGTCCTGGAGTTTGACGAGGCCAGGCGGAAGCAGCTCTTCTGGAGGGCCCAGGAGATC

T.scotSA01      TGGGCCGAGGAGCTGCCTGCCTTGCCCCTCTACTTCCGCGCTAACCCCTACGTGGTGCGG
6/pET-22        TGGGCCGAGGAGCTGCCTGCCTTGCCCCTCTACTTCCGCGCTAACCCCTACGTGGTGCGG

T.scotSA01      AAGGGCCTGGTCAACTACGTGGCCAGCGCTTACGCGGGCGGCTACGGTTACCCCGGCTGG
6/pET-22        AAGGGCCTGGTCAACTACGTGGCCAGCGCTTACGCGGGCGGCTACGGTTACCCCGGCTGG

T.scotSA01      AACGCTTGGGAGATCGGCTGGGAGAGCCGCGGCGCCGTGAAGAAGTGGGACCAGGCGAAG
6/pET-22        AACGCTTGGGAGATCGGCTGGGAGAGCCGCGGCGCCGTGAAGAAGTGGGACCAGGCGAAG

T.scotSA01      TACGCTCTTTCCGTCAAGTAA
6/pET-22        TACGCTCTTTCCGTCAAGTAA
```

Figure 4.6: Sequence alignments of the ABC transporter, peptide-binding gene from *T. scotoductus* SA-01 and clone 6 in pET-22b(+) (Construct 1), showing 100% identity.

4.3.4 Cloning into pWUR and pMK184

The pWUR and pMK184 vectors were propagated in *E. coli* One Shot TOP10 competent cells as described in section 4.2.10. Plasmids were isolated and the insert sizes were evaluated by double digestion with the restriction enzymes, *Eco*RI and *Xba*I, as described in section 4.2.9, to yield compatible cohesive ends. RFLP, confirming the empty, digested pWUR and pMK184 vectors, can be seen in figure 4.7A.

The ± 1.9 kb inserts for all three constructs, purified from the agarose gel, were ligated into both the pWUR and pMK184 vectors, as described in section 4.2.10. The ligated plasmid reactions were transformed into *E. coli* One Shot TOP10 competent cells, as

described in section 4.2.10. Plasmids were isolated from 10 clones for each construct in each vector and the insert sizes were evaluated through double digestion with the restriction enzymes *Eco*RI and *Xba*I, as described in section 4.2.9. RFLP, confirming the insertion of the ABC transporter, peptide-binding gene into the pWUR vector for all three constructs, can be seen in figure 4.7B and insertion into the pMK184 vector for all three constructs, can be seen in figure 4.7C. One clone for each of the three constructs in pWUR and one clone for two of the three constructs in pMK184 were selected for downstream experiments. Construct 1 in pMK184 did not yield the correct insert and was not used for further experiments. The selected clones for downstream experiments were clone 10 (Construct 1; Lane 11; Figure 4.7B); clone 2 (Construct 2; Lane 13; Figure 4.7B) and clone 7 (Construct 3; Lane 28, Figure 4.7B) for pWUR and clone 4 (Construct 2; Lane 15; Figure 4.7C) and clone 4 (Construct 3; Lane 25; Figure 4.7C) for pMK184.

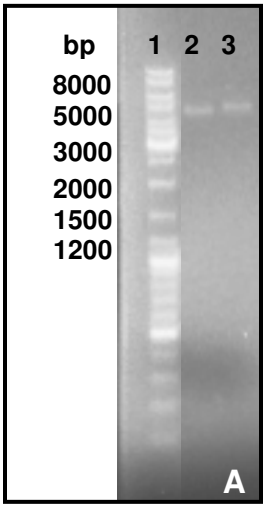

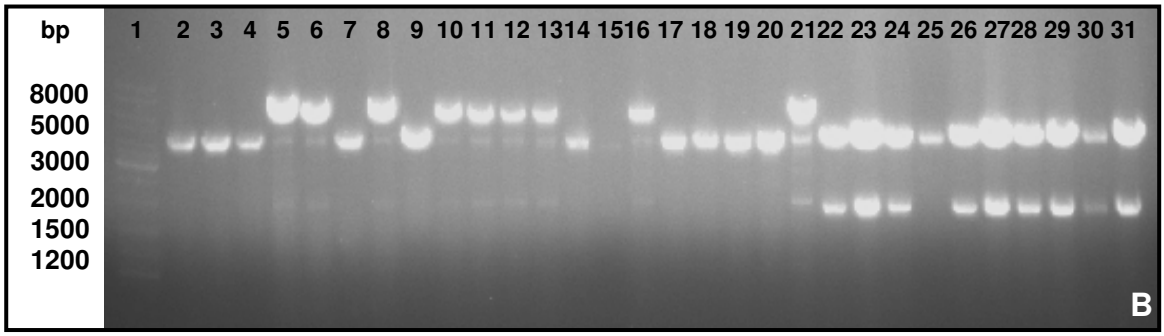

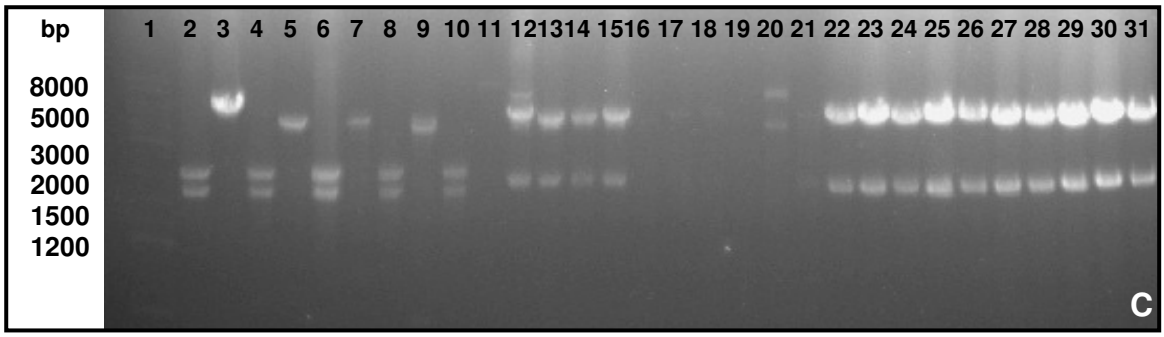

Figure 4.7: (A) The empty, digested pWUR and pMK184 vectors (Lanes 2 and 3 respectively), and the GeneRuler™ DNA ladder (Lane 1). (B) The ABC transporter, peptide-binding gene of ± 1.9 kb, inserted into pWUR of ± 4.5 kb. Construct 1 (Lanes 2 - 11); construct 2 (Lanes 12 - 21); construct 3 (Lanes 22 - 31) and the GeneRuler™ DNA ladder (Lane 1). (C) The ABC transporter, peptide-binding gene of ± 1.9 kb, inserted into pMK184 of ± 5 kb. Construct 1 (Lanes 2 - 11); construct 2 (Lanes 12 - 21); construct 3 (Lanes 22 - 31) and the GeneRuler™ DNA ladder (Lane 1).

The five selected clones were sequenced for confirmation of the nucleotide composition of the ABC transporter, peptide-binding gene, as described in section 4.2.11. The data was analyzed and contigs were formed, using ContigExpress (Vector NTI Suite 9). Analyzed sequences were used to search the Genbank Database, using BLAST (NCBI, 2009) and alignments were done using ClustalW (EBI, 2009). Sequence results of the inserts showed 100% identity to ABC transporter, peptide-binding gene of *T. scotoductus* SA-01 (Figure 4.8) and were confirmed with BLAST analysis to be an ABC transporter, peptide-binding protein. The results all five clones were identical and therefore only the alignment from clone 2 in pWUR (Construct 2) is shown here as a representation.

*T.scot*SA01 ATGAGAAAAGTAGGCAAGCTGGCTGTATTCGGTTTAGCCGCCCTGGGCTTGGCCCTGGCG
2/pWUR ATGAGAAAAGTAGGCAAGCTGGCTGTATTCGGTTTAGCCGCCCTGGGCTTGGCCCTGGCG

*T.scot*SA01 GGGCCCCAGGACAACAGCCTGGTCATAGGGGCTTCGCAGGAGCCCCGGGTTCTGGCGGGG
2/pWUR GGGCCCCAGGACAACAGCCTGGTCATAGGGGCTTCGCAGGAGCCCCGGGTTCTGGCGGGG

*T.scot*SA01 GACTTCCTAAGCATCATCTCCAACCAGTCCATCAAGTTGGAGATCGAGCAGTACCTCTTC
2/pWUR GACTTCCTAAGCATCATCTCCAACCAGTCCATCAAGTTGGAGATCGAGCAGTACCTCTTC

*T.scot*SA01 GCCCCCCTCATCGGTTTCAACGCCAACAGCGAAAACTTTCCCGTGCTGGTCACCGAGGTG
2/pWUR GCCCCCCTCATCGGTTTCAACGCCAACAGCGAAAACTTTCCCGTGCTGGTCACCGAGGTG

*T.scot*SA01 CCCACCCGGCAAAACGGGCGTTTGCGGGTGACGGACATCGGCGGGGGCAAGAAGCGCTTG
2/pWUR CCCACCCGGCAAAACGGGCGTTTGCGGGTGACGGACATCGGCGGGGGCAAGAAGCGCTTG

*T.scot*SA01 GAGATGGACCTCACCATCCGGCCCGATGCCCGCTGGTCCGACGGCAAGCCCATCACCACC
2/pWUR GAGATGGACCTCACCATCCGGCCCGATGCCCGCTGGTCCGACGGCAAGCCCATCACCACC

*T.scot*SA01 GAGGATGTGGCCTTCTACTACGAGGTGGGCAAGGCCAAGGGGATGCCGGTGCTCAACCCG
2/pWUR GAGGATGTGGCCTTCTACTACGAGGTGGGCAAGGCCAAGGGGATGCCGGTGCTCAACCCG

*T.scot*SA01 GACTACTGGGAGCGGGTGAACCTCCGGGTCAGGGACGCCCGCAACTTCACCGTGATCTTT
2/pWUR GACTACTGGGAGCGGGTGAACCTCCGGGTCAGGGACGCCCGCAACTTCACCGTGATCTTT

*T.scot*SA01 GAGCCCGCCTACTACTACGACACCTACGGCGGCACCTACGGCTCCCCCATCGGCTACGCT
2/pWUR GAGCCCGCCTACTACTACGACACCTACGGCGGCACCTACGGCTCCCCCATCGGCTACGCT

*T.scot*SA01 CCCAAGCACATCATGGGCGCCGAGTGGGAGAAGGTGAAAGCGGCGGCCCGGAACCTGGAT
2/pWUR CCCAAGCACATCATGGGCGCCGAGTGGGAGAAGGTGAAAGCGGCGGCCCGGAACCTGGAT

*T.scot*SA01 CCCGATAAGGATGCGGAGAGGCTCAACGAGCTCTACCGCAACTTCTTCCTCAAGTTCGCC
2/pWUR CCCGATAAGGATGCGGAGAGGCTCAACGAGCTCTACCGCAACTTCTTCCTCAAGTTCGCC

*T.scot*SA01 ACTCCCCAGGCCCTAAACCGGGGAGCCATGGTCTACTCGGGGGCCTTCAAGCTGCGGCGC
2/pWUR ACTCCCCAGGCCCTAAACCGGGGAGCCATGGTCTACTCGGGGGCCTTCAAGCTGCGGCGC

*T.scot*SA01 TGGGTGCCGGGGAACTCCATTGAGATGGAGCGGAACCCCAACTTCCCCATCAAGCCCGAG
2/pWUR TGGGTGCCGGGGAACTCCATTGAGATGGAGCGGAACCCCAACTTCCCCATCAAGCCCGAG

*T.scot*SA01 GGTGGGGAGAGCCGGTACGTGCAGAGGGTGGTCTACCGCTTCATCCAGAACACCAACTCC
2/pWUR GGTGGGGAGAGCCGGTACGTGCAGAGGGTGGTCTACCGCTTCATCCAGAACACCAACTCC

*T.scot*SA01 CTCCTGGTGGCCGTCCTGGGCGGGAGCATTGACGCCACCTCCAGCGTCTCCCTCACCTTT
2/pWUR CTCCTGGTGGCCGTCCTGGGCGGGAGCATTGACGCCACCTCCAGCGTCTCCCTCACCTTT

*T.scot*SA01 GACCAAGGCCGTAGCCGCCAGCTCACCTCCCGGGCCCCTGGCCGCTTTGACATCTGGTTC
2/pWUR GACCAAGGCCGTAGCCGCCAGCTCACCTCCCGGGCCCCTGGCCGCTTTGACATCTGGTTC

*T.scot*SA01 GTGCCCGGGGCCATCTGGGAGCACATTGACGTCAACAAGTTTGAGAACTGCCAGGCGGTC
2/pWUR GTGCCCGGGGCCATCTGGGAGCACATTGACGTCAACAAGTTTGAGAACTGCCAGGCGGTC

*T.scot*SA01 CGCGACTTGGGCCTGAACGACGTCCGCACCCGTCGGGCCCTCCTCCACGCTCTGAACCGC
2/pWUR CGCGACTTGGGCCTGAACGACGTCCGCACCCGTCGGGCCCTCCTCCACGCTCTGAACCGC

*T.scot*SA01 GAGGGGTTGGTCAAGGCCTTCTTTGACGGCCTCCAGCCCGTGGCCCACACCTGGATCGCC
2/pWUR GAGGGGTTGGTCAAGGCCTTCTTTGACGGCCTCCAGCCCGTGGCCCACACCTGGATCGCC

*T.scot*SA01 CCCGTCAACCCCCTCTTCAACCCCAATGTGCGGAAGTACGAGTTTGACCTGAAGAAGGCG
2/pWUR CCCGTCAACCCCCTCTTCAACCCCAATGTGCGGAAGTACGAGTTTGACCTGAAGAAGGCG

*T.scot*SA01 GAGGCGCTCTTGGCGGAGATGGGCTGGAGGAAGGGGCCGGACGGCATCCTTCAGCGCACC
2/pWUR GAGGCGCTCTTGGCGGAGATGGGCTGGAGGAAGGGGCCGGACGGCATCCTTCAGCGCACC

```
T.scotSA01      GTGGGTGGCCGCACCGTGCGCTTTGAGATTGAGTTCGTCACCACCGCGGGCAACGCTATC
2/pWUR          GTGGGTGGCCGCACCGTGCGCTTTGAGATTGAGTTCGTCACCACCGCGGGCAACGCTATC

T.scotSA01      CGGGAGCGCACCCAGCAGTTCTTCGCCGAGGACCTGAAGAAGATCGGCATCGCCGTCAAG
2/pWUR          CGGGAGCGCACCCAGCAGTTCTTCGCCGAGGACCTGAAGAAGATCGGCATCGCCGTCAAG

T.scotSA01      ATCAATAACGCCCCCAGCGCCGTGGTCTTCGCCGACGACTACATCCAGCGGGCCAGCGAG
2/pWUR          ATCAATAACGCCCCCAGCGCCGTGGTCTTCGCCGACGACTACATCCAGCGGGCCAGCGAG

T.scotSA01      TGCAAGTGGACCGGGCTGTTTGAGTTCGCTTGGGTTTCCAACCTGGCCGAGGATGGCTCC
2/pWUR          TGCAAGTGGACCGGGCTGTTTGAGTTCGCTTGGGTTTCCAACCTGGCCGAGGATGGCTCC

T.scotSA01      CTCTTCCAGTACAAGAACCTGAACACCGGGGCCATCATGGTGCCCACCAAGGAGAACAAC
2/pWUR          CTCTTCCAGTACAAGAACCTGAACACCGGGGCCATCATGGTGCCCACCAAGGAGAACAAC

T.scotSA01      TACCAGGGGCAGAACATCGGCGGCTGGCGCAACGACGAGTTTGACCGTCTGACGAGCCAG
2/pWUR          TACCAGGGGCAGAACATCGGCGGCTGGCGCAACGACGAGTTTGACCGTCTGACGAGCCAG

T.scotSA01      GGTGTCCTGGAGTTTGACGAGGCCAGGCGGAAGCAGCTCTTCTGGAGGGCCCAGGAGATC
2/pWUR          GGTGTCCTGGAGTTTGACGAGGCCAGGCGGAAGCAGCTCTTCTGGAGGGCCCAGGAGATC

T.scotSA01      TGGGCCGAGGAGCTGCCTGCCTTGCCCCTCTACTTCCGCGCTAACCCCTACGTGGTGCGG
2/pWUR          TGGGCCGAGGAGCTGCCTGCCTTGCCCCTCTACTTCCGCGCTAACCCCTACGTGGTGCGG

T.scotSA01      AAGGGCCTGGTCAACTACGTGGCCAGCGCTTACGCGGGCGGCTACGGTTACCCCGGCTGG
2/pWUR          AAGGGCCTGGTCAACTACGTGGCCAGCGCTTACGCGGGCGGCTACGGTTACCCCGGCTGG

T.scotSA01      AACGCTTGGGAGATCGGCTGGGAGAGCCGCGGCGCCGTGAAGAAGTGGGACCAGGCGAAG
2/pWUR          AACGCTTGGGAGATCGGCTGGGAGAGCCGCGGCGCCGTGAAGAAGTGGGACCAGGCGAAG

T.scotSA01      TACGCTCTTTCCGTCAAGTAA
2/pWUR          TACGCTCTTTCCGTCAAGTAA
```

Figure 4.8: Sequence alignments of the ABC transporter, peptide-binding gene from *T. scotoductus* SA-01 and clone 2 in pWUR (Construct 2), showing 100% identity.

4.3.5 Expression of the ABC Transporter, Peptide-Binding Protein

The five selected clones were used for expression of the ABC transporter, peptide-binding protein, as described in section 4.2.13. Since expression in *T. thermophilus* was constitutive from the PslpA promoter, no induction was required and after an absorbance of 0.4 - 0.8 at 600 nm was reached, the cells were harvested and washed as described in section 3.2.13 and subjected for SDS-PAGE analysis (Figure 4.9), as described in section 3.2.15.1. The expression levels were notably lower than when expression was done with the pET vectors in chapter 3 and the expressed protein of ± 70 kDa in size could only be detected at very low levels. This is probably due to the weaker PslpA promoter in *T. thermophilus*, as compared to the strong T7 promoter system in *E. coli*.

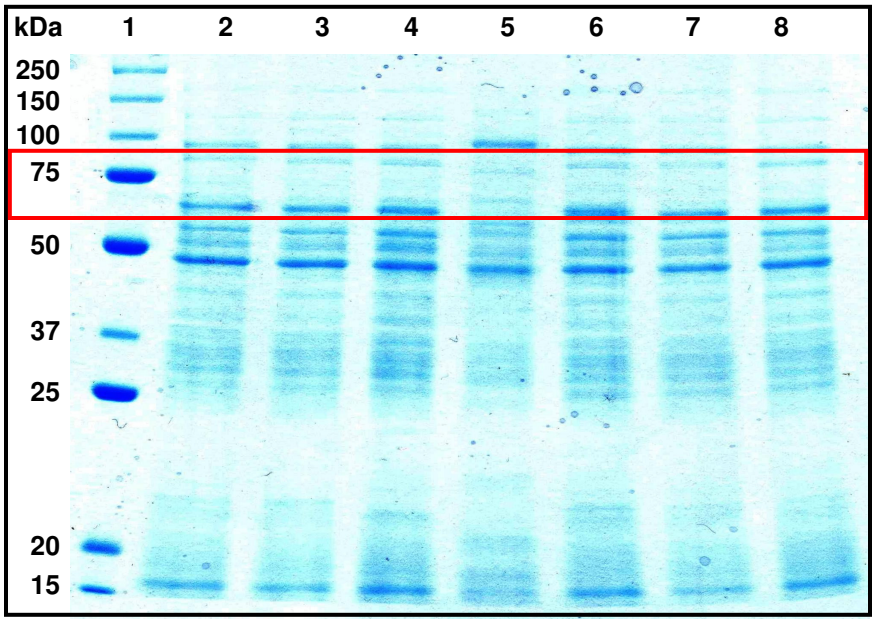

Figure 4.9: Expression of the ABC transporter, peptide-binding protein of ± 70 kDa. Lane 1 represents the Precision Plus Protein™ Standard. Lanes 2 and 6 are the negative controls of pWUR and pMK184 respectively. Lanes 3 – 5 are the expressed clone 10 (Construct 1); clone 2 (Construct 2) and clone 7 (Construct 3) in pWUR respectively. Lanes 7 and 8 are the expressed clone 4 (Construct 2) and clone 4 (Construct 3) in pMK184 respectively.

4.3.6 Purification of the ABC Transporter, Peptide-Binding Protein

4.3.6.1 Expression in pWUR and pMK184

After fractionation, as described in section 3.2.13, the soluble fractions for expression in pWUR and pMK184 were used for purification purposes, using a 5 ml Nickel NTA (HisTrapFF) column (Amersham Biosciences), as described in section 3.2.14.2. An elution profile was obtained for each clone (Figure 4.10) and used to select fractions for SDS-PAGE analysis (Figure 4.11 and Figure 4.12) and Western blot analysis (Figure 4.13), as described in section 4.2.15.1.

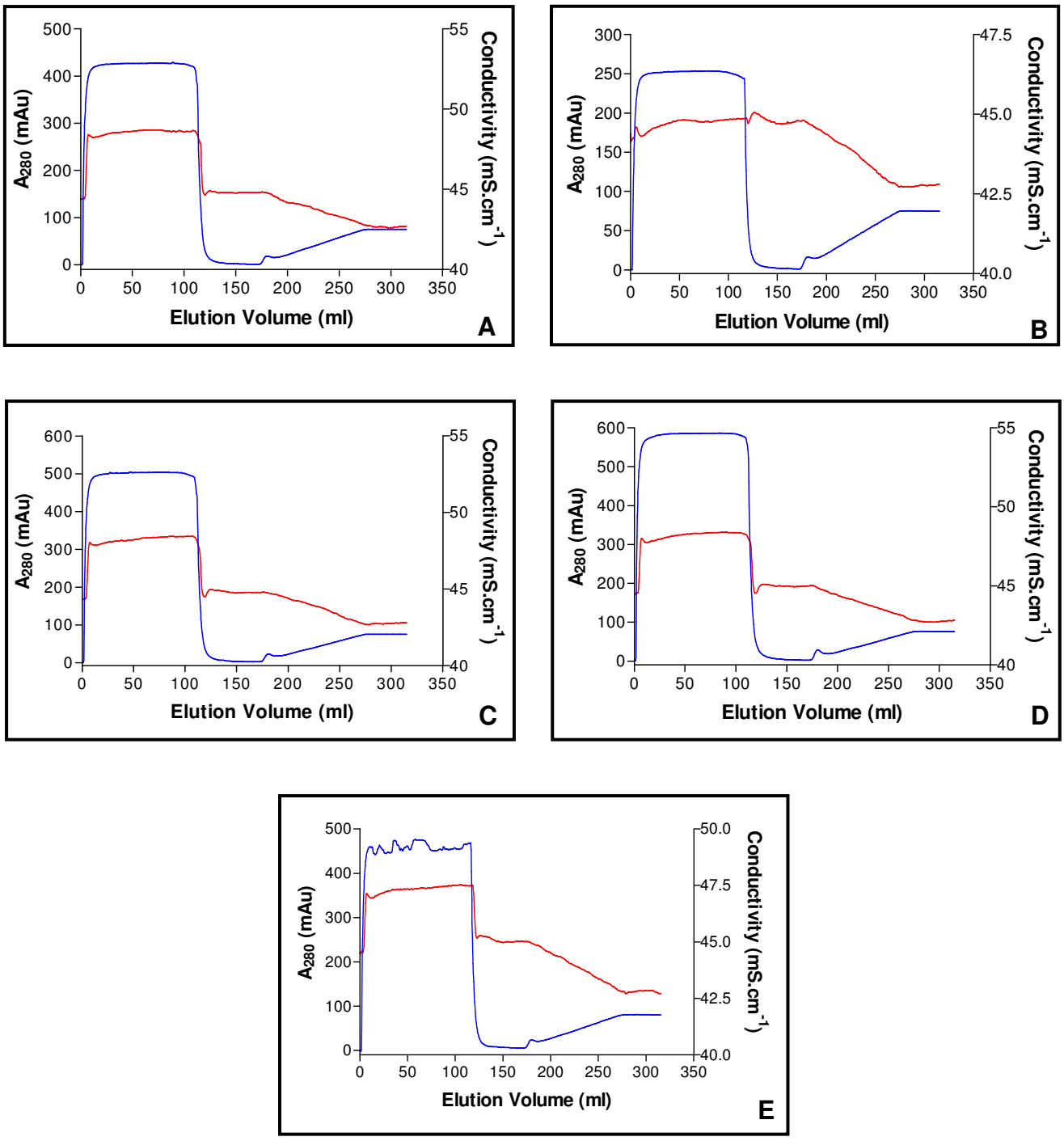

Figure 4.10: Elution profiles obtained after purification with the Nickel NTA (HisTrapFF) column, showing the protein eluted between ± 170 and 200 ml [A_{280} (▬); Conductivity (▬)]. (A) Clone 10 (Construct 1) in pWUR. (B) Clone 2 (Construct 2) in pWUR. (C) Clone 7 (Construct 3) in pWUR. (D) Clone 4 (Construct 2) in pMK184. (E) Clone 4 (Construct 3) in pMK184.

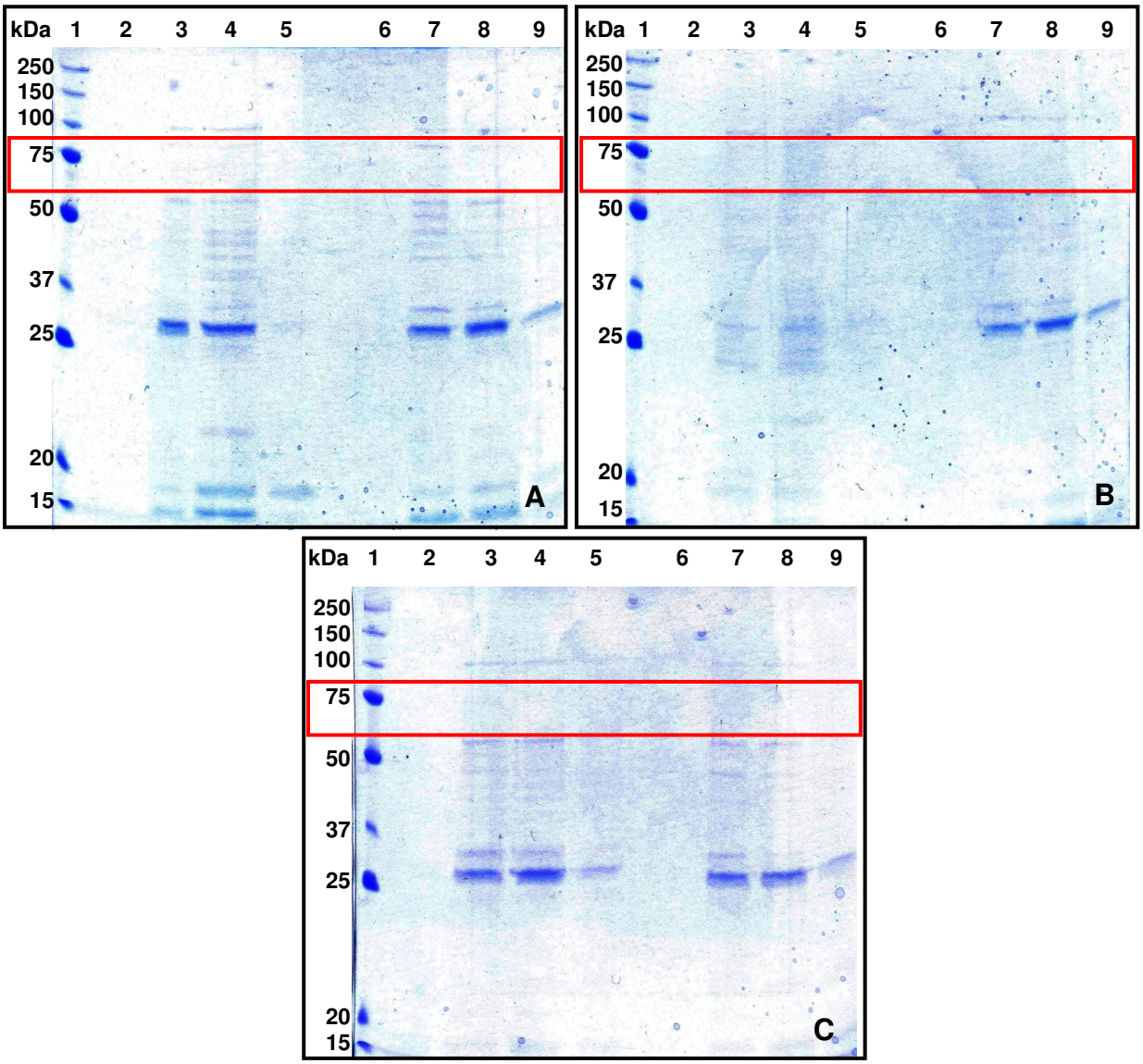

Figure 4.11: SDS-PAGE with Coomassie blue staining, for the fractions selected from the elution profile to determine which fractions contained the ± 70 kDa protein. (A) The Precision Plus Protein™ Standard (Lane 1); pWUR negative control (Lanes 2 – 5) and Clone 10 (Construct 1) in pWUR (Lanes 6 – 9). (B) The Precision Plus Protein™ Standard (Lane 1); Clone 2 (Construct 2) in pWUR (Lanes 2 – 5) and Clone 7 (Construct 3) in pWUR (Lanes 6 – 9). (C) The Precision Plus Protein™ Standard (Lane 1); Clone 4 (Construct 2) in pMK184 (Lanes 2 – 5) and Clone 4 (Construct 3) in pMK184 (Lanes 6 – 9).

After staining of the SDS-gels with Coomassie blue, the purified protein of ± 70 kDa in size could not be detected for all the clones and Silver staining was done on the gels; however the purified protein could still only be detected in extremely low levels. The

protein was detected in Clone 10 (Construct 1) in pWUR (Figure 4.12A; Lanes 6 – 9), Clone 7 (Construct 3) in pWUR (Figure 4.12 B; Lanes 6 – 9) and Clone 4 (Construct 3) in pMK184 (Figure 4.12C; Lanes 6 – 9). This is due to the low levels achieved with the expression.

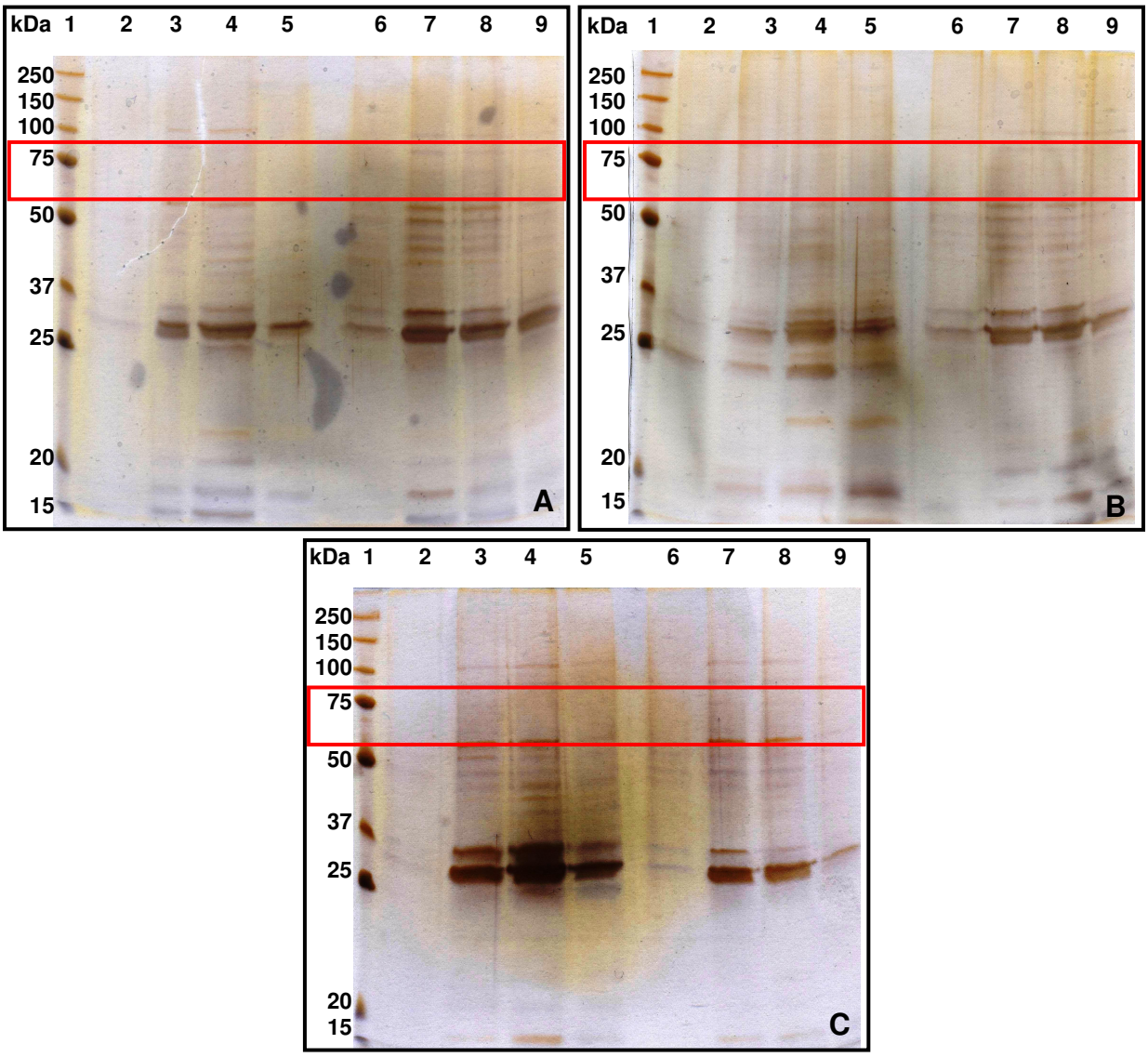

Figure 4.12: SDS-PAGE with Silver staining, for the fractions selected from the elution profile to determine which fractions contained the ± 70 kDa protein. (A) The Precision Plus Protein™ Standard (Lane 1); pWUR negative control (Lanes 2 – 5) and Clone 10 (Construct 1) in pWUR (Lanes 6 – 9). (B) The Precision Plus Protein™ Standard (Lane 1); Clone 2 (Construct 2) in pWUR (Lanes 2 – 5) and Clone 7 (Construct 3) in pWUR (Lanes 6 – 9). (C) The Precision Plus Protein™ Standard (Lane 1); Clone 4 (Construct 2) in pMK184 (Lanes 2 – 5) and Clone 4 (Construct 3) in pMK184 (Lanes 6 – 9).

Western blot analysis with His-Tag detection was performed on Clone 2 (Construct 2) in pWUR and Clone 4 (Construct 2) in pMK184 to confirm the presence of the expressed protein (Figure 4.13).

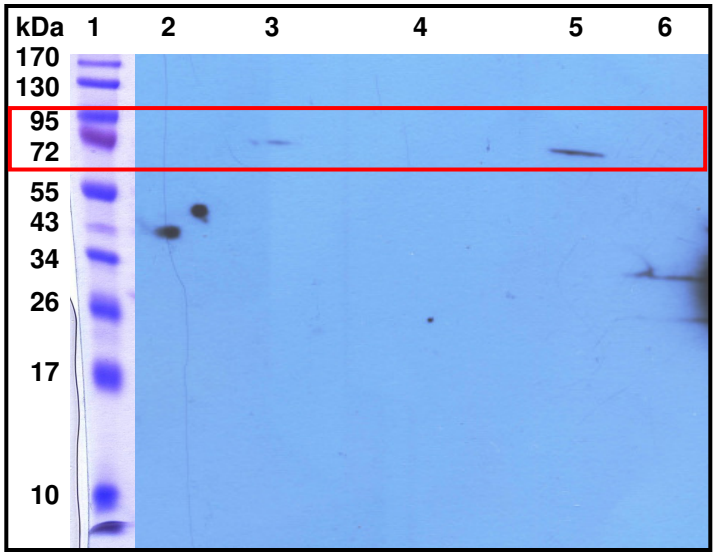

Figure 4.13: Western blot with His-Tag detection, confirming the presence of the protein of ± 70 kDa, for Clone 2 (Construct 2) in pWUR and Clone 4 (Construct 2) in pMK184 (Lanes 3 and 5 respectively). The PageRuler™ Prestained Protein Ladder can be seen in lane 1, the pWUR negative control in lane 4 and a positive control of ± 40 kDa in lane 2.

Fractions that contained the protein of expected size (± 70 kDa) were pooled and dialysed overnight with 20 mM phosphate buffer (pH 7.4) to remove the imidazole. Activity was assessed at 65ºC and 85ºC on combined fractions (Figure 4.14) to determine if the protein was capable of gold reduction, using the gold reduction assay as described in section 4.2.15.3. Enhanced activity was detected at 85ºC that, in accordance with thermodynamic principles, applies only if the proteins are thermostable. This suggested that the thermostable protein expressed in a thermophilic host is more active at higher temperatures, in comparison to the protein expressed in a mesophilic host, as described in chapter 3.

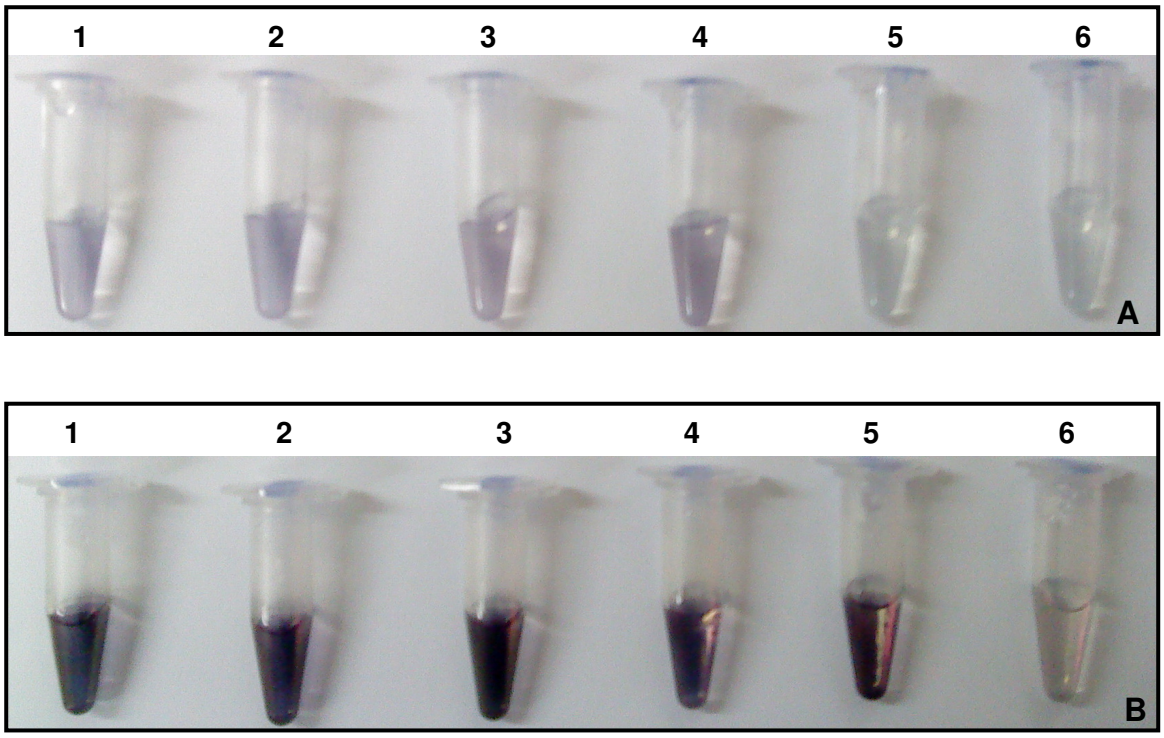

Figure 4.14: Activity determinations done at (A) 65ºC and (B) 85ºC, with tube 6 representing the blank reaction, containing no protein and showing no activity and tubes 1 – 5 are the pooled fractions for Clone 10 (Construct 1) in pWUR; Clone 2 (Construct 2) in pWUR; Clone 7 (Construct 3) in pWUR; Clone 4 (Construct 2) in pMK184 and Clone 4 (Construct 3) in pMK184, respectively, showing a pink/purple colour, which proved that the protein has gold reduction activity.

Purified proteins, containing a C-terminal and/or an N-terminal His-Tag and either included or excluded the leader peptide, were used for downstream experiments.

4.3.7 Characterization of the ABC Transporter, Peptide-Binding Protein in *Thermus thermophilus* HB27

The results revealed no specific differences between the five different constructs, expressed in either pWUR or pMK184, containing a C-terminal and/or an N-terminal His-Tag and either including or excluding the leader peptide. If there are differences, these will be highlighted. This again indicated that the His-Tag and the leader peptide had no influence on the gold reduction and nanoparticle formation process and only results for Clone 10 (Construct 1) in pWUR will be shown here as a representation. Furthermore, only results that had shown significant differences will be discussed.

In all characterization steps, the protein mediated reduction and nanoparticle formation reactions were done, using protein at a starting concentration of 100 $\mu g.ml^{-1}$, except for when the effect of protein concentrations on gold reduction and nanoparticle formation were tested. All protein concentrations were determined with the Micro BCA™ Protein Assay Kit (PIERCE), as described in section 3.2.15.2. A blank reaction was made for each parameter tested, containing additional buffer instead of the protein. This was done to compensate for chemical reduction that might occur and again demonstrated the differences in nanoparticle formations from the protein reactions, proving the significant role of the protein in the nanoparticle formation process. All gold reduction and nanoparticle formation experiments were done with the gold reduction assay, as described in section 3.2.15.3. In all the experiments, gold reduction and nanoparticle formation is displayed in figures and please note that protein reactions can be seen with an odd number and their respective blank reactions with an even number. The SPR band was recorded for all the samples from each parameter, to verify gold reduction and nanoparticle formation. This was done through UV-Vis wave scans in the range of 300-800 nm, as described in section 3.2.15.4. As described in section 3.3.7, samples subjected for TEM and EDX analysis, were selected simply based on the SPR obtained through UV-Vis spectra and visual observations in the colour obtained through the gold reduction assay, and was done as described in sections 3.2.15.5 and 3.2.15.6 respectively. Furthermore, the samples that were subjected for SAED analysis, as described in sections 3.2.15.6, were only tested for additional confirmation of elemental analysis and only a few samples for this analysis were randomly selected.

4.3.7.1 The Effect of the Assay Components (Sodium Dithionite and Methyl Viologen) on Gold Reduction and Nanoparticle Formation

The effect of sodium dithionite and methyl viologen on gold reduction and nanoparticle formation was tested using three different ways at 65ºC and 85ºC. Either both components were present simultaneously in the reaction (Tubes 1 – 4), or only sodium dithionite (Tubes 5 – 8) or only methyl viologen (Tubes 9 – 12). This was done to determine the influence of these assay components on the gold reduction and nanoparticle formation process. When comparing the reactions through the visual assay (Figure 4.15) and the SPR, obtained through UV-Vis spectra (Figure 4.16), nanoparticle

formation was obtained in all three reactions with no real differences between them. This can be seen due to a change in the absorbance around 540 – 570 nm in the protein reactions (Figure 4.16A) with no change in the respective blank reactions (Figure 4.16B). Clear differences in the blank reactions could be detected and overall enhanced activity was obtained at 85ºC and SPR and TEM were thus performed on particles obtained at only 85ºC.

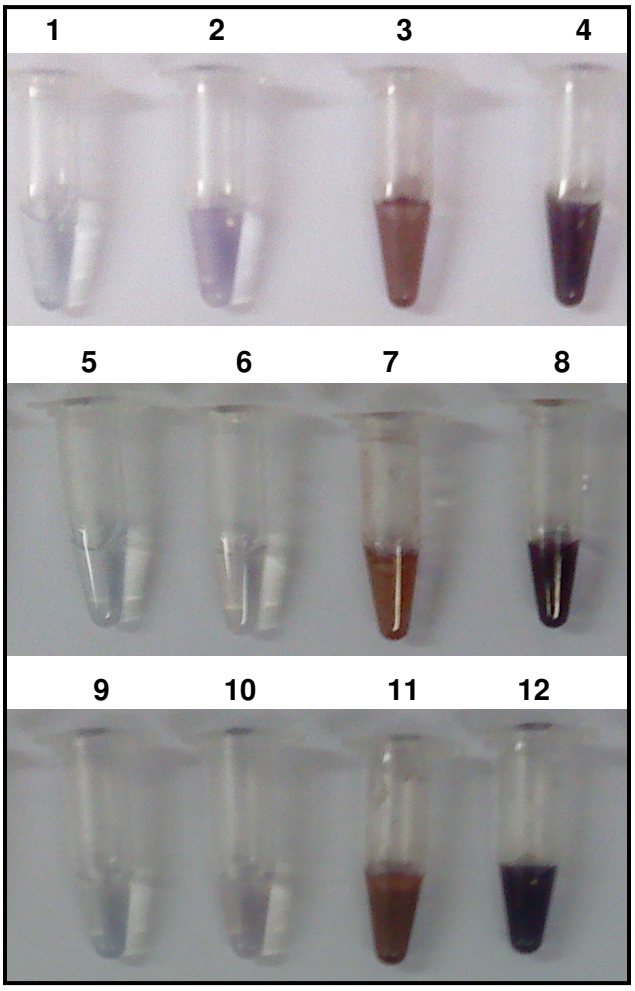

Figure 4.15: The different colours obtained through the gold reduction assay with or without sodium dithionite and methyl viologen, indicating gold nanoparticle formation at 65ºC and 85ºC. The odd numbers (1 and 3; 5 and 6; 9 and 10) indicate protein reactions for both components, only dithionite and only methyl viologen respectively and the even numbers (2 and 4; 6 and 8; 10 and 12) the corresponding blank reactions.

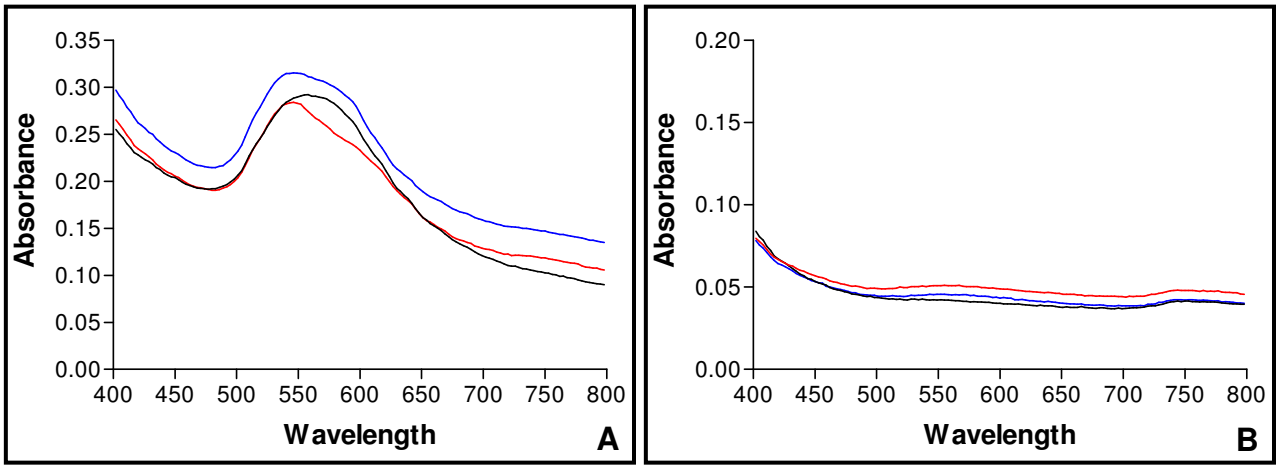

Figure 4.16: UV-Vis absorption spectra of the surface plasmon resonance recorded for with or without sodium dithionite and methyl viologen at 85ºC, indicating gold nanoparticle production through a change in the absorbance around 540 - 570 nm. (A) The protein reactions and (B) the corresponding blank reactions. [Sodium dithionite and methyl viologen ( ); Sodium dithionite ( ); Methyl viologen ( )].

When compared with the results for the expression in *E. coli* (Sections 3.3.7.1 and 3.3.7.2), similar results were obtained, indicating that no matter how the protein was expressed, methyl viologen was not needed and only results in chemical reduction. Whereas sodium dithionite is needed in the reaction for the protein, to play a role in the gold reduction and nanoparticle formation process.

The TEM micrographs (Figure 4.17) confirmed that particles were formed with all three reactions and that all the particles are in the nano size range but not monodispersed. Nanoparticles formed in the presence of only methyl viologen were slightly less, but other than the amount of particles, no real differences were obtained between the three reactions. SAED was performed on the nanoparticles with sodium dithionite and methyl viologen present and EDX was done on all the samples and nanoparticles were confirmed to be gold, as can be seen in figure 4.17B and figure 4.18 respectively. In figure 4.17B the micro-diffraction pattern for gold can be seen.

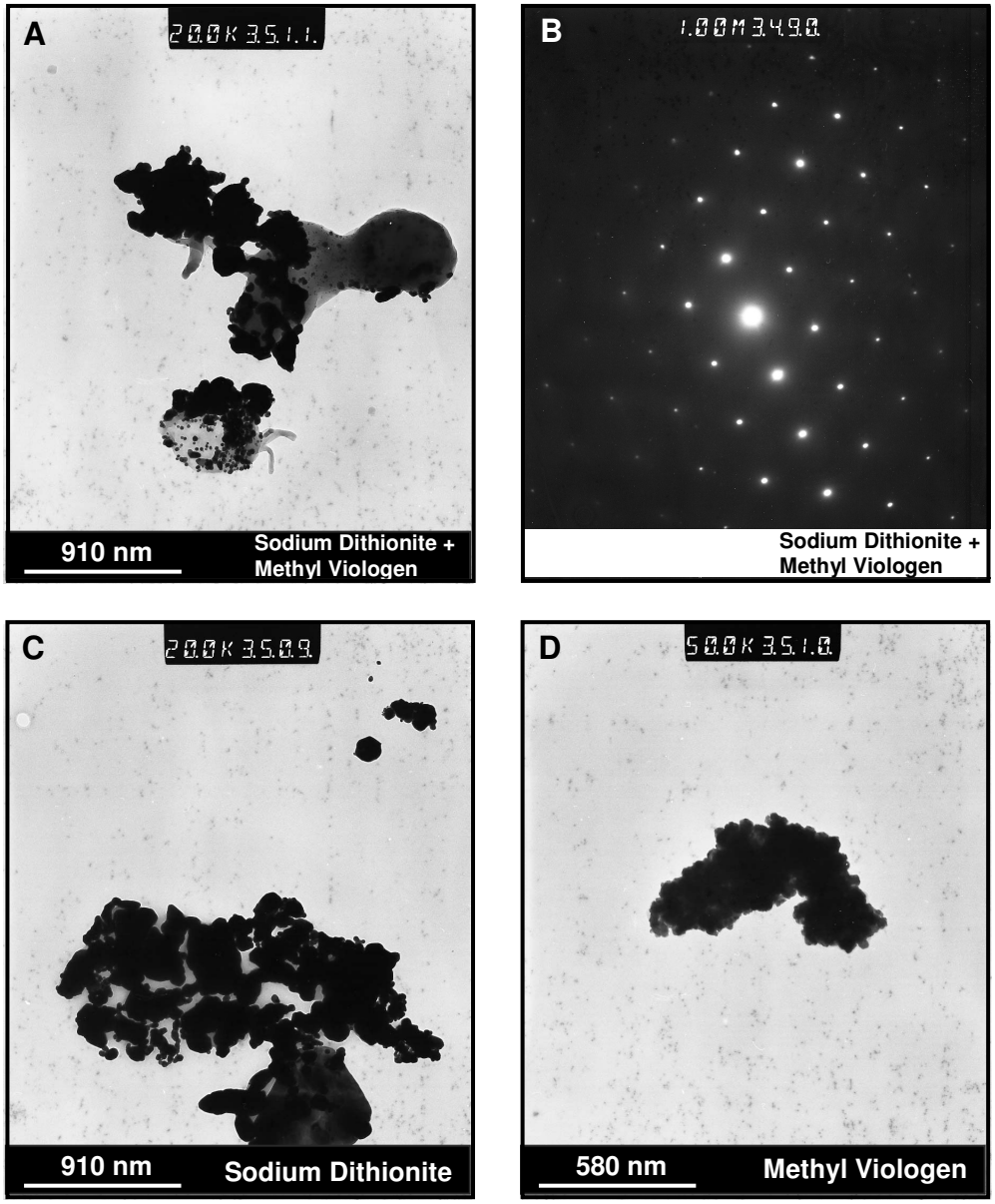

Figure 4.17: (A, C and D) TEM micrographs for the different assay components at 85ºC, indicating the shapes, sizes and amounts of gold nanoparticles obtained with (B) corresponding selected-area electron micro-diffraction pattern for sodium dithionite and methyl viologen. Scale bars in A, C and D are equal to 910 nm; 910 nm and 580 nm respectively.

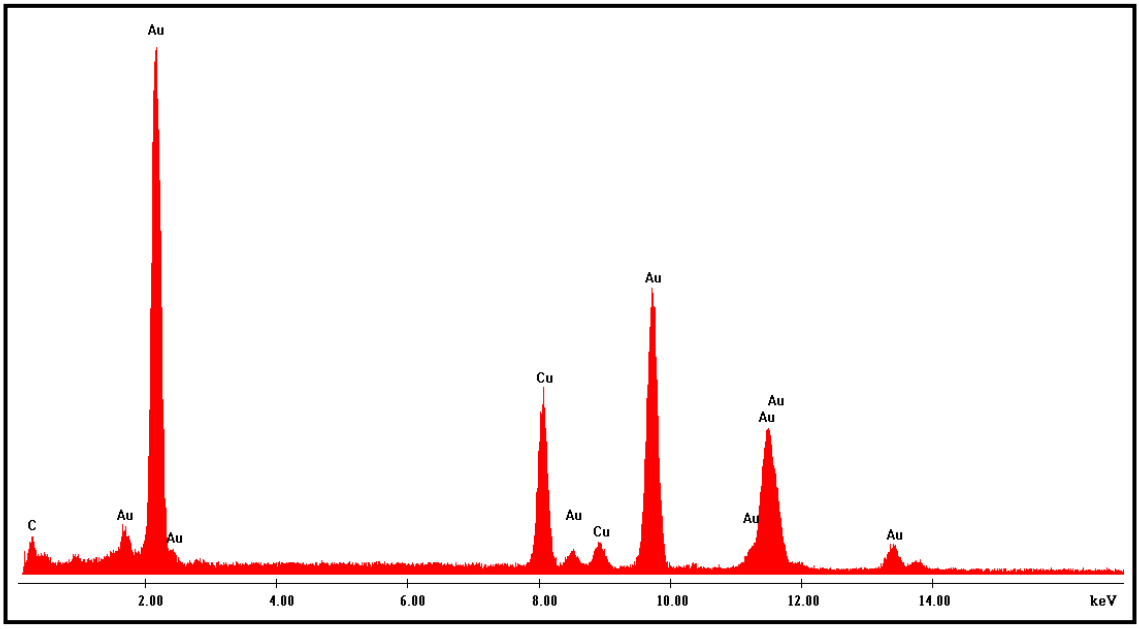

Figure 4.18: EDX spectrum recorded for the nanoparticles produced with the different assay components at 85ºC, showing a typical pattern for all the samples and indicates that the nanoparticles are gold.

From this, it can be concluded that methyl viologen had no effect on gold reduction and nanoparticle formation and is thus not needed in the gold reduction assay, since nanoparticles were obtained in the absence of methyl viologen and in the presence of sodium dithionite alone. The mechanism for methyl viologen and sodium dithionite on gold reduction can be seen in section 3.3.7.1.

4.3.7.2 The Effect of Denatured Protein on Gold Reduction and Nanoparticle Formation

The effect of denatured protein on gold reduction and nanoparticle formation was tested with protein that was boiled for 3 hours to become denatured and inactive and sodium dithionite, dithiothreitol (DTT) and β-mercaptoethanol were used as electron donors and reducing agents respectively. When comparing the reactions through the visual assay (Figure 4.19) and the SPR, obtained through UV-Vis spectra (Figure 4.20), insignificant changes were observed with all three components, indicating that in comparison with the activity obtained in section 4.3.7.6 where folded protein was used, gold reduction and nanoparticle formation was not very effective when the protein is not active. This can be

seen through the absence of any changes in the absorbance around 540 – 560 nm in the protein reactions (Figure 4.20A) and in the respective blank reactions (Figure 4.20B). The slight change in colour is due to chemical reduction and again proves that the protein has to be present in an active form and the disulphide bond should be reduced for nanoparticle formation to take place. Clear differences in the blank reactions could be detected and overall enhanced activity was again obtained at 85ºC, therefore SPR was performed on 85ºC only.

When comparing the results obtained in this section with those from section 4.3.7.6, a clear difference was obtained. This again indicate that the presence of the folded protein play a significant role in gold reduction and nanoparticle formation, yielding a level of control over the rate of the process and (as discussed before in sections 1.6 and 3.3.7.1), the rate of particle formation can also influence the type of particle formed.

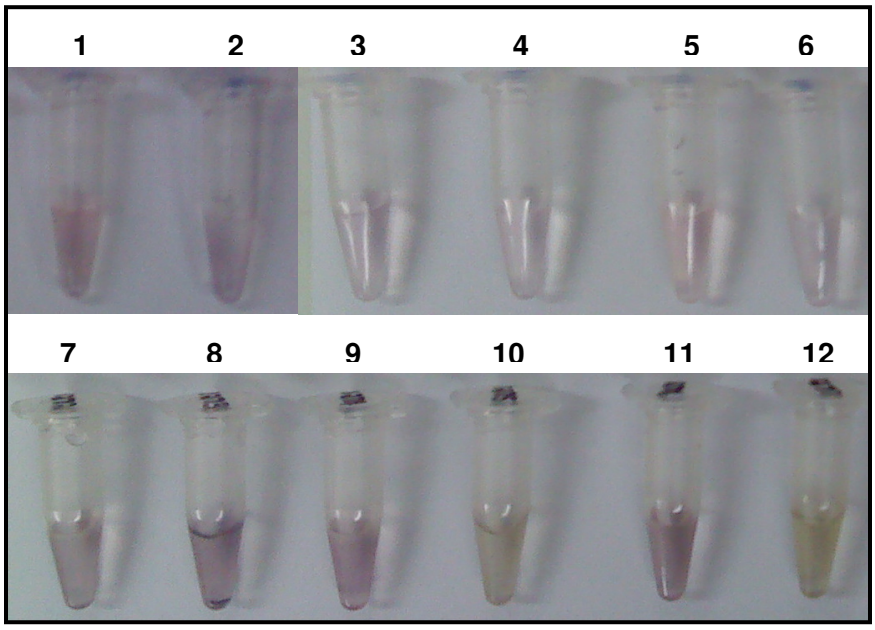

Figure 4.19: The different colours obtained through the gold reduction assay with denatured protein and various electron donors, indicating gold nanoparticle formation for 65ºC (1 – 6) and 85ºC (7 – 12). The odd numbers (1 – 5 and 7 - 11) indicate protein reactions for sodium dithionite; dithiothreitol and β-mercaptoethanol respectively and the even numbers (2 – 6 and 8 - 12) the corresponding blank reactions.

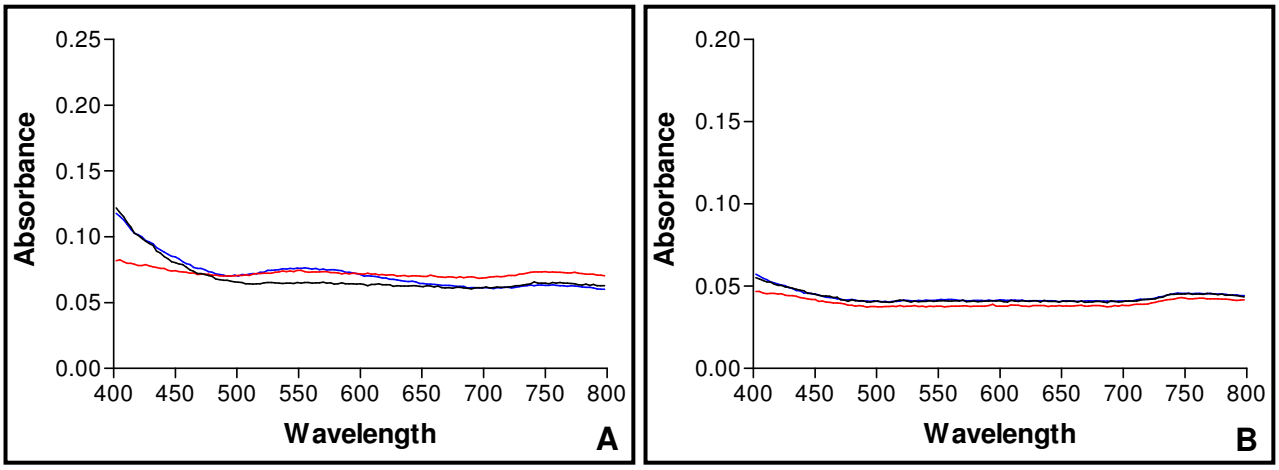

Figure 4.20: UV-Vis absorption spectra of the surface plasmon resonance recorded for the denatured protein and various electron donors at 85ºC, indicating insignificant nanoparticle production through no change in the absorbance around 540 - 560 nm. (A) The protein reactions and (B) the corresponding blank reactions. [Sodium dithionite ( ); Dithiothreitol ( ); β-mercaptoethanol ( )].

Similar results were obtained with protein expressed in a mesophilic host (Section 3.3.7.4); therefore TEM analysis was not performed on these samples.

4.3.7.3 The Effect of $HAuCl_4$ Concentrations on Gold Reduction and Nanoparticle Formation

The effect of gold(III) concentrations on gold reduction and nanoparticle formation was tested at 0 mM; 0.5 mM; 1.0 mM; 2.0 mM; 5.0 mM; 7.5 mM and 10 mM final concentrations of $HAuCl_4$ respectively, to determine the optimum gold(III) concentration for nanoparticle formation with the best defined shapes. This was done at both 65ºC and 85ºC. When comparing the reactions through the visual assay (Figure 4.21) and the SPR, obtained through UV-Vis spectra (Figure 4.22), optimum nanoparticle formation took place from 0.5 mM to 2 mM (Tubes 3 – 8 and 17 - 23). Nanoparticle formations can be seen through a change in the absorbance around 540 – 550 nm in the protein reactions (Figure 4.22A) with no change in the respective blank reactions (Figure 4.22B). At 0 mM (Tubes 1 and 15) no reaction took place, again indicating no interference by any of the assay components that could have influenced nanoparticle formations. At 5.0 mM to 10 mM (Tubes 9 – 14 and 23 - 28), big particles were expected which are most

likely not in the nano size range, due to the gold colours obtained and they contained particles that had already precipitated out of solution. Clear differences in the blank reactions could be detected. Overall enhanced activity was obtained at 85ºC and SPR and TEM were thus performed on particles obtained at only 85ºC.

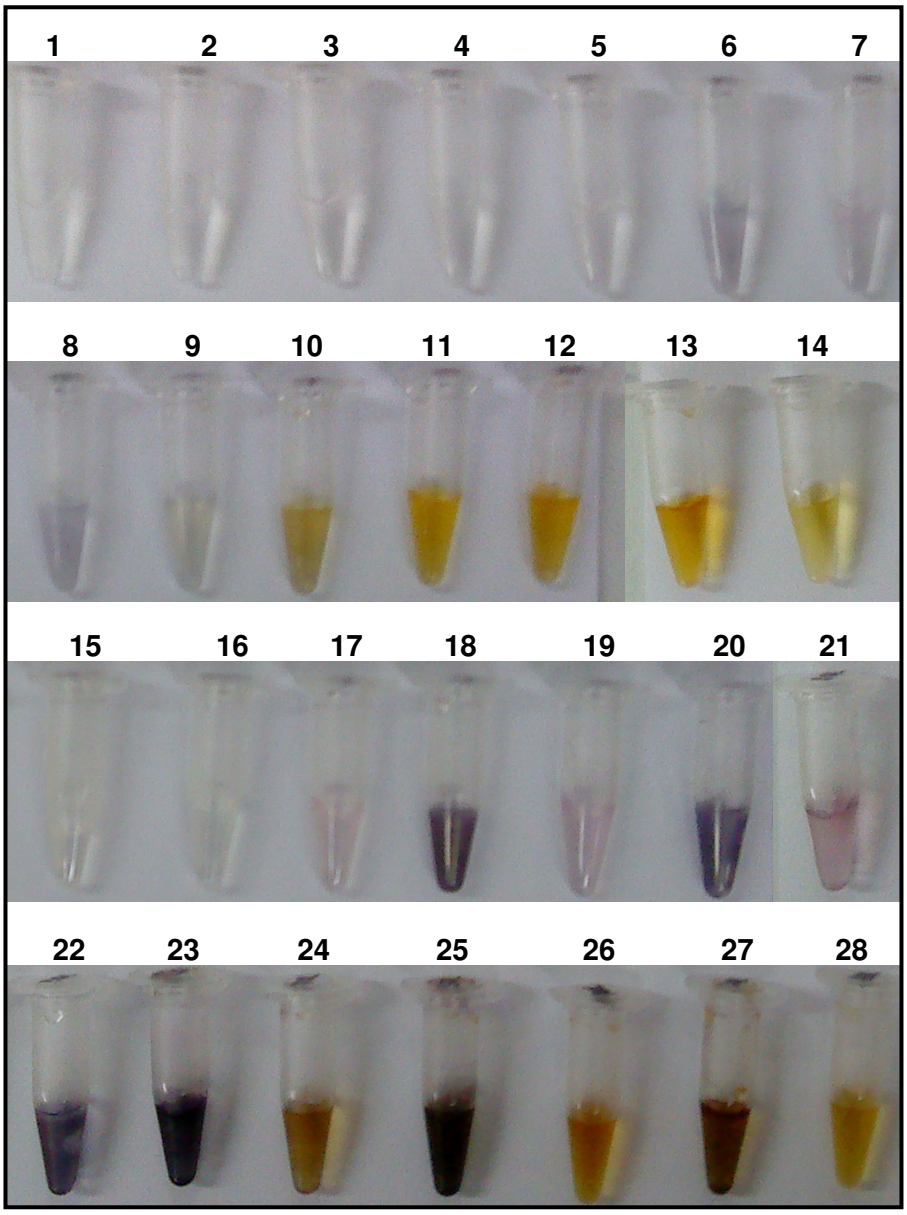

Figure 4.21: The different colours obtained through the gold reduction assay at varying $HAuCl_4$ concentrations, indicating gold nanoparticle formation for 65ºC (1 – 14) and 85ºC (15 – 28) respectively. The odd numbers (1 – 13 and 15 - 27) indicate protein reactions for 0 mM; 0.5 mM; 1.0 mM; 2.0 mM; 5.0 mM; 7.5 mM and 10 mM respectively and the even numbers (2 – 14 and 16 - 28) the corresponding blank reactions.

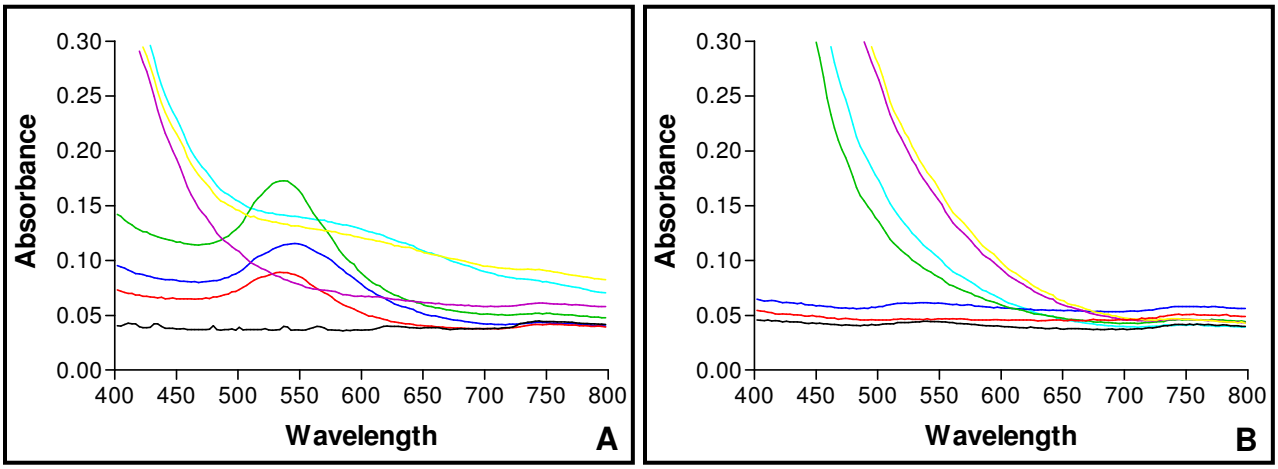

Figure 4.22: UV-Vis absorption spectra of the surface plasmon resonance recorded for the different $HAuCl_4$ concentrations at 85ºC, indicating gold nanoparticle production through a change in the absorbance around 540 - 550 nm. (A) The protein reactions and (B) the corresponding blank reactions. [0 mM ( ); 0.5 mM ( ); 1.0 mM ( ); 2.0 mM ( ); 5.0 mM ( ); 7.5 mM ( ); 10 mM ( )].

When compared with the results for the expression in *E. coli* (Section 3.3.7.6), similar results were obtained, indicating that no matter how the protein was expressed, if the gold concentration is too high and the protein aids not only in gold reduction but also nanoparticle formation, it might be a plausible explanation for the differences in the stoichiometry, therefore leading to uncontrolled particle formation at higher concentrations.

The TEM micrographs (Figure 4.23) confirmed that gold nanoparticles were formed at gold concentrations of 0.5 mM – 2.0 mM, but no observable differences were obtained using similar gold concentrations together with the protein expressed in a mesophilic host (Section 3.3.7.6). SAED (Figure 4.23D) was performed on the 2.0 mM and EDX (Figure 4.24) was done on all the samples, confirming that the nanoparticles were gold. In figure 4.23D the ring pattern for gold can be seen.

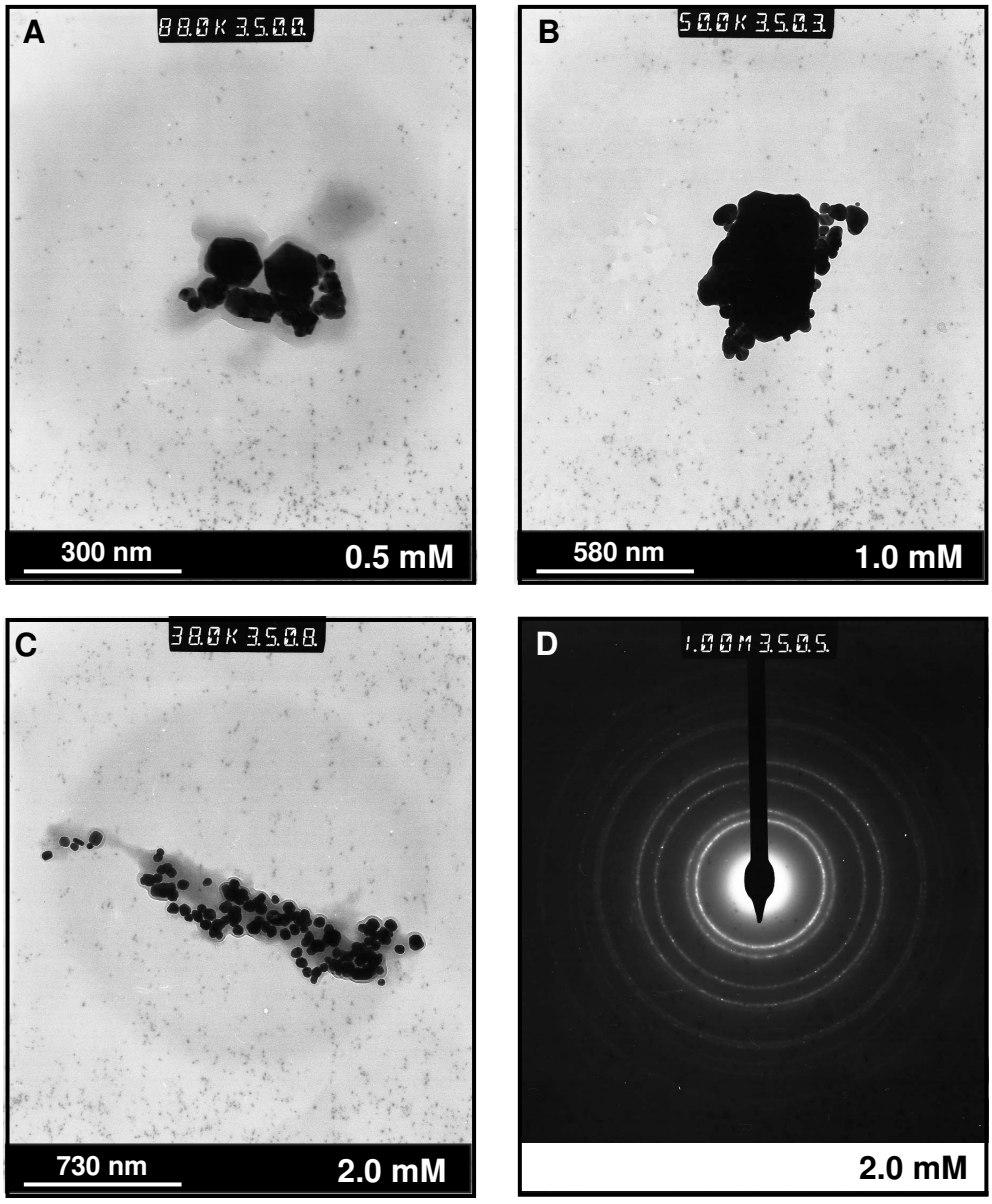

Figure 4.23: (A, B and C) TEM micrographs for the different $HAuCl_4$ concentrations at 85ºC, indicating the shapes, sizes and amounts of gold nanoparticles obtained with (D) corresponding selected-area electron ring pattern for 2.0 mM. Scale bars in A, B and C are equal to 300 nm; 580 nm and 730 nm respectively.

From this it can be concluded that expression in a thermophilic host had no influence on the nanoparticles obtained with different gold(III) concentrations.

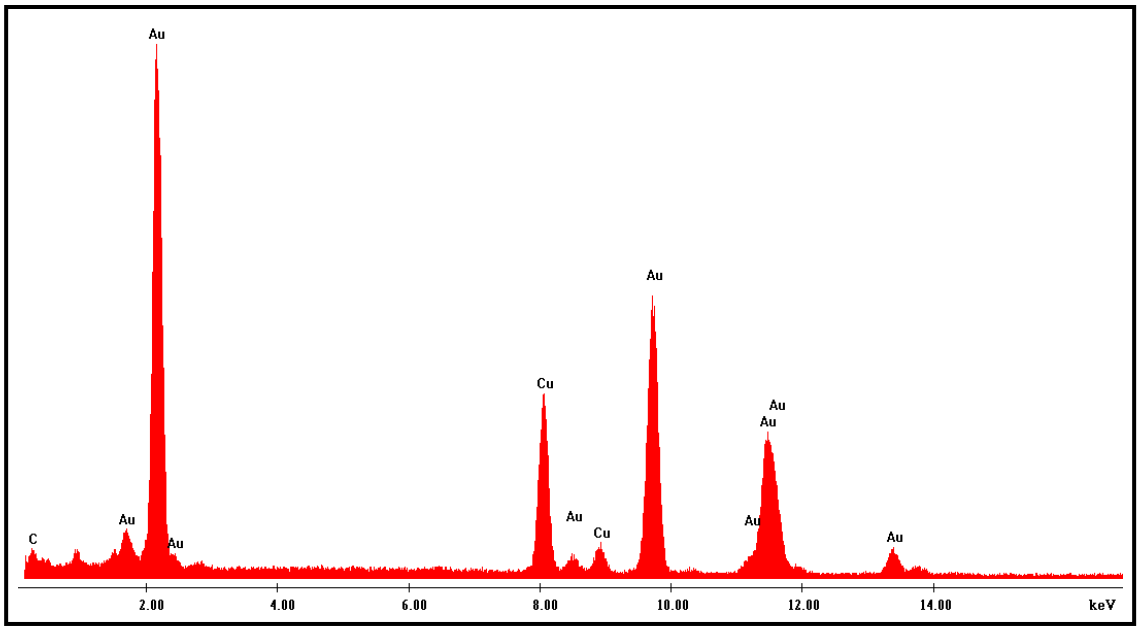

Figure 4.24: EDX spectrum recorded for the nanoparticles produced at different $HAuCl_4$ concentrations at 85ºC, showing a typical pattern for all the samples and indicates that the nanoparticles are gold.

4.3.7.4 The Effect of Temperature on Gold Reduction and Nanoparticle Formation

The effect of temperature on gold reduction and nanoparticle formation was tested through incubation at 30ºC; 37ºC; 42ºC; 55ºC; 65ºC and 85ºC respectively, to determine the optimum temperature for nanoparticle formation with the best defined shapes. When comparing the reactions through the visual assay (Figure 4.25) and the SPR, obtained through UV-Vis spectra (Figure 4.26), effective nanoparticle formation occurred at only 65ºC and 85ºC (Tubes 9 - 12) with optimum formation at 85ºC (Tubes 11 and 12). Nanoparticle formations can be seen through a change in the absorbance around 540 – 560 nm in the protein reactions (Figure 4.26A) with no change in the respective blank reactions (Figure 4.26B). High levels of chemical reduction were obtained with the blank reaction of 85ºC, but with a clear difference in its corresponding protein reaction and no change in the absorbance were detected, again indicating purely chemical reduction and no nanoparticle formation and proving the significant role played by the protein in slowing down the reaction rate. At 30ºC – 42ºC (Tubes 1 – 6), no differences were obtained, indicating that nanoparticle formation was very slow and not very effective, if any at all. At 55ºC (Tubes 7 and 8), a small change was observed with a low absorbance value, indicating insignificant nanoparticle formation.

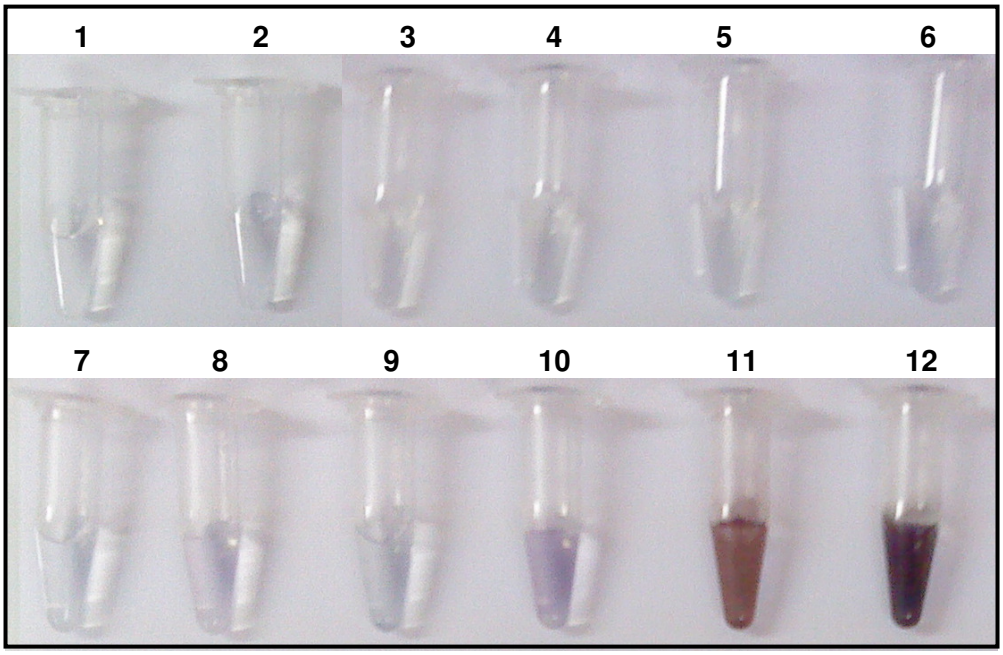

Figure 4.25: The different colours obtained through the gold reduction assay at varying temperatures, indicating gold nanoparticle formation. The odd numbers (1 – 11) indicate protein reactions for 30ºC; 37ºC; 42ºC; 55ºC; 65ºC and 85ºC respectively and the even numbers (2 – 12) the corresponding blank reactions.

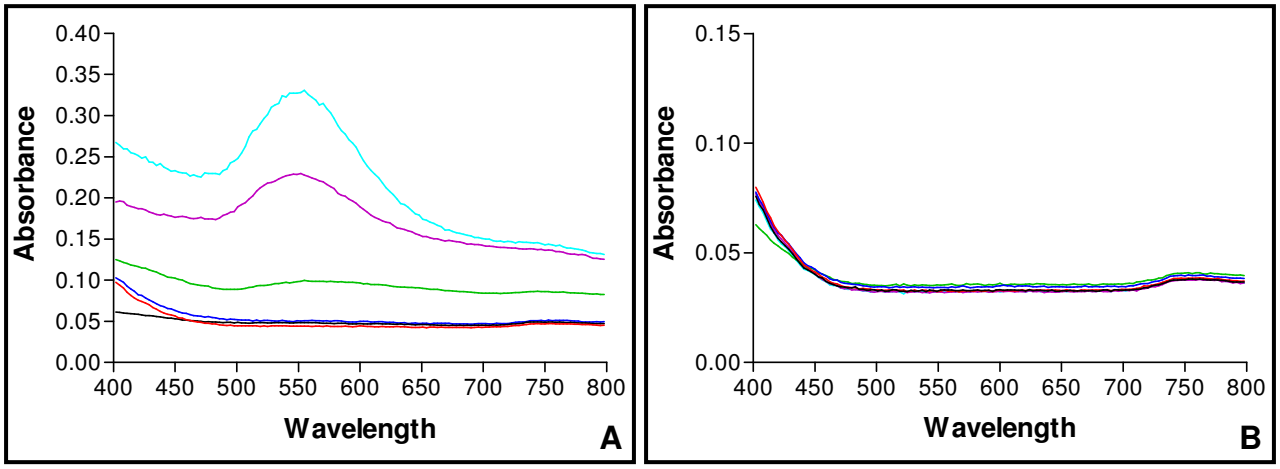

Figure 4.26: UV-Vis absorption spectra of the surface plasmon resonance recorded for the different temperatures, indicating gold nanoparticle production through a change in the absorbance around 540 - 560 nm. (A) The protein reactions and (B) the corresponding blank reactions. [30ºC ( ); 37ºC ( ); 42ºC ( ); 55ºC ( ); 65ºC ( ); 85ºC ( )].

The TEM micrographs (Figures 4.27A and C) confirmed that particles were formed at 65ºC and 85ºC, and that all the particles are in the nano size range, but not monodispersed. The particles obtained were mostly hexagon, elongated hexagon and rod like shapes. SAED and EDX was performed on the nanoparticles from 65ºC and 85ºC and the nanoparticles were confirmed to be gold, as can be seen in figures 4.27B and D and figure 4.28 respectively. In figure 4.27B the micro-diffraction pattern for gold can be seen in and figure 4.27D, the ring pattern for gold. In all the figures with EDX spectra from here onwards, the carbon and copper detected in the samples is due to the TEM grids, since analysis was done on Formvar carbon-coated 200-mesh copper grids (Section 3.2.15.5).

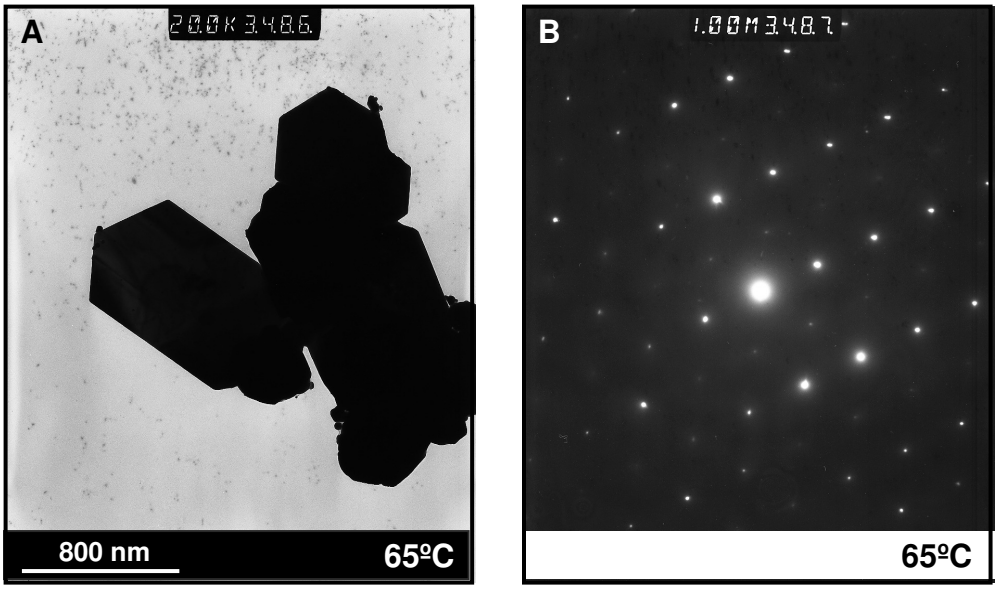

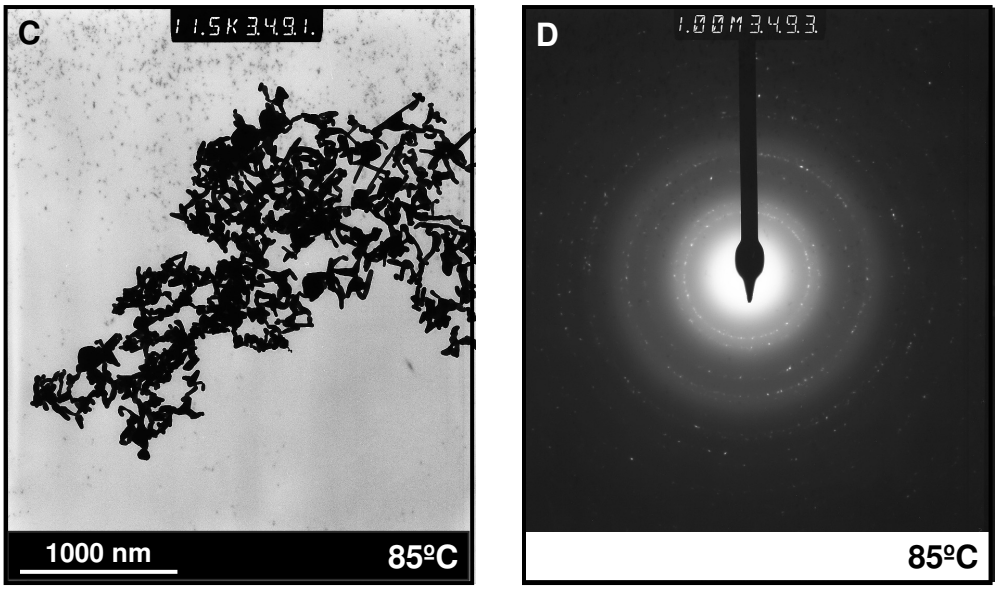

Figure 4.27: (A and C) TEM micrographs for gold nanoparticles with (B and D) corresponding selected-area electron micro-diffraction and ring pattern for 65ºC and 85ºC respectively, indicating the shapes, sizes and amounts of gold nanoparticles obtained. Scale bars in A and C are equal to 800 nm and 1000 nm respectively.

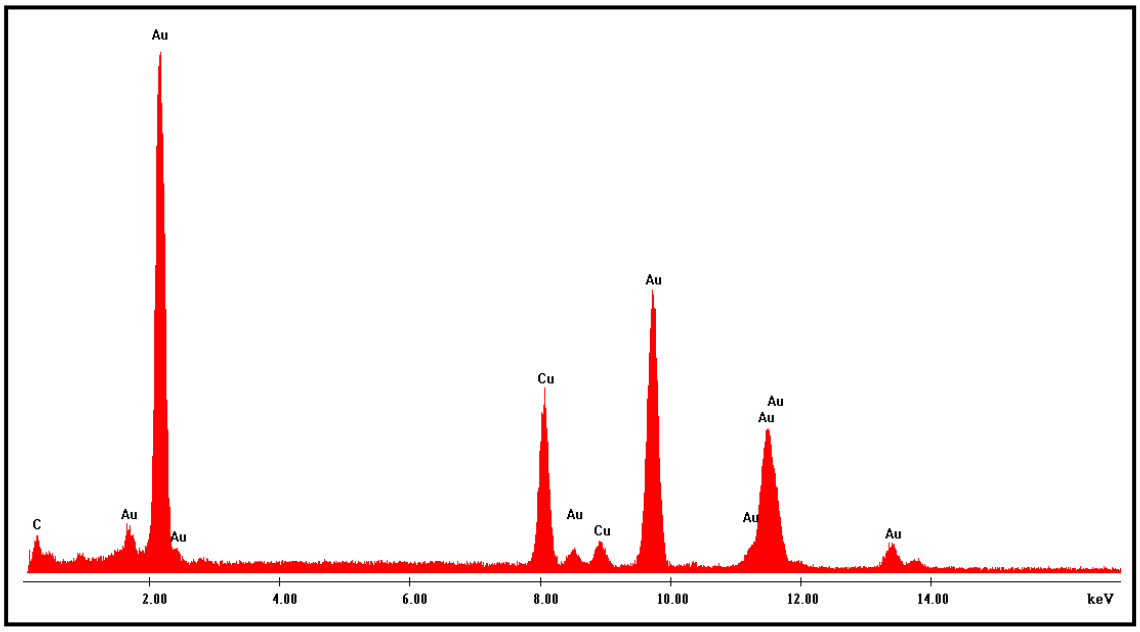

Figure 4.28: EDX spectrum recorded for the nanoparticles produced at 65ºC and 85ºC, showing a typical pattern for all the samples and indicates that the nanoparticles are gold.

From this it can be concluded that enhanced activity was detected at higher temperatures which concurs with the thermodynamic principles for thermostable proteins as discussed in section 4.3.6. This confirms that the thermostable protein expressed in a thermophilic host is more active at higher temperatures with optimum nanoparticle formation at 85ºC, in comparison to the protein expressed in a mesophilic host, with optimum nanoparticle formation at 65ºC (Section 3.3.7.7). As discussed in section 4.1, Bruins *et al.*, (2001); Hidalgo *et al.*, (2004) and Moreno *et al.*, (2005) found that there are several drawbacks and limitations that prevent proteins to fold correctly. One of these drawbacks includes temperature and therefore it might be that the expression host have an influence on the protein folding, which in turn, can influence that activity of the protein; therefore the protein showed less activity at higher temperatures when expressed in a mesophilic host (Chapter 3).

4.3.7.5 The Effect of pH on Gold Reduction and Nanoparticle Formation

The effect of pH on gold reduction and nanoparticle formation was tested at pH values of 3.6; 5.5; 7.5 and 9.0 at both 65ºC and 85ºC respectively, to determine the optimum pH for nanoparticle formation with the best defined shapes. When comparing the reactions through the visual assay (Figure 4.29) and the SPR, obtained through UV-Vis spectra (Figure 4.30), nanoparticles were formed at all pH values, except pH 3.6 (Tubes 1, 2 and 9, 10), with optimum formation at pH 7.5 – 9.0 (Tubes 5 – 8 and 13 - 16). Nanoparticle formations can be seen through a change in the absorbance around 550 – 650 nm in the protein reactions (Figure 4.30A) with no change in the respective blank reactions (Figure 4.30B). At pH 3.6 a black precipitate was formed and together with an insignificant change detected in the absorbance, this indicated that particles formed were not anymore in the nano size range. At pH 5.5 (Tubes 3 and 11), nanoparticles were obtained indicated by a pink colour, but without a clear difference in the blank reaction (Tubes 4 and 12). pH 7.5 and 9.0 gave efficient nanoparticle formations, due to the pink, purple and blue colours and clear differences were obtained in the blank reactions. The blue colour for pH 9.0 at 85ºC (Tube 15), together with a shift in the wavelength, indicates bigger nanoparticles were formed. Overall enhanced activity was obtained at 85ºC and SPR and TEM were thus performed on particles obtained at only 85ºC.

When compared with the results for the expression in *E. coli* (Section 3.3.7.8), enhanced activity was obtained at pH 7.5 – 9.0, whereas in *E. coli*, pH 5.5 also had effective nanoparticle formation. This may be again due to the folding of the protein that differs with the expression host and influencing the activity of the protein, and therefore was more active at pH values closer to the pI of the protein (pI 9.54).

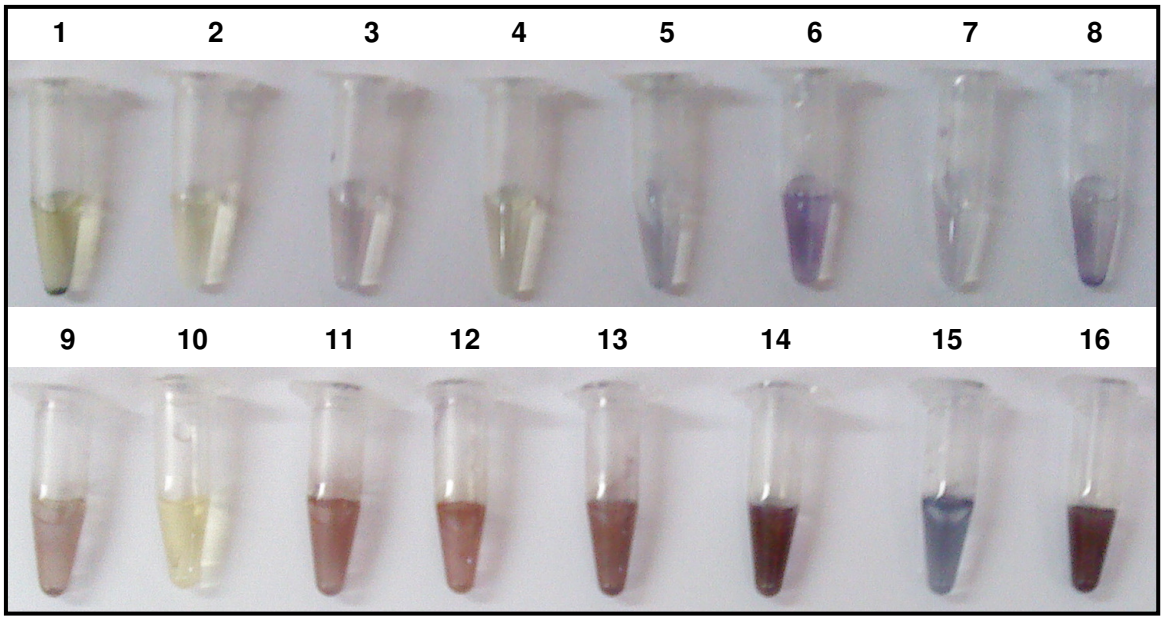

Figure 4.29: The different colours obtained through the gold reduction assay at varying protein concentrations, indicating gold nanoparticle formation for 65ºC (1 – 8) and 85ºC (9 – 16) respectively. The odd numbers (1 – 7 and 9 - 15) indicate protein reactions for pH 3.6; 5.5; 7.5 and 9.0 respectively and the even numbers (2 – 8 and 10 - 16) the corresponding blank reactions.

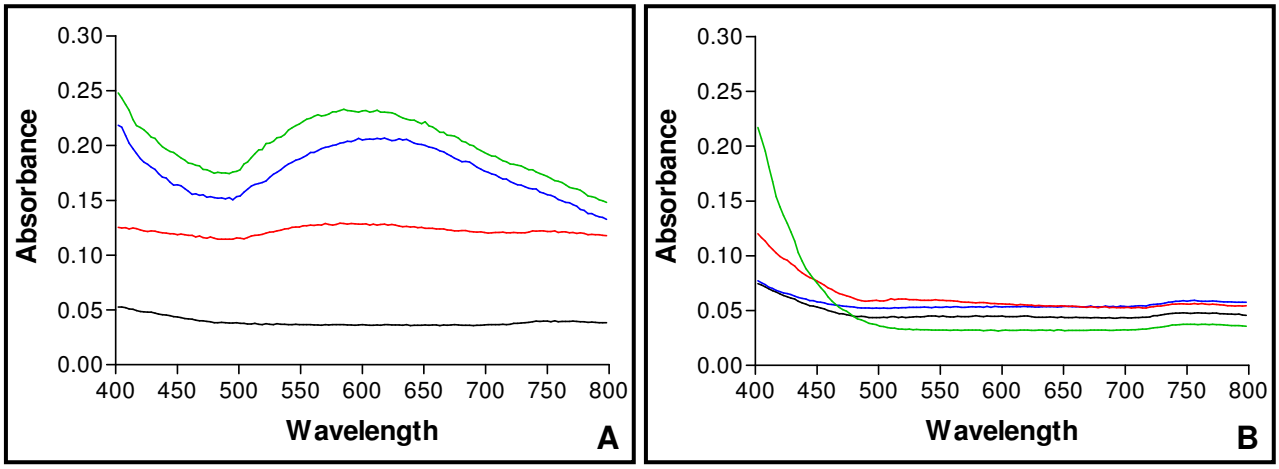

Figure 4.30: UV-Vis absorption spectra of the surface plasmon resonance recorded for the different pH values at 85ºC, indicating gold nanoparticle production through a change in the absorbance around 550 - 650 nm. (A) The protein reactions and (B) the corresponding blank reactions. [pH 3.6 ( ); pH 5.5 ( ); pH 7.5 ( ); pH 9.0 ( )].

The TEM micrographs (Figure 4.31) confirmed that particles formed are in the nano size range, but not monodispersed. The particles were mostly spherical and overall bigger than the ones obtained with expression in *E. coli* (Section 3.3.7.8). Nanoparticles for pH 9.0 were also notably bigger than those for pH 7.5. Therefore it can be concluded that bigger nanoparticles can be obtained at higher pH values.

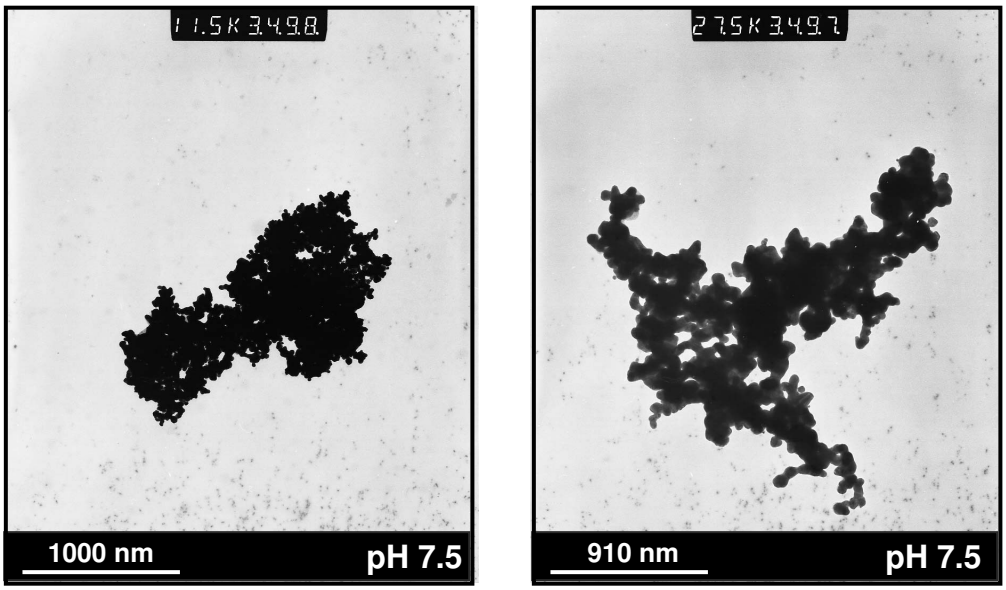

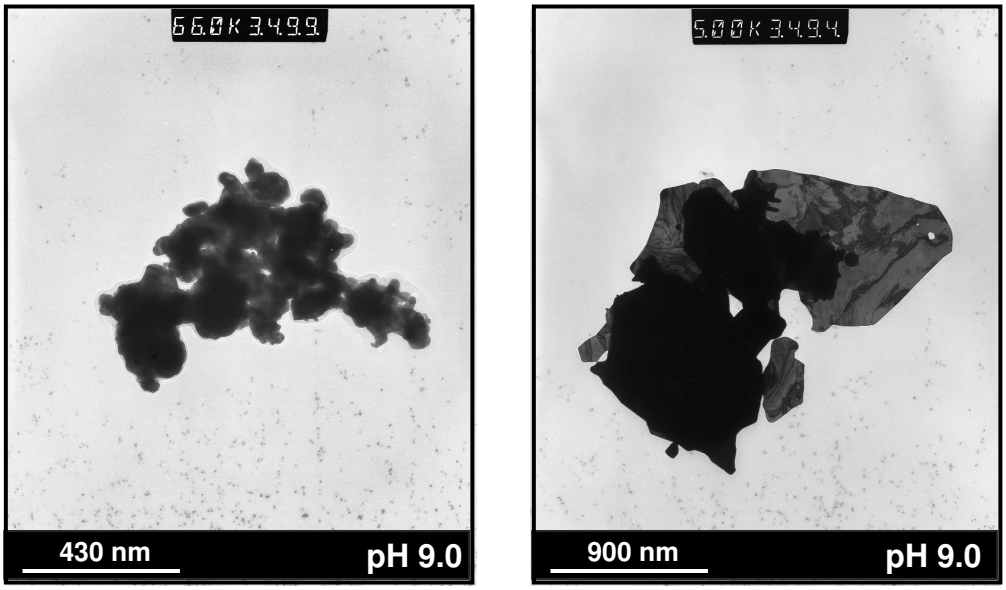

Figure 4.31: TEM micrographs for the different pH values at 85ºC, indicating the shapes, sizes and amounts of gold nanoparticles obtained. Scale bars are equal to 1000 nm; 910 nm; 430 nm and 900 nm respectively.

SAED was performed on the nanoparticles from pH 9.0 at 85ºC and EDX was done on all the samples and the nanoparticles were confirmed to be gold, as can be seen in figure 4.32 and figure 4.33 respectively. In figure 4.32B the micro-diffraction pattern for gold can be seen.

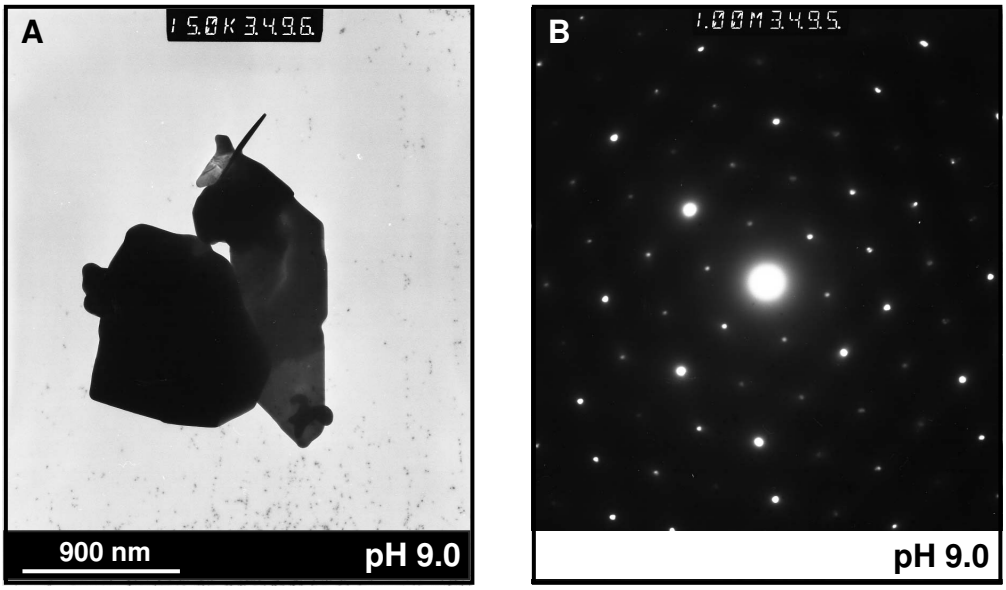

Figure 4.32: (A) TEM micrograph of gold nanoparticles with (B) corresponding selected-area electron micro-diffraction pattern for pH 9.0 at 85ºC. The scale bar in A is equal to 900 nm.

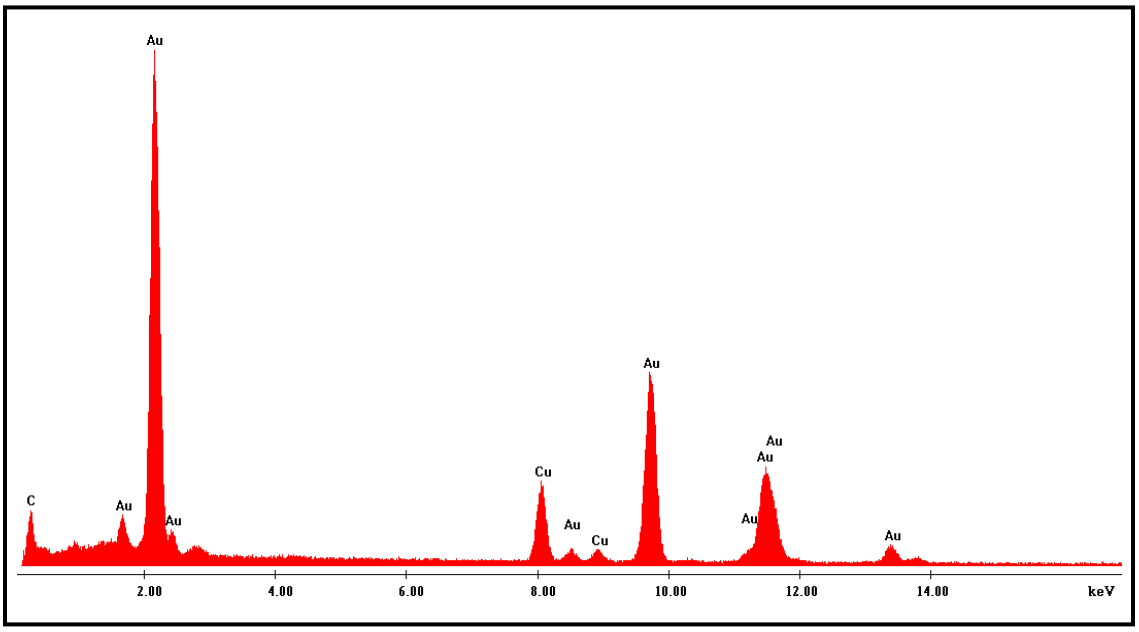

Figure 4.33: EDX spectrum recorded for the nanoparticles produced at different pH values at 85ºC, showing a typical pattern for all the samples and indicates that the nanoparticles are gold.

4.3.7.6 The Effect of Different Disulphide Bond Reducing Agents on Gold Reduction and Nanoparticle Formation

The effect of different disulphide bond reducing agents on gold reduction and nanoparticle formation was tested, using sodium dithionite, dithiothreitol (DTT) and β-mercaptoethanol as electron donors and reducing agents respectively. All three components were used without the addition of methyl viologen at 65ºC and 85ºC and the same principle applies for the mechanism of gold reduction and nanoparticle formation as discussed in section 3.3.7.1. When comparing the reactions through the visual assay (Figure 4.34) and the SPR, obtained through UV-Vis spectra (Figure 4.35), effective nanoparticle formation was obtained with all three components and can be seen due to a change in the absorbance around 550 – 600 nm in the protein reactions (Figure 4.35A) with no change in the respective blank reactions (Figure 4.35B). No significant differences were obtained in the activity of the three components and since they are all disulphide bond reducing agents, the proposed mechanism hypothesis, as discussed in section 3.2.16, can be applied to all three these electron donors. The shift in wavelength

indicates bigger nanoparticles were formed. Overall, enhanced activity was again obtained at 85ºC, therefore SPR and TEM was performed on 85ºC only.

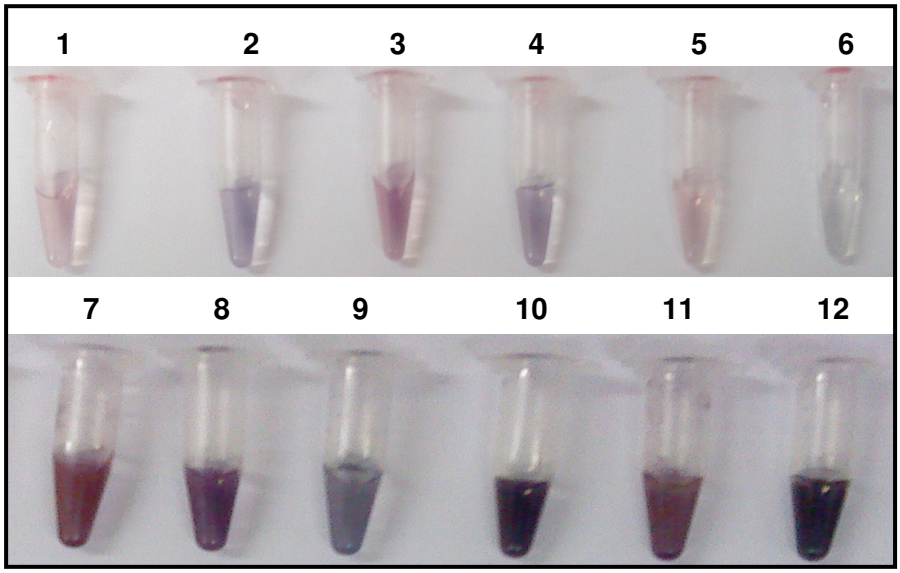

Figure 4.34: The different colours obtained through the gold reduction assay with various electron donors, indicating gold nanoparticle formation for 65ºC (1 – 6) and 85ºC (7 – 12) respectively. The odd numbers (1 – 5 and 7 - 11) indicate protein reactions for sodium dithionite; dithiothreitol and β-mercaptoethanol respectively and the even numbers (2 – 6 and 8 - 12) the corresponding blank reactions.

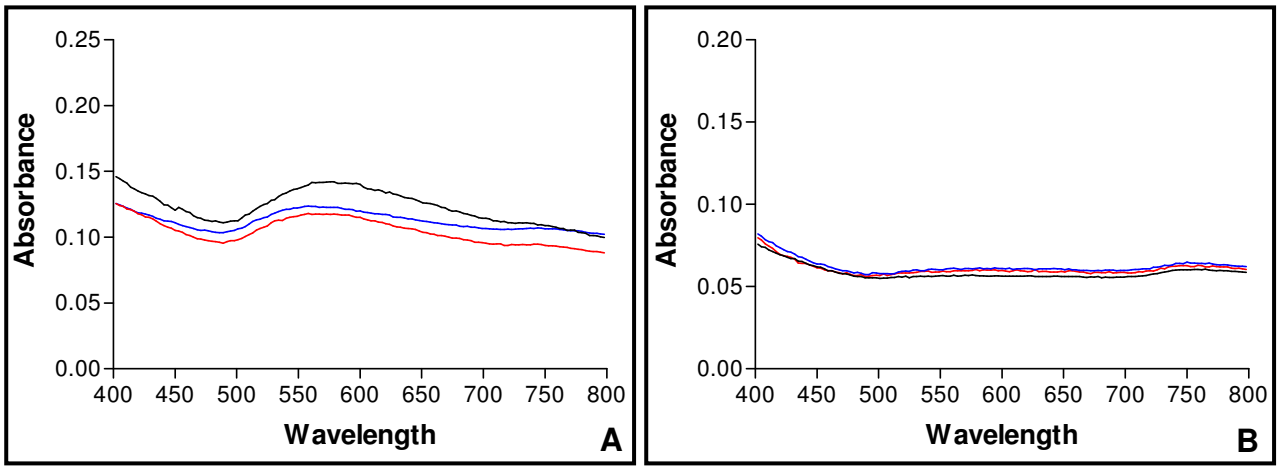

Figure 4.35: UV-Vis absorption spectra of the surface plasmon resonance recorded for the different electron donors at 85ºC, indicating gold nanoparticle production through a change in the absorbance around 550 - 600 nm. (A) The protein reactions and (B) the corresponding blank reactions. [Sodium dithionite (▬); Dithiothreitol (▬); β-mercaptoethanol (▬)].

When compared with the results for the expression in *E. coli* (Sections 3.3.7.9), similar results were obtained, indicating that no matter how the protein was expressed, the different disulphide bond reducing agents had no effect on particle formation and might be due to all three yielding a reduced protein through reduction of the disulphide bond.

The TEM micrographs (Figure 4.36) confirmed that particles were formed with all three electron donors and that all the particles are in the nano size range, with no real differences amongst the three components. SAED (Figure 4.36B) was performed on the sodium dithionite as electron donor and EDX (Figure 4.37) was done on all the samples and the nanoparticles were confirmed to be gold. In figure 4.36B the micro-diffraction pattern for gold can be seen.

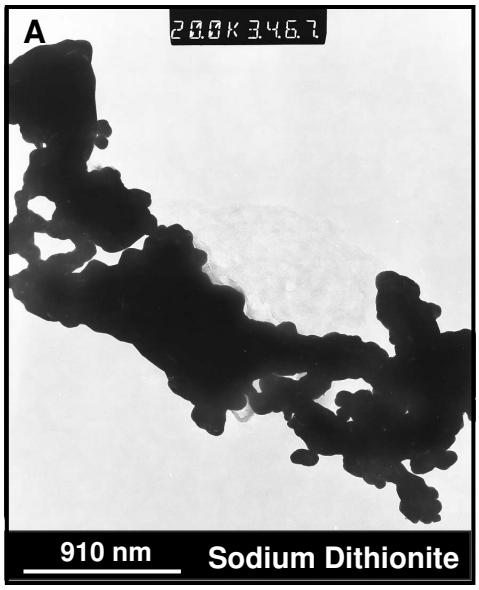

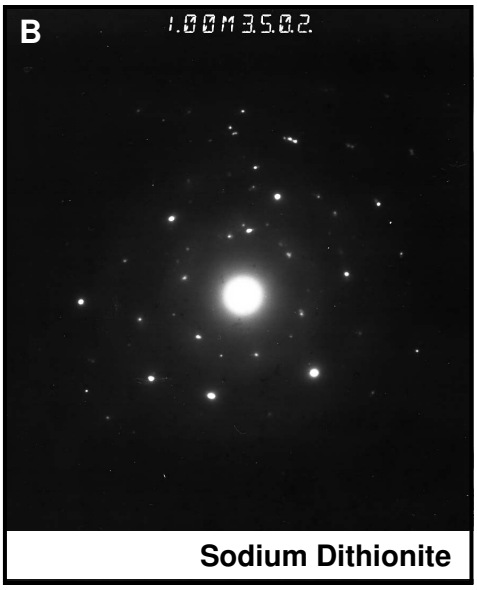

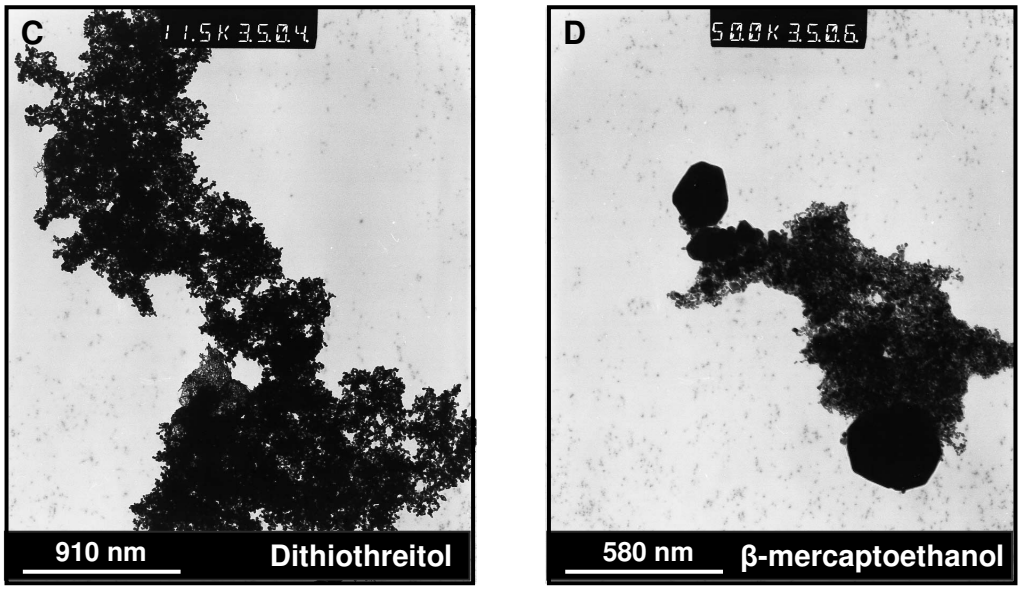

Figure 4.36: (A) TEM micrograph of gold nanoparticles with (B) corresponding selected-area electron micro-diffraction pattern for sodium dithionite as electron donor at 85ºC. (C and D) TEM micrographs for dithiothreitol and β-mercaptoethanol at 85ºC respectively, indicating the shapes, sizes and amounts of gold nanoparticles obtained. The scale bars in A, C and D are equal to 910 nm; 910 nm and 580 nm respectively.

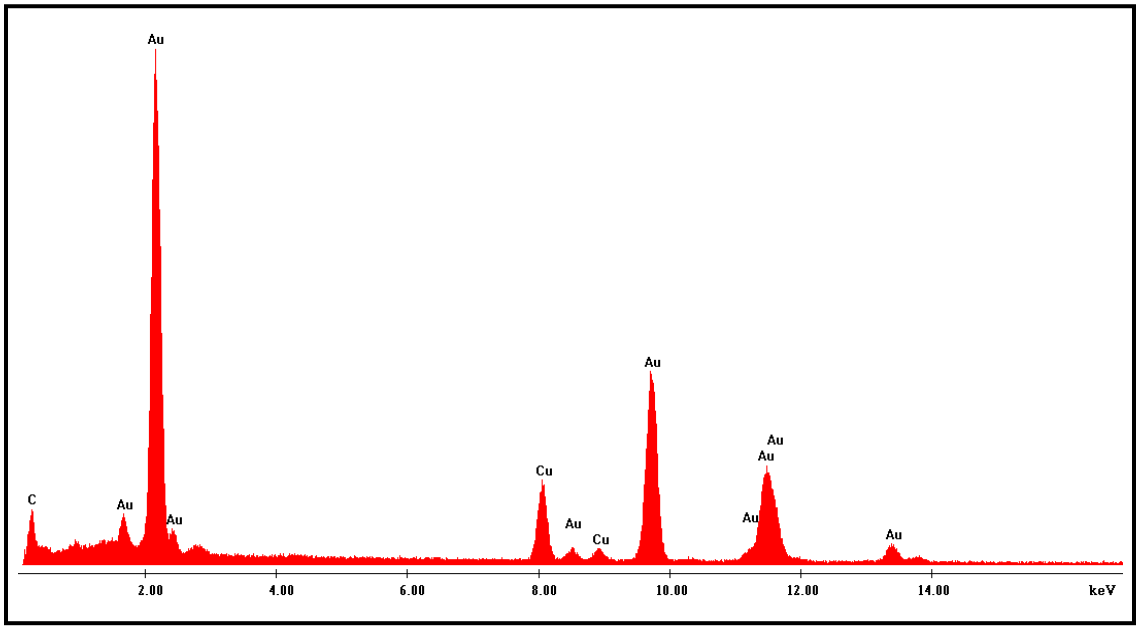

Figure 4.37: EDX spectrum recorded for the nanoparticles produced with the different electron donors at 85ºC, showing a typical pattern for all the samples and indicates that the nanoparticles are gold.

From this it can be concluded that the different electron donors and reducing agents did not had any real influence on the gold reduction and nanoparticle formation process.

4.3.8 Mechanism Hypothesis

The mechanism hypothesis, as discussed in section 3.2.16, was verified by testing the effect of the sulphydryl blocking agent, iodoacetic acid, on sodium dithionite, dithiothreitol (DTT) and β-mercaptoethanol for gold reduction and nanoparticle formation. When comparing the reactions through the visual assay (Figure 4.38) and the SPR, obtained through UV-Vis spectra (Figure 4.39), only a slight change in colour was observed with all three the components, indicating that gold reduction and nanoparticle formation did took place but not very effectively. This can be seen through the presence of a small, but not significant changes in the absorbance around 540 – 560 nm in the protein reactions with the electron donors (Figure 4.39A) with no change in the respective blank reactions (Figure 4.39B). Clear differences in the blank reactions could be detected and overall enhanced activity was again obtained at 85ºC, therefore SPR was performed on 85ºC only.

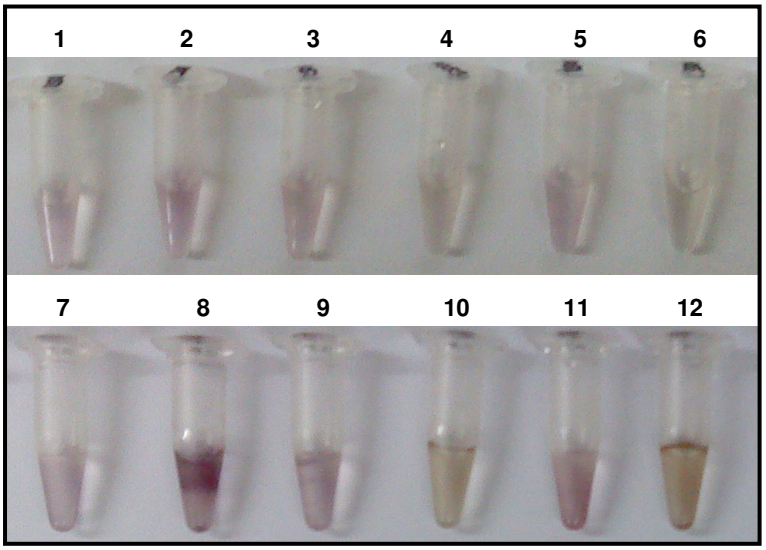

Figure 4.38: A slight change in colour obtained through the gold reduction assay with iodoacetic acid and the various electron donors, indicating ineffective nanoparticle formation for 65ºC (1 – 6) and 85ºC (7 – 12). The odd numbers (1 – 5 and 7 - 11) indicate protein reactions for sodium dithionite; dithiothreitol and β-mercaptoethanol respectively and the even numbers (2 – 6 and 8 - 12) the corresponding blank reactions.

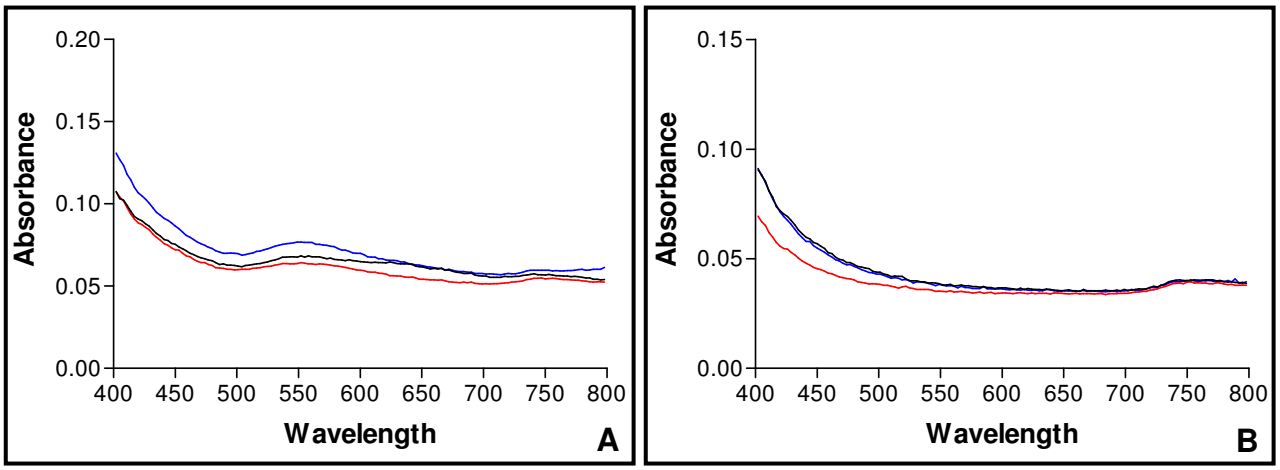

Figure 4.39: UV-Vis absorption spectra of the surface plasmon resonance recorded for the iodoacetic acid with the various electron donors at 85ºC, indicating ineffective nanoparticle production through small changes in the absorbance around 540 - 560 nm. (A) The protein reactions and (B) the corresponding blank reactions. [Sodium dithionite ( ); Dithiothreitol ( ); β-mercaptoethanol ( )].

Similar results were obtained with the gold reduction assay and the SPR when compared to section 4.3.7.2 where denatured protein was used as a parameter. Therefore TEM analysis was not performed on these samples, since the results would be similar, showing no significant nanoparticle formation with all three the electron donors.

When comparing the results obtained in this section with those from section 4.3.7.6, ineffective gold reduction and nanoparticle formation was obtained when iodoacetic acid was added as a sulphydryl blocking agent. Expression in a thermophilic host influence protein folding, as discussed in section 4.1, and it might be that the disulphide bond was folded inwards and was not completely accessible for the iodoacetic acid to block the reduction of the protein. Therefore gold reduction and nanoparticle formation could be detected in the slight change in colour that occurred, but it was insignificant and thus collaborates with the hypothesis of Van Marwijk, (2009), stating that gold reduction takes place *via* reduction of a surface exposed disulphide bond which in turns reduces the gold to elemental gold and yielding a change in colour; however with the addition of the sulphydryl blocking agent, iodoacetic acid, the disulphide bond can't become reduced, thereby preventing the protein to become reduced and therefore no reduction of gold should take place, giving no change in colour when the gold reduction assay is used.

4.4 CONCLUSIONS

The ABC transporter, peptide-binding protein from *Thermus scotoductus* SA-01 was successfully cloned and expressed in the thermophilic host, *Thermus thermophilus*. Expressed protein was obtained in very low levels, but was effectively purified, with and without the N-terminal His-Tag and leader peptide. Characterization studies showed that the neither the His-Tag nor the leader peptide had significant influences on the gold reduction and nanoparticle formation process, since no real differences were obtained in the characterization studies.

The ABC transporter, peptide-binding protein was also successful in the reduction of gold(III) to gold(0) and in the formation of gold nanoparticles, at various parameters. Nanoparticles of different shapes, sizes and distributions were obtained, but these particles were not monodispersed at most parameters tested. The particles obtained were overall bigger, but not well defined. Nanoparticle formation was dependant on environmental parameters but control of the process was not complete. Chemical reduction did have an influence in some instances, but overall it could again be seen that the presence of the protein played a significant role in slowing down the reaction rate, yielding a level of control over the nanoparticles produced.

For the mechanism hypothesis, it was confirmed that when reduction of the disulphide bond was blocked with a sulphydryl blocking agent, insignificant gold reduction and nanoparticle formation was obtained, proving that the hypothesis might be true, but also that expression in a thermophilic host influences the folding of the protein and have an effect on nanoparticle formation.

Overall, the best nanoparticles were obtained at pH values closest to the pI of the protein, at lower gold(III) concentrations and at higher temperatures, indicating the influence of the thermophilic expression host on the folding and activity of the protein.

REFERENCES

- **Averhoff, B.** (2006) Genetic Systems for *Thermus*. *Methods in Microbiology.* **35**:279-309.

- **Brouns, S.J.J., Wu, H., Akerboom, J., Turnbull, A.P., de Vos, W.M. and van der Oost, J.** (2005) Engineering a Selectable Marker for Hyperthermophiles. *The Journal of Biological Chemistry.* **280**:11422-11431.

- **Bruins, M.E., Janssen, A.E.M. and Boom, R.M.** (2001) Thermozymes and their Applications. *Applied Biochemistry and Biotechnology.* **90**:155-186.

- **De Grado, M., Castán, P. and Berenguer, J.** (1999) A High-Transformation Efficiency Cloning Vector for *Thermus thermophilus*. *Plasmid.* **42**:241-245.

- **Fairbanks, G., Steck, T.L. and Wallach, D.F.H.** (1971) Electrophoretic Analysis of the Major Polypeptides of the Human Erythrocyte Membrane. *Biochemistry.* **10**:2606-2617.

- **Hanahan, D.** (1983) Studies on Transformation of *E. coli* with Plasmid. *Journal of Molecular Biology.* **166**:557-580.

- **Hidalgo, A., Betancor, L., Moreno, R., Zafra, O., Cava, F., Fernández-Lafuente, R., Guisán, J.M. and Berenguer, J.** (2004) *Thermus thermophilus* as a Cell Factory for the Production of a Thermophilic MN-Dependant Catalase which Fails to be Synthesized in an Active Form in *Escherichia coli*. *Applied and Environmental Microbiology.* **70**:3839-3844.

- **Koyama, Y., Hoshino, T., Tomizuka, N. and Furukawa, K.** (1986) Genetic Transformation of the Extreme Thermophile *Thermus thermophilus* and of other *Thermus* spp. *J. Bacteriol.* **166**:338-340.

- **Laemmli, U.K.** (1970) Cleavage of Structural Proteins during the Assembly of the Head of Bacteriophage T4. *Nature.* **227**:680-685.

- **Lasa, I., De Grado, M., De Pedro, M.A. and Berenguer, J.** (1992) Development of *Thermus-Escherichia* Shuttle Vectors and their Use for Expression of the *Clostridium thermocellum celA* Gene in *Thermus thermophilus*. *Journal of Bacteriology.* **174**:6424-6431.

- **Moreno, R., Haro, A., Castellanos, A. and Berenguer, J.** (2005) High-Level Overproduction of His-Tagged *Tth* DNA Polymerase in *Thermus thermophilus*. *Applied and Environmental Microbiology.* **71**:591-593.

- **Moreno, R., Zafra, O., Cava, F. and Berenguer, J.** (2003) Development of a Gene Expression Vector for *Thermus thermophilus* Based on the Promoter of the Respiratory Nitrate Reductase. *Plasmid.* **49**:2-8.

- **Rabilloud, T., Carpentier, G. and Tarroux, P.** (1988) Improvement and Simplification of Low Background Silver Staining of Proteins by using Sodium Dithionite. *Electrophoresis.* **9**:288-291.

- **Ramírez-Arcos, S., Fernández-Herrero, L.A., Marín, I. and Berenguer, J.** (1998) Anaerobic Growth, a Property Horizontally Transferred by an Hfr-Like Mechanism among Extreme Thermophiles. *Journal of Bacteriology.* **180**:3137-3143.

- **Smith, P.K., Krohn, R.I., Hermanson, G.T., Mallia, A.K., Gartner, F.H., Provenzano, M.D., Fujimoto, E.K., Goeke, N.M., Olson, B.J. and Klenk, D.C.** (1985) Measurement of Protein using Bicinchoninic Acid. *Analytical Biochemistry.* **150**:76-85.

- **Towner, P.** (1991) Isolation of DNA by SDS-Proteinase K Treatment. *In* T.A. Brown (Ed.). *Essential Molecular Biology. A Practical Approach.* **1**:52-53. Oxford University Press. United Kingdom.

- **Turner, P., Mamo, G. and Karlsson, E.N.** (2007) Potential and Utilization of Themophiles and Thermostable Enzymes in Biorefining. *Microbial Cell Factories.* **6**:9-31.

- **Van Marwijk, J.** (2009) Biological Synthesis of Gold Nanoparticles by *Thermus scotoductus* SA-01. *PhD. Thesis.* University of the Free State. Bloemfontein. South Africa.

CHAPTER 5

CONCLUSIONS

The production of gold nanoparticles with unique shapes, sizes and dispersity are important properties that may lead to an increase in the applications of gold in the industry. However, methods used for the production of these nanomaterials have to be selected with great care, keeping in mind the safety of the environment and the public, and especially concerning human health. In this study, gold nanoparticles were produced through biological synthesis, making use of an ABC transporter, peptide-binding protein from *Thermus scotoductus* SA-01.

The ABC transporter, peptide-binding protein, a thermostable protein of ± 70 kDa, was shown to be capable of reducing soluble gold(III) to insoluble gold(0) with subsequent nanoparticle formation through reduction of a surface exposed disulphide bond. Expression studies were carried out in *Escherichia coli*, a mesophilic expression host, with pET-22b(+) and pET-28b(+) and in *Thermus thermophilus*, a thermophilic expression host, with pWUR and pMK184. The oligonucleotide primers used were designed to yield constructs that either included or excluded the leader peptide, the C-terminal and/or the N-terminal His-Tag when cloned in pET-22b(+) and pET-28b(+). This was done to determine the influence (if any) of the His-Tag and the leader peptide on gold reduction and nanoparticle formation. The His-Tags were also added for purification purposes.

All variations of the protein were successfully purified, either through size-exclusion or nickel affinity columns; however, expression and purification levels were notably lower in the thermophilic expression host, probably due to weaker PslpA promoter in *T. thermophilus*, as compared to the strong T7 promoter system in *E. coli*. Purified protein was used for characterization studies with different parameters, to determine how they will influence the gold reduction and nanoparticle formation process. It was found that

the leader peptide and His-Tags had no effect on the nanoparticles obtained, but the expression host and the different parameters had significant influences.

Overall, bigger particles were obtained with the thermophilic expression and optimum activity was obtained at 85ºC, as compared to a 65ºC optimum for the mesophilic expression. The pH of the solution played a significant role in obtaining better defined particles specifically when a pH value closer to the pI of the protein was used. The temperature at which the reactions were performed also had a significant influence. At lower temperatures the particles formed were smaller and fewer were formed, but with better defined shapes. This may be due to the nanoparticle formation process taking place at a slower rate, yielding a measure of control over this process to form particles that are well shaped and clearly defined. At higher temperatures, the process takes place much faster; yielding unusual shapes or not giving enough time to form defined particles and the reaction is thus completed before complete particle formation. Therefore, it might be possible to obtain more nanoparticles with better defined shapes through incubation at lower temperatures, but for longer time intervals.

When denatured protein was added to the reaction, clear differences were detected when compared with results obtained when correctly folded protein were present in the reaction. Chemical reduction was obtained, but when comparing the results, it was apparent that the presence of the folded protein played a significant role in gold reduction and nanoparticle formation by slowing down the process, yielding a level of control over the rate of gold reduction and influencing the type of particles formed.

It was found that sodium dithionite are oxidized with molecular oxygen and can be used to release two hydrogen ions (H^+), which will cleave the surface exposed disulphide bond (S-S) of the protein to yield a reduced protein (SH-SH). This reduced protein can then convert gold(III) to gold(0) with subsequent nanoparticle formation. Furthermore, the addition of methyl viologen in the gold reduction assay did not influence the nanoparticles obtained and it can be concluded that methyl viologen is not needed in this assy. When iodoacetic acid, a sulphydryl blocking agent, was added to the reaction, no gold reduction activity and nanoparticle formations were obtained, proving that the mechanism hypothesis might be true. In this case, no colour formation was observed with protein from the mesophilic host; indicating that gold reduction did not take place

and therefore the disulphide bond was not reduced and no gold nanoparticles were produced. When using protein from the thermophilic host, a slight change in colour was observed; however, particle formation was ineffective. This might be due to a change in the folding of the protein in the thermophilic host resulting in the disulphide bond being folded inwards and not completely accessible for the iodoacetic acid to block the reduction of the protein. Although low levels of nanoparticle formation could be detected, due to the slight change in colour, it can again be concluded that the hypothesis might be true.

In general, effective reduction of gold(III) was obtained with the ABC transporter, peptide-binding protein from both mesophilic and thermophilic expressions and nanoparticles produced were all in the nano range, except for when excessive concentrations of gold(III) were added. Particles sizes, shapes and distributions could be manipulated to some extent, but control thereof was not complete and it was not possible to obtain monodisperse particles, although in some cases it was near monodisperse. The majority of nanoparticles obtained were spherical, but several well defined, non-spherical shapes were obtained.

Therefore, by using the ABC transporter, peptide-binding protein, successful reduction of gold(III) and formation of nanoparticles can be obtained, resulting in an increase in the applications of gold through a method that is environmentally friendly method and safe for human health.

SUMMARY

Developments in the biosynthesis of nanoparticles have increased significantly during the last few years as a result of the growing interest in the unique properties displayed by nanoparticles. These particles are extremely small in size and have a large surface to volume ratio, giving them unique physical and chemical properties at this scale that differs considerably from when they are used in larger form. These exceptional properties are used in a wide variety of applications, ensuing nanotechnology to become a multidisciplinary field. Research into application structure types are extended daily and as a result, the next few years will be crucial as applications for nanomaterials in the industry are most likely to be increased.

Gold nanoparticles is receiving more and more attention because of its wide variety of uses in optical, electronic, magnetic, catalytic, and biomedical applications, but even more due to them being the most stable of all the metal nanoparticles. Several methods are used to produce these metal nanoparticles, but are mostly making use of toxic chemicals in the synthesis protocol, which are harmful to the environment and human health. To overcome this problem, researchers are making use of more “greener” alternatives through the use of biological systems and microorganisms in nanoscience and nanotechnology. These microorganisms have unique potential in producing nanoparticles that are environmentally friendly and display different shapes, sizes and distributions. Among the different microorganisms used, bacteria have received the most attention in the nanoparticle production process, but have not been as successful as chemical synthesis to produce monodisperse noble metal nanoparticles.

In this study, successful gold reduction and nanoparticle formation with different shapes, sizes and distribution was obtained; however, these particles were not monodisperse. This was achieved with a thermostable protein of ± 70 kDa that was identified as an ABC transporter, peptide-binding protein and which was purified from *Thermus scotoductus* SA-01; an extremophile and thermophilic bacterium that was isolated from groundwater

samples from Mponeng (a deep South African gold mine in the Witwatersrand Supergroup operated by AngloGold Ashanti) at a depth of 3.2 km with ambient rock temperature of 60ºC. The protein was expressed in *Escherichia coli* and *Thermus thermophilus* HB27, a mesophilic and a thermophilic expression host respectively. It was found that the expression host might have an influence on the way the protein is folded and therefore influence nanoparticle formation. Expression studies was also done on the protein that either included or excluded Histidine-Tags and a leader peptide, but it was found that neither the His-Tags nor the leader peptide had any influence on the nanoparticles produced.

Gold reduction and nanoparticle formation was obtained through reduction of a surface exposed disulphide bond in the ABC transporter, peptide-binding protein, using sodium dithionite as electron donor and reducing agent. In general it was found that nanoparticle formation was dependant on environmental parameters but control of this process was not complete. Chemical reduction did influence the nanoparticle formation process in some instances, but overall it could be seen that the presence of the protein played a significant role in slowing down the reaction rate, yielding a level of control over the nanoparticles produced and ensuring a more environmentally friendly, biological process for the production of gold nanoparticles.

Key words: Metal nanoparticles; biosynthesis; gold reduction; *Thermus scotoductus* SA-01; ABC transporter, peptide-binding protein; mesophilic and thermophilic expression host.

OPSOMMING

Ontwikkelings in die biosintese van nanopartikels het gedurende die laaste paar jaar aansienlik verhoog as gevolg van die toenemende belangstelling in die unieke eienskappe van nanopartikels. Hierdie partikels is uitsonderlik klein en het ‘n groot oppervlakte tot volume verhouding. Op hierdie skaal gee dit aan hulle unieke fiesiese en chemiese eienskappe wat, aansienlik verskil van die gebruik daarvan in groter vorme. Hierdie uitsonderlike eienskappe word in ‘n wye verskeidenheid toepassings gebruik wat veroorsaak het dat nanotegnologie ‘n multidissiplinêre veld geword het. Ondersoek na toepassing-struktuur-tipes word daagliks uitgebrei, en as gevolg daarvan, sal die volgende paar jaar krities wees soos wat toepassings in die nanomateriaalbedryf waarskynlik behoort toe te neem.

Goud nanopartikels ontvang meer en meer aandag as gevolg van die wye verskeidenheid van gebruike in optiese, elektroniese, magnetiese, katalitiese, en biomediese toepassings, maar veral omdat hulle die mees stabielste van al die metaal nanopartikels is. Verskeie metodes word gebruik om die metaal nanopartikels te produseer, maar giftige chemikalieë word meestal gebruik in die produksie proses wat skadelik is vir die omgewing en vir menslike gesondheid. Om hierdie probleem te oorkom maak navorsers gebruik van meer "groener" alternatiewe deur die gebruik van biologiese sisteme en mikroörganismes in die nanowetenskap en nanotegnologie. Hierdie mikroörganismes het unieke potensiaal in die vervaardiging van nanopartikels wat omgewingsvriendelik is en lei tot verskillende vorms, groottes en verspreiding van nanopartikels. Tussen die verskillende mikro-organismes wat gebruik word, ontvang bakterieë die meeste aandag in die nanopartikel produksie proses, maar is nie so suksesvol soos chemiese sintese in die produsering van egalig verspreide edel metaal nanopartikels.

In hierdie studie was suksesvolle goud reduksie en nanopartikel vorming met verskillende vorms, groottes en verspreiding verkry, maar hierdie deeltjies is nie egalig

verspreid nie. Dit is bereik met ‘n termostabiele proteïen van ± 70 kDa wat as ‘n ABC-vervoerder-peptied-bindings-proteïen geïdentifiseer is. Hierdie proteïen is gesuiwer vanuit *Thermus scotoductus* SA-01, ‘n ekstremofiele en termofiele bakterie wat in grondwater monsters van Mponeng (‘n diep Suid-Afrikaanse goudmyn aan die Witwatersrand Supergroep, beheer deur AngloGold Ashanti) op ‘n diepte van 3,2 km met omringende rots temperatuur van 60ºC geïsoleer is. Die proteïen is uitgedruk in *Escherichia coli* en *Thermus thermophilus* HB27, ‘n mesofieliese en ‘n termofieliese uitdrukkingsgasheer onderskeidelik. Dit is bevind dat die uitdrukkingsgasheer ‘n invloed het op die manier waarop die proteïen is gevou en dus die vorming van nanoprtikels beïnvloed het. Uitdrukking studies is ook gedoen op die proteïen wat of ‘n Histidien-aanhangsel of ‘n leierpeptied of beide bevat het. Dit is egter gevind dat nie die Histidien-aanhangsel of die leierpeptied enige invloed gehad het op die nanopartikels wat verkry is nie.

Goud reduksie en nanopartikel vorming is verkry deur die reduksie van ‘n disulfied binding, geleë op die oppervlak van die ABC-vervoerder-peptied-bindings-proteïen, met behulp van natrium ditioniet as elektron skenker en reduseermiddel. In die algemeen is daar gevind dat nanopartikels se vorming afhanklik is van die omgewingsparameters, maar beheer van hierdie proses is nie volledig nie. Chemiese reduksie het in sommige gevalle ‘n invloed gehad op die vorming van nanopartikels, maar in geheel kan dit gesien word dat die teenwoordigheid van die proteïen ‘n baie belangrike rol speel in die vertraging van die reaksietempo. Dit kan sorg vir ‘n mate van beheer oor die vorming van nanopartikels en lei tot ‘n meer omgewingsvriendelike, biologiese proses vir die produksie van goud nanopartkels.

Sleutelterme: Metaal nanopartikels; biosintese; goud reduksie; *Thermus scotoductus* SA-01; ABC-vervoerder, peptied-gebinde proteïen; mesofieliese en termofieliese uitdrukkingsgasheer